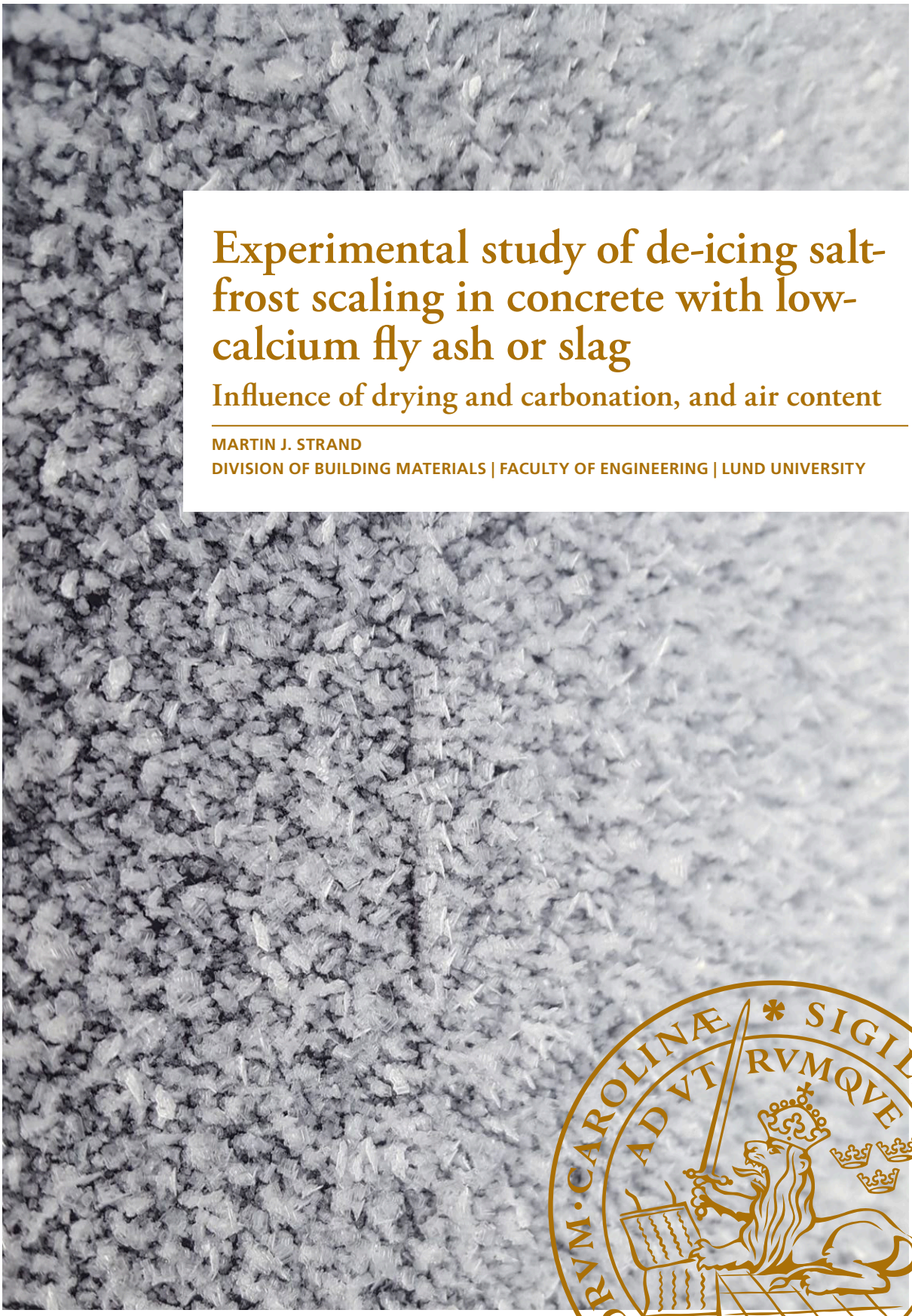

Experimental study of de-icing salt-frost scaling in concrete with low-calcium fly ash or slag

Influence of drying and carbonation, and air content

MARTIN J. STRAND
DIVISION OF BUILDING MATERIALS | FACULTY OF ENGINEERING | LUND UNIVERSITY

Experimental study of de-icing salt-frost scaling in concrete with low-calcium fly ash or slag

Influence of drying and carbonation, and air content

Martin J. Strand

LUND
UNIVERSITY

DOCTORAL DISSERTATION
with due permission from the Faculty of Engineering, Lund University, Sweden.
To be defended at V-huset, John Ericssons väg 1, Lund, Sweden, lecture hall V:B
1 February 2019 at 10:15.

Faculty opponent
Associate Professor Marianne Tange Hasholt
From the Technical University of Denmark,
Department of Civil Engineering

Cover photo by Linnea Gard

Lund University
Faculty of Engineering
Department of Building & Environmental Technology
Division of Building Materials

ISBN 978-91-7753-940-7 (Print)
ISBN 978-91-7753-941-4 (Pdf)
ISSN 0348-7911
ISRN LUTVDG/TVBM--18/1038--SE(1-73)

Printed in Sweden by Media-Tryck, Lund University
Lund 2018

Dedicated to Linnea and my family

Table of contents

Preface

I would like to thank Professor Emeritus Göran Fagerlund and Dr Kyösti Tuutti (Skanska) for making the project possible, and the SBUF and Cementa AB for the funding.

Moreover, I wish to thank the following people who assisted me during the project:

- My supervisors—Dr Katja Fridh, Professor Lars Wadsö, and Dr Maria Fredriksson;
- Members of the reference group who expressed great interest in the project—Dr Anders Lindvall, Dr Arvid Hejll, Erik Viggh, lic. Mikael Westerholm, Dr Nils Rydén, Dr Peter Utgenannt, Dr Staffan Hintze, Dr Ulf Håkansson, and Ulf Jönsson;
- Dr Sture Lindmark and Professor George Scherer for answering my questions to enhance my understanding of the salt-frost scaling mechanisms;
- Dr Jan-Erik Lindqvist for helping me with the microscopic analysis.

I also wish extend my gratitude to the employees at the division of Building Materials who created a pleasant working environment.

My special gratitude goes to Linnea, my family, and friends for their moral support until the completion of this work.

Summary

In order to reduce the net climate impact of concrete production, it is necessary for the industry to undertake several actions. Among these is to include fly ash and slag as supplementary cementitious materials. Accordingly, this project has studied concrete containing low-calcium fly ash or ground-granulated blast-furnace slag. In incorporating fly ash or slag as supplementary material, the cement reaction is affected and the products of reaction are not the same. Consequently, the material properties and durability also change.

This PhD-project has studied a superficial damage on concrete called de-icing salt-frost scaling (DISFS), which occurs when a solution with a low concentration of de-icing agent freezes in contact with concrete. DISFS has been studied ever since the beginning of the 20th century in order to understand the damage mechanism, and how concrete recipes should be designed to minimize the damage. Early studies have shown that a salt solution with a low concentration (approx. 3%) results in more DISFS damage than when the concentration is 0 or 10%. Moreover, studies have shown that an entrained air void content, created by using an air entraining agent, reduces the DISFS. Furthermore, studies have also shown that preconditioning of the concrete surface, especially drying and carbonation, also have an effect on the DISFS. The reason for this is that the microstructure changes depending on the preconditioning process. If a sample is cured for a longer period, more products are created from the binder reaction and the microstructure becomes denser. Two factors that affect this are carbonation and drying. Carbonation is the reaction between the concrete surface and CO_2 (carbon dioxide), which changes the microstructure of the surface. Drying does not by itself affect the microstructure, but it can cause micro cracks to form and it lowers the initial moisture content.

Prior studies have resulted in some theories that try to explain the mechanism causing DISFS. However, there is a lack of studies that have tested what influence the factors mentioned above (drying and carbonation, air content, and varying salt solution concentrations) have on the DISFS on concrete containing fly ash or slag.

Concrete containing fly ash or slag has different microstructures compared to ordinary concrete containing 100% cement. Because curing and carbonation change the microstructures of the material, there is a need for a broad study analysing how these different factors (drying and carbonation, air content, and varying salt solution concentrations) affect the DISFS in concrete containing fly ash or slag. As the microstructures change with time due to curing and carbonation, there can be preconditioning processes that are favourable to some materials and unfavourable to others.

This project has focused on how drying, carbonation, air content, and salt concentration affect the DISFS in concrete containing fly ash or slag. To determine

the influence of air content on the DISFS, concrete batches with various air contents are required. A method was developed to find one combination of admixtures (one superplasticiser and one air-entraining agent) for each binder. Linear traverse analysis was used to quantify the varied air-void systems created by the air-entraining agent. Furthermore, other measurements have been performed to characterise the materials. Low-temperature calorimetry has been conducted to assess the amount of ice formed and acquire information on the microstructure of pores with sizes below 50 nm. Because a coarse porosity results in a high absorption rate, and a fine porosity results in a low absorption rate, capillary absorption measurements have been conducted to obtain some information on capillary porosity (pores over 50 nm in size); moreover, total porosities are also determined. Measurements of pH have been conducted to determine whether the samples used for low-temperature calorimetry and capillary absorption measurements are completely carbonated. To analyse the effect of carbonation on the DISFS, thin-slice analysis has been performed to measure the carbonation depth on the samples used for the DISFS test. It is possible to correlate the carbonation depth with the DISFS mass by using the approximation that 1 kg/m² equals a 1-mm scaling depth. A DISFS test is developed and designed to contribute to a small variation in the DISFS results.

A study has been made where different characteristics of the porosity have been correlated to the DISFS for concrete that have hydrated for over 300 d. The binder combinations used for these tests were CEM I mixed with 20, 35% LCFA, or 20, 35, 70% slag, or 25+10% slag+limestone filler. These tests focused on the effect on the DISFS from the increased fraction of SCM, the effect from drying and carbonation, and the effect from various air contents for each binder combination. Moreover, a broader DISFS study was performed on concrete with 100% CEM I, 35% LCFA, or 35% slag, where the concrete hydrated for 8 to 63 d. These tests were conducted for several reasons. Partly to acquire more knowledge regarding how different preconditioning processes, air contents, and salt solution concentrations affect the DISFS in concrete containing fly ash or slag exposed to a short period of hydration. The results also bridge the gap between the effect drying and carbonation has of the DISFS on concrete exposed to a short period of hydration in relation to well hydrated concrete (results from concrete that have hydrated for over 300 days). Moreover, they bridge the gap between the effect air content has on the DISFS of concrete exposed to a short period of hydration in relation to well hydrated concrete (results from concrete that have hydrated for over 300 days). The broad approach on this DIFS study contributed to some interesting and unexpected results.

The study that aimed to correlate different characteristics of the porosity with DISFS showed that carbonation contribute to a lower DISFS for concrete containing 100% CEM I, 20, and 35% slag, unchanged DISFS for concrete containing 20% LCFA,

or 25+10% slag+limestone filler, and increased DISFS for concrete containing 35% LCFA, or 70% slag. The study also found a correlation between the carbonation depth and the DISFS with the approximation that 1 kg/m² DISFS equals to 1 mm DISFS depth. Thereby the following conclusions could be made. A fine structure of pores below 50 nm (that reduces the fraction of ice that can form at a given temperature), combined with low permeability according to the capillary suction measurements (which infer a fine porosity for the structure of pores larger than 50 nm), generally results in a low DISFS. (The only exception was the noncarbonated concrete with 25% slag and 10% limestone filler). A coarse structure of pores below 50 nm (which enable more water to freeze at a given temperature), with a high permeability according to the capillary suction measurements (which infer a coarse porosity for the structure of pores larger than 50 nm) generally results in a high DISFS. The DISFS results on the concrete that have hydrated for 8 to 63 d clearly show that the preconditioning process affect the DISFS. The different materials can be affected by the same preconditioning process in various ways. The results also show that the air content has different effects on the DISFS depending on whether or not the test surface is dried and carbonated. The tests with different NaCl concentrations resulted in some unexpected results where a high NaCl concentration resulted in a high DISFS in two cases. The cause for these two unique cases for 35% LCFA is believed to be that the critical degree of saturation was exceeded. Otherwise the results seemed to agree with the so called ‘glue spall theory’ where a high salt solution concentration results in a low DISFS.

This project has shown that these three factors (drying and carbonation, air content, and NaCl concentration) affect the DISFS in various ways depending on the material. Accordingly, this highlights the complexity of attempting to test the DISFS in the laboratory. Some researchers have criticised the standard test methods for being too conservative and so that some concrete recipes containing fly ash or slag which seem DISFS resistant in the field do not pass. Because, there is a critical need to lower the CO_2 emissions due to global warming, there is a reason to fine-tune the standard preconditioning process making it less conservative, so that concrete containing fly ash or slag that reduce the net CO_2 emissions, which works in the field tests, does not fail the test. This thesis contributes with important information if a fine-tuning of the standard preconditioning process would be carried through of the European standard DISFS test method.

Sammanfattning

För att minska klimatpåverkan från cementproduktionen krävs många olika åtgärder. En åtgärd för att minska cementanvändandet är att använda tillsatsmaterial, som flygaska eller slagg. Därför har detta projekt testat betong som innehåller antingen flygaska med lågt kalciuminnehåll, eller granulerad masugnsslagg. När betongreceptet innehåller flygaska eller slagg ändras reaktionen och därmed produkterna (den resulterande hårdnade pastan) från reaktionen. Som en följd därav ändras även materialegenskaperna och beständigheten av betongen.

Detta doktorandprojekt har studerat tösaltfrostavskalning, en ytlig skada på betong som sker då en saltlösning med låg saltkoncentration fryser i kontakt med betongytan. Tösaltfrostavskalning har studerats sedan början av 1900-talet för att förstå skademekanismen och hur betongrecept behöver utformas för att minimera potentiell skada. Tidigare studier har visat att en låg saltlösningskoncentration (ca 3%) resulterar i mer tösaltfrostavskalning jämfört med 0 eller 10%. Vidare har även studier visat att lufthalten i betong, som bildats från en luftporbildare, reducerar tösaltfrostavskalningen. Studier har även påvisat att förkonditioneringen av betongytan, särskilt torkning och karbonatisering, påverkar tösaltfrostavskalningen. Anledningen till detta är att mikrostrukturen ändras beroende på vilken förkonditioneringsprocess som betongprovet utsätts för. Om ett prov får hydratisera under en längre tid kommer mer produkter bildas från bindemedelsreaktionen och vilket innebär att mikrostrukturen blir tätare. Två faktorer som påverkar detta är karbonatisering och torkning. Karbonatisering innebär att betongytan binder CO_2 (koldioxid), vilket förändrar ytans mikrostruktur. Endast uttorkning påverkar inte mikrostrukturen, däremot kan torkning bidra till att mikrosprickor bildas och den initiala vattenhalten i betongen minskar.

Tillsammans har tidigare studier resulterat i teorier som försöker förklara skademekanismen som skapar tösaltfrostavskalningsskadan. Dock finns en brist på studier som har testat vilken påverkan de ovan nämnda faktorerna (torkning och karbonatisering, lufthalten, och saltlösningskoncentrationen) har på tösaltfrostavskalningen i betong som innehåller flygaska eller slagg, varför detta projekt genomförts. Betong som innehåller flygaska eller slagg har mikrostrukturer som skiljer sig från betong som endast innehåller cement. Eftersom härdning och karbonatisering förändrar mikrostrukturen av materialet så behövdes en bred studie som studerar hur respektive faktor (torkning och karbonatisering, lufthalten, och saltlösningskoncentrationen) påverkar tösaltfrostavskalningen i betong med flygaska eller slagg. Då mikrostrukturen ändras över tiden, beroende på härdningen och karbonatiseringen, kan vissa förkonditioneringsprocesser vara fördelaktiga för vissa material och ofördelaktiga för andra.

På grund av bristen av studier av hur tösaltfrostavskalningen i betong med flygaska eller slag påverkas av torkning och karbonatisering, lufthalten, och saltkoncentrationen så har detta projekt genomförts. För att bestämma vilken inverkan lufthalten har på avskalningen krävdes det att flera satser gjöts där endast lufthalten varieras. En metod har utvecklats för att hitta en kombination av tillsatsmedel (ett flyttillsatsmedel och en luftporbildare) för respektive bindemedel. Linjär traversanalys har utförts för att kvantifiera de olika luftporssystemen skapade av luftporbildaren. Vidare har fler mätningar utförts för att karaktärisera materialen. Lågtemperaturkalorimetrimätningar har utförts för att få information om isbildningen och mikrostrukturen av porer med radier under 50 nm. Eftersom en grov porositet ger en hög absorptionshastighet och en fin porositet ger en låg absorptionshastighet, har kapillärsugningsförsök utförts, vilket ger information om kapillärporositeten (porer med radier över 50 nm). Dessutom utfördes mätningar på den totala porositeten. Mätningar av pH-värde har utförts för att bestämma om de karbonatiserade proverna som användes för lågtemperaturkalorimetrin och kapillärsugningen var genomkarbonatiserade. För att undersöka karbonatiseringens inverkan på avskalningen mättes karbonatiseringsdjupet med tunnslipsanalys på de karbonatiserade proverna som saltfrosttestades. En tösaltfrosttestmetod med låg spridning i avskalningsresultaten har även utvecklats och använts för att kvantifiera tösaltfrostavskalningen.

Försök har utförts där olika egenskaper hos porositeten har kopplats till tösaltfrostavskalningen för betong som härdat över 300 d. Bindemedels-kombinationerna som testades vid dessa försök var CEM I blandat med 20, 35% flygaska med låg kalciumhalt, eller 20, 35, 70% slagg, eller 25% slagg med 10% kalkfiller. Vid dessa försök var fokus på att se inverkan hos en ökande mängd tillsatsmaterial, effekten från karbonatisering, samt effekten från en ökande lufthalt hos respektive bindemedelskombination. Vidare utfördes även en bredare tösaltfroststudie där yngre betong testades med 100% CEM I, 35% flygaska, eller 35% slagg, där proverna härdats i 8 till 63 d. Dessa tester utfördes på grund av flera anledningar. Dels för att få mer kunskap om hur olika förkonditioneringar, lufthalter och saltkoncentrationer påverkar avskalningen hos betong innehållande flygaska eller slag som hydratiserat en kort tid. Resultaten överbrygger resultaten för hur uttorkning och karbonatisering påverkar tösaltfrostbeständigheten ung betong jämfört med välhärdad betong (resultaten från betong som härdat över 300 d). Även för att överbrygga resultaten för hur olika lufthalter påverkar tösaltfrostavskalningen i ung betong jämfört med välhärdad betong (resultaten från betong som härdat över 300 d). På grund av bredden av tösaltfrostavskalningstesterna i ung betongen hittades flera intressanta och oväntade resultat.

Vid försöken där egenskaper hos porositeten påverkar tösaltfrostavskalningen visade resultaten att karbonatisering bidrar till en minskad tösaltfrostavskalningen för välhydratiserad betong med 100% CEM I, samt 20, och 35% slagg, en

oförändrad tösaltfrostavskalning för välhydratiserad betong med 20% flygaska eller 25+10% slagg+kalkfiller, och en ökad tösaltfrostavskalning för välhydratiserad betong med 35% flygaska eller 70% slagg. Resultaten visar även på en korrelation mellan karbonatiseringsdjupet och avskalningsmängden genom att approximera 1 kg/m² tösaltfrostavskalning till 1 mm avskalningsdjup. Därigenom kunde följande slutsatser dras från resultaten. En fin porositet under 50 nm (vilket innebär att mindre vatten fryser vid en specifik temperatur), tillsammans med en låg permeabilitet enligt kapillärsugningsförsöken (vilket innebär en fin porositet för strukturen över 50 nm), bidrar generellt sett till en låg tösaltfrostavskalning. (Det enda undantaget var okarbonatiserad betong med 25% slagg och 10% kalkfiller). En grov porositet under 50 nm (vilket innebär att mer vatten kan frysa vid en specifik temperatur), tillsammans med en hög permeabilitet enligt kapillärsugningsförsöken (vilket innebär en grov porositet för strukturen över 50 nm), bidrar generellt sett till en hög tösaltfrostavskalning. Resultaten för saltfrostförsöken på den betong som hydratiserat 8 till 63 d visar tydligt att förkonditioneringsprocesserna påverkar materialens tösaltfrostavskalningen. De olika materialen påverkas även olika mycket av samma förkonditioneringsprocess. Resultaten visar även att lufthalten har olika inverkan på tösaltfrostavskalningen beroende på om ytan har torkat och karbonatiserat eller inte. NaCl koncentrationerna visade även några oväntade resultat där en hög NaCl koncentration resulterade i en hög saltfrostavskalning i två fall. Dessa två unika fall för 35% flygaska tros bero på att den kritiska vattenmättnadsgraden överskrids. I övrigt verkar den s.k. ”glue spall teorin” stämma med resultaten då en hög tösaltkoncentration resulterar i en låg avskalning.

Detta doktorandprojekt har visat att de tre studerade faktorerna (torkning och karbonatisering, lufthalt, och NaCl koncentration) påverkar avskalning på olika sätt beroende på materialet. Därmed påvisas komplexiteten i att testa saltfrostavskalning i laboratorier. Några forskare har kritiserat standardmetoderna för att vara alltför konservativa och underkänna betong med flygaska eller slagg som klarar sig i fält. Då det finns ett kritiskt behov av att sänka CO_2 utsläppen på grund av den globala uppvärmningen, finns det en anledning att finjustera standardmetodernas förkonditioneringsprocess för att vara mindre konservativ så att färre betongrecept med flygaska eller slagg som bidrar till en minskning i netto CO_2 emissionerna underkänns av standardmetoden som tycks klara sig i fält. Denna doktorsavhandling bidrar med viktig information om en sådan finjustering av förkonditioneringsprocessen till den europeiska standardmetoden för tösaltfrostavskalningen skulle genomföras.

List of appended publications

This thesis is based on the following publications appended at the end of the thesis.

Paper I Strand, M.J., Fridh, K., *Methodology to Analyse the Salt-Frost scaling Mechanism(s) in Concrete with Different binders*, Materials, Systems and Structures in Civil Engineering 2016, Segment on Frost action in Concrete, Proceeding pro114, Lyngby, Denmark. https://www.rilem.net/publication/publication/473

My contributions were the performance of all laboratory measurements presented in the paper and all complementary laboratory work (such as the preconditioning of samples and planning of all measurements), evaluation of results, and writing the paper. KF provided some inputs during the work and commented on the paper.

Paper II Strand, M.J., Fridh, K., *Test Method for De-Icing Salt-Frost Scaling in High-Performance Concrete*, MethodsX, 2018.

My contributions were the development of the salt-frost scaling method including the performance of all tests during the development to minimise the risk of errors. Moreover, I participated in teaching, assisting, and co-supervising a master student, Henrik Sjöbeck, who performed a third of the de-icing salt-frost scaling measurements presented in the paper. I performed all measurements not made by HS and wrote the paper. KF provided some input during the work and commented on the paper. Doctor Maria Fredriksson commented on the paper; Dr Sture Lindmark and Dr Peter Utgenannt provided some inputs during the development of the method and sample setup.

Paper III Strand, M.J., Fridh, K., *The Air Void Contents Effect on the Salt Frost Scaling of Uncarbonated Concrete containing Siliceous Fly Ash or Slag*, Nordic Concrete Research, Proceeding of the XXIII Nordic concrete research symposium, Segment on air entraining agents and frost action, Aalborg, Denmark, 2017

My contributions were the performance of all laboratory measurements presented in the paper and all complementary laboratory work (such as the preconditioning of samples and planning of all measurements), evaluation of results, and writing the paper. KF provided some input during the work and commented on the paper.

Paper IV Strand, M.J., Fridh, K., *De-Icing Salt-frost Scaling part 1: Concrete Containing Low-Calcium Fly Ash—Comparison between carbonated and noncarbonated samples, and the effect of various air contents*, Manuscript.

My contributions were the performance of all laboratory measurements presented in the paper and all complementary laboratory work (such as the preconditioning of samples and planning of all measurements), evaluation of results, and writing the paper. KF provided some input during the work and commented on the paper. Professor Lars Wadsö commented on the paper.

Paper V Strand, M.J., Fridh, K., *De-Icing Salt-frost Scaling part 2: Concrete Containing Ground Granulated Blast-Furnace Slag—Comparison between carbonated and noncarbonated samples, and the effect of various air contents*, Manuscript.

My contributions were the performance of all laboratory measurements presented in the paper and all complementary laboratory work (such as the preconditioning of samples and planning of all measurements), evaluation of results, and writing the paper. KF provided some input during the work and commented on the paper. Professor Lars Wadsö commented on the paper.

Paper VI Strand, M.J., *De-Icing Salt-Frost Scaling in Concrete Containing Fly-Ash or Slag—Influence of Drying and Carbonation, Air Content, and Salt Solution Concentration*, Manuscript.

My contributions were the performance of all laboratory measurements presented in the paper and all complementary laboratory work (such as the preconditioning of samples and planning of all measurements), evaluation of results, and writing the paper. Doctor Katja Fridh and Professor Lars Wadsö commented on the paper.

1 Introduction

1.1 Background

Concrete is a widely used building material because of its formability, high compressive strength, and durability. However, 5–8% of all man-made CO_2 emissions are contributed by cement production [1]. Considering the potential risks posed by man-made emissions to climate change, it is crucial to reduce such emissions in order to minimise their negative impact on the climate in the future. The CO_2 emissions from cement production can be reduced by replacing a fraction of the cement with some other supplementary cementitious material (SCM). Two examples of SCMs are low-calcium fly ash (LCFA) and ground-granulated blast-furnace slag, which are waste products from coal power plants and steel industries, respectively. However, when these SCMs are mixed with concrete, they change the latter's microstructure including some of its properties. It is important that this change does not jeopardise the durability of concrete.

This project has studied concrete or micro-concrete with a water–binder ratio of 0.40 that could be used in structures, such as bridge decks that are exposed to harsh environments and several concurrent deterioration mechanisms. One important deterioration mechanism is the de-icing salt-frost scaling (DISFS). This phenomenon occurs when a solution of water with a low concentration of de-icing salt freezes in contact with a concrete surface. In studying the DISFS, the concrete test surface is in contact with a solution with a specific salt concentration. Thereafter, this setup is exposed to freeze–thaw cycles. After a certain number of cycles, the scaling is brushed off, dried, and weighed. The mass of this material is used as a measure of the DISFS degradation of concrete.

When fly ash or slag is included as a binder in a concrete recipe, the properties of concrete, including its durability, are modified [2-16]. In the past, several researchers have studied the DISFS mechanisms; the effect of various factors on the DISFS [2-33] has also been investigated. These studies clearly demonstrate that such an undertaking is not a simple task because several factors significantly influence the results. Three of the most important and complex factors that have a considerable impact on the DISFS are the preconditioning of the test surface [4-6, 11, 14, 16, 20, 26, 31, 32, 34], the air content and porosity of the concrete [5, 8, 10, 26, 35-42], and the concentration of the de-icing agent [17, 18, 26, 43-49]. If

concrete properties vary, then the above factors will affect the DISFS to various extents. For example, the rates of hydration and dehydration, and the carbonation of concrete containing LCFA or slag differ when compared with concrete that has 100% CEM I. The aim of this project is to contribute to the knowledge pertaining to the effect of drying, carbonation, air content, and salt concentration on the DISFS in concrete containing various fractions of the LCFA or slag.

1.2 Research questions

In each paper, some specific questions are discussed and answered. This thesis aims to answer the general questions stated below. In order to accomplish that, information pertaining to the salt-frost scaling behaviour in concrete containing LCFA or slag in relation to concrete with 100% CEM I is discussed.

1. How do various fractions of added LCFA or slag affect the salt-frost scaling on the surface of a never-dried and never-carbonated, or dried and carbonated sawed concrete?
2. How does drying and carbonation affect the salt-frost scaling on the surface of sawed concrete containing various fractions of added LCFA or slag?
3. How do various air contents affect the salt-frost scaling on the surface of a never-dried and never-carbonated, or dried and carbonated sawed concrete containing various fractions of added LCFA or slag?

1.3 Thesis structure

Figure 1 presents the thesis structure and provides information pertaining to different parts that comprise the project in order to answer the research questions in the best way possible. Because this project has been centred on experiments and methods, the focus on these areas is reflected in the literature study, which has been continuously conducted during the project. The majority of papers perused are experimental studies on the de-icing salt-frost scaling and various factors that affect it. Some of the aforementioned have a large influence on the design of the DISFS method as well as its testing and validation. Moreover, these articles motivated the use of the test matrix of complementary studies presented in paper 6.

The literature study is followed by the de-icing salt-frost scaling study. First, the materials that have been used in this project are presented. This project is aimed at explaining (among other things) the effect of different air-void contents on the DISFS in concrete containing various fractions of the LCFA or slag. Accordingly,

a methodology that enables the creation of concrete casts containing the LCFA and slag with various air contents is developed. This technique and the other methods used in the study are described in this paper. These methods are pH measurement, low-temperature calorimetry (LTC) measurement, capillary suction measurement, DISFS measurement, thin-section analysis (samples were prepared by Research Institutes of Sweden (RISE)), and linear traverse analysis (performed by Pelcon AB). Moreover, to characterise the binders, the following measurements are performed by Cementa: X-ray fluorescence (XRF), Blaine, inductively coupled plasma (ICP), laser diffraction, compressive strength, and loss on ignition (LOI).

After describing the methods, results from the appended papers (4, 5, and 6) are summarised. In papers 4 and 5, results from the LTC and capillary suction measurements demonstrate how carbonation affects the porosities of different binder combinations. Paper 4 presents results from recipes containing 20 and 35 mass% LCFA, and paper 5 presents results from recipes containing 20, 35, and 70 mass% slag, and 25+10 mass% slag+lime stone filler. These results provide information on the porosities of noncarbonated and carbonated binders. Consequently, this enables the discussion of the effect of porosities in each binder on the DISFS, which has been hydrated over an extended period. Furthermore, the foregoing results show the effect of various air contents in each binder on the DISFS. Thereafter, paper 6—a comprehensive study of the DISFS tests for concrete (which has not been hydrated for as long a time as the concrete discussed in papers 4 and 5) is summarised. The DISFS results show the effect of drying and carbonation, air content, and various NaCl concentrations on the DISFS in concrete with 35% LCFA or slag. All the DISFS tests are implemented according to the method presented in paper 2. The results clearly show that the three tested factors (drying and carbonation, air content, and NaCl concentration) affect the DISFS in various ways depending on the binder. Consequently, this provides some clarifications on the complexity of testing the de-icing salt-frost scaling.

Subsequent to the summaries, some interesting comparisons are made between the DISFS results presented in papers 4, 5, and 6; in particular, those results that do not receive any attention in other papers. These comparisons show that drying and carbonation affect the DISFS in various ways depending on the type of binder and the time of favourable hydration that the sample has been exposed to prior to the DISFS test.

After the complementary comparisons, the conclusions that have been reached in each paper are presented along with the general conclusions that have been drawn according to the results presented in the thesis. The conclusions are then followed by suggestions for future research projects.

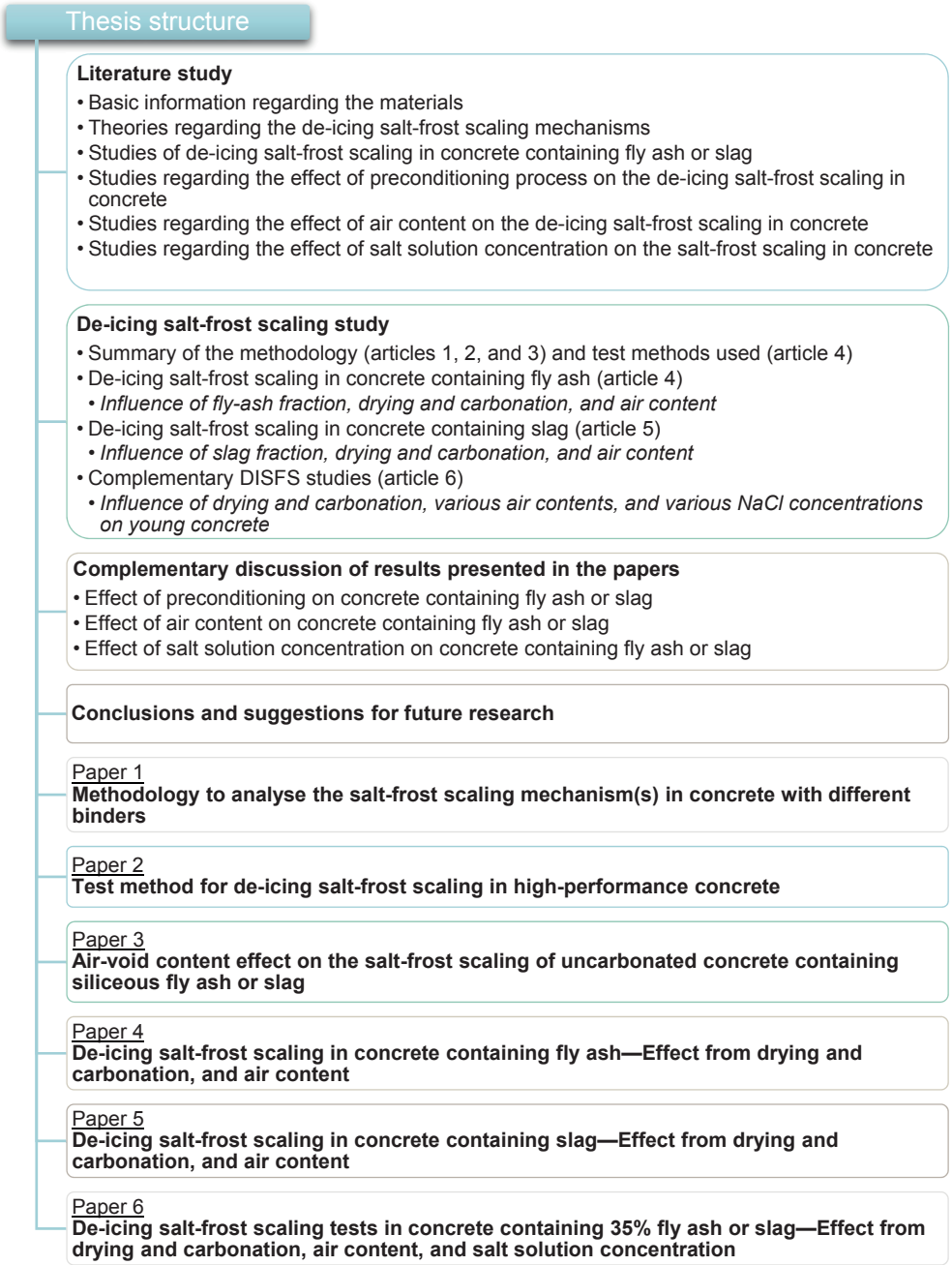

Figure 1
Structure of the thesis.

2 Literature study

The literature study summarises information pertaining to materials used in this project, the salt-frost scaling mechanism, and previous studies regarding salt-frost scaling in concrete containing fly ash or slag.

2.1 Concrete materials

This PhD project has studied concretes where the base recipe contains low-alkali CEM I (appendix B). Recipes with various fractions of either low-calcium fly ash (LCFA) or ground-granulated blast-furnace slag have been made to determine how these additions modify concrete properties and salt-frost scaling resistance. This section provides basic information regarding concrete durability, and fly ash, slag, and admixtures that have been used.

2.1.1 Concrete durability

Fly ash and slag change the material properties and durability of concrete [50-55]. Different types of deterioration mechanisms are related to conditions that concrete is exposed to. The European standard [56] defines various exposure classes and sets some minimum requirements on the concrete subjected to various exposure classes. If these minimum requirements are satisfied, concrete durability should be sufficiently high for a certain service life. Furthermore, these minimum requirements also specify the limits of SCM fractions that can be added. As an example, for concrete exposed to sulphates (e.g., in sewer pipes), it is advantageous to have a significant fraction of slag because it increases resistance against sulphate attack. However, in the case of concrete exposed to freezing and thawing in combination with de-icing salts, the standards have relatively low limits for fractions of the SCM replacements. These limits have been set because studies have indicated that an increased fraction of the SCMs results in an increased mass of the DISFS (i.e., lower DISFS resistance).

Besides those pertaining to the durability of hardened concrete, there are also other properties that change when SCMs are added. One example is that the total heat

produced from reactions during the first day is reduced. This is because the dissolutions of LCFA and slag are slow. The reactions of LCFA and slag consume calcium hydroxide; this means that the LCFA and slag are dependent on the cement reaction. When these reactions begin, they mostly yield calcium silica hydrates. Because the LCFA and slag reactions start at a later time than the cement reaction does, a lower temperature inside the young concrete results—a condition particularly beneficial to thick cast structures, or when casting in environments with high temperatures. High temperatures inside the concrete during the hydration period can cause problems, such as shrinkage during cooling; this leads to large tensile stresses, which can cause cracks in the concrete. However, a low heat of hydration can also be a disadvantage when casting in a cold climate because the reaction rate will then become even slower. It will result in a lower hydration rate and a slower increase in the early compressive strength; consequently, the necessary time before the formwork can be removed is increased. These simple examples demonstrate that it is important to consider the several changes in concrete properties when adding SCMs in order to utilise them advantageously.

2.1.2 Low-calcium fly ash

Fly ash consists of spheres of practically completely burnt ash (SiO_2). It is a waste product from coal power plants collected by filters installed in the chimneys to prevent the fly ash from polluting the environment. Thereafter, this waste product can be used as a supplementary cementitious material mixed with cement. Furthermore, it contributes to a few modifications in concrete properties through pozzolanic reaction.

Low-calcium fly ash, which consists mostly of silicon dioxide (SiO_2) and aluminium oxide (Al_2O_3), is used in this project. The sizes of these fly-ash spheres range from 5 to 150 μm (appendix B).

2.1.3 Ground-granulated blast-furnace slag

Slag is created inside a blast furnace during the production of iron. It is a waste product that mainly consists of calcium oxide (CaO), silicon dioxide (SiO_2), and aluminium oxide (Al_2O_3). After cooling, it is ground into powder with a similar (or slightly smaller) particle size as cement. The particle sizes of the slag used in this project range from 3 to 56 μm (appendix B).

2.1.4 Limestone filler

The filler is limestone ($CaCO_3$), which has been ground down to a particle size distribution similar to that of cement. The limestone filler contributes by increasing the fraction of calcium in the paste mix. The increased calcium contributes to a faster early hydration because of the seeding effect, which increases the rate of nucleation. In this PhD project, low-alkali CEM I contains 2.36% limestone filler.

2.1.5 Superplasticiser

Superplasticisers are used to increase the workability of concrete, i.e., make it flow without increasing the water–binder ratio [57]. These can generally be classified into four categories: sulphonated melamine formaldehyde condensates, sulphonated naphthalene formaldehyde condensates, modified lignosulphonates, and synthetic polymers (e.g., hydroxylated carboxylic acids and polyether–polycarboxylates) [58]. They adsorb to cement grains, disperse them, and prevent early agglomeration; thereby, the workability of fresh concrete is increased. The dispersion is also positive for cement hydration because more cement grains have direct contact with water; consequently, the paste can reach a higher degree of hydration (hydrated cement mass in relation to the initial total mass of cement) in a shorter time. This is a positive effect because concrete strength increases with an increased degree of hydration.

2.1.6 Air-entraining agent

Air-entraining agents are surfactants that end up at the interface between air and water inside the cement paste [40, 57]. The surfactants have one end that is hydrophilic (negatively charged) and another end (usually resembling a tail), which is non-polar (or hydrophobic) [57]. One aspect that can be designed for a synthetic surfactant is the length of this non-polar tail, which can have an impact on some properties of the air-entraining agent [57]. Some examples of air-entraining agents are neutralised wood resin and synthetic detergents from salts of organic acids and sulphonated hydrocarbons [57]. These should not bind chemically with cement or any other SCMs and should only contribute by encapsulating air inside the cement paste [57].

2.1.7 Aggregates

Usually, aggregates compose approximately 75 mass% of a normal concrete mix; this implies that aggregates have a significant impact on concrete properties. Among the factors to consider in the choice of aggregates is their size distribution. This is

important for workability, which has an effect on concrete compaction; hence influencing its strength. Furthermore, the aggregate size distribution determines the required minimum cement content because it is dependent on the total surface area of aggregates. Generally, a smaller total surface area should require a lower minimum cement content; by reducing the cement content, the total CO_2 emissions are also reduced.

One additional factor that can be considered in relation to concrete strength is that aggregates contain various minerals, which have different Young's modulus and maximum compressive strengths; this will affect the strength of concrete. Nevertheless, considering that the concrete compressive strength is a combination of the strengths of hardened cement paste and aggregates, the effect of the aggregate is dependent on the strength of the hardened cement paste. If the water binder ratio is low, e.g., 0.40, and the concrete is well-hydrated, the hardened cement paste can have approximately the same compressive strength as the aggregates. Under this condition, any concrete fracture will go through both the cement paste and aggregates, i.e., the aggregate strength impacts the total concrete strength. However, if the water–binder ratio is high, e.g., 0.60, then the fractures will most probably go through the cement paste and around the aggregates. This means that aggregates with a high Young's modulus and high compressive strength will not contribute to a significant increase in the total compressive strength of a concrete recipe with a high water–binder ratio.

When considering durability, there are also some factors to consider before choosing aggregates. Amorphous quartz aggregates, such as flint, can yield alkali–silica reactions; the product from the reaction has an increased volume and therefore creates a pressure that can crack the concrete and thereby destroy it. This can be avoided by using cement with low-alkali content and/or aggregates with low-amorphous silica content.

For concrete structures that would be exposed to freezing temperatures, i.e., the risk of frost damage exists, frost-resistant aggregates should be used in the concrete mix. Generally, frost-resistant aggregates have high strengths and low water absorption. To determine whether aggregates are frost-resistant or not, some standard tests can be implemented [59-62]. Petrographic examination can show whether there are some generally weak minerals or particles (with low compressive and tensile strengths) that are present. Water absorption tests can also indicate whether aggregates are frost-resistant or not. If an aggregate has a large volume of small voids that can be filled easily with water, then the risk of frost damage is high. Aggregates that are frost-resistant generally have either a low volume of large voids that are not easily filled with water, or a low volume of small air voids where the amount of water that can freeze is small. The absorption rate and the rate at which water can be transported through the pore structure are also important factors.

Another test is to allow the aggregates to absorb water and thereafter have these exposed to freeze–thaw cycles. After exposure, the frost resistance is based on whether any cracks have formed, there is a loss in mass, or concrete strength has been reduced. In some particular cases, such as when concrete is extremely exposed to salt and de-icing agents, the aforementioned test can be conducted using a salt solution or urea instead of pure water.

In Sweden, the bedrock largely consists of granite, which is an igneous rock that contains the mineral quartz feldspar and mica (biotite); granite is usually frost-resistant.

The interfacial transitional zone (ITZ) is a layer of paste around aggregates that is known to be more porous than the bulk cement paste [63]. The reason for such porosity is 'the wall effect', which draws smaller cement grains towards the aggregate surface [63]. Thus, the formation of this zone depends on the cement grain sizes [63]. When normal cement is used with cement grains from less than 1 to 100 μm, the most significant change in properties is found at an area that is 15–20 μm from the aggregate surface [63]. Scrivener et al. [63] makes it clear that this is a gradual transition and not a distinct zone. Moreover, the wall effect increases the effective water–cement ratio, which contributes to a more porous layer [63]. One of the conclusions in the paper is that, if smaller particles, such as silica fume, are added to the mix, then the ITZ can be modified [63].

Silica fume is not used in this project. However, it can be noted that the slag used in this study has a larger fraction of small particles than the LCFA, which means that the ITZ in the tested concretes containing LCFA and slag will most probably differ. Considering that the ITZ is more porous, the probability of ice nucleation starting in this zone is high. Concurrently, the tensile strength should naturally be lower in the ITZ; that would also make the probability higher for a crack to start and propagate from this zone. Hence, the ITZ may have a significant impact on the mass of the DISFS created.

The effect of three different types of aggregates on the ITZ and how the DISFS mass changes depending on different aggregates are reported in [64]. The three are carbonated steel slag, normal, and crushed steel slag aggregates. It is concluded that the ITZ properties change when one of these three types of aggregates is employed. Furthermore, results regarding the ITZ properties have a strong correlation with results from the DISFS tests. In changing the aggregates from normal to carbonated steel, the permeability seems to decrease, the hardness increases, and the frost and DISFS resistances increase. The reason for these changes is presumed to be because the high water absorption of carbonated steel aggregates contributes to a lower water–binder ratio in the ITZ around the aggregates. This means that the layer becomes denser.

Reference [65] presents variations in the ITZ formed when different fractions of the limestone filler (LF) and slag are added. Both the LF and slag have slightly smaller particle size distributions in comparison with the cement used in the study. Results show that the incorporation of LF and slag reduces the porosity in the ITZ, the chloride migration coefficient, and the high absorption capacity of the concrete.

2.2 De-icing salt-frost scaling

This section provides information on de-icing agents that can come into contact with concrete and cause the DISFS; the information is necessary in the study of salt-frost scaling mechanisms. Moreover, it includes a summary of a few previous studies regarding the pessimum concentration. Thereafter, theories regarding the DISFS mechanism are briefly described.

For the DISFS to occur, a de-icing agent that reduces the thawing temperature of ice is required [17, 18]. Because no superficial scaling occurs when only pure water is present, this is presumed to be a separate mechanism from the internal frost damage that is caused by a high hydraulic pressure. Accordingly, information regarding changes that occur when a de-icing agent is added to water is required. Two changes transpire when a de-icing agent is added: the amount of ice formed at a given temperature becomes lower, and the liquid uptake is slightly increased.

2.2.1 Theories regarding de-icing salt-frost scaling

The following section presents three theories regarding the de-icing salt-frost scaling mechanism: hydraulic pressure, micro-ice lens formation, and glue-spall mechanisms.

2.2.1.1 Hydraulic pressure theory

The theory of hydraulic pressure contributing to the DISFS is presented by Powers in [66] and subsequently further developed and tested [5, 26, 42, 67-72]. The underlying mechanism is that, when water freezes, its volume increases and generates a hydraulic pressure from the pore solution being squeezed through the microstructure [42]. This mechanism is dependent on the permeability, degree of saturation, and freezing rate [42]. The maximum hydraulic pressure, P_{max} (Pa), can be calculated for a non-saturated paste, according to Eqs. 1–4 presented in [42].

$$P_{max} = \frac{\eta}{3}\left(1.09 - \frac{1}{s}\right)\frac{uR}{K}\Phi(L) \quad \text{Eq. 1}$$

P_{max} = maximum hydraulic pressure, Pa

η = coefficient of viscosity of water, Pa

s = degree of saturation (amount of capillary water/capillary porosity)

$$u = \frac{dw_f}{d\theta} \quad \text{Eq. 2}$$

dw_f = ice mass formed per volume of paste, kg/m³

$d\theta$ = temperature change, °C

$$R = \frac{d\theta}{dt} \quad \text{Eq. 3}$$

R = rate of cooling, °C/s

dt = time change, s

K = coefficient of permeability of paste, m

$$\Phi(L) = \frac{L^3}{r_b} + \frac{3L^2}{2} \quad \text{Eq. 4}$$

L = distance from the bubble boundary to that of the sphere of influence (paste that surrounds an air void; the moisture inside the sphere of influence of a certain air void can be expelled to the air void), m

r_b = radius of air void, m

The pressure is relieved if there is an empty air void into which the solution can drain. As the distance to the closest air void where the pore solution can drain increases, the hydraulic pressure also increases. Therefore, the increased amounts of air voids (of the same sizes) decrease these distances and hydraulic pressures. If the amount of large air voids distributed in the paste matrix is sufficient, the hydraulic pressure will never contribute to a pressure that is sufficiently large to fracture the concrete.

2.2.1.2 Micro-ice lens formation

Lindmark studied the DIFSF and presented results that support the theory of micro-ice lens formation [26]. One of the tests presented shows that samples that have been stored in low concentrations of NaCl solutions (close to pessimum concentrations)

and thereafter submerged in precooled salt solutions, gained more weight than samples that have been stored in higher concentrations of salt solutions [26]. The mass increase is higher when the temperature of the precooled solution is lower. Cryogenic suction (absorption at low temperatures) has also been analysed in a study by Liu and Hansen [73]. The results clearly show the increase in absorption because of the cryogenic suction of salt solution and water [73]. However, cryogenic suction is approximately the same for water and a 3% NaCl solution [73]. This indicates that the cryogenic suction effect is not related to the salt-frost scaling. The amount of scaling in concrete exposed to pure water is insignificant compared with that in concrete exposed to a low-concentration salt solution [73].

The ice-lens growth mechanism is presented by Powers in [69] and subsequently further developed and tested by Powers and Helmuth, Lindmark, and Liu [26, 68, 70]. The driving force that contributes to the ice-body growth is the imbalance between the free energy in water and ice [69]. This energy imbalance attracts water to ice and consequently contributes to the growth of ice crystals. An increased free energy results in a lower freezing point, i.e., the freezing point suppression is increased [69]. An increase in ion concentration increases the free energy of the pore solution [69]. Furthermore, the free energy increases when the sizes of voids decrease because the smaller curvature of the surrounding matrix increases the suction pressure. When ice nucleation starts, only water freezes; this creates differences among the ion concentrations and among the free energy values of unfrozen water surrounding the ice body [69]. This driving force, which results from differences among the free energies, is called osmotic pressure; it results in the transport of water from the small voids to the larger voids where ice nucleation started [69]. Moreover, on the concrete surface (outside the concrete matrix), there will be an unfrozen solution, which will contribute to the transport of water to the ice bodies in the concrete matrix [69].

2.2.1.3 Glue spall

The glue-spall mechanism theory presented by Valenza and Scherer [39] is based on the difference between the thermal expansion coefficients of concrete and ice. The salt solution freezes and strongly adheres to the concrete. When the temperature decreases, the ice shrinks and cracks because of the unfrozen brine pockets inside the ice layer; this results in high superficial stresses on the concrete surface. This theory was tested by warping measurements conducted by Valenza II and Scherer [74]. The warping test setup is basically a beam of cement paste on which a solution is frozen. The ice shrinks more than the cement paste does and causes the beam to bend; the beam deflection is measured, and the stresses are calculated. Results from these tests are presented in [74].

According to the theory, any decrease in the tensile strength of the concrete surface results in the increased mass of scaling. One example that leads to a decrease in the

tensile strength is the increased surface water–binder ratio when bleeding occurs on the concrete surface. Similarly, an increased porosity should result in a decrease in the tensile strength. However, a well-connected air-void system with large entrained voids (approximately 300 μm in diameter) should result in a smaller difference between the thermal coefficients of the ice layer and concrete. This could explain why entrained air decreases the mass of scaling.

2.2.2 Drying and carbonation

The research has shown that the preconditioning of the test surface has a significant influence on the DISFS. When a standard test method is used, it is important to be aware that different materials are affected by the preconditioning stages in various ways. For example, some reach a higher degree of hydration, whereas others dry faster and start with a lower water content. Moreover, the carbonation of different materials results in different chemical products; this in turn affects the DISFS.

In the current study, the preconditioning of samples before the DISFS tests are implemented has been divided into three stages. The first stage, named ‘internal curing’ (IC), is defined as the time from casting until the test surface dries. When testing sawed surfaces, it is the time from casting until sawing. When testing cast surfaces, curing compounds can be applied to prevent drying. In such cases, the time during which the curing compound remains on the sample surface is also considered as the IC. The second stage, named ‘drying and carbonation’ (DC), is defined as the time during which the samples are exposed to air at a specific temperature, relative humidity, and CO_2 concentration. The third stage, named ‘resaturation’ (RS), is defined as the time during which the samples are submerged in water, after the DC period and before the DISFS test begins.

Some studies present results, which indicate that curing compounds decrease the mass of DISFS [6, 11, 14, 20, 33]; all studies disregard the curing compound even before testing starts. A study of Ahani and Nokken [32] presents results that show an increase in the DISFS in concrete with fly ash in which the curing compound is not ignored.

The effect of drying and carbonation on salt-frost scaling has been previously studied to some extent [5, 24]. A study by Jacobsen on salt-frost scaling [24] focused on the effect of evaporation; how the water content at the start of the salt-frost scaling test affected salt-frost scaling was also examined to a certain degree. Utgenannt [5] focused on the effect of carbonation on concrete containing slag and silica. Results showed that the carbonation changed the concrete’s microstructure, which significantly affected the salt-frost scaling resistance. Concrete containing only CEM I experienced a reduction in scaling after carbonation. When the slag content was increased, the carbonation resulted in an increased mass of scaling.

Results indicated that concrete containing 60 mass% slag was affected to the largest extent. The carbonation seemed to increase both the capillary porosity and scaling mass. This resulted in a large scaling mass during the first freeze–thaw cycles; thereafter, the scaling mass decreased when the carbonated surface layer was scaled off.

Bleeding (water separation from the paste) seems to increase when fly ash is used. This means that the effective water–binder ratio on the concrete surface increases; this increases the autogenous shrinkage and leads to an increase in the DISFS mass [31]. An increasing loss on ignition (fraction of unburnt carbon in fly ash) increases the DISFS when the water–binder ratio is 0.45 [15].

However, an agreement between the results from the standard DISFS methods and field tests is insufficient to some extent [16, 20, 33]. The DISFS mass increases as the degree of hydration decreases in concrete with CEM I [5, 18] and CEM I blended with fly ash [16, 20, 27] with a water–binder ratio of 0.45; the DISFS mass increases when the binder content decreases [10, 19].

2.2.2.1 Comparison between DISFS methods

This section presents a comparison among some of the standardised DISFS methods. The comparison shows the differences among the preconditioning processes of test surfaces and some pieces of information relating to the differences among the freeze–thaw cycles. Because the preconditioning process affects the DISFS, results vary among the different methods. This is presented to emphasise the point that the results presented in this thesis (produced with a specific DISFS method) are not directly comparable to results from the other DISFS methods. Moreover, the comparison is made because some studies have criticised the lack of agreement between the standard DISFS methods and field tests [2, 4, 16, 20, 21, 28, 30, 33].

Table 1
Comparison among preconditioning processes of four standard DISFS methods [75-77] based on [9].

DISFS method	Internal curing (IC) or 100% RH	Drying and carbonation[1] (DC)	Resaturation (RS)	Min temperature		De-icer
				°C	h	
Slab[2] [76]	21	7	3	−18–(−22)	0–4	3% NaCl
CDF[2] [76]	7	21	7 (3% NaCl)	−20	3	3% NaCl
ASTM 672[3] [75]	14	14	0	−18		4% $CaCl_2$
BNQ[3] [77]	14	14	7	−18	7–12	3% NaCl

[1] Test surface is exposed to air at 20 °C and 50–70% RH (which is favourable for carbonation); the atmospheric CO_2 concentration is 0.04%.
[2] Used in Europe; sawed test surface.
[3] Used in USA and Canada; finished test surface.

2.2.3 Air content

The positive effect of an increased air content by using air-entraining agents has been known and studied since the mid-20th century [42, 69]. According to the glue-spall theory, when the air-void system is good, there is a reduction in the DISFS because the system contributes compressive stresses when the ice body causes water suction from adjacent capillary pores. This suction, in combination with ice in the matrix, contributes to the increase in thermal expansion; consequently, this results in a smaller difference in shrinkage between the concrete surface and ice [78]. According to the theory of ice-lens growth, the reduction in the DISFS mass resulting from the presence of the air-void system is because of the shortened water transport distance—from a point in the capillary pore to an air void [68].

It is necessary to quantify the air-void system to make it possible to decide whether the system has the appropriate features (that is, the number of voids are sufficient and the voids are small resulting in short distances among them but sufficiently large so as not to be easily filled with water). The measurements from which these factors are calculated are made on two-dimensional sections of a concrete sample. To identify the air voids, the concrete is painted black and air voids are filled with zinc paste; thereby, a contrast is created between the concrete and air voids. When this is accomplished, a linear traverse measurement can be performed.

2.2.3.1 Linear traverse

Linear traverse measurement is accomplished by focusing a small light beam, ca 2 μm in diameter, on the painted concrete surface (black concrete surface and air voids filled with white zinc), and thereafter measuring the reflection of light. When the light is focused on the black area, the reflection is low (i.e., solid concrete), whereas on the white area, the reflection is high (i.e., air void filled with zinc paste); this enables the measurement of the length of each white area crossed. These so-called cords are the length of each line over an air void that the light has traversed. However, note that the light practically never goes through the middle of each air void; this introduces some problems. Therefore, in order to make the results statistically reliable for a sample, several lines have to be measured [79].

2.2.3.2 Air-void system relationships

The theory of micro ice-lens growth has led Powers [42] to analyse the relationship between the average distance from any point in a cement paste to an air void and the DISFS mass. With more entrained air, there will be more small air voids with a shorter average distance between them; the so-called spacing factor. Powers concluded that concrete should have a spacing factor of approximately 0.01 in (0.25 mm); however, this value is only approximate and does not guarantee frost resistance [42]. The paper presents the following equations developed by Powers with contributions from Willis.

Equation 5 calculates the total air content by multiplying the number of voids intersected (cords) during the measurement with the average distance across all intersections (symbols are described on page VI).

$$A = n \cdot l \quad \text{Eq. 5}$$

A = Total volume of air voids per unit volume of concrete (usually called 'total air content'), m³/m³

n = Number of voids intersected per unit length of traverse

l = Average distance across intersected voids along the line of traverse, m

Willis concluded that the boundary area of air voids per unit volume of air (m²/m³) can also be determined from the average cord length, l [42].

$$\alpha = \frac{4}{l} \quad \text{Eq. 6}$$

α = Volumetric surface of air voids; boundary area per unit volume of air, m²/m³

Equations 1 and 2 yield Eq. 3

$$\alpha = \frac{4n}{A} \quad \text{Eq. 7}$$

The third equation of interest presented in the paper is the void spacing factor that is calculated according to Eq. 4.

$$L = \frac{3}{\alpha}\left(1.4\left(\frac{p}{A}+1\right)^{\frac{1}{3}} - 1\right) \quad \text{Eq. 8}$$

p = Paste content; volume of paste per unit volume of concrete, m³/m³

L = Spacing factor, m

After the spacing factor, other similar factors have been suggested to describe the DISFS resistance: the Philleo factor [80], mean spacing factor [81], and flow length [82]. These three are based on the same concept as the spacing factor, and all quantify the average distance to the nearest air void.

Plante et al. [83] has suggested an air-void stability index, which is defined as the largest spacing factor minus the smallest spacing factor between two mixes (with the same recipe), where, for example, the mixing time has been changed to evaluate the air-void system. The index could give some indications concerning the variation of air-void systems created; however, it should be noted that the spacing factors themselves must also considered. If the air-void stability index is low (which is considered to be good) but the spacing factors are high, the quality of the air-void

system remains considerably low. This index has been used in the evaluation process in reference [84].

In a more recent paper by Hasholt [85], scaling results are presented in relation to the total air content, specific surface, spacing factor, and total surface area of voids. The paper states that the total surface area of voids is as good as or better than the spacing factor in indicating the DISFS resistance. The total surface area of voids is proportional to the total surface area multiplied by the specific surface area. The main difference between the spacing factor and total surface area of voids is explained as follows:

'The spacing factor expresses the likelihood that a capillary pore is located in the vicinity of an air void. The total surface area expresses the likelihood that the capillary pore is connected to an air void'.

The foregoing suggests that the DISFS is more dependent on the connectivity between the air-void system and capillary pore system than the shortest distances from different points inside the capillary pore system to air voids [85].

2.2.4 De-icing agent solutions

The DISFS mechanisms that inflict superficial damage have been studied for a considerable time. Among the oldest and most famous papers is that written by Henry Arnfelt and published in 1943 [18]. He studied the various effects of de-icing agents on the DISFS mass and identified the concentrations that yielded the largest scaling mass. Verbeck and Klieger published a paper in 1957 [17] where they reported the use of a similar test matrix with both salt and non-salt de-icing agents. After these two studies of considerable scales, it was concluded that there exists a so-called 'pessimum concentration' for each de-icing agent, which yields the largest damage mass.

To understand this pessimum concentration, it is important to have a basic comprehension of what transpires when a solution with a low concentration of a de-icing agent freezes. Under normal conditions, without any de-icing agents, water freezes at 0 °C (or slightly below 0 °C if the water is supercooled). However, when a de-icing agent is mixed with water, the freezing temperature of water in the solution becomes lower. This enables de-icing agents to thaw ice on top of roads and bridges during winter. Because the NaCl solution is used in several DISFS tests, it is used here as an example to visualise the effect of a de-icing agent. Figure 2 presents a sodium chloride–water phase diagram. Area 1 in the figure shows the temperatures and concentrations at which NaCl is completely dissolved when mixed with water. When the concentration increases from 0 to approximately 23 mass%, the freezing depression of water in the solution is lowered from 0 to −21.12 °C. The point where areas 1, 2, 3, and 4 meet in the diagram is called the eutectic point.

When a 23.3 mass% NaCl solution is cooled below −21.12 °C, it will change to an ice phase and a crystal phase of $NaCl{\cdot}2H_2O$; the foregoing indicates that salt does not have any de-icing function below the eutectic point.

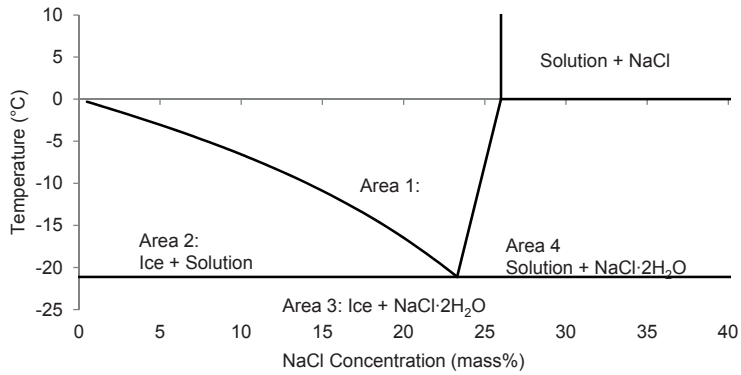

Figure 2
NaCl–water system phase diagram [18].

Figure 3 presents a part of areas 1 and 2. It shows the equilibrium of a 3 mass% NaCl solution when the temperature is between 0 and −21.12 °C.

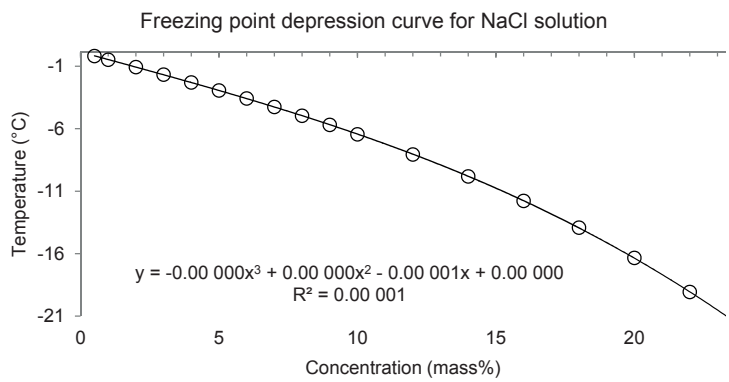

Figure 3
Freezing point depression curve of NaCl mixed with H_2O in thermodynamic equilibrium [86]. Data points of the freezing suppression are from [86], and the equation has been generated from the measurement points.

According to Figure 3, for a solution with 3 mass% NaCl, the freezing suppression is −1.79 °C. When this solution is exposed to temperatures below −1.79 °C, only a part of H_2O freezes, whereas NaCl has to be dissolved in the solution; this means that there will be one part ice and one part solution. Because a part of water has frozen, the mass ratio between NaCl and unfrozen water has increased;

consequently, the NaCl concentration of the solution has increased. The ice fraction can be calculated according to Eq. 9$A = n \cdot l$

Eq. 5:

$$Y_T = \frac{c_T - c_i}{c_T} \quad \text{Eq. 9}$$

Y_T = Ice fraction at a temperature, T

c_T = Equilibrium concentration at a temperature, T, %

c_i = Initial concentration, %

where the concentration at temperature T is given by the equation presented in Figure 3.

In the following example, the temperature is reduced to −6.6 °C for a solution with an initial concentration of 3 mass% NaCl. According to Figure 3, the concentration at a temperature of −6.56 °C is 10 mass%. The ice fraction can then be determined according to the following calculation.

$$\frac{10 - 3}{10} = 0.70 = 70\%$$

This indicates that 70% of the NaCl solution consists of ice, whereas the remaining part (30 mass%) consists of a 10 mass% NaCl solution, which can remain as a solution at −6.56 °C. In Figure 4, the ice fraction formed at a given temperature is calculated by employing Eq. 1 and the data given in Figure 3. The various lines present solutions with different initial concentrations—from 1 (curve with the highest fraction of ice at −21 °C) to 10 mass% NaCl (curve with the lowest fraction of ice at −21 °C). [87]

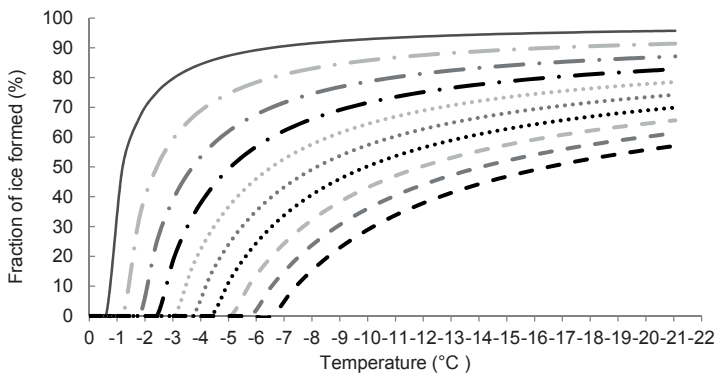

Figure 4
Fraction of ice formed at a certain temperature of NaCl solution, from 1 to 10 mass% NaCl at 1 mass% increments.

The following are some concluding notes pertaining to the function of de-icing agents.

- The addition of a de-icing agent to ice lowers the freezing point; thereby, ice is thawed when the addition is sufficiently high.
- When the temperature of a salt solution is lowered, only water freezes, whereas NaCl remains in the solution and increases the solution concentration.
- During the freezing of a solution with a low concentration of de-icing agent (when freezing starts from just below 0 to −21.1 °C), the ice fraction increases with the concentration of the surrounding solution.

2.2.4.1 Pessimum concentrations of de-icing agent solutions

A pessimum concentration of de-icing agents that contributes to the largest DISFS mass during freezing–thawing exists. This means that when water with 0.1, 3, and 10 mass% NaCl freezes, the 3 mass% solution yields a larger DISFS mass compared with the 0.1 and 10 mass% solutions.

Previous studies (identified from the literature review) that have implemented the DISFS tests at various concentrations of de-icing agents are [17, 18, 26, 44, 45, 47-49]. Table 2 partially summarises these studies; some of the notable findings from the results are listed in Table 3.

Table 2
Summary of studies of pessimum salt concentration where different factors have been varied.

Researcher(s) [Article]	De-icing agents	Concentrations [mass%]	Material
Arnfelt [18]	$CaCl_2$ NaCl	1–10, 20, 30, 40, 50, 60 0, 2, 4, 6, 8, 10, 20, 30	OPC, concrete samples taken from road, unknown water–binder ratio
Verbeck and Klieger [17]	$CaCl_2$ NaCl Urea Ethyl alcohol	2, 4, 8, 16 2, 4, 8, 16 2, 4, 8, 16 2, 4, 8, 16	OPC, Non-air entrained (ca 2 vol% ac) + Air entrained (ca 7 vol% ac) water–binder ratios: 0.42 and 0.63[1)]
Sellevold and Farstad [49]	NaCl	0.5, 1, 1.5, 2, 3, 4, 4.5, 6, 8	OPC, OPC+silica fume, water binder–ratios: 0.55, 0.45, 0.36, and 0.27, initial salt solutions in pores
Fagerlund [48]	NaCl	0.0, 2.5, 5.0, 10.0	OPC, three various air contents, three water–binder ratios: 0.40, 0.60, and 0.70
Lindmark [26]	NaCl	1.0, 1.5, 2.0, 2.5, 3.0, 3.5, 4.0, 4.5, 5.0	OPC, 0.35 initial salt solutions in pores Dried and remoistened, and never-dried specimens
Marchand [47]	NaCl	1.5, 3, 6, 9, 12	OPC, initial and no-initial salt solutions in pores water–binder ratios: 0.25, 0.35, and 0.45 hydrated 180 d in lime solution, dried and carbonated for 21 d
Setzer [46]	NaCl	0.1, 0.5, 1, 2, 3, 6, 8, 9, 10, 11, 12, 15, 18	OPC,
Liu and Hansen [44]	NaCl	0, 0.5, 1.5, 3, 6, 9, 12	OPC, water–binder ratio: 0.45

[1)] 4.8 and 7.2 gallons of water per sack of cement = 7.2×3.785/43 = 0.63; mass of 1 sack of cement is uncertain (here, it is assumed to be 43 kg).

Table 3
Notable comments from pessimum studies [17, 18, 26, 44, 45, 47-49].

Author	Notable comments
Arnfelt [18]	Older and less permeable concrete (i.e., has a longer hydration time and therefore most probably has a higher degree of hydration) creates smaller DISFS mass. The chemical effect from the salt solution seems insignificant. Results show that there exists a pessimum concentration both for NaCl and CaCl. Results also indicate that seven other chemicals produce more severe damage than pure water does when mixed to have a freezing point depression of 1.5 °C.
Verbeck and Klieger [17]	Dissimilar de-icing agents can cause the DISFS. Low concentrations of de-icing agents with a pessimum of 2 to 4 mass% contribute to a larger DISFS mass when they freeze in contact with concrete. Results indicate that a larger DISFS mass is produced when the same solution is kept in contact with the concrete during the freeze–thaw cycle in comparison to that when water has frozen then salt is applied (which thaws the ice). Finally, the solution is rinsed from the surface and replaced with new water. No DISFS occurs when the concrete test surface is only damp (i.e., there is no layer of solution on top of the concrete that freezes and thaws).
Sellevold and Farstad [49]	Concrete mixes with a water–binder ratio of 0.27 and a compressive strength of approximately 115 MPa seem to be unaffected by the DISFS. Concrete mixes with a water–binder ratio of 0.36 and a compressive strength of approximately 91.5 MPa are clearly affected by the DISFS, and the pessimum concentration of the NaCl appear to be 4.5–6 mass%. Concrete mixes with a water–binder ratio of 0.55 and a compressive strength of approximately 50 MPa are clearly affected by the DISFS, and the pessimum concentration of the NaCl seems to be 1–3 mass% NaCl. No damage is produced in concrete with a water–binder ratio of 0.5 when water is used, whereas a 0.5 mass% NaCl concentration contributes to a significant DISFS mass. When an initial NaCl concentration is present inside the pores before the test begins (with a 3 mass% NaCl outer solution), the DISFS mass decreases compared to that when the initial inner concentration is 0%.
Fagerlund [48]	Results indicate that the pessimum NaCl concentration for the DISFS is higher in a saturated sample (from approximately 2.5 mass% for a dried sample to 5 (or 10) mass% for a saturated sample). Results indicate that the uptake of NaCl solution is higher during freezing and thawing than during isothermal capillary suction with +20 °C; the uptake of NaCl solution is generally higher than the water uptake. The DISFS mass decreases when the air content increases or when the water–binder ratio decreases. Results from freezing samples saturated with either water or various NaCl solutions (with constant degrees of saturation) show the largest strain in the samples with 2.5 mass% NaCl, which indicates a pessimum concentration.
Lindmark [26]	There is no clear pessimum between 1.0 and 5.0 mass% NaCl solutions (with a w/c of 0.35). The DISFS mass is generally higher when the outer concentration is 3 mass% NaCl regardless of the inner concentration.
Marchand [47]	A consistent pessimum of approximately 1.5–3 mass% (for favourably hydrated concrete with a w/c of 0.25, 0.35, and 0.45) suggests that the pessimum chloride concentration is not related to concrete quality. It is reported that the DISFS mass is related to the ice formation, and therefore, to the pore structure. A low water–binder ratio contributes to a denser pore structure and lesser ice formation. This is assumed to be the reason for the lower scaling mass in concrete with a low water–binder ratio. Results suggest that the outer solution has a more significant influence on the DISFS.
Setzer [46]	Results indicate that a minimum temperature of −20 °C results in larger DISFS mass than when the minimum temperature is −10 °C. A pessimum NaCl concentration can be observed at approximately 3 mass% when the minimum temperature is −10 and −20 °C. The pessimum NaCl concentration seems to be the same for CEM I and CEM III/B with a water–binder ratio of 0.60 and bc of 320 kg/m³. There is a clear difference between the DISFS of a 0.0 mass% NaCl (water) solution and that of a 0.1 mass% NaCl solution.
Liu and Hansen [44]	Results indicate that when the NaCl concentration is approximately 0.5–6.0 mass%, the largest DISFS mass is produced.

2.2.5 Conclusions derived from literature study

There is a lack of research regarding the following factors:

- the effect of various preconditioning processes, i.e., time of hydration and drying, and carbonation of concrete containing the LCFA and slag;
- the effect of various air contents on the DISFS in concrete containing the LCFA and slag;
- the effect of various NaCl concentrations on the DISFS in concrete containing the LCFA and slag.

This study aims to determine the foregoing by means of a broad approach that enables relative comparisons between the various factors that affect the DISFS of each material. Furthermore, it aims to relate the experimental results to the theories related to the mechanism causing the DISFS.

3 De-icing salt-frost scaling study

This section presents the materials and methods employed in the project and provides a complementary presentation of results. The discussion focuses on the effects of drying and carbonation, air content, and salt concentration on the DISFS.

3.1 Materials

3.1.1 Binders

4 summarises the binders and abbreviation of each binder used in this study; the corresponding product names and producers are similarly listed. To characterise the binders, the cement manufacturer, Cementa AB, made the measurements given below (appendix B).

Table 4.
Binder combinations and abbreviations of concrete recipes containing binders.

Binder abbreviation	Blended content	Product name
CEM I	100% CEM I 42.5 N - SR 3 MH LA[1)]	'Degerhamn anläggningscement' from Cementa
F20	80 mass% CEM I 42.5 N - SR 3 MH LA[1)] 20 mass% LCFA[2)]	'Degerhamn anläggningscement' from Cementa Low calcum fly ash from Emineral A/S
F35	65 mass% CEM I 42.5 N - SR 3 MH LA[1)] 35 mass% LCFA[2)]	'Degerhamn anläggningscement' from Cementa Low calcum fly ash from Emineral A/S
S20	80 mass% CEM I 42.5 N - SR 3 MH LA[1)] 20 mass% slag[3)]	'Degerhamn anläggningscement' from Cementa Merit 5000 from Merox
S35	65 mass% CEM I 42.5 N - SR 3 MH LA[1)] 35 mass% slag[3)]	'Degerhamn anläggningscement' from Cementa Merit 5000 from Merox
S70	80 mass% CEM I 42.5 N - SR 3 MH LA[1)] 20 mass% slag[3)]	'Degerhamn anläggningscement' from Cementa Merit 5000 from Merox
K35	65 mass% CEM I 42.5 N - SR 3 MH LA[1)] 25 mass% slag[3)] 10 mass% LF[4)]	'Degerhamn anläggningscement' from Cementa Merit 5000 from Merox Limus 25 from Nordkalk

The loss on ignition is measured with a thermogravimetric analyser, which measures mass loss when the binder is heated up to 950 °C. This mass loss is possibly caused by the evaporation of bound water and the release of carbon dioxide from

carbonated cement or unburnt coal when fly ash is tested. When slag is tested, the oxidation of sulphur can contribute to a negative loss on ignition, i.e., mass increase.

The XRF measures secondary X-rays that have been reflected by the material, which usually consists of powder. This is an elemental analysis that identifies the oxides and fraction size of each oxide present in cement. From these results, a Bogue calculation, which yields the potential amount of alite, belite, tri-calcium aluminate, and tetra-calcium alumina ferrite, can be made.

The Blaine fineness measurement [88] is used to determine air permeability by drawing a defined quantity of air through a bed of cement with a specific porosity. Based on the permeability, the Blaine value—the specific surface area of particles per mass of material (m^2/kg)—can be calculated; a high Blaine value indicates small particles in the cement and vice versa. This surface area is important to consider when making comparison with other studies of the LCFA or slag, for example. This is because the particle size has an impact on the hydration process; larger specific grain surfaces contribute to more reactions [4].

A laser diffraction measurement of the particle size distribution is performed to complement the Blaine measurement. Considering that the particle size distribution of the binder can affect the ITZ (which could be a crucial area for the DISFS), this additional information could be an interesting factor to evaluate. The results are presented as a particle size distribution from 1 to 315 μm.

The Vicat test [89] consists of a needle pressed down into the fresh cement paste with a certain force at different specified times after water is added to the cement. As the cement reacts with water, the paste becomes stiffer, and the penetration depth of the needle decreases. The result indicates the time it takes for the fresh paste to set, harden, and cease its flow. Accordingly, the measurements provide the initial and final setting times, and yield information on early hydration.

The ICP analysis is conducted to investigate the amount of K_2O and Na_2O from the cement dissolved in the pore water. This is interesting because the dissolved alkali content is presumed to affect the formation of air voids in the fresh paste.

The measurements of SO_3, CO_2, and limestone contents are similarly conducted. Because the measurements are performed on CEM I, these yield some information on 5% of the cement, which is not a clinker but consists of limestones.

3.1.2 Aggregates

Three types of aggregates have been used in the study. In this chapter, these are referred to as ‘0-8 sand’, ‘8-12 stones’, and ‘12-16 stones’. The 0-8 sand is from ‘Kvidinge stenkross AB’ and mainly consists of quartz and feldspar. The 8-12 and 12-16 stones are from ‘Hardeberga stenkross’ and mostly consist of quartzite.

The volume of concrete per cast is approximately 22 dm³; the main reason for the small mixing size is that several batches have been discarded because of unwanted air content in the fresh concrete. Figure 5 presents the sieving curves of each aggregate type and the combined curve '50-20-30', which is used in the concrete recipes.

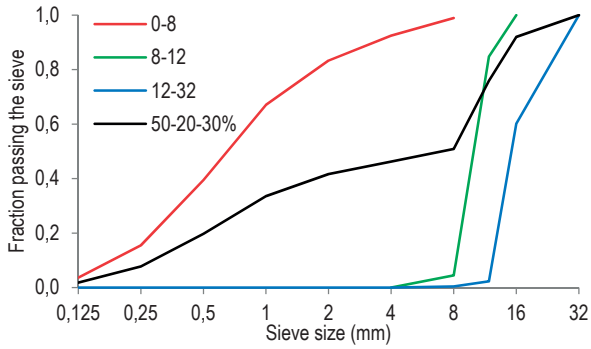

Figure 5.
Sieving curves of aggregates together with the combined sieving curve used in the recipes.

3.1.3 Superplasticisers

In the test of superplasticiser combinations and air-entraining agents, six different types of superplasticisers are tested with each air-entraining agent. Five of these are modified polycarboxylates, and one is a sulphonate melamine formaldehyde condensate. Six superplasticisers are tested. Pozzolith 475-S is selected for the concrete recipes containing fly ash (used for the DISFS test), and ViscoCrete RMC-520 is selected for the concrete recipes (used for the DISFS test) containing slag and 100% CEM I.

3.1.4 Air-entraining agents

In the test of combinations of superplasticisers and air-entraining agents, three different types of air-entraining agents are tested with each superplasticiser. Two of these are synthetic detergents; one is a vinsol resin. Sika AirPRO is selected for all concrete recipes.

3.2 Methods

3.2.1 Test of admixture combinations

To study the effect of various air contents on the DISFS, it is necessary to create a stable air-void system in each concrete recipe. Therefore, the method presented in [90] is developed. The conference paper in [90] presents the method and some results; the selection process of different combinations is reported as well, and all results are shown in appendix A. However, it is important to indicate that at this time, these results are probably outdated. This is because the producers of these admixtures could have possibly continued to develop and make changes to these products (or possibly even replaced them with completely new improved products, but retained the brand names). Nevertheless, the method that is employed for identifying a combination of admixtures that worked well with each binder combination has been proven effective.

3.2.2 Measurement of pH in samples exposed to accelerated carbonation

In papers 4 and 5, the goal of the LTC and capillary suction measurements is to compare noncarbonated and carbonated samples. The noncarbonated samples are dried in 0% CO_2 (using a CO_2 absorbent) inside a glovebox with a 35% relative humidity (RH). The carbonated samples are exposed to an accelerated carbonation (approximately 1 vol% CO_2 and 56% RH for 83 d). However, by the end of the accelerated carbonation period, the CO_2 concentration has continued to decrease by a few thousand ppmv each day. Therefore, there is a need to quantify the extent of carbonation. Thymol blue is initially used in the testing; however, it could not show whether the small 5-mm concrete samples are completely carbonated or not. Accordingly, pH measurements are performed on crushed noncarbonated and carbonated samples similar to those used in the LTC measurements. The pH in noncarbonated concrete is expected to be 12.7–13.1 for the low-alkali cement [44] that is used in the present study. The pH in carbonated concrete is expected to be below 10 [45].

The 2–5-mm particles, similar to those used in the LTC, are ground into powder by hand and placed in deionised water (10-g powder in 200 g of deionised H_2O). The pH meter (Orion 720A) is first calibrated with two buffer solutions (pH of 7 and 12). After the calibration, the measurements are made by rinsing the meter with deionised H_2O, taking measurements in the sample solution for 5 min, and rinsing the meter with deionised water before testing the next sample.

3.2.3 Low-temperature calorimetry measurements

The LTC results of concrete batches tested in papers 4 and 5 show the amount of ice that is formed at each temperature. According to the Gibbs–Thomson equation, the melting point is dependent on the pore size [91]. The thawing curves of these measurements are used to acquire information regarding the pore size distribution where the pore radius is below 50 nm [91]. The method used in the present study is the same as that used in [92], which is shown to be reliable for investigating pores between 2 and 50 nm.

The hysteresis between the freezing and thawing curves provides some information regarding the microstructure based on the theory presented in [93]. The hysteresis is caused by the stochastic process of freezing and the large pores surrounded by smaller pores [93]. The water inside the large pores cannot freeze before the water in the smaller surrounding pores has frozen [93]. However, when the ice thaws, the ice inside the small pores thaws before the surrounding ice in the larger pores thaws [93]. Therefore, the LTC results enable an analysis of the carbonation effect on the amount of ice that is formed at different temperatures, as well as the effect of carbonation on hysteresis, i.e., changes in the microstructure because of the carbonation of each binder.

The 2–5-mm concrete particles are saturated with water after the drying period. One 3-ml plastic container is filled with vacuum-saturated 2–5-mm concrete particles, each weighing approximately 0.3 g; the total mass of each sample is 2.0–2.5 g. For each measurement, two samples are used: one vacuum-saturated sample and one reference sample dried at 105 °C. Both have approximately the same mass and are obtained from the same crushed concrete cylinder.

The LTC measurements are made with a Setaram BT 2.15 temperature-scanning calorimeter. The results show the heat flow produced by the exothermic phase-change of water to ice, and the reverse during thawing. The temperature cycle started at +20 °C with a ramp of −6 °C/h to the minimum temperature of −80 °C; thereafter, a ramp of +6 °C/h back to +20 °C. Because the samples are small, the temperature is approximately the same through the entire sample at a given time. To evaluate the results, the baseline and amount of ice formed are calculated according to the J-method presented in [94].

3.2.4 Capillary absorption measurements

Capillary absorption measurements are conducted in samples obtained from concrete batches tested in papers 4 and 5 to acquire information on the permeability and water absorption of the total pore volume, and how these change with carbonation. Hence, this measurement complements the LTC, which measures porosity of voids with a radius <50 nm.

To quantify the properties related to moisture absorption, three factors are calculated according to Eqs. 10–12. This enables an analysis to determine the effect of these factors on the DISFS. The samples are first dried at a 35% RH and room temperature; thereafter, at 105 °C. An RH of 35% dries all pores larger than approximately 2 nm [51]; a temperature of 105 °C overestimates the total porosity because some amount of the chemically bound water evaporates [52]. Because the samples are dried at a 35% RH and vacuum-saturated before they are heated at 105 °C, the damage caused by drying at such a temperature does not affect the previous measurements. Drying at 105 °C is performed to enable comparisons with studies that have similarly dried samples at this temperature.

$$m = \frac{t}{h^2} \qquad \text{Eq. 10}$$

m = resistance to water penetration, s/mm²

t = time when knickpoint is reached, s

h = specimen thickness, mm

$$c = \frac{W_n - W_i}{\sqrt{t}} \qquad \text{Eq. 11}$$

c = coefficient of capillarity, kg/s$^{0.5}$

W_n = mass of absorbed water per unit area at knickpoint, kg

W_i = initial mass of water in sample at start of test, kg

$$P_{tot} = \frac{V_{open}}{V_{tot}} = \left(\frac{Q_{sat,air} - Q_{dry}}{\rho_w}\right) / \left(\frac{Q_{sat,air} - Q_{sat,water}}{\rho_w}\right) \qquad \text{Eq. 12}$$

P_{tot} = porosity

V_{open}=open pore volume, m³

V_{tot}=total sample volume, m³

$Q_{sat,a}$=mass of vacuum-saturated sample in air, kg

$Q_{sat,w}$=mass of vacuum-saturated sample in water, kg

$Q_{dry,35\%}$=mass of sample dried at 35% RH, kg

$Q_{dry,105\ °C}$=mass of sample dried at 105 °C, kg

ρ_w=density of water, kg/m³

Measurements are performed on samples that are 100 mm in diameter and 5-mm thick in Petri dishes with a cellulose-based cloth that is saturated with deionised water; the samples lay on the cloth. Each sample is taken from the Petri dish and placed on a slightly wet cellulose-based cloth before it is placed on a balance, and

then returned to the Petri dish. Each measurement lasted approximately 20 s. A minimum of 12 measurements are performed during the first eight hours; thereafter, four additional measurements are made in the course of two weeks after the first measurements. Measurements are made on three samples for each binder

3.2.5 Air-void analysis by linear traverse measurements

The air-void analysis using linear traverse (explained in section 2.2.3.1) is conducted to quantify the air-void system in the concrete batches tested in papers 4 and 5. This enables an analysis of the effect of increased air content in concrete on the DISFS. The air-void system is quantified by calculating the specific surface, spacing factor, and approximate air-void size distribution.

Linear traverse measurements are performed by Pelcon Materials & Testing ApS (Copenhagen, Denmark) according to ASTM C457 [39]. One sample of each binder with a 150×100-mm surface tested in papers 4 and 5 is analysed. All results are presented in appendix C.

3.2.6 Thin-section analysis

Microscopic analysis is performed on thin-section samples that are preconditioned in the same way as the carbonated DISFS samples in papers 4 and 5. This is implemented to quantify the carbonation depth, locate microcracks, analyse the homogeneity in the paste, and determine whether water separation and agglomeration of air voids occurred. This confirms that the combination of the superplasticiser and air-entraining agent works well together in each binder.

The samples are sent to RISE (Research Institutes of Sweden) to prepare them for microscopy. The thin-section samples are cut to dimensions of 90×40 mm² with a thickness of approximately 25 μm obtained from samples similar to the DISFS samples (100 mm in diameter and 50-mm high); one thin-section sample is made from each binder. The microscopic analysis is implemented with fluorescent and polarised lights. The fluorescent light enables the quantification of microcracks, analysis of the homogeneity and denseness of the paste, and water separation and agglomeration of air voids. Figure 6 presents a picture exposed to fluorescent light. When polarised light is used, the carbonated layer is seen as a beige colour that enables a quantification of the carbonation depth. Figure 7 presents a picture exposed to polarised light.

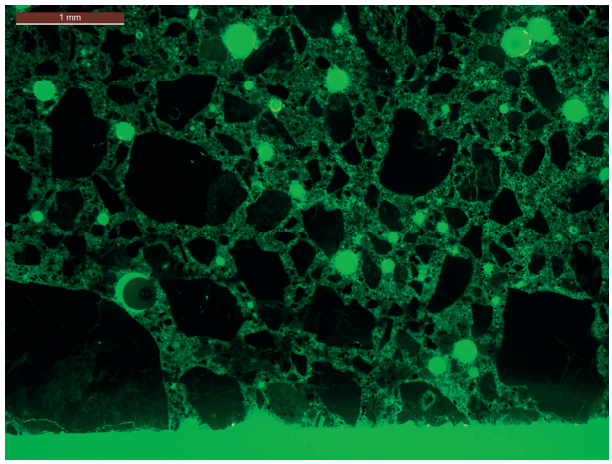

Figure 6
Sample with a 35% LCFA and 5.1% air content exposed to fluorescent light. The bottom of the picture is the surface that has been exposed to drying and carbonation. The black areas show aggregates, and the light green colours show entrained air voids.

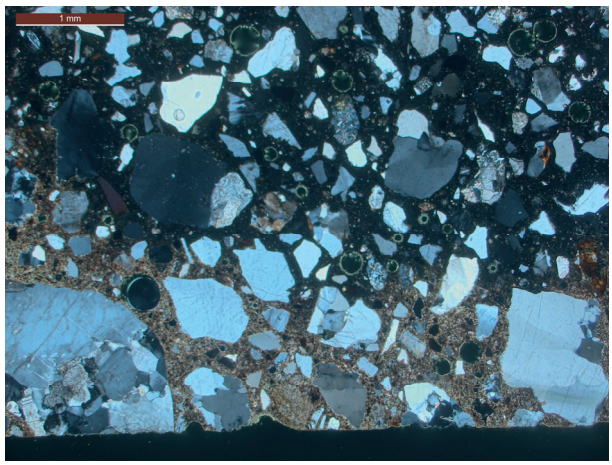

Figure 7
The same sample and sample position shown in Figure 6 exposed to polarised light. The beige colour shows the carbonated layer.

3.2.7 De-icing salt-frost scaling test

The de-icing salt-frost scaling test used in the current project is presented in [27]. Cylindrical samples, 100 mm in diameter and 50-mm thick, are fabricated. This size is chosen to have sufficiently large concrete samples for testing salt-frost scaling; it is also sufficiently small to enable several tests to run in parallel. In each freezer, 63 samples can fit. The samples are exposed to the same temperature cycle regardless

of their placement inside the freezer because of their size and setup. Hence, if three identical samples are fabricated for each factor, then the influence of 21 different factors on salt-frost scaling can be studied simultaneously in one freezer. However, the salt-frost scaling tests consume a considerable amount of time. Nevertheless, the method enables either the broad study of several different factors in order to determine that with the most influence, or the testing of a few different factors with several samples that increases the reliability of results.

The test surface is submerged 2 mm into a 3 mass% NaCl solution. The freeze–thaw cycle, to which the samples are subjected inside the freezer, results in a large DISFS mass. The freezing and thawing temperatures that the samples are exposed to only have small variations regardless of the sample placement inside the freezer. All aspects of the method presented in [27] have been designed to minimise the variation caused by the method on the DISFS results. The assessment criterion to estimate the concrete destruction is the mass of scaling produced from the test. Because different methods yield different DISFS masses, it is the relative DISFS that should be compared when the results from various studies are assessed.

In the DISFS tests, the preconditioning processes have been varied to investigate the research questions. The concrete in [95, 96] is hydrated for a long time (308 d). This has allowed all concrete samples to reach a high degree of hydration, regardless of the added LCFA or slag that can have a slower hydration rate. To complement these results, the samples in [97] are hydrated for short periods. In addition to the preconditioning processes, the air content is varied in [95-97]; because salt concentrations affect the capillary absorption [72], the salt concentration is also varied in [97]. Therefore, the results provide a broad overview of the effect of different factors on the DISFS in concrete recipes used.

3.3 Results and discussion

All measurement results obtained in this project are presented in the appended papers. This section first summarises the results from papers 4, 5, and 6; thereafter, some complementary comparisons are made between the DISFS in concrete, which has been hydrated for a long time [95, 96], and the DISFS in concrete or micro-concrete (containing the same binder combinations), which has been hydrated for a shorter period [97].

3.3.1 Summary of fly ash paper

The LTC and capillary suction measurements are used to characterise the concrete. These measurements are made on carbonated and noncarbonated concrete

(however, pH measurements show that the concrete containing 100% CEM I and 20% LCFA (F20) are more probably not completely carbonated). The LTC measurements show that an increased LCFA fraction increased the fraction of freezable water to −50 °C. Moreover, carbonation of concrete containing the LCFA increased the fraction of freezable water content. The capillary suction measurements show that an increased LCFA fraction decreases permeability (the coefficient of capillarity is decreased and the resistance to water penetration is increased).

The thin-section analysis shows that an increased LCFA fraction increases the carbonation rate. The concrete containing 35 mass% LCFA (F35) approximately has a 2-mm carbonation depth after 735 days of carbonation in 60% RH and 400 ppmv CO_2; concretes with F20 and CEM I have carbonation depths of 1 and 0.2 mm, respectively. When it is assumed that a 1-mm scaling depth is approximately 1 kg/m², the scaling rate for CEM I is lower until the 0.2-mm carbonated layer (0.2 kg/m²) has scaled off, as shown Figure 8. Furthermore, the figure shows that the scaling rate is higher in F35 until the 2-mm carbonated layer has scaled off. Because each horizontal axis in Figure 8 shows the accumulated scaling, the number of cycles that has passed when the accumulated DISFS is 0.2, 1, and 2 kg/m² (the accumulated scaling that corresponds to the carbonated layer) differs between the noncarbonated and carbonated samples. To aid in the analysis of Figure 8, the cycles that have passed for the noncarbonated and carbonated batches are summarised in Table 5.

Scrutinising the seven-cycle scaling (the DISFS per seven freeze–thaw cycles) in CEM I, it is seen that the average scaling rate is lower in carbonated samples (dashed lines) compared to that in noncarbonated samples (solid lines) until the scaling rate is 0.2 kg/m²; thereafter, the scaling rates are approximately equal. The various colours represent different air contents: the black line (lowest air content) represents the highest DISFS; the blue, green, and red lines (increasing air content) indicate lower scaling. Focusing on F35, the scaling rate is higher in carbonated samples (dashed lines) until the accumulated scaling rate is approximately 2 kg/m². The black, blue, green, and red lines show that the noncarbonated samples have approximately the same scaling, and the DISFS does not seem to be affected by the increased air content. However, when the samples have carbonated (dashed lines), the increased air content has an effect on the DISFS; because the black line represents the highest air content, the blue, green, and red lines indicate decreasing DISFS rates. In F20, carbonation does not seem to have any effect because the carbonated samples (dashed lines) have the same scaling rate as the noncarbonated samples (solid lines). However, the carbonated F20 samples with the lowest air content (black dashed line) have significantly larger DISFS rates compared to those in the noncarbonated F20 samples.

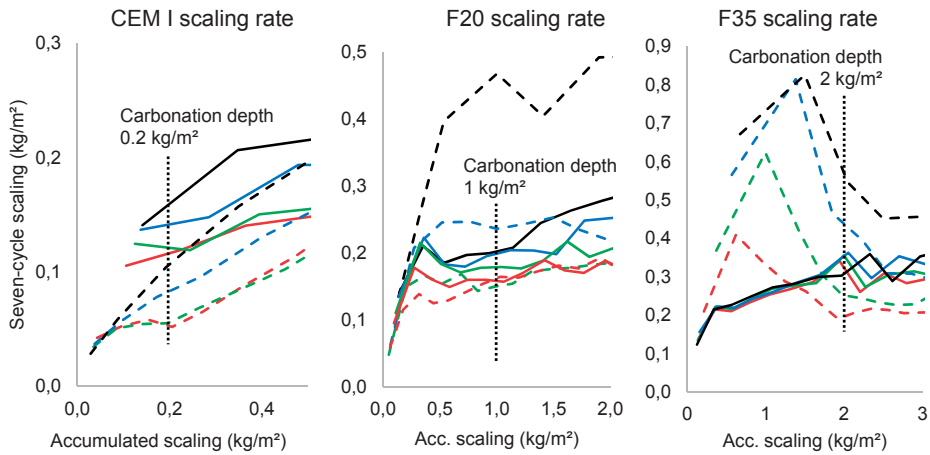

Figure 8
Correlation between the scaling rate (as a function of the accumulated scaling) and carbonation depth (where carbonation depths of 0.2, 1, and 2 mm are assumed to be approximately 0.2, 1, and 2 kg/m², respectively). Note that the vertical and horizontal axes are not of the same scale.

Table 5
Cycles when the accumulated scalings are 0.2, 1.0, and 2.0 kg/m² for CEM I, F20, and F35, respectively.

Binder	Noncarbonated	Carbonated	Difference
CEM I-1	9	21	12
CEM I-2	10	23	13
CEM I-3	11	28	17
CEM I-4	12	27	15
F20-1	37	21	−16
F20-2	38	35	−3
F20-3	41	50	9
F20-4	46	55	9
F35-1	57	20	−37
F35-2	55	24	−31
F35-3	56	36	−20
F35-4	58	52	−6

3.3.2 Summary of slag paper

The measurements that have been made to characterise the concrete are the same as those conducted on the fly ash samples, as discussed above (the LTC and capillary suction measurements). The pH measurements show that the concrete samples containing 100% CEM I, and 20 and 35% slag (S20 and S35, respectively) along

with 25+10% slag+lime filler (K35) are more probably not completely carbonated. The LTC measurements show that for S20, S35, and K35, the fraction of water freezable to −50 °C only increased slightly in noncarbonated or carbonated samples when compared with that in CEM I samples. The concrete containing 70 mass% slag has a higher fraction of freezable water content both in the noncarbonated and carbonated samples. The capillary suction measurements show that an increased slag fraction decreases the permeability (the coefficient of permeability decreases, and the resistance to water penetration increases) of noncarbonated samples. When the samples have carbonated, CEM I has practically the same permeability as S20 and S70, whereas S35 and K35 have the lowest permeability.

The thin-section analysis shows that S20, S35, and K35 do not significantly affect the carbonation rate compared to that in CEM I. All of these samples have a carbonation depth of approximately 0.2 mm after 735 d of carbonation in 60% RH and 400 ppmv CO_2. The concrete containing 70 mass% slag (S70) has a carbonation depth of approximately 2 mm after 735 days of carbonation in 60% RH and 400 ppmv CO_2. If it is assumed that a 1-mm scaling depth is approximately 1 kg/m², the scaling rate is lower in S20 and S35 until the 0.2-mm carbonated layer (0.2 kg/m²) has scaled off, as shown in Figure 9. Moreover, the figure shows that the scaling rate is higher in S70 until the 2-mm carbonated layer has scaled off. Because each horizontal axis in Figure 9 shows the accumulated scaling, the number of cycles that has passed when the accumulated DISFS is 0.2 and 2 kg/m² (the accumulated scaling that corresponds to the carbonated layer) differs between the noncarbonated and carbonated samples. To aid in the analysis of Figure 9, the cycles that have passed for the noncarbonated and carbonated batches are summarised in Table 6.

Scrutinising the seven-cycle scaling (DISFS per seven freeze–thaw cycles) in S20, the average scaling rate is lower in the carbonated samples (dashed lines) compared to that in the noncarbonated samples (solid lines) until 0.2 kg/m². Thereafter, the scaling rates are approximately the same as that in CEM I samples. The different colours represent the various air contents. These show that air content does not affect the DISFS in noncarbonated samples, whereas an increased air content decreases the DISFS in carbonated samples. In S35, the scaling rate is initially lower in the carbonated samples (dashed lines) compared to that in the noncarbonated samples (not as distinct as S20; nevertheless, it still provides a clear benefit). The air content does not seem to affect the DISFS in noncarbonated or carbonated S35 samples. In S70, the carbonated samples have a higher scaling rate compared to that in the noncarbonated samples until the rate of approximately 2.5 kg/m². The estimated average carbonation depth is 2 mm, which would suggest a 2-kg/m² accumulated scaling. However, the density of S70 is lower because the slag has a lower density than CEM I. This could contribute to the small difference between the 2 and 2.5-

kg/m² scaling rates. The air content does not seem to affect the DISFS in noncarbonated or carbonated samples. However, the reason for this could be that the difference between the lowest and highest air content is negligible. In K35, the results are approximately the same as those in F20, where carbonation does not seem to have any significant effect on the DISFS. The increased air content does not seem to have any effect on the DISFS in K35, except for the following: the carbonated K35 concrete with the lowest air content (dashed black line) has a significantly higher scaling rate compared with those of other concrete samples.

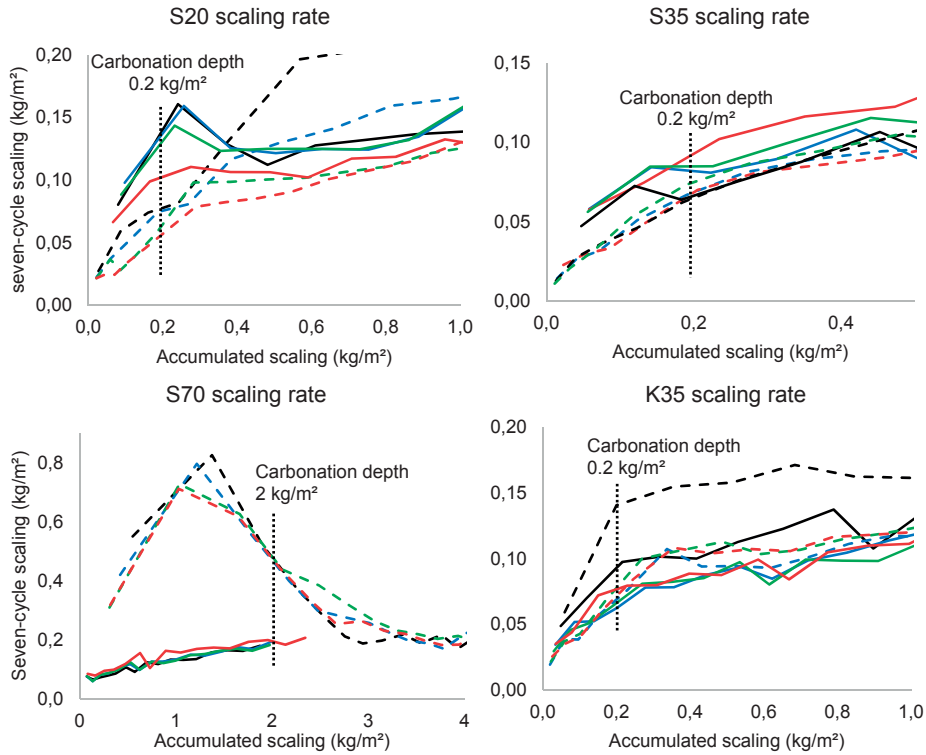

Figure 9
Correlations between the scaling rate (as a function of the accumulated scaling) and the carbonation depth (where carbonation depths of 0.2 and 2 mm are assumed to be approximately 0.2 and 2 kg/m², respectively). Note that the vertical axes are not of the same scale.

Table 6
Number of cycles when the accumulated scaling is 0.2 kg/m² for CEM I, S20, S35, and K35, and the number of cycles when the accumulated scaling is 2.0 kg/m² for S70.

Binder	Noncarbonated	Carbonated	Difference
CEM I-1	9	21	12
CEM I-2	10	23	13
CEM I-3	11	28	17
CEM I-4	12	27	15
S20-1	12	24	12
S20-2	11	29	18
S20-3	12	36	24
S20-4	16	41	25
S35-1	22	34	12
S35-2	19	36	17
S35-3	19	36	17
S35-4	19	36	17
S70-1	>112	23	<−89
S70-2	>112	25	<−87
S70-3	>112	26	<−86
S70-4	100	27	−73
K35-1	20	14	−6
K35-2	28	32	4
K35-3	29	30	1
K35-4	25	31	6

3.3.3 Summary of complementary tests

This study is aimed at performing complementary measurements on concrete and micro-concrete to bridge the gap between well-hydrated (exposed to IC300) samples and young samples (exposed to IC63, IC29, IC22, and IC8). Moreover, these tests investigate the effect of a shorter period of drying and carbonation on young samples; these processes are more similar to the preconditioning processes that are used in the standard test methods. To compare the air content between micro-concrete and concrete, the air content in hardened paste (ACP) is calculated in each batch. The ACP is the air content measured in the fresh concrete divided by the fraction of paste; the definition is presented in [97].

The results in [97], pertaining to young concrete and micro-concrete, show that drying and carbonation have different effects on the DISFS depending on the binder.

Figure 10 shows some examples of results presented in [97]. The samples have 8 d or 30 d of internal curing (IC), and drying and carbonation periods (DC), compared with the 30 d of IC of samples that have never been dried or carbonated. These are compared with preconditioning processes IC23 DC7 and RS1 (RS is resaturation before testing), which are similar to the process in the standardised slab method according to [76].

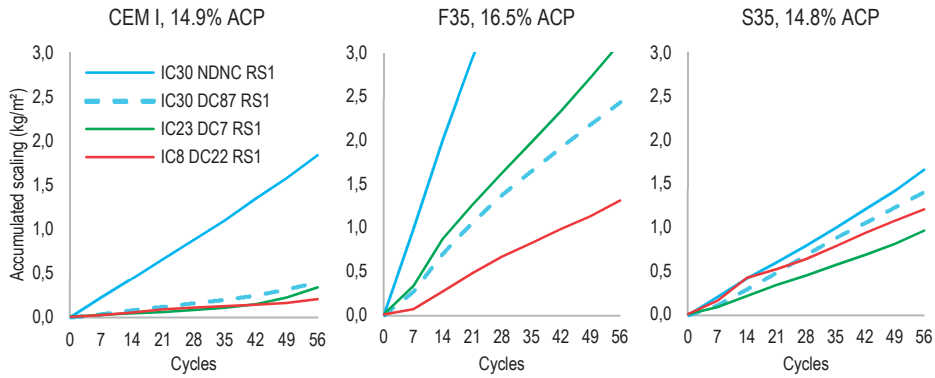

Figure 10
Average accumulated scaling of three samples containing 100% CEM I, 35% LCFA, and 35% slag exposed to various preconditioning processes.

The results also show that the air content has various effects on the DISFS depending on the preconditioning process and binder. This is demonstrated by the comparison between Figure 11 and Figure 12. The effect of air content when the samples have never been dried or carbonated is shown in Figure 11. Figure 12 shows the effect of air content when the same samples have been exposed to a shorter IC combined with a DC period. There is an evident difference, and the preconditioning process clearly influences the effect of air content (on the DISFS) on all three binders.

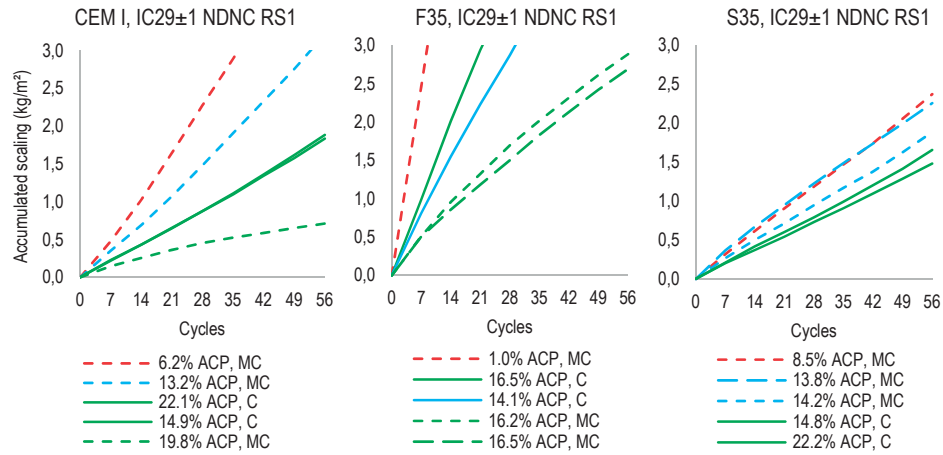

Figure 11
Average accumulated scaling of three samples containing 100% CEM I, 35% LCFA, and 35% slag exposed to IC29±1 (has never been dried and never been carbonated) with various air contents.

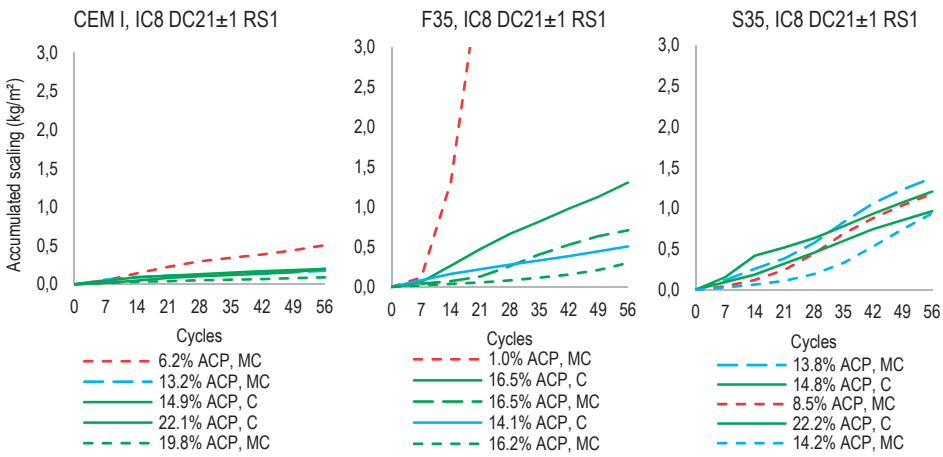

Figure 12
Average accumulated scaling of three samples containing 100% CEM I, 35% LCFA, and 35% slag exposed to IC8 DC21±1 with various air contents.

The results presented in paper 6 also show that various NaCl concentrations affect the DISFS in different ways depending on the preconditioning process and binder. Considering the previous research that has studied the pessimum concentration, low concentrations are expected to result in more DISFS. This is generally the case for both preconditioning processes according to Figure 13 and Figure 14. Figure 13 shows never-dried and never-carbonated samples exposed to IC29. Figure 14 shows samples from the same batches exposed to IC29 followed by a period of drying and

carbonation. However, there is one unexpected result: the exposure of samples containing 35% LCFA (which have never been dried or carbonated) to 9% NaCl concentration has resulted in a large DISFS. Otherwise, drying and carbonation reduce the DISFS; the same effects are shown in Figure 11 and Figure 12.

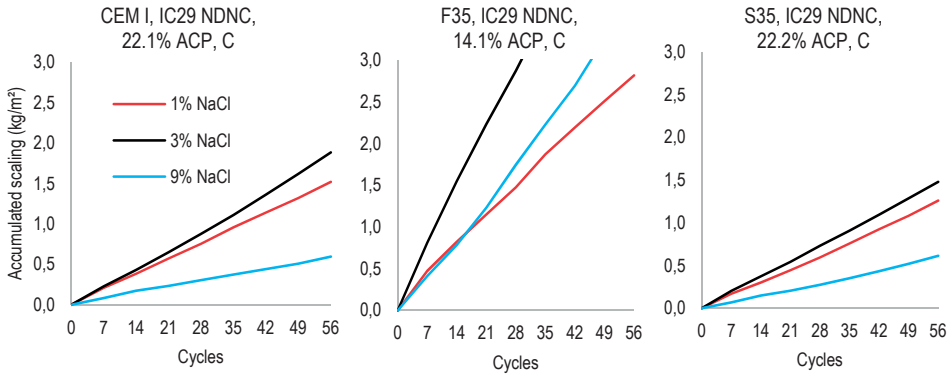

Figure 13
Average accumulated scaling of three samples 100% CEM I, 35% LCFA, and 35% slag exposed to IC29 (has never been dried and never been carbonated) and various NaCl concentrations.

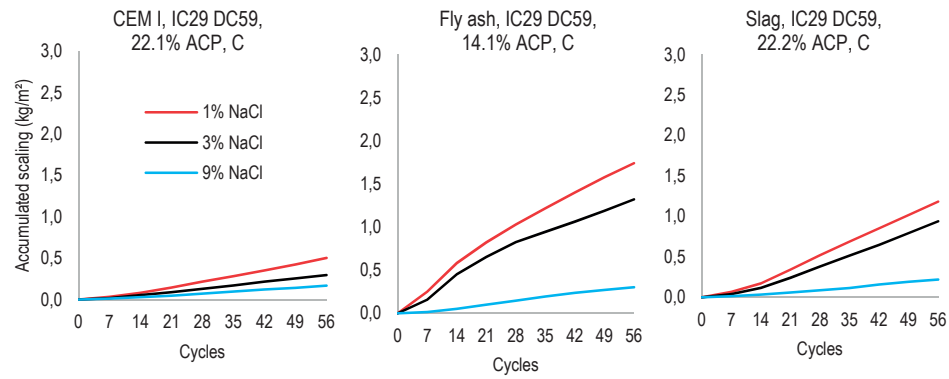

Figure 14
Average accumulated scaling of three samples containing 100% CEM I, 35% LCFA, and 35% slag exposed to IC29 DC59 and various NaCl concentrations.

3.3.4 Complementary comparisons among the papers

The binders used in [97] are 100% CEM I, 35% LCFA, and 35% slag. Because these binders are similarly tested in [95, 96], comparisons can be made among the results presented in these papers. Such comparisons enable an analysis of the influence of drying and carbonation on the DISFS in concrete that has been hydrated for an extended period of time (presented in [95, 96]) and samples that have been hydrated

for a short period (presented in [97]). Each diagram presents the binder, the preconditioning process, and the ACP (air content of paste) for each line. In the label, 'C' denotes concrete recipes with aggregate sizes up to 32 mm, and 'MC' denotes micro-concrete recipes with aggregate sizes up to 8 mm.

3.3.4.1 Low-calcium fly ash

Figure 15–17 present comparisons between the results presented in [96] and [97].

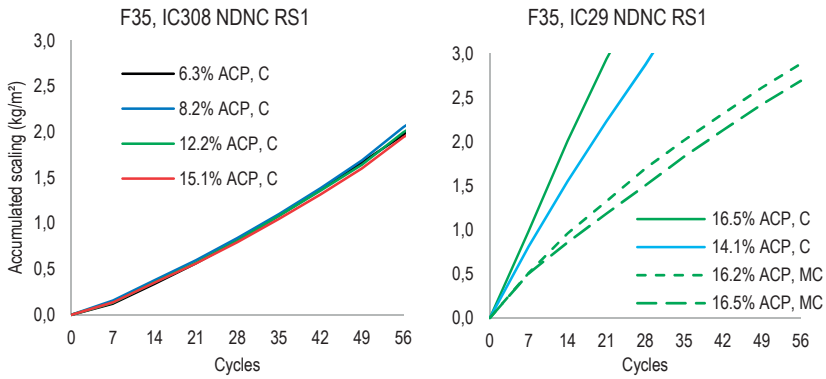

Figure 15
Left shows results presented in [96]; solid lines show concrete samples exposed to IC308 and NDNC. Right shows results presented in [97]. Samples have been exposed to IC29 ±1 NDNC. Solid and dashed lines represent concrete and micro-concrete, respectively. Air content in the paste is according to definition given in [97]. In the label, 'C' denotes concrete recipe with aggregate sizes up to 32 mm, whereas 'MC' denotes micro-concrete recipe with aggregate sizes up to 8 mm.

The results in [97] show that concrete exposed to 29±1 d of IC and NDNC (never-dried and never-carbonated) has higher DISFS compared to samples exposed to 308 d presented in [96]. These show that an increased IC period decreases the DISFS in concrete with 35 mass% LCFA when the samples have never been dried or carbonated.

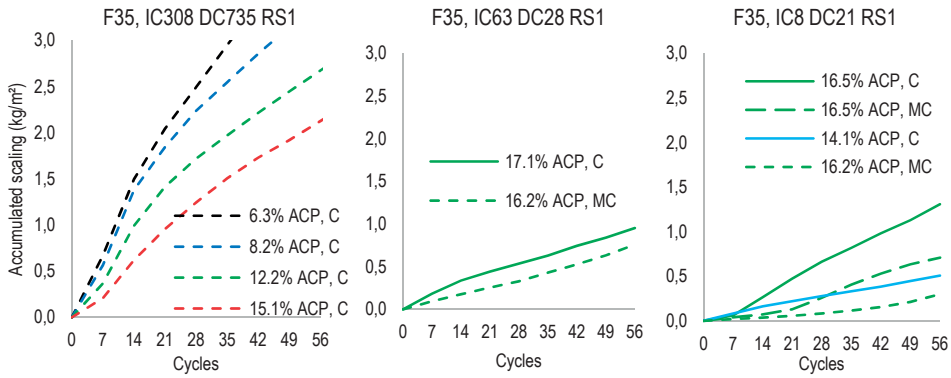

Figure 16
Left shows results from [96] of concrete samples exposed to IC308 and DC735 with varying air contents. Centre and right show results presented in [97]. All samples are exposed to IC8 followed by 20±1 DC. In the label, 'C' denotes concrete recipe with aggregate sizes up to 32 mm, whereas 'MC' denotes micro-concrete recipe with aggregate sizes up to 8 mm.

The results presented in [96] show that drying and carbonation increase the DISFS in concrete with 35 mass% LCFA. This concrete has been exposed to 308 d of IC and 735 of DC (the increased DISFS in Figure 16, left, is because of the decreased air content). However, results presented in [97] show that concrete exposed to 8 d of IC and 22 d of DC has the lowest DISFS among all samples with 35 mass% LCFA.

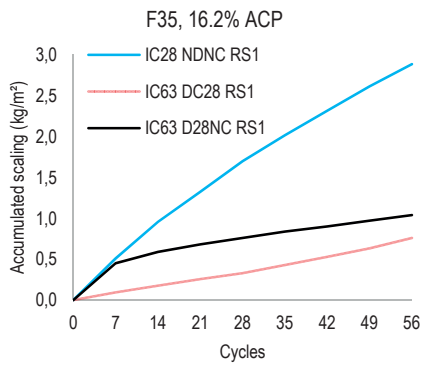

Figure 17
Micro-concrete that has never been dried and never been carbonated (blue line), has been dried and carbonated (red line), and has been dried and never been carbonated (black line). Results are presented in [97].

Figure 17 shows results presented in [97], where the effect of drying is tested. In comparing the black and blue lines in Figure 17, drying seems to have a positive impact. In comparing results between samples that have been dried and carbonated and those of samples that have been dried and never been carbonated, the

carbonation of concrete with 35 mass% LCFA similarly appears to reduce the DISFS (these results are presented in [97]).

3.3.4.2 Ground-granulated blast furnace slag

Figure 18–20 present comparisons between the results presented in [95] and [97].

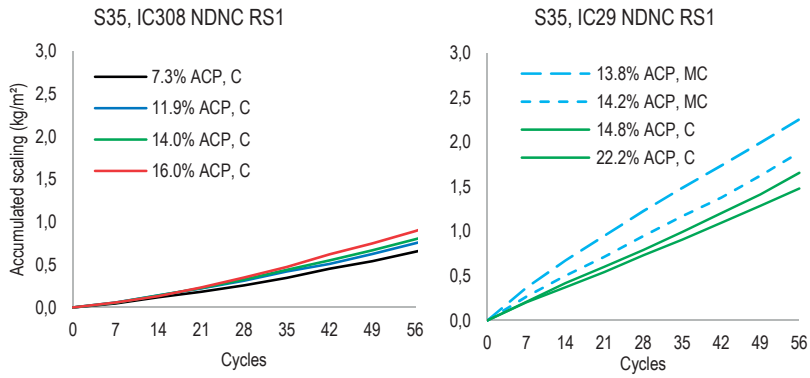

Figure 18
Left shows results from [95]. Solid lines show concrete samples exposed to IC308 and NDNC. Right shows results presented in [97]; all samples are exposed to IC29 ±1 NDNC. Solid lines are concrete and dashed lines are micro-concrete with air content in the paste according to the definition given in [97]. In the label, 'C' denotes concrete recipe with aggregate sizes up to 32 mm, whereas 'MC' denotes micro-concrete recipe with aggregate sizes up to 8 mm.

The results in [97] show that concrete exposed to 29±1 d of IC and NDNC has a higher DISFS compared to concrete exposed to 308 d (presented in [95]). This shows that an increased IC period decreases the DISFS in concrete with 35 mass% slag (the same as that with LCFA).

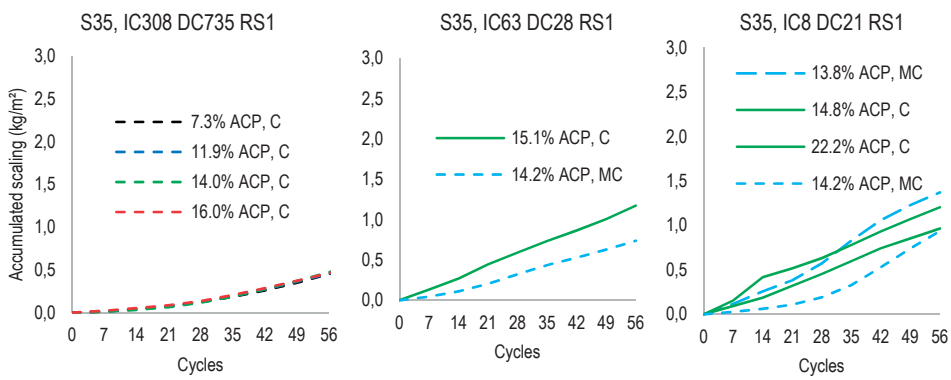

Figure 19
Left shows results from [95] of concrete samples exposed to IC308 and DC735 with varying air contents. Centre and right show results presented in [97].

The results presented in [95] show that drying and carbonation decrease the DISFS in concrete with 35 mass% slag. This concrete has been exposed to 308 d of IC and 735 d of DC. Apparently, the increased air content has no effect, as indicated in Figure 19, left. Results presented in [97] show that concrete or micro-concrete with 35 mass% slag exposed to IC8 and DC22, or IC63 and DC28 has a higher DISFS compared to concrete exposed to IC308 and DC735. Hence, an increased hydration period decreases the DISFS in dried samples. Figure 20 shows results presented in [97] where the effect of drying is tested.

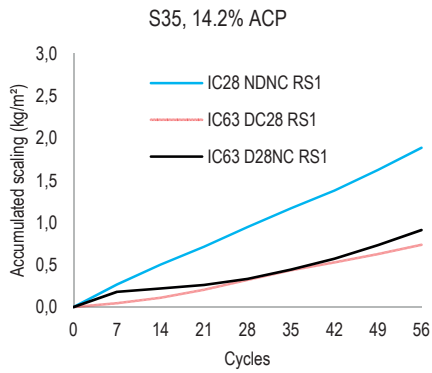

Figure 20
Micro-concrete that has never been dried and never been carbonated (blue line), has been dried and carbonated (red line), and has been dried and never been carbonated (black line). Results are presented in [97].

In comparing the black and blue lines in Figure 20, it is observed that drying has a positive impact. In comparing the dried and carbonated samples with those that have been dried and never been carbonated, the carbonation of concrete with 35 mass% slag slightly reduces or does not affect the DISFS (these results are presented in [97]). These trends are the same in samples with 35 mass% slag and 35 mass% LCFA. However, drying has no positive effect on concrete with 100% CEM I, as shown in Figure 21.

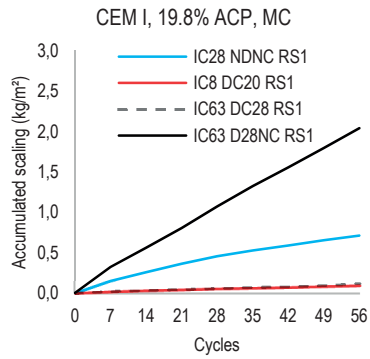

Figure 21
Micro-concrete that has never been dried and never been carbonated (blue line), has been dried and carbonated (red line), and has been dried and never been carbonated (black line). Results are presented in [97].

In comparing the black and red lines in Figure 21, it is observed that the combined drying and carbonation result in a large decrease in the DISFS. In comparing the black and blue lines, drying increases the DISFS (these results are presented in [97]). Accordingly, drying increases the DISFS in concrete with 100% CEM I, whereas carbonation contributes to a large decrease in the DISFS. The foregoing deviates from the results of micro-concrete with 35 mass% LCFA or slag.

3.4 Conclusions

Specific questions are discussed in the papers. In this section, the general conclusions from the papers are presented. These are followed by some general conclusions drawn regarding the main research questions stated at the beginning of this dissertation.

3.4.1 General conclusions from papers 4 and 5.

- A fine structure of mesopores that reduce the ice fraction, which can form at a given temperature combined with a low permeability in the structure of pores with a radius greater than 50 nm, results in a low DISFS. This has only one exception—noncarbonated concrete with 25+10% slag+LF that has a fine structure of mesopores and a coarse structure of pores with a radius larger than 50 nm with an extremely low DISFS.
- A coarse structure of mesopores with a medium or high permeability in the pore structure with a radius longer than 50 nm results in the largest DISFS.

3.4.2 General conclusions from paper 6.

- The DISFS is highly dependent on the hydration time, drying and carbonation, air content, and salt solution. The largest influencing factor on concrete containing CEM I is surface carbonation. The preconditioning process with short favourable hydration followed by drying and carbonation have the most significant influence among all tested factors on concrete containing 35% LCFA. All tested factors appear to have the lowest influence on concrete containing 35% slag; this suggests that it is more robust than the other recipes. The largest influencing factors on concrete containing 35% slag are drying and carbonation.

3.4.3 General conclusions on the main research questions

1. How do various fractions of added LCFA or slag affect the salt-frost scaling on a never-dried and never-carbonated, or dried and carbonated sawed concrete surface?

This question is discussed more extensively in paper 4 and 5 [95, 96]. According to paper 4 [96], an increased LCFA fraction results in an increased DISFS in concrete with an extended period of internal curing. The present results show that this is true in both never-dried and never-carbonated concrete, as well as in dried and carbonated concrete. According to paper 5 [95], a fraction of up to 70 mass% slag results in a decreased DISFS in a never-dried and never-carbonated concrete with a long period of internal curing. For dried and carbonated concrete, the DISFS is low when the replacement is up to 35 mass% slag. When the concrete has been dried and carbonated, and the replacement of slag is 70 mass%, the DISFS is high.

2. How does drying and carbonation affect the salt-frost scaling in concrete containing various fractions of added LCFA or slag on a sawed concrete surface?

According to Figure 15, an increased period of internal curing decreases the DISFS when the samples have never been dried or carbonated. However, according to paper 4 [96] and paper 6 [97], the most favourable preconditioning (out of the processes tested) of concrete containing 35 mass% LCFA is 8 d of internal curing and 21 d of drying and carbonation. The results also show that long periods of drying and carbonation, for concrete with 35 mass% LCFA exposed to a long period of hydration, increase the DISFS. According to paper 5 [95] and paper 6 [97], drying and carbonation are favourable in concrete containing up to 35 mass% slag. The drying and carbonation of well-hydrated concrete with 70 mass% slag increase the DISFS.

3. How do various air contents affect the salt-frost scaling in concrete containing various fractions of added LCFA or slag in a never-dried and never-carbonated, or dried and carbonated sawed concrete surface?

According to results shown in paper 4 [96] and paper 6 [97], an increased air content decreases the DISFS in both carbonated and noncarbonated well-hydrated concrete containing 20 mass% LCFA. The increased air content does not affect the DISFS in well-hydrated never-dried and never-carbonated concrete that contains 35 mass% LCFA. However, an increased air content decreases the DISFS in dried and carbonated concrete containing 35 mass% LCFA that has been hydrated for a long period.

An increased air-void content has a positive effect on concrete containing 20 mass% slag. However, it has no positive effect on the DISFS in concrete with more than 20 mass% slag. The reason for this low effect could be that the low permeability of pores, with a radius longer than 50 nm, counteracts the protective effect of air voids. The reason for the low effect of the increased air content on the scaling in the concrete with 70 mass% slag presented in [95] could be the low increase in the air-void content.

Another hypothesis that explains why the increased air-void content does not reduce the DISFS in noncarbonated F35 and noncarbonated S70 is that considerable impediments (according to the LTC measurements) disable the effect of the increased air-void content.

3.5 Future research

It would be of particular interest to further study young concrete. Some examples of the preconditioning processes could be IC1DC27, IC7DC21, IC14DC14, IC27DC1, IC28DC0, IC1DC6, and IC7DC7. After preconditioning, some samples should be used for the DISFS test and some samples should be used to measure material properties (thin slice analysis, low temperature calorimetry, and capillary absorption). Moreover, the comparison should be made with samples that are exposed to the same processes; however, drying and carbonation have to be changed from the normal atmosphere to a condition with 0 ppmv CO_2 and 10 000 ppmv CO_2, for example. Two batches should be fabricated with each binder—one with an air-entraining agent (ca 20% ACP) and another without. Furthermore, the addition of supplementary cementitious materials should be varied. All studies, where the factors are structurally varied, can contribute to the enhancement of knowledge regarding the de-icing salt-frost scaling mechanism. The low correlation between field results and those of standard test methods in concrete containing the LCFA or slag has been criticised. Therefore, these results should also be used as base knowledge in order to enable a calibration of the standard preconditioning process. The aim should be to acquire a higher correlation between the DISFS results from standard test methods and the DISFS in real structures containing the LCFA or slag.

It would be interesting to test more LCFA/slag concentrations. If two preconditioning processes are chosen (e.g., IC1DC21 and IC28DC0), and three samples of each recipe are to be tested, two freezers can test 21 different recipes (e.g., CEM I, F5–F35, and S5–S65 with 5% increments). The results from such a test would show whether the changes that are observed among the different recipes (CEM I – FA35, and CEM I – S65) are continuous; in such a case, it would be appropriate to interpolate among the results obtained from different LCFA/slag concentrations.

It would be noteworthy to study two unexpected outlying results. First, why is IC8 DC21 RS1 the most favourable preconditioning process for F35 concrete? In comparing F35 samples, the capillary porosity of those that have been exposed to IC8 DC21 RS1 should be coarser than those that have been exposed to IC63 DC28 RS1. Accordingly, it would be interesting to measure the pore size distribution and total volume of pores with a radius longer than 50 nm of different materials. This should then be correlated with the DISFS to determine whether a certain pore volume distribution results in a lower DISFS. Second, why does noncarbonated K35 have a considerably low DISFS when it seems to have a coarse porosity based on the capillary suction measurement? In noncarbonated K35, the DISFS is low. On the other hand, in noncarbonated CEM I, the DISFS is large. Both have coarse capillary porosities according to the capillary absorption measurements. Thus, it would be interesting to study the volume of pores with a radius longer than 50 nm as well to determine whether the capillary porosities differ between these binders.

Another interesting study would be to vary the DISFS test. As an example: samples exposed to continuous cycling in constant contact the NaCl solution (such as the method used in this thesis) are compared to samples that are exposed to seven cycles of freezing and thawing followed by seven days of drying and carbonation. The drying and carbonation could also be varied, e.g. some samples that are dried and carbonated in 35 % RH, and others that are dried and carbonated in 90 % RH. The samples exposed to 35 % RH will dry out more water from the samples which will give information how drying during the test affect the DISFS. Because the RH is approx. 90 % during the winter, the samples exposed to 90 % RH will most likely give some information closer related to the DISFS in field during winter.

The goal of the DISFS research should be to identify the combination of material properties that invariably results in a high DISFS resistance. This would enable faster tests that can measure these properties to answer the question of whether or not a specific type of concrete can be used in an environment where it is exposed to de-icing salt-frost scaling. One interesting test would be to study whether a certain correlation exists among warping test measurements (e.g., deflection when various binders are exposed to different salt concentrations), according to [74] and the DISFS.

References

1. Scrivener, K.L., *Options for the future of cement.* The Indian Concrete Journal, 2014. **88**(7): p. 11.
2. Boubitsas, D., et al., *Frost resistance of concrete - Experience from long term exposure*, in *Materials, Systems and Structures in Civil Engineering 2016*, M.T. Hasholt, K. Fridh, and R.D. Hooton, Editors. 2016, RILEM publications S.A.R.L: Technical University of Denmark, Lyngby, Denmark. p. 21-30.
3. Helsing, E. and P. Utgenannt, *The salt-frost resistance of concrete with supplementary cementitoius materials (SCM)*, in *Materials, Systems and Structures in Civil Engineering 2016*, M.T. Hasholt, K. Fridh, and R.D. Hooton, Editors. 2016, RILEM publications S.A.R.L: Technical University of Denmark, Lyngby, Denmark. p. 51-60.
4. Löfgren, I., O. Esping, and A. Lindvall, *The influence of carbonation and age on salt frost scaling of concrete with mineral additions*, in *Materials, Systems and Structures in Civil Engineering 2016*, M.T. Hasholt, K. Fridh, and R.D. Hooton, Editors. 2016, RILEM publications S.A.R.L: Technical University of Denmark, Lyngby, Denmark. p. 91-100.
5. Utgenannt, P., *The influence of ageing on the salt-frost resistance of concrete*, in *Department och Building and Environmental Technology*. 2004, Faculty of Engineering, LTH, Lund University: Lund. p. 346.
6. Bilodeau, A. and V.M. Malhotra. *Deicing salt scaling resistance of concrete incorporating supplementary cementing materials CANMET research*. in *Freeze-Thaw Durability of Concrete - rilem proceedings 30*. 1997. E & FN SPON.
7. Panesar, D.K. and S.E. Chidiac, *Multi-variable statistical analysis for scaling resistance of concrete containing GGBFS.* Cement and Concrete Composites, 2007. **29**(1): p. 39-48.
8. Giergiczny, Z., et al., *Air void system and frost-salt scaling of concrete containing slag-blended cement.* Construction and Building Materials, 2009. **23**(6): p. 2451-2456.
9. Hooton, R.D. and D. Vassilev, *Deicer Scaling Resistance of Concrete Pavements, Bridge Decks, and Other Structures Containing Slag Cement: Phase 2: Evaluation of Different Laboratory Scaling Test Methods*. 2012.
10. Sun, C.T., W.H. Li, and B.R. Hou, *Study on Frost-Salt Resistance of Fly Ash Concrete.* Architecture and Urban Development, 2012. **598**: p. 432-437.

11. Zhang, M.H., et al., *De-Icing Salt Scaling of Concrete Incorporating Different Types and Percentages of Fly Ashes*, in *Sixth CANMET/ACI International Conference on Fly Ash, Silica Fume, Slag, and Natural Pozzolans in Concrete*, V.M. Malhotra, Editor. 1998, ACI: Bangkok, Thailand. p. 493-525.

12. Marchand, J., et al., *Effects of fly ash on microstructure and deicer salt scaling resistance of concrete*, in *Frost Resistance of Concrete*, M.J. Setzer and R. Auberg, Editors. 1997, E&FN Spon: University of Essen. p. 11-20.

13. Baert, G., A.-M. Poppe, and N. De Belie, *Evaluation and comparison of mechanical characteristics and durability of concrete with different cement replacement levels by fly ash*, in *Cement Combinations for Durable Concrete*, R.K. Dhir, T.A. Harrison, and M.D. Newlands, Editors. 2005, MPG Books: University of Dundee, Scotland, UK. p. 787-797.

14. Bilodeau, A., et al., *Effect of Curing Methods and Conditions on the Performance of Fly Ash Concrete in De-Icing Salt Scaling*, in *Sixth CANMET/ACI International Conference on Fly Ash, Silica Fume, Slag, and Natural Pozzolans in Concrete*, V.M. Malhotra, Editor. 1998, ACI: Bangkok, Thailand. p. 361-384.

15. Nowak-Michta, A., *Water-binder Ratio Influence on De-icing Salt Scaling of Fly Ash Concretes.* Procedia Engineering, 2013. **57**: p. 823-829.

16. Bouzoubaâ, N., et al., *Deicing salt scaling resistance of concrete incorporating supplementary cementing materials: laboratory and field test data.* Canadian Journal of Civil Engineering, 2008. **35**: p. 1261-1275.

17. Verbeck, G.J. and P. Klieger, *Studies of "Salt" Scaling of Concrete*, H.R.B. 150, Editor. 1957: Washington D.C. p. 13.

18. Arnfelt, H., *Damage on Concrete Pavements by Wintertime Salt Treatment*. 1943, Statens Väginstitut. p. 28.

19. Nili, M. and M. Zaheri, *Deicer salt-scaling resistance of non-air-entrained roller-compacted concrete pavements.* Construction and Building Materials, 2011. **25**(4): p. 1671-1676.

20. Marchand, J., M. Jolin, and Y. Machabée, *Deicer salt scaling resistance of supplementary cementing material concrete: laboratory results against field performance*, in *Cement Combinations for Durable Concrete*, R.K. Dhir, T.A. Harrison, and M.D. Newlands, Editors. 2005, MPG Books: University of Dundee, Scotland, UK. p. 579-590.

21. Hooton, R.D. and A. Boyd, *Effect of finishing, forming and curing on de-icer salt scaling resistance of concretes*, in *Frost Resistance of Concrete*, M.J. Setzer and R. Auberg, Editors. 1997, E&FN Spon: University of Essen. p. 174-183.

22. Jacobsen, S., D.H. Saether, and E.J. Sellevold, *Frost testing of high strength concrete: Frost/salt scaling at different cooling rates.* Materials and Structures/Materiaux et Constructions, 1997. **30**(195): p. 33-42.

23. Powers, T.C., *Basic Considerations Pertaining to Freezing-and-Thawing Tests.* ASTM Proceedings, 1955. **55**: p. 24.

24. Jacobsen, S., et al., *Frost deicer salt scaling testing of concrete: Effect of drying and natural weathering.* Cement Concrete and Aggregates, 1997. **19**(1): p. 8-16.

25. Setzer, M.J. and R. Auberg. *Testing of Freeze Thaw and Deicing Salt Resistance*. in *CBP Second International Workshop*. 1994. Oslo, Norway.

26. Lindmark, S., *Mechanisms of Salt Frost Scaling of Portland Cement-bound Materials: Studies and Hypothesis*, in *Department of Building and Environmental Technology*. 1998, Faculty of Engineering, LTH, Lund University: Lund. p. 266.

27. Strand, M.J. and K. Fridh, *Test Method for De-Icing Salt Frost Scaling in High Performance Concrete.* MethodsX, 2018.

28. Krishnan, A., et al., *Technical issues related to the use of fly ash and slag during late-fall (low temperature) construction season*. 2006, Indiana department of transportation, Purdue University. p. 358.

29. Deja, J., *Freezing and de-icing salt resistance of blast furnace slag concretes.* Cement and Concrete Composites, 2003. **25**(3): p. 357-361.

30. Boyd, A.J. and R.D. Hooton, *Long-Term Scaling Performance of Concretes Containing Supplementary Cementing Materials.* Journal of Materials in Civil Engineering, 2007. **19**(10): p. 820-825.

31. Pigeon, M., et al., *Surface microstructure and scaling resistance of concrete.* Cement and Concrete Research, 1996. **26**(10): p. 1555-1566.

32. Ahani, R.M. and M.R. Nokken, *Salt scaling resistance – The effect of curing and pre-saturation.* Construction and Building Materials, 2012. **26**(1): p. 558-564.

33. Bouzoubaâ, N., et al., *Deicing salt scaling resistance of concrete incorporating fly ash and (or) silica fume - laboratory and field sidewalk test data.* Canadian Journal of Civil Engineering, 2011. **38**: p. 373-382.

34. Thomas, M.D.A., *Laboratory and field studies of salt scaling in fly ash concrete*, in *Frost Resistance of Concrete*, M.J. Setzer and R. Auberg, Editors. 1997, E&FN Spon: University of Essen. p. 21-30.

35. Yuan, J., Y. Wu, and J. Zhang, *Characterization of air voids and frost resistance of concrete based on industrial computerized tomographical technology.* Construction and Building Materials, 2018. **168**: p. 975-983.

36. Shon, C.-S., et al., *Determination of air-void system and modified frost resistance number for freeze-thaw resistance evaluation of ternary blended concrete made of ordinary Portland cement/silica fume/class F fly ash.* Cold Regions Science and Technology, 2018. **155**: p. 127-136.

37. Van den Heede, P., J. Furniere, and N. De Belie, *Influence of air entraining agents on deicing salt scaling resistance and transport properties of high-volume fly ash concrete.* Cement and Concrete Composites, 2013. **37**: p. 293-303.

38. Valenza II, J.J. and G.W. Scherer, *A review of salt scaling: I. Phenomenology.* Cement and Concrete Research, 2007. **37**(7): p. 1007-1021.

39. Valenza II, J.J. and G.W. Scherer, *A review of salt scaling: II. Mechanisms.* Cement and Concrete Research, 2007. **37**(7): p. 1022-1034.

40. Du, L. and K.J. Folliard, *Mechanisms of air entrainment in concrete.* Cement and Concrete Research, 2005. **35**(8): p. 1463-1471.

41. Powers, T.C., *Void spacing as a basis for producing air-entrained concrete.* Journal of the American Concrete Institute, 1954. **50**(9): p. 741-760.

42. Powers, T.C. *The Air Requirement of Frost-Resistant Concrete*. 1949. Highway Research Board 29, PCA Bull 33.

43. Ghazy, A. and M.T. Bassuoni, *Resistance of concrete to different exposures with chloride-based salts.* Cement and Concrete Research, 2017. **101**: p. 144-158.

44. Liu, Z. and W. Hansen, *Freezing characteristics of air-entrained concrete in the presence of deicing salt.* Cement and Concrete Research, 2015. **74**: p. 10-18.

45. Setzer, M.J., *Frost-attack on concrete - modeling by the micro-ice-lens model - evaluating by RILEM CIF test.* Creep, Shrinkage and Durability Mechanics of Concrete and Concrete Structures, 2009: p. 971-977.

46. Setzer, M.J., S. Palecki, and F. Tauscher, *Einfluss der NaCl konzentration auf das abwitterungsverhalten von beton unter frost-tausalzbelastung.* Forschungsbericht BAST, 2007.

47. Marchand, J., et al., *Influence of Chloride Solution Concentration on Deicer Salt Scaling Deterioration of Concrete.* ACI Materials Journal, 1999. **96**(4): p. 429-435.

48. G., F., *Studies of the Scaling, the Water Uptake and the Dilation of Mortar Specimens Exposed to Freezing and Thawing in NaCl Solutions*, in *Freeze-Thaw and De-Icing Resistance of Concrete*, G. Fagerlund and M.J. Setzer, Editors. 1992, Lund Institute of Technology: Lund, Sweden. p. 36-66.

49. Sellevold, E.J. and T. Farstad, *Frost/Salt-testing of Concrete: Effect of Test Parameters and Concrete Moisture History.* 1991.

50. Thomas, M., *Optimizing the use of fly ash in concrete*, in *Portland Cement Association*. 2007: IL, Skokie, 5420 Old Orchard Road.

51. Uysal, M. and V. Akyuncu, *Durability performance of concrete incorporating Class F and Class C fly ashes.* Construction and Building Materials, 2012. **34**: p. 170-178.

52. Lothenbach, B., K. Scrivener, and R.D. Hooton, *Supplementary cementitious materials.* Cement and Concrete Research, 2011. **41**(12): p. 1244-1256.

53. Toutanji, H., et al., *Effect of supplementary cementitious materials on the compressive strength and durability of short-term cured concrete.* Cement and Concrete Research, 2004. **34**(2): p. 311-319.

54. Papadakis, V.G., *Effect of supplementary cementing materials on concrete resistance against carbonation and chloride ingress.* Cement and Concrete Research, 2000. **30**(2): p. 291-299.

55. J., T.C.P.M.M. *Influence of supplementary cementing materials on the de-icer salt scaling resistance of concrete*. in *Proceeding of the 7th international conference on durability of building materials and components, 7DBMC*. 1996. Stockholm, Sweden.

56. Anonymous, *SS-EN 1097-6:2013*, in *Tests for mechanical and physical properties of aggregates - Part 6: Determination of particle density and water absorption*. 2013.

57. E-701, A.C., *Chemical admixtures for concrete*, in *ACI Education Bulletin E4-12*. 2013.

58. Edmeades, R.M. and P.C. Hewlett, *15 - Cement Admixtures*, in *Lea's Chemistry of Cement and Concrete (Fourth Edition)*. 1998, Butterworth-Heinemann: Oxford. p. 841-905.

59. SS-EN1367-1, *SS-EN 1367-1:2007*, in *Tests for thermal and weathering properties of aggregates - Part 1: Determination of resistance to freezing and thawing*. 2007.

60. SS-EN12620, *SS-EN 12620+A1:2008*, in *Aggregates for concrete*. 2008.

61. Standard, S., *SS-EN 1097-6:2013 Tests for mechanical and physical properties of aggregates - Part 6: Determination of particle density and water absorption*. 2013.

62. SS-EN1367-2, *SS-EN 1367-2:2009*, in *Tests for thermal and weathering properties of aggregates - Part 2: Magnesium sulfate test*. 2009.

63. Scrivener, K.L., A.K. Crumbie, and P. Laugesen, *The interfacial transition zone (ITZ) between cement paste and aggregate in concrete.* Interface science, 2004. **12**(4): p. 411-421.

64. Pang, B., et al., *ITZ properties of concrete with carbonated steel slag aggregate in salty freeze-thaw environment.* Construction and Building Materials, 2016. **114**: p. 162-171.

65. Wu, K., et al., *Microstructural characterization of ITZ in blended cement concretes and its relation to transport properties.* Cement and Concrete Research, 2016. **79**: p. 243-256.

66. Powers, T.C., *A Working Hypothesis for Further Studies of Frost Resistance of Concrete.* Journal of the American Concrete Institute, 1945. **16**(4): p. 245-272.

67. Terzaghi, R.D., et al., *Discussion of the paper A working hypothesis for further studies of frost resistance of concrete.* Journal of the American Concrete Institute, 1946. **41**: p. 272-1 to 272-20.

68. Powers, T.C. and R.A. Helmuth, *Theory of volume changes in hardened portland-cement paste during freezing.* Proceedings, Highway Research Board 32, PCA Bull 46, 1953.

69. Powers, T.C., *The mechanism of frost action in concrete (Part II).* Cement, Lime and Gravel, 1966. **41**(6): p. 5.

70. Liu, Z., *Frost Deterioration in Concrete due to Deicing Salt Exposure: Mechanism, Mitigation and Conceptual Surface Scaling Model*. 2014, University of Michigan. p. 211.

71. Liu, Z., W. Hansen, and F. Wang, *Pumping effect to accelerate liquid uptake in concrete and its implications on salt frost durability.* Construction and Building Materials, 2018. **158**: p. 181-188.

72. Yuan, J., et al., *Mechanisms on the Salt–Frost Scaling of Concrete.* Journal of Materials in Civil Engineering Structures, 2017. **29**(3).

73. Liu, Z. and W. Hansen, *A hypothesis for salt frost scaling in cementitious materials.* Journal of Advanced Concrete Technology, 2015. **13**: p. 403-414.

74. Valenza II, J.J., *Mechanism for Salt Scaling*, in *Civil and Environmental Engineering*. 2005, Princeton University. p. 362.

75. ASTM, *ASTM C672/C672M-12*, in *Standard test method for scaling resistance of concrete surfaces exposed to deicing chemicals*. 2012.

76. CEN/TS, *CEN/TS 12390-9* in *Testing hardened concrete - Part 9: Freeze-thaw resistance - Scaling*. 2006. p. 24.

77. BNQ, S.o.t.P.o.Q., *NQ 2621-900*. 2002: Montréal, Quebec, Canada.

78. Sun, Z. and G.W. Scherer, *Effect of air voids on salt scaling and internal freezing.* Cement and Concrete Research, 2009. **40**: p. 260-270.

79. ASTM, *ASTM C457 / C457M - 12, Standard Test Method for Microscopical Determination of Parameters of the Air-Void System in Hardened Concrete*. 2012.

80. Philleo, R., *A method for analysing void distribution in air-entrained concrete.* Cement, Concrete and Aggregates, 1983. **5**(2): p. 128-130.

81. Attiogbe, E.K., *Mean Spacing of Air Voids in Hardened Concrete.* Aci Materials Journal, 1993. **90**(2): p. 174-181.

82. Pleau, R. and M. Pigeon, *The use of the flow length concept to assess the efficiency of air entrainment with regards to frost durability: Part I - Description of the test method.* Cement, Concrete and Aggregates, 1996. **18**(1): p. 19-29.

83. Plante, P., M. Pigeon, and F. Saucier, *Air-Void Stability .2. Influence of Superplasticizers and Cement.* Aci Materials Journal, 1989. **86**(6): p. 581-589.

84. Pigeon, M., et al., *Influence of soluble alkalies on the production and stability of the air-void system in superplasticized and nonsuperplasticized concrete.* ACI Materials Journal, 1992. **89**(1): p. 24-31.

85. Hasholt, M.T., *Air void structure and frost resistance: a challenge to Powers' spacing factor.* Materials and Structures, 2012. **47**(5): p. 911-923.

86. Haynes, W.M., *CRC Handbook of Chemistry and Physics 93rd edition*, ed. W.M. Haynes. 2012.

87. Matalkah, F. and P. Soroushian, *Freeze thaw and deicer salt scaling resistance of concrete prepared with alkali aluminosilicate cement.* Construction and Building Materials, 2018. **163**: p. 200-213.

88. EN196-6, *Methods of testing cement- Part 6: Determination of fineness*. 2010.

89. EN196-3, *Methods of testing cement - Part 3: Determination of setting times and soundness*. 2005.

90. Strand, M.J. and K. Fridh, *Methodology to analyse the salt frost scaling mechanism(s) in concrete with different binders*, in *Materials, Systems and Structures in Civil Engineering 2016*. 2016: Technical University of Denmark, Copenhagen, Denmark.

91. Scherer, G.W., *Crystallization in pores.* Cement and Concrete Research, 1999. **29**(8): p. 1347-1358.

92. Wu, M. and B. Johannesson, *Impact of sample saturation on the detected porosity of hardened concrete using low temperature calorimetry.* Thermochimica Acta, 2014. **580**: p. 66-78.

93. Fagerlund, G., *Non-freezable water contents of porous building materials*. 1974, Lund Institute of Technology: Lund, Sweden. p. 186.

94. Wu, M., B. Johannesson, and M. Geiker, *Determination of ice content in hardened concrete by low-temperature calorimetry Influence of baseline calculation and heat of fusion of confined water.* Journal of Thermal Analysis and Calorimetry, 2014. **115**(2): p. 1335-1351.

95. Strand, M.J. and K. Fridh, *De-Icing Salt Frost Scaling part 2: Concrete containing Ground Granulated Blast-Furnace Slag*. Manuscript, Lund University.

96. Strand, M.J. and K. Fridh, *De-Icing Salt Frost Scaling part 1: Concrete containing Low Calcium Fly Ash*. Manuscript, Lund University.

97. Strand, M.J. and K. Fridh, *De-Icing Salt Frost Scaling in Concrete containing Fly Ash or Slag - Influence from Drying and Carbonation, Air Content, and Concentration of Salt Solution*. Manuscript, Lund University.

Appendix

Appendix A – Test of admixture combinations

Materials and results

The method and materials are presented in [90]. A 6-kg mass of aggregates with fraction sizes between 0 and 8 mm is mixed with a 2-kg binder. The water–binder ratio is 0.40, and the amount of air-entraining agent is set as the average amount recommended by the manufacturer in relation to the binder mass. The superplasticiser is added until one of two events occurs during mixing—either the workability would be 130 mm when measured with a Hägermann cone, or bleeding would occur on the surface.

Table 7
XRF analysis of CEM I and binder combinations.

Binder	CaO[1] [%]	SiO_2[1] [%]	Al_2O_3[1] [%]	Fe_2O_3[1] [%]	MgO[1] [%]	K_2O[1] [%]	Na_2O [%]	Na_2Oe[2] [%]	SO_3[1] [%]	LOI[1] [%]
CEM I	63.60	21.30	3.80	4.56	0.86	0.65	0.07	0.50	2.45	1.84
LCFA	3.53	57.00	21.60	7.33	1.95	2.16	0.00	1.42	0.65	2.71
F20	52.40	28.60	7.38	5.17	1.09	1.00	0.25	0.91	2.05	2.00
F35	44.00	33.50	9.88	5.52	1.26	1.24	0.38	1.20	1.78	2.09
Slag[3]	33.08	34.11	13.01	0.50	15.07	0.92	0.59	1.20	3.27	
S20	57.80	23.90	5.61	3.78	3.68	0.699	0.17	0.63	2.60	1.17
S35	52.70	25.90	7.10	3.11	5.92	0.748	0.26	0.75	2.76	0.56
S70	41.60	29.90	10.20	1.67	10.7	0.842	0.44	1.00	3.02	-0.59
K35	54.10	22.90	5.94	3.11	4.77	0.685	0.21	0.66	2.40	5.04

[1] The measurement precisions are CaO±0.233%, SiO_2±0.100%, Al_2O_3±0.052%, Fe_2O_3±0.019%, MgO±0.025%, K_2O±0.032%, SO_3±3%, and (loss on ignition=) LOI ±0.18%.

[2] Na_2O-equivalent from K_2O and Na_2O.

[3] Average values calculated based on measurements performed on S20, S35, and S70.

The XRF analysis shows that the LCFA has its Na_2O-equivalent approximately three times larger than that of CEM I. The slag has a slightly lower Na_2O-equivalent compared with that of the LCFA.

Table 8
ICP analysis of CEM I and binder combination with low-calcium fly ash.

Binder	ICP analysis[1] [%]		
	K_2O	Na_2O	Na_2Oe
CEM I	0.44	0.03	0.32
F20	0.35	0.03	0.26
F35	0.29	0.04	0.23

[1] ICP analysis of soluble K_2O, Na_2O and Na_2O-equivalent in H_2O according to 'CR 0401' method.

The ICP results and soluble alkalis in water show that alkalis in the fly ash are not as soluble in water as do alkalis in CEM I.

Table 9–

Table 16 summarise the amount of superplasticisers added in relation to the maximum recommended amount, indication of water separation, measured air content, workability using the Hägermann cone, and amount of foam created in the dispersion test.

Table 9
Test of admixture combination with CEM I as binder.

Combination	Superplasticiser[1], %	Indication of water separation	Air content, %	Workability, mm	Foam
SP1[2]+AEA1[3]	112.0	Slight	9.6	170	Medium
SP2[2]+AEA1	126.8	Clear	5.2	170	Medium
SP3[2]+AEA1	126.5	Clear	7.2	175	Medium
SP4[2]+AEA1	257.8	Slight	15.1	155	Considerable'
SP5[2]+AEA1	196.7	No	12.5	170	Considerable'
SP1+AEA2[3]	417.3	Clear	4.3	175	Low
SP2+AEA2	244.8	Clear	6.0	165	Medium
SP3+AEA2	103.8	Clear	18.5	120	Medium
SP4+AEA2	318.0	Slight	5.2	150	Medium
SP5+AEA2	125.7	No	11.5	180	Considerable'
SP1+AEA3[3]	65.0	Slight	13.5	225	Considerable'
SP2+AEA3	37.0	Slight	18,5	140	Considerable'
SP3+AEA3	33.0	Slight	15.0	185	Considerable'
SP4+AEA3	69.5	No	20.0	120	Considerable'
SP5+AEA3	68.3	No	21.5	130	Considerable'

Table 10
Test of admixture combination with 20 mass% LCFA + 80 mass% CEM I as binder.

Combination	Superplasticiser[1], %	Indication of water separation	Air content, %	Workability, mm	Foam
SP1[2]+AEA1[3]	65.3	Slight	11.0	135	Medium
SP2[2]+AEA1	97.0	Slight	9.7	135	Considerable'
SP3[2]+AEA1	87.3	Slight	8.3	120	Considerable'
SP4[2]+AEA1	97.8	Slight	9.8	115	Considerable'
SP5[2]+AEA1	129.7	Slight	14.8	125	Considerable'
SP1+AEA2[3]	137.3	Clear	4.8	110	Low
SP2+AEA2	60.0	Clear	8.0	155	Medium
SP3+AEA2	49.8	Clear	6.1	125	Medium
SP4+AEA2	117.0	Slight	9.5	110	Considerable'
SP5+AEA2	75.0	Slight	11.5	165	Considerable'
SP1+AEA3[3]	60.3	Slight	9.8	180	Considerable'
SP2+AEA3	57.0	No	15.0	145	Considerable'
SP3+AEA3	31.8	No	14.2	135	Considerable'
SP4+AEA3	44.5	No	15.2	110	Considerable'
SP5+AEA3	21.7	Slight	17.5	110	Considerable'

Table 11
Test of admixture combination with 35 mass% LCFA + 65 mass% CEM I as binder.

Combination	Superplasticiser[1], %	Indication of water separation	Air content, %	Workability, mm	Foam
SP1[2]+AEA1[3]	93.0	Slight	8.9	150	Considerable'
SP2[2]+AEA1	67.3	Slight	10.6	150	Considerable'
SP3[2]+AEA1	85.3	Slight	7.8	120	Considerable'
SP4[2]+AEA1	143.0	Slight	9.0	120	Medium
SP5[2]+AEA1	111.7	Slight	14.5	140	Considerable'
SP1+AEA2[3]	109.0	Clear	3.2	115	Low
SP2+AEA2	130.0	Clear	5.3	135	Medium
SP3+AEA2	156.3	Slight	4.8	110	Low
SP4+AEA2	100.5	Clear	8.0	155	Medium
SP5+AEA2	183.0	Clear	5.2	120	Medium
SP1+AEA3[3]	118.0	Clear	6.5	120	Medium
SP2+AEA3	80.0	Slight	9.8	160	Medium
SP3+AEA3	82.3	Slight	6.6	135	Medium
SP4+AEA3	78.5	No	13.1	140	Considerable'
SP5+AEA3	115.7	Slight	15.1	150	Considerable'

Table 12
Test of admixture combination with 20 mass% slag + 80 mass% CEM I as binder.

Combination	Superplasticiser[1], %	Indication of water separation	Air content, %	Workability, mm	Foam
SP1[2]+AEA1[3]	33.7	Slight	14.6	130	Considerable'
SP2[2]+AEA1	12.3	Slight	14.0	115	Considerable'
SP3[2]+AEA1	11.5	Slight	16.7	110	Considerable'
SP4[2]+AEA1	18.0	Slight	16.5	110	Considerable'
SP5[2]+AEA1	91.0	Slight	16.8	110	Considerable'
SP1+AEA2[3]	50.7	Slight	9.4	175	Considerable'
SP2+AEA2	37.5	Slight	9.8	190	Considerable'
SP3+AEA2	75.5	Clear	6.2	115	Low
SP4+AEA2	57.8	Slight	15.5	110	Medium
SP5+AEA2	119.3	Slight	12.9	150	Considerable'
SP1+AEA3[3]	74.3	Slight	13.6	170	Considerable'
SP2+AEA3	69.0	Slight	14.9	170	Considerable'
SP3+AEA3	77.0	Slight	10.7	160	Considerable'
SP4+AEA3	84.0	Slight	16.7	110	Considerable'
SP5+AEA3	96.3	No	19.8	140	Considerable'

Table 13
Test of admixture combination with 35 mass% slag + 65 mass% CEM I as binder.

Combination	Superplasticiser[1], %	Indication of water separation	Air content, %	Workability, mm	Foam
SP1[2]+AEA1[3]	126.0	Clear	6.6	125	Medium
SP2[2]+AEA1	93.8	Clear	9.9	135	Considerable'
SP3[2]+AEA1	100.8	Clear	7.7	130	Considerable'
SP4[2]+AEA1	111.3	Slight	11.3	130	Considerable'
SP5[2]+AEA1	105.7	No	16.8	145	Considerable'
SP1+AEA2[3]	125.7	Clear	5.5	120	Medium
SP2+AEA2	78.3	Clear	10.7	125	Considerable'
SP3+AEA2	57.3	Clear	7.5	145	Considerable'
SP4+AEA2	80.5	Slight	17.0	125	Considerable'
SP5+AEA2	79.0	No	15.5	150	Considerable'
SP1+AEA3[3]	58.3	Slight	13.2	190	Considerable'
SP2+AEA3	62.8	Slight	15.8	180	Considerable'
SP3+AEA3	71.0	Clear	11.0	180	Considerable'
SP4+AEA3	69.0	Slight	14.6	105	Considerable'
SP5+AEA3	82.7	No	21.0	150	Considerable'

Table 14
Test of admixture combination with 70 mass% slag + 30 mass% CEM I as binder.

Combination	Superplasticiser[1], %	Indication of water separation	Air content, %	Workability, mm	Foam
SP1[2]+AEA1[3]	113.3	Clear	5.9	120	Considerable'
SP2[2]+AEA1	45.5	No	15.4	150	Considerable'
SP3[2]+AEA1	51.3	Slight	9.5	185	Considerable'
SP4[2]+AEA1	60.8	Slight	18.5	125	Considerable'
SP5[2]+AEA1	81.7	No	18.0	150	Considerable'
SP1+AEA2[3]	72.0	Clear	6.6	155	Considerable'
SP2+AEA2	41.5	No	14.2	150	Considerable'
SP3+AEA2	48.8	Slight	9.6	145	Considerable'
SP4+AEA2	56.0	No	15.7	130	Considerable'
SP5+AEA2	52.7	No	17.0	130	Considerable'
SP1+AEA3[3]	55.7	Slight	11.5	225	Considerable'
SP2+AEA3	29.8	No	20.0	130	Considerable'
SP3+AEA3	37.5	Slight	16.5	165	Considerable'
SP4+AEA3	41.8	Slight	19.0	115	Considerable'
SP5+AEA3	51.7	Slight	20.5	125	Considerable'

Table 15
Test of admixture combination with 25 mass% slag + 10 mass% LF + 65 mass% CEM I as binder.

Combination	Superplasticiser[1], %	Indication of water separation	Air content, %	Workability, mm	Foam
SP1[2]+AEA1[3]	91.3	Slight	8.5	125	Medium
SP2[2]+AEA1	81.5	Slight	10.7	135	Considerable'
SP3[2]+AEA1	119.3	Clear	5.3	120	Medium
SP4[2]+AEA1	79.3	Slight	13.4	110	Considerable'
SP5[2]+AEA1	91.0	Slight	18.2	125	Considerable'
SP1+AEA2[3]	17.0	Clear	5.0	120	Low
SP2+AEA2	81.0	Clear	8.3	110	Medium
SP3+AEA2	72.5	Clear	5.8	120	Considerable'
SP4+AEA2	91.3	Slight	16.0	130	Considerable'
SP5+AEA2	71.7	No	16.8	125	Considerable'
SP1+AEA3[3]	67.3	Slight	11.0	170	Considerable'
SP2+AEA3	62.3	Slight	15.2	180	Considerable'
SP3+AEA3	59.0	Slight	11.2	170	Considerable'
SP4+AEA3	80.3	Slight	11.1	110	Considerable'
SP5+AEA3	90.3	No	19.5	155	Considerable'

Table 16
Summary of combinations used.

Binders	Superplasticiser[1)] [%]	Indication of water separation	Air content [%]	Workability [mm]	Foam
CEM I	68,3	No	21,5	130	Considerable'
F20	44.5	No	15.2	110	Considerable'
F35	78.5	No	13.1	140	Considerable'
S20	96.3	No	19.8	140	Considerable'
S35	82.7	No	21.0	150	Considerable'
S70	51.7	Slight	20.5	125	Considerable'
K35	90.3	No	19.5	155	Considerable'

The results enable a choice of admixture combination for each binder to minimise the risk of bleeding.

SWEDAC ACKREDITERING
2026
ISO/IEC 17025

PROVRESULTAT

utfärdat av ackrediterat provningslaboratorium

CEMENTA
HEIDELBERGCEMENT Group
Cementa Research

Provnr: 168949

Cementa AB
Stefan Sandelin, ref 205875
Box 47210
10074 STOCKHOLM

2015-10-05

Provnr	168949		
Märkning	LTH Referensprov 0; Degerhamn anläggningscement		
Uppdrag / grupp	Analyser för LTH-doktorand		
Variant		Ankomstdatum	2015-06-18
Handläggare	Karin Lindhe	Klardatum	2015-10-05
Provtagningsdatum	2015-06-17		
Provtagning	Insänt av kund		
Provtagare			

Namn (Karin Fagerström)

* ej ackrediterad analys

Analys	Metod	Resultat	Mätosäkerhet	Kommentar
Leco Apparatur				
Gl.f 950°C	ER 9213 :2005	1,84 **%**	**0,18 %**	
Bogue Beräkningar				
* C2S	Saknas	15,7 **%**		
* C3S	Saknas	60,4 **%**		
C3A	ER 9226	2,4 **%**		
* C4AF	Saknas	13,9 **%**		
Fysikaliska Bestämningar				
Densitet	ER 9228	3226 **kg/m3**	**40 kg/m3**	
Blaine, manuell	EN 196-6 :2010	343 **m2/kg**	**3 %**	
Bindetid				
Vatten	EN 196-3 :2005	26,0 **%**	**3,7 %**	
Vicat vatten	EN 196-3 :2005	195 **min**	**4 %**	
Normprov Tryckhållfasthet				
2 d	EN 196-1 :2005	21,8 **MPa**	**5 %**	
28 d	EN 196-1 :2005	55,1 **MPa**	**5 %**	
56 d	EN 196-1 :2005	62,3 **MPa**	**5 %**	
91 d	EN 196-1 :2005	66,1 **MPa**	**5 %**	
Std.av. 2 dygn	EN 196-1 :2005	0,3 **MPa**	**5 %**	
Std.av. 28 dygn	EN 196-1 :2005	0,3 **MPa**	**5 %**	
Std.av. 56 dygn	EN 196-1 :2005	1,2 **MPa**	**5 %**	
Std.av. 91 dygn	EN 196-1 :2005	2,0 **MPa**	**5 %**	
ICP-Analys				
* K2O H2O-lösl	CR 0401	0,21 **%**		
* Na2O H2O-lösl	CR 0401	0,02 **%**		
XRF - Cement - wroxi				
Na2O-ekvivalent	ER 9214	0,50 **%**		
CaO	ER 9214	63,6 **%**	**0,233 %abs**	
SiO2	ER 9214	21,3 **%**	**0,100 %abs**	
Al2O3	ER 9214	3,80 **%**	**0,052 %abs**	
Fe2O3	ER 9214	4,56 **%**	**0,019 %abs**	

Cementa Research
Skeppargatan 1
P.O Box 104
SE-624 22 Slite
Sweden

Phone +46 (0)498-28 11 00
Fax +46 (0)498-28 13 91
www.cementaresearch.se
johan.larsson@cementa.se
VAT no. SE556102778901

MgO	ER 9214	0,856 **%**	**0,025 %abs**
K2O	ER 9214	0,650 **%**	**0,032 %abs**
Na2O	ER 9214	0,07 **%**	
Partikelstorleksdistribution (Laserdiffraktionsteknik)			
D(0.5)	ER 9322	17,305 **µm**	
LECO instrument CS 230			
SO3	ER 9212	2,45 **%**	**3 %**
CO2	ER 9212	0,93 **%**	**3 %**
* Kalksten beräknad Degerhamn	Saknas	2,36 **%**	

Partikelstorleksdistribution (Laserdiffraktionsteknik)

Analys	**Siktstorlek**	**Passerande på sikt**
Enhet	µm	%
Metod	ER 9322	ER 9322
Mätosäkerhet		
RAD		
1	1,00	0,49
2	1,20	0,86
3	1,40	1,30
4	1,60	1,78
5	1,80	2,32
6	2,00	2,90
7	2,20	3,51
8	2,60	4,81
9	3,00	6,20
10	3,50	7,99
11	4,00	9,83
12	4,50	11,68
13	5,00	13,52
14	5,50	15,34
15	6,30	18,19
16	7,00	20,62
17	8,00	23,98
18	9,00	27,22
19	10,00	30,33
20	12,00	36,23
21	15,00	44,33
22	16,00	46,85
23	18,00	51,62
24	20,00	56,04
25	22,00	60,13
26	25,00	65,67
27	28,00	70,54
28	32,00	76,07
29	36,00	80,65
30	40,00	84,41
31	45,00	88,16
32	50,00	91,06
33	56,00	93,68
34	63,00	95,84
35	75,00	98,06
36	90,00	99,35
37	106,0	99,93
38	125,0	100,0

Cementa Research
Skeppargatan 1
P.O Box 104
SE-624 22 Slite
Sweden

Phone +46 (0)498-28 11 00
Fax +46 (0)498-28 13 91
www.cementaresearch.se
johan.larsson@cementa.se
VAT no. SE556102778901

39	150,0	100,0
40	175,0	100,0
41	200,0	100,0
42	225,0	100,0
43	250,0	100,0
44	280,0	100,0
45	315,0	100,0

Delges **Cementa AB , Stefan Sandelin, ref 205875**
Cementa AB , Erik Viggh, ref 183100
Cementa AB , Mikael Westerholm

Mätosäkerhet enligt "SWEDAC:s policy för mätosäkerhet vid kalibrering och provning", SWEDAC DOC 04:05. Den angivna mätosäkerheten är beräknad med täckningsfaktor 2, vilket ger konfidensnivå på ca 95%. Mätosäkerheten anges som (%) relativ eller absolut(abs%) eller i övrigt gällande enhet t.ex. Mpa, mg/kg.

* SLUT PÅ RAPPORTEN *

Cementa Research
Skeppargatan 1
P.O Box 104
SE-624 22 Slite
Sweden

Phone +46 (0)498-28 11 00
Fax +46 (0)498-28 13 91
www.cementaresearch.se
johan.larsson@cementa.se
VAT no. SE556102778901

PROVRESULTAT

CEMENTA
HEIDELBERGCEMENT Group
Cementa Research

Cementa AB
Erik Viggh, ref 183100
Dockplatsen 1
211 19 MALMÖ

2016-04-29

Provnr	171102		
Märkning	Anl.cem.		
Uppdrag / grupp	Analyser för LTH-doktorand - Refnr: 121034856142		
Variant		Ankomstdatum	2016-04-11
Handläggare	Stina Hammar	Klardatum	2016-04-29
Provtagningsdatum	2016-04-25		
Provtagning	Insänt av kund		
Provtagare			

Namn (Stina Hammar)

* ackrediterad analys

Analys	Metod	Resultat	Mätosäkerhet	Kommentar
ICP-Analys				
Na2O-ekvivalent H2O-löslig	Saknas	0,32 %		
K2O H2O-lösl	CR 0401	0,44 %		
Na2O H2O-lösl	CR 0401	0,03 %		

Delges **Cementa AB , Erik Viggh, ref 183100**
Cementa AB , Mikael Westerholm

Mätosäkerhet enligt "SWEDAC:s policy för mätosäkerhet vid kalibrering och provning", SWEDAC DOC 04:05. Den angivna mätosäkerheten är beräknad med täckningsfaktor 2, vilket ger konfidensnivå på ca 95%. Mätosäkerheten anges som (%) relativ eller absolut(abs%) eller i övrigt gällande enhet t.ex. Mpa, mg/kg.

* SLUT PÅ RAPPORTEN *

Cementa Research
Skeppargatan 1
P.O Box 104
SE-624 22 Slite
Sweden

Phone +46 (0)498-28 11 00
Fax +46 (0)498-28 13 91
www.cementaresearch.se
johan.larsson@cementa.se
VAT no. SE556102778901

SWEDAC ACKREDITERING
2026
ISO/IEC 17025

PROVRESULTAT

utfärdat av ackrediterat provningslaboratorium

CEMENTA
HEIDELBERGCEMENT Group
Cementa Research

Cementa AB
Stefan Sandelin, ref 205875
Box 47210
10074 STOCKHOLM

2015-10-14

Provnr	168951		
Märkning	LTH F20; Degerhamn anläggningscement + FA		
Uppdrag / grupp	Analyser för LTH-doktorand		
Variant		Ankomstdatum	2015-06-18
Handläggare	Karin Lindhe	Klardatum	2015-10-14
Provtagningsdatum	2015-06-17		
Provtagning	Insänt av kund		
Provtagare			

Namn (Karin Lindhe)

* ej ackrediterad analys

Analys	Metod	Resultat	Mätosäkerhet	Kommentar
Leco Apparatur				
Gl.f 950°C	ER 9213 :2005	2,00 **%**	**0,18 %**	
Gravimetrisk Analys				
* Flygaska-halt inkl. gips	Saknas	17,4 **%**		
Fysikaliska Bestämningar				
Densitet	ER 9228	2988 **kg/m3**	**40 kg/m3**	
Blaine, manuell	EN 196-6 :2010	340 **m2/kg**	**3 %**	
Bindetid				
Vatten	EN 196-3 :2005	26,0 **%**	**3,7 %**	
Vicat vatten	EN 196-3 :2005	215 **min**	**4 %**	
Normprov Tryckhållfasthet				
2 d	EN 196-1 :2005	17,0 **MPa**	**5 %**	
28 d	EN 196-1 :2005	45,5 **MPa**	**5 %**	
56 d	EN 196-1 :2005	56,4 **MPa**	**5 %**	
91 d	EN 196-1 :2005	62,7 **MPa**	**5 %**	
Std.av. 2 dygn	EN 196-1 :2005	0,3 **MPa**	**5 %**	
Std.av. 28 dygn	EN 196-1 :2005	1,0 **MPa**	**5 %**	
Std.av. 56 dygn	EN 196-1 :2005	0,6 **MPa**	**5 %**	
Std.av. 91 dygn	EN 196-1 :2005	1,5 **MPa**	**5 %**	
ICP-Analys				
* K2O H2O-lösl	CR 0401	0,35 **%**		
* Na2O H2O-lösl	CR 0401	0,03 **%**		
TGA				
* CaCO3	Saknas	2,12 **%**		
XRF - Cement - wroxi				
Na2O-ekvivalent	ER 9214	0,91 **%**		
CaO	ER 9214	52,4 **%**	**0,233 %abs**	
SiO2	ER 9214	28,6 **%**	**0,100 %abs**	
Al2O3	ER 9214	7,38 **%**	**0,052 %abs**	
Fe2O3	ER 9214	5,17 **%**	**0,019 %abs**	
MgO	ER 9214	1,09 **%**	**0,025 %abs**	

Cementa Research
Skeppargatan 1
P.O Box 104
SE-624 22 Slite
Sweden

Phone +46 (0)498-28 11 00
Fax +46 (0)498-28 13 91
www.cementaresearch.se
johan.larsson@cementa.se
VAT no. SE556102778901

K2O	ER 9214	0,996 **%**	**0,032 %abs**
Na2O	ER 9214	0,25 **%**	

Partikelstorleksdistribution (Laserdiffraktionsteknik)

D(0.5)	ER 9322	18,097 **µm**	

LECO instrument CS 230

SO3	ER 9212	2,05 **%**	**3 %**

Partikelstorleksdistribution (Laserdiffraktionsteknik)

Analys	**Siktstorlek**	**Passerande på sikt**
Enhet	µm	%
Metod	ER 9322	ER 9322
Mätosäkerhet		
RAD		
1	1,00	0,46
2	1,20	0,86
3	1,40	1,33
4	1,60	1,85
5	1,80	2,43
6	2,00	3,04
7	2,20	3,69
8	2,60	5,07
9	3,00	6,50
10	3,50	8,36
11	4,00	10,23
12	4,50	12,10
13	5,00	13,95
14	5,50	15,77
15	6,30	18,61
16	7,00	21,00
17	8,00	24,27
18	9,00	27,38
19	10,00	30,34
20	12,00	35,85
21	15,00	43,26
22	16,00	45,53
23	18,00	49,80
24	20,00	53,73
25	22,00	57,34
26	25,00	62,22
27	28,00	66,52
28	32,00	71,43
29	36,00	75,54
30	40,00	78,98
31	45,00	82,50
32	50,00	85,33
33	56,00	88,00
34	63,00	90,37
35	75,00	93,13
36	90,00	95,17
37	106,0	96,43
38	125,0	97,29
39	150,0	97,92
40	175,0	98,29
41	200,0	98,56
42	225,0	98,77

Cementa Research
Skeppargatan 1
P.O Box 104
SE-624 22 Slite
Sweden

Phone +46 (0)498-28 11 00
Fax +46 (0)498-28 13 91
www.cementaresearch.se
johan.larsson@cementa.se
VAT no. SE556102778901

43	250,0	98,95
44	280,0	99,13
45	315,0	99,32
46	355,0	99,48
47	400,0	99,63
48	450,0	99,77
49	500,0	99,88
50	560,0	99,97
51	600,0	100,0
52	677,0	100,0

Delges **Cementa AB , Mikael Westerholm**
Cementa AB , Erik Viggh, ref 183100
Cementa AB , Stefan Sandelin, ref 205875

Ingen hänsyn tagen till renheten på kalkstenen.

Mätosäkerhet enligt "SWEDAC:s policy för mätosäkerhet vid kalibrering och provning", SWEDAC DOC 04:05. Den angivna mätosäkerheten är beräknad med täckningsfaktor 2, vilket ger konfidensnivå på ca 95%. Mätosäkerheten anges som (%) relativ eller absolut(abs%) eller i övrigt gällande enhet t.ex. Mpa, mg/kg.

* SLUT PÅ RAPPORTEN *

Cementa Research
Skeppargatan 1
P.O Box 104
SE-624 22 Slite
Sweden

Phone +46 (0)498-28 11 00
Fax +46 (0)498-28 13 91
www.cementaresearch.se
johan.larsson@cementa.se
VAT no. SE556102778901

PROVRESULTAT

Cementa Research

Cementa AB
Erik Viggh, ref 183100
Dockplatsen 1
211 19 MALMÖ

2016-04-29

Provnr	171103		
Märkning	F20		
Uppdrag / grupp	Analyser för LTH-doktorand - Refnr: 121034856142		
Variant		Ankomstdatum	2016-04-11
Handläggare	Stina Hammar	Klardatum	2016-04-29
Provtagningsdatum	2016-04-25		
Provtagning	Insänt av kund		
Provtagare			

Namn (Stina Hammar)

* ackrediterad analys

Analys	Metod	Resultat	Mätosäkerhet	Kommentar
ICP-Analys				
Na2O-ekvivalent H2O-löslig	Saknas	0,26 %		
K2O H2O-lösl	CR 0401	0,35 %		
Na2O H2O-lösl	CR 0401	0,03 %		

Delges **Cementa AB , Mikael Westerholm**
Cementa AB , Erik Viggh, ref 183100

Mätosäkerhet enligt "SWEDAC:s policy för mätosäkerhet vid kalibrering och provning", SWEDAC DOC 04:05. Den angivna mätosäkerheten är beräknad med täckningsfaktor 2, vilket ger konfidensnivå på ca 95%. Mätosäkerheten anges som (%) relativ eller absolut(abs%) eller i övrigt gällande enhet t.ex. Mpa, mg/kg.

* SLUT PÅ RAPPORTEN *

Cementa Research
Skeppargatan 1
P.O Box 104
SE-624 22 Slite
Sweden

Phone +46 (0)498-28 11 00
Fax +46 (0)498-28 13 91
www.cementaresearch.se
johan.larsson@cementa.se
VAT no. SE556102778901

SWEDAC ACKREDITERING 2026 ISO/IEC 17025

PROVRESULTAT

utfärdat av ackrediterat provningslaboratorium

CEMENTA HEIDELBERGCEMENT Group
Cementa Research

Cementa AB
Stefan Sandelin, ref 205875
Box 47210
10074 STOCKHOLM

2015-10-14

Provnr	168952		
Märkning	LTH F35; Degerhamn anläggningscement + FA		
Uppdrag / grupp	Analyser för LTH-doktorand		
Variant		Ankomstdatum	2015-06-18
Handläggare	Karin Lindhe	Klardatum	2015-10-14
Provtagningsdatum	2015-06-17		
Provtagning	Insänt av kund		
Provtagare			

Namn (Karin Lindhe)

* ej ackrediterad analys

Analys	Metod	Resultat	Mätosäkerhet	Kommentar
Leco Apparatur				
Gl.f 950°C	ER 9213 :2005	2,09 **%**	**0,18 %**	
Gravimetrisk Analys				
* Flygaska-halt inkl. gips	Saknas	33,4 **%**		
Fysikaliska Bestämningar				
Densitet	ER 9228	2822 **kg/m3**	**40 kg/m3**	
Blaine, manuell	EN 196-6 :2010	328 **m2/kg**	**3 %**	
Bindetid				
Vatten	EN 196-3 :2005	26,0 **%**	**3,7 %**	
Vicat vatten	EN 196-3 :2005	210 **min**	**4 %**	
Normprov Tryckhållfasthet				
2 d	EN 196-1 :2005	13,3 **MPa**	**5 %**	
28 d	EN 196-1 :2005	37,4 **MPa**	**5 %**	
56 d	EN 196-1 :2005	49,6 **MPa**	**5 %**	
91 d	EN 196-1 :2005	56,9 **MPa**	**5 %**	
Std.av. 2 dygn	EN 196-1 :2005	0,2 **MPa**	**5 %**	
Std.av. 28 dygn	EN 196-1 :2005	0,4 **MPa**	**5 %**	
Std.av. 56 dygn	EN 196-1 :2005	1,1 **MPa**	**5 %**	
Std.av. 91 dygn	EN 196-1 :2005	0,6 **MPa**	**5 %**	
ICP-Analys				
* K2O H2O-lösl	CR 0401	0,28 **%**		
* Na2O H2O-lösl	CR 0401	0,04 **%**		
TGA				
* CaCO3	Saknas	1,75 **%**		
XRF - Cement - wroxi				
Na2O-ekvivalent	ER 9214	1,19 **%**		
CaO	ER 9214	44,0 **%**	**0,233 %abs**	
SiO2	ER 9214	33,5 **%**	**0,100 %abs**	
Al2O3	ER 9214	9,88 **%**	**0,052 %abs**	
Fe2O3	ER 9214	5,52 **%**	**0,019 %abs**	
MgO	ER 9214	1,26 **%**	**0,025 %abs**	

Cementa Research
Skeppargatan 1
P.O Box 104
SE-624 22 Slite
Sweden

Phone +46 (0)498-28 11 00
Fax +46 (0)498-28 13 91
www.cementaresearch.se
johan.larsson@cementa.se
VAT no. SE556102778901

K2O	ER 9214	1,24 %	**0,032 %abs**
Na2O	ER 9214	0,38 %	

Partikelstorleksdistribution (Laserdiffraktionsteknik)

D(0.5)	ER 9322	18,556 µm	

LECO instrument CS 230

SO3	ER 9212	1,78 %	**3 %**

Partikelstorleksdistribution (Laserdiffraktionsteknik)

Analys	**Siktstorlek**	**Passerande på sikt**
Enhet	µm	%
Metod	ER 9322	ER 9322
Mätosäkerhet		
RAD		
1	1,00	0,56
2	1,20	0,88
3	1,40	1,22
4	1,60	1,58
5	1,80	1,96
6	2,00	2,38
7	2,20	2,84
8	2,60	3,85
9	3,00	4,98
10	3,50	6,55
11	4,00	8,25
12	4,50	10,04
13	5,00	11,88
14	5,50	13,74
15	6,30	16,71
16	7,00	19,26
17	8,00	22,78
18	9,00	26,13
19	10,00	29,30
20	12,00	35,08
21	15,00	42,58
22	16,00	44,81
23	18,00	48,93
24	20,00	52,65
25	22,00	56,03
26	25,00	60,54
27	28,00	64,49
28	32,00	69,00
29	36,00	72,81
30	40,00	76,04
31	45,00	79,40
32	50,00	82,15
33	56,00	84,84
34	63,00	87,31
35	75,00	90,37
36	90,00	92,88
37	106,0	94,63
38	125,0	96,02
39	150,0	97,22
40	175,0	98,04
41	200,0	98,62
42	225,0	99,04

Cementa Research
Skeppargatan 1
P.O Box 104
SE-624 22 Slite
Sweden

Phone +46 (0)498-28 11 00
Fax +46 (0)498-28 13 91
www.cementaresearch.se
johan.larsson@cementa.se
VAT no. SE556102778901

43	250,0	99,36
44	280,0	99,64
45	315,0	99,85
46	355,0	99,94
47	400,0	99,99
48	450,0	100,0

Delges **Cementa AB , Stefan Sandelin, ref 205875**
Cementa AB , Erik Viggh, ref 183100
Cementa AB , Mikael Westerholm

Ingen hänsyn tagen till renheten på kalkstenen.

Mätosäkerhet enligt "SWEDAC:s policy för mätosäkerhet vid kalibrering och provning", SWEDAC DOC 04:05. Den angivna mätosäkerheten är beräknad med täckningsfaktor 2, vilket ger konfidensnivå på ca 95%. Mätosäkerheten anges som (%) relativ eller absolut(abs%) eller i övrigt gällande enhet t.ex. Mpa, mg/kg.

* SLUT PÅ RAPPORTEN *

Cementa Research
Skeppargatan 1
P.O Box 104
SE-624 22 Slite
Sweden

Phone +46 (0)498-28 11 00
Fax +46 (0)498-28 13 91
www.cementaresearch.se
johan.larsson@cementa.se
VAT no. SE556102778901

PROVRESULTAT

Cementa Research

Cementa AB
Erik Viggh, ref 183100
Dockplatsen 1
211 19 MALMÖ

2016-04-29

Provnr	171104		
Märkning	F35		
Uppdrag / grupp	Analyser för LTH-doktorand - Refnr: 121034856142		
Variant		Ankomstdatum	2016-04-11
Handläggare	Stina Hammar	Klardatum	2016-04-29
Provtagningsdatum	2016-04-25		
Provtagning	Insänt av kund		
Provtagare			

Namn (Stina Hammar)

* ackrediterad analys

Analys	Metod	Resultat	Mätosäkerhet	Kommentar
ICP-Analys				
Na2O-ekvivalent H2O-löslig	Saknas	0,23 %		
K2O H2O-lösl	CR 0401	0,29 %		
Na2O H2O-lösl	CR 0401	0,04 %		

Delges **Cementa AB , Mikael Westerholm**
Cementa AB , Erik Viggh, ref 183100

Mätosäkerhet enligt "SWEDAC:s policy för mätosäkerhet vid kalibrering och provning", SWEDAC DOC 04:05. Den angivna mätosäkerheten är beräknad med täckningsfaktor 2, vilket ger konfidensnivå på ca 95%. Mätosäkerheten anges som (%) relativ eller absolut(abs%) eller i övrigt gällande enhet t.ex. Mpa, mg/kg.

* SLUT PÅ RAPPORTEN *

Cementa Research
Skeppargatan 1
P.O Box 104
SE-624 22 Slite
Sweden

Phone +46 (0)498-28 11 00
Fax +46 (0)498-28 13 91
www.cementaresearch.se
johan.larsson@cementa.se
VAT no. SE556102778901

SWEDAC ACKREDITERING
2026
ISO/IEC 17025

PROVRESULTAT

utfärdat av ackrediterat provningslaboratorium

CEMENTA
HEIDELBERGCEMENT Group
Cementa Research

Cementa AB
Stefan Sandelin, ref 205875
Box 47210
10074 STOCKHOLM

2015-10-14

Provnr	168953		
Märkning	LTH S20; Degerhamn anläggningscement+ Slagg(Merit)		
Uppdrag / grupp	Analyser för LTH-doktorand		
Variant		Ankomstdatum	2015-06-18
Handläggare	Karin Lindhe	Klardatum	2015-10-14
Provtagningsdatum	2015-06-17		
Provtagning	Insänt av kund		
Provtagare			

Namn (Karin Lindhe)

* ej ackrediterad analys

Analys	Metod	Resultat	Mätosäkerhet	Kommentar
Leco Apparatur				
Gl.f 950°C	ER 9213 :2005	1,17 **%**	**0,18 %**	
Fysikaliska Bestämningar				
Densitet	ER 9228	3167 **kg/m3**	**40 kg/m3**	
Blaine, manuell	EN 196-6 :2010	371 **m2/kg**	**3 %**	
Bindetid				
Vatten	EN 196-3 :2005	26,0 **%**	**3,7 %**	
Vicat vatten	EN 196-3 :2005	215 **min**	**4 %**	
Normprov Tryckhållfasthet				
2 d	EN 196-1 :2005	16,5 **MPa**	**5 %**	
28 d	EN 196-1 :2005	52,1 **MPa**	**5 %**	
56 d	EN 196-1 :2005	63,3 **MPa**	**5 %**	
91 d	EN 196-1 :2005	65,3 **MPa**	**5 %**	
Std.av. 2 dygn	EN 196-1 :2005	0,2 **MPa**	**5 %**	
Std.av. 28 dygn	EN 196-1 :2005	0,8 **MPa**	**5 %**	
Std.av. 56 dygn	EN 196-1 :2005	1,3 **MPa**	**5 %**	
Std.av. 91 dygn	EN 196-1 :2005	1,3 **MPa**	**5 %**	
ICP-Analys				
* K2O H2O-lösl	CR 0401	0,35 **%**		
* Na2O H2O-lösl	CR 0401	0,03 **%**		
XRF - Cement - wroxi				
Na2O-ekvivalent	ER 9214	0,63 **%**		
CaO	ER 9214	57,8 **%**	**0,233 %abs**	
SiO2	ER 9214	23,9 **%**	**0,100 %abs**	
Al2O3	ER 9214	5,61 **%**	**0,052 %abs**	
Fe2O3	ER 9214	3,78 **%**	**0,019 %abs**	
MgO	ER 9214	3,68 **%**	**0,025 %abs**	
K2O	ER 9214	0,699 **%**	**0,032 %abs**	
Na2O	ER 9214	0,17 **%**		
Partikelstorleksdistribution (Laserdiffraktionsteknik)				
D(0.5)	ER 9322	16,142 **µm**		

Cementa Research
Skeppargatan 1
P.O Box 104
SE-624 22 Slite
Sweden

Phone +46 (0)498-28 11 00
Fax +46 (0)498-28 13 91
www.cementaresearch.se
johan.larsson@cementa.se
VAT no. SE556102778901

LECO instrument CS 230

SO3	ER 9212	2,60 %	3 %
CO2	ER 9212	0,84 %	3 %
* Kalksten beräknad Degerhamn	Saknas	2,12 %	

Partikelstorleksdistribution (Laserdiffraktionsteknik)

Analys	**Siktstorlek**	**Passerande på sikt**
Enhet	µm	%
Metod	ER 9322	ER 9322
Mätosäkerhet		
RAD		
1	1,00	0,63
2	1,20	1,05
3	1,40	1,52
4	1,60	2,05
5	1,80	2,63
6	2,00	3,26
7	2,20	3,93
8	2,60	5,38
9	3,00	6,93
10	3,50	8,95
11	4,00	11,02
12	4,50	13,09
13	5,00	15,15
14	5,50	17,18
15	6,30	20,33
16	7,00	22,98
17	8,00	26,60
18	9,00	30,02
19	10,00	33,25
20	12,00	39,25
21	15,00	47,23
22	16,00	49,66
23	18,00	54,22
24	20,00	58,39
25	22,00	62,21
26	25,00	67,33
27	28,00	71,80
28	32,00	76,85
29	36,00	81,01
30	40,00	84,42
31	45,00	87,81
32	50,00	90,45
33	56,00	92,82
34	63,00	94,80
35	75,00	96,86
36	90,00	98,10
37	106,0	98,66
38	125,0	98,91
39	150,0	99,04
40	175,0	99,14
41	200,0	99,27
42	225,0	99,41
43	250,0	99,55
44	280,0	99,71

Cementa Research
Skeppargatan 1
P.O Box 104
SE-624 22 Slite
Sweden

Phone +46 (0)498-28 11 00
Fax +46 (0)498-28 13 91
www.cementaresearch.se
johan.larsson@cementa.se
VAT no. SE556102778901

45	315,0	99,86
46	355,0	99,96
47	400,0	100,0
48	450,0	100,0

Delges **Cementa AB , Stefan Sandelin, ref 205875**
Cementa AB , Erik Viggh, ref 183100
Cementa AB , Mikael Westerholm

Mätosäkerhet enligt "SWEDAC:s policy för mätosäkerhet vid kalibrering och provning", SWEDAC DOC 04:05. Den angivna mätosäkerheten är beräknad med täckningsfaktor 2, vilket ger konfidensnivå på ca 95%. Mätosäkerheten anges som (%) relativ eller absolut(abs%) eller i övrigt gällande enhet t.ex. Mpa, mg/kg.

* SLUT PÅ RAPPORTEN *

Cementa Research
Skeppargatan 1
P.O Box 104
SE-624 22 Slite
Sweden

Phone +46 (0)498-28 11 00
Fax +46 (0)498-28 13 91
www.cementaresearch.se
johan.larsson@cementa.se
VAT no. SE556102778901

SWEDAC ACKREDITERING
2026
ISO/IEC 17025

PROVRESULTAT

utfärdat av ackrediterat provningslaboratorium

CEMENTA
HEIDELBERGCEMENT Group
Cementa Research

Cementa AB
Stefan Sandelin, ref 205875
Box 47210
10074 STOCKHOLM

2015-10-14

Provnr	168954		
Märkning	LTH S35; Degerhamn anläggningscement + Slagg (Merit)		
Uppdrag / grupp	Analyser för LTH-doktorand		
Variant		Ankomstdatum	2015-06-18
Handläggare	Karin Lindhe	Klardatum	2015-10-14
Provtagningsdatum	2015-06-17		
Provtagning	Insänt av kund		
Provtagare			

Namn (Karin Lindhe)

* ej ackrediterad analys

Analys	Metod	Resultat	Mätosäkerhet	Kommentar
Leco Apparatur				
Gl.f 950°C	ER 9213 :2005	0,56 **%**	**0,18 %**	
Fysikaliska Bestämningar				
Densitet	ER 9228	3123 **kg/m3**	**40 kg/m3**	
Blaine, manuell	EN 196-6 :2010	395 **m2/kg**	**3 %**	
Bindetid				
Vatten	EN 196-3 :2005	26,0 **%**	**3,7 %**	
Vicat vatten	EN 196-3 :2005	230 **min**	**4 %**	
Normprov Tryckhållfasthet				
2 d	EN 196-1 :2005	12,9 **MPa**	**5 %**	
28 d	EN 196-1 :2005	53,9 **MPa**	**5 %**	
56 d	EN 196-1 :2005	63,5 **MPa**	**5 %**	
91 d	EN 196-1 :2005	67,4 **MPa**	**5 %**	
Std.av. 2 dygn	EN 196-1 :2005	0,1 **MPa**	**5 %**	
Std.av. 28 dygn	EN 196-1 :2005	0,6 **MPa**	**5 %**	
Std.av. 56 dygn	EN 196-1 :2005	0,7 **MPa**	**5 %**	
Std.av. 91 dygn	EN 196-1 :2005	0,5 **MPa**	**5 %**	
ICP-Analys				
* K2O H2O-lösl	CR 0401	0,27 **%**		
* Na2O H2O-lösl	CR 0401	0,03 **%**		
XRF - Cement - wroxi				
Na2O-ekvivalent	ER 9214	0,75 **%**		
CaO	ER 9214	52,7 **%**	**0,233 %abs**	
SiO2	ER 9214	25,9 **%**	**0,100 %abs**	
Al2O3	ER 9214	7,10 **%**	**0,052 %abs**	
Fe2O3	ER 9214	3,11 **%**	**0,019 %abs**	
MgO	ER 9214	5,92 **%**	**0,025 %abs**	
K2O	ER 9214	0,748 **%**	**0,032 %abs**	
Na2O	ER 9214	0,26 **%**		
Partikelstorleksdistribution (Laserdiffraktionsteknik)				
D(0.5)	ER 9322	15,339 **µm**		

Cementa Research
Skeppargatan 1
P.O Box 104
SE-624 22 Slite
Sweden

Phone +46 (0)498-28 11 00
Fax +46 (0)498-28 13 91
www.cementaresearch.se
johan.larsson@cementa.se
VAT no. SE556102778901

LECO instrument CS 230

SO3	ER 9212	2,76 %	3 %
CO2	ER 9212	0,73 %	3 %
* Kalksten beräknad Degerhamn	Saknas	1,84 %	

Partikelstorleksdistribution (Laserdiffraktionsteknik)

Analys	**Siktstorlek**	**Passerande på sikt**
Enhet	µm	%
Metod	ER 9322	ER 9322
Mätosäkerhet		
RAD		
1	1,00	0,71
2	1,20	1,17
3	1,40	1,70
4	1,60	2,28
5	1,80	2,91
6	2,00	3,59
7	2,20	4,32
8	2,60	5,88
9	3,00	7,54
10	3,50	9,70
11	4,00	11,90
12	4,50	14,11
13	5,00	16,29
14	5,50	18,44
15	6,30	21,75
16	7,00	24,53
17	8,00	28,29
18	9,00	31,83
19	10,00	35,14
20	12,00	41,22
21	15,00	49,18
22	16,00	51,57
23	18,00	56,02
24	20,00	60,06
25	22,00	63,73
26	25,00	68,63
27	28,00	72,87
28	32,00	77,64
29	36,00	81,57
30	40,00	84,78
31	45,00	87,98
32	50,00	90,47
33	56,00	92,72
34	63,00	94,60
35	75,00	96,57
36	90,00	97,79
37	106,0	98,38
38	125,0	98,69
39	150,0	98,92
40	175,0	99,13
41	200,0	99,36
42	225,0	99,57
43	250,0	99,76
44	280,0	99,92

Cementa Research
Skeppargatan 1
P.O Box 104
SE-624 22 Slite
Sweden

Phone +46 (0)498-28 11 00
Fax +46 (0)498-28 13 91
www.cementaresearch.se
johan.larsson@cementa.se
VAT no. SE556102778901

45	315,0	99,99
46	355,0	100,0
47	400,0	100,0
48	450,0	100,0

Delges **Cementa AB , Erik Viggh, ref 183100**
Cementa AB , Stefan Sandelin, ref 205875
Cementa AB , Mikael Westerholm

Mätosäkerhet enligt "SWEDAC:s policy för mätosäkerhet vid kalibrering och provning", SWEDAC DOC 04:05. Den angivna mätosäkerheten är beräknad med täckningsfaktor 2, vilket ger konfidensnivå på ca 95%. Mätosäkerheten anges som (%) relativ eller absolut(abs%) eller i övrigt gällande enhet t.ex. Mpa, mg/kg.

* SLUT PÅ RAPPORTEN *

Cementa Research
Skeppargatan 1
P.O Box 104
SE-624 22 Slite
Sweden

Phone +46 (0)498-28 11 00
Fax +46 (0)498-28 13 91
www.cementaresearch.se
johan.larsson@cementa.se
VAT no. SE556102778901

SWEDAC ACKREDITERING
2026
ISO/IEC 17025

PROVRESULTAT

utfärdat av ackrediterat provningslaboratorium

CEMENTA
HEIDELBERGCEMENT Group
Cementa Research

Cementa AB
Stefan Sandelin, ref 205875
Box 47210
10074 STOCKHOLM

2015-10-14

Provnr	168955		
Märkning	LTH S70; Degerhamn anläggningscement + Slagg		
Uppdrag / grupp	Analyser för LTH-doktorand		
Variant		Ankomstdatum	2015-06-18
Handläggare	Karin Lindhe	Klardatum	2015-10-14
Provtagningsdatum	2015-06-17		
Provtagning	Insänt av kund		
Provtagare			

Namn (Karin Lindhe)

* ej ackrediterad analys

Analys	Metod	Resultat	Mätosäkerhet	Kommentar
Leco Apparatur				
Gl.f 950°C	ER 9213 :2005	-0,59 **%**	**0,18 %**	
Fysikaliska Bestämningar				
Densitet	ER 9228	3025 **kg/m3**	**40 kg/m3**	
Blaine, manuell	EN 196-6 :2010	448 **m2/kg**	**3 %**	
Bindetid				
Vatten	EN 196-3 :2005	26,0 **%**	**3,7 %**	
Vicat vatten	EN 196-3 :2005	330 **min**	**4 %**	
Normprov Tryckhållfasthet				
2 d	EN 196-1 :2005	4,4 **MPa**	**5 %**	
28 d	EN 196-1 :2005	42,4 **MPa**	**5 %**	
56 d	EN 196-1 :2005	49,3 **MPa**	**5 %**	
91 d	EN 196-1 :2005	51,8 **MPa**	**5 %**	
Std.av. 2 dygn	EN 196-1 :2005	0,1 **MPa**	**5 %**	
Std.av. 28 dygn	EN 196-1 :2005	0,4 **MPa**	**5 %**	
Std.av. 56 dygn	EN 196-1 :2005	0,9 **MPa**	**5 %**	
Std.av. 91 dygn	EN 196-1 :2005	1,1 **MPa**	**5 %**	
ICP-Analys				
* K2O H2O-lösl	CR 0401	0,14 **%**		
* Na2O H2O-lösl	CR 0401	0,02 **%**		
XRF - Cement - wroxi				
Na2O-ekvivalent	ER 9214	1,00 **%**		
CaO	ER 9214	41,6 **%**	**0,233 %abs**	
SiO2	ER 9214	29,9 **%**	**0,100 %abs**	
Al2O3	ER 9214	10,2 **%**	**0,052 %abs**	
Fe2O3	ER 9214	1,67 **%**	**0,019 %abs**	
MgO	ER 9214	10,7 **%**	**0,025 %abs**	
K2O	ER 9214	0,842 **%**	**0,032 %abs**	
Na2O	ER 9214	0,44 **%**		
Partikelstorleksdistribution (Laserdiffraktionsteknik)				
D(0.5)	ER 9322	13,957 **µm**		

Cementa Research
Skeppargatan 1
P.O Box 104
SE-624 22 Slite
Sweden

Phone +46 (0)498-28 11 00
Fax +46 (0)498-28 13 91
www.cementaresearch.se
johan.larsson@cementa.se
VAT no. SE556102778901

LECO instrument CS 230

SO3	ER 9212	3,02 %	3 %
CO2	ER 9212	0,54 %	3 %
* Kalksten beräknad Degerhamn	Saknas	1,38 %	

Partikelstorleksdistribution (Laserdiffraktionsteknik)

Analys	Siktstorlek	Passerande på sikt
Enhet	µm	%
Metod	ER 9322	ER 9322
Mätosäkerhet		
RAD		
1	1,00	0,82
2	1,20	1,42
3	1,40	2,11
4	1,60	2,86
5	1,80	3,67
6	2,00	4,54
7	2,20	5,45
8	2,60	7,35
9	3,00	9,32
10	3,50	11,83
11	4,00	14,33
12	4,50	16,78
13	5,00	19,18
14	5,50	21,49
15	6,30	25,02
16	7,00	27,94
17	8,00	31,83
18	9,00	35,43
19	10,00	38,78
20	12,00	44,80
21	15,00	52,53
22	16,00	54,82
23	18,00	59,04
24	20,00	62,84
25	22,00	66,26
26	25,00	70,78
27	28,00	74,67
28	32,00	79,00
29	36,00	82,53
30	40,00	85,40
31	45,00	88,26
32	50,00	90,46
33	56,00	92,45
34	63,00	94,12
35	75,00	95,88
36	90,00	97,00
37	106,0	97,58
38	125,0	97,97
39	150,0	98,34
40	175,0	98,71
41	200,0	99,07
42	225,0	99,40
43	250,0	99,67
44	280,0	99,89

Cementa Research
Skeppargatan 1
P.O Box 104
SE-624 22 Slite
Sweden

Phone +46 (0)498-28 11 00
Fax +46 (0)498-28 13 91
www.cementaresearch.se
johan.larsson@cementa.se
VAT no. SE556102778901

45	315,0	99,98
46	355,0	100,0
47	400,0	100,0
48	450,0	100,0
49	500,0	100,0
50	560,0	100,0

Delges **Cementa AB , Erik Viggh, ref 183100**
Cementa AB , Stefan Sandelin, ref 205875
Cementa AB , Mikael Westerholm

Mätosäkerhet enligt "SWEDAC:s policy för mätosäkerhet vid kalibrering och provning", SWEDAC DOC 04:05. Den angivna mätosäkerheten är beräknad med täckningsfaktor 2, vilket ger konfidensnivå på ca 95%. Mätosäkerheten anges som (%) relativ eller absolut(abs%) eller i övrigt gällande enhet t.ex. Mpa, mg/kg.

* SLUT PÅ RAPPORTEN *

Cementa Research
Skeppargatan 1
P.O Box 104
SE-624 22 Slite
Sweden

Phone +46 (0)498-28 11 00
Fax +46 (0)498-28 13 91
www.cementaresearch.se
johan.larsson@cementa.se
VAT no. SE556102778901

SWEDAC ACKREDITERING 2026 ISO/IEC 17025

PROVRESULTAT

utfärdat av ackrediterat provningslaboratorium

CEMENTA HEIDELBERGCEMENT Group
Cementa Research

Cementa AB
Stefan Sandelin, ref 205875
Box 47210
10074 STOCKHOLM

2015-10-14

Provnr	168956		
Märkning	LTH K35; Degerhamn anläggningscement + Slagg och Kalksfiller		
Uppdrag / grupp	Analyser för LTH-doktorand		
Variant		Ankomstdatum	2015-06-18
Handläggare	Karin Lindhe	Klardatum	2015-10-14
Provtagningsdatum	2015-06-17		
Provtagning	Insänt av kund		
Provtagare			

Namn (Karin Lindhe)

* ej ackrediterad analys

Analys	Metod	Resultat	Mätosäkerhet	Kommentar
Leco Apparatur				
Gl.f 950°C	ER 9213 :2005	5,04 **%**	**0,18 %**	
Fysikaliska Bestämningar				
Densitet	ER 9228	3104 **kg/m3**	**40 kg/m3**	
Blaine, manuell	EN 196-6 :2010	397 **m2/kg**	**3 %**	
Bindetid				
Vatten	EN 196-3 :2005	26,0 **%**	**3,7 %**	
Vicat vatten	EN 196-3 :2005	210 **min**	**4 %**	
Normprov Tryckhållfasthet				
2 d	EN 196-1 :2005	12,8 **MPa**	**5 %**	
28 d	EN 196-1 :2005	47,9 **MPa**	**5 %**	
56 d	EN 196-1 :2005	55,2 **MPa**	**5 %**	
91 d	EN 196-1 :2005	58,3 **MPa**	**5 %**	
Std.av. 2 dygn	EN 196-1 :2005	0,3 **MPa**	**5 %**	
Std.av. 28 dygn	EN 196-1 :2005	1,2 **MPa**	**5 %**	
Std.av. 56 dygn	EN 196-1 :2005	0,6 **MPa**	**5 %**	
Std.av. 91 dygn	EN 196-1 :2005	0,6 **MPa**	**5 %**	
ICP-Analys				
* K2O H2O-lösl	CR 0401	0,20 **%**		
* Na2O H2O-lösl	CR 0401	0,02 **%**		
TGA				
* CaCO3	Saknas	10,60 **%**		
XRF - Cement - wroxi				
Na2O-ekvivalent	ER 9214	0,66 **%**		
CaO	ER 9214	54,1 **%**	**0,233 %abs**	
SiO2	ER 9214	22,9 **%**	**0,100 %abs**	
Al2O3	ER 9214	5,94 **%**	**0,052 %abs**	
Fe2O3	ER 9214	3,11 **%**	**0,019 %abs**	
MgO	ER 9214	4,77 **%**	**0,025 %abs**	
K2O	ER 9214	0,685 **%**	**0,032 %abs**	
Na2O	ER 9214	0,21 **%**		

Cementa Research
Skeppargatan 1
P.O Box 104
SE-624 22 Slite
Sweden

Phone +46 (0)498-28 11 00
Fax +46 (0)498-28 13 91
www.cementaresearch.se
johan.larsson@cementa.se
VAT no. SE556102778901

Partikelstorleksdistribution (Laserdiffraktionsteknik)

D(0.5)	ER 9322	16,439 **µm**	

LECO instrument CS 230

SO3	ER 9212	2,40 **%**	**3 %**

Partikelstorleksdistribution (Laserdiffraktionsteknik)

Analys	**Siktstorlek**	**Passerande på sikt**
Enhet	µm	%
Metod	ER 9322	ER 9322
Mätosäkerhet		
RAD		
1	1,00	0,59
2	1,20	1,16
3	1,40	1,83
4	1,60	2,58
5	1,80	3,39
6	2,00	4,24
7	2,20	5,11
8	2,60	6,91
9	3,00	8,72
10	3,50	10,96
11	4,00	13,16
12	4,50	15,28
13	5,00	17,33
14	5,50	19,30
15	6,30	22,31
16	7,00	24,79
17	8,00	28,13
18	9,00	31,26
19	10,00	34,20
20	12,00	39,64
21	15,00	46,86
22	16,00	49,06
23	18,00	53,19
24	20,00	56,99
25	22,00	60,47
26	25,00	65,16
27	28,00	69,28
28	32,00	73,98
29	36,00	77,90
30	40,00	81,17
31	45,00	84,50
32	50,00	87,15
33	56,00	89,63
34	63,00	91,80
35	75,00	94,26
36	90,00	96,00
37	106,0	97,00
38	125,0	97,65
39	150,0	98,11
40	175,0	98,41
41	200,0	98,65
42	225,0	98,88
43	250,0	99,09
44	280,0	99,30

Cementa Research
Skeppargatan 1
P.O Box 104
SE-624 22 Slite
Sweden

Phone +46 (0)498-28 11 00
Fax +46 (0)498-28 13 91
www.cementaresearch.se
johan.larsson@cementa.se
VAT no. SE556102778901

45	315,0	99,51
46	355,0	99,67
47	400,0	99,81
48	450,0	99,91
49	500,0	99,99
50	560,0	100,0

Delges **Cementa AB , Stefan Sandelin, ref 205875**
Cementa AB , Erik Viggh, ref 183100

Ingen hänsyn tagen till renheten på kalkstenen.

Mätosäkerhet enligt "SWEDAC:s policy för mätosäkerhet vid kalibrering och provning", SWEDAC DOC 04:05. Den angivna mätosäkerheten är beräknad med täckningsfaktor 2, vilket ger konfidensnivå på ca 95%. Mätosäkerheten anges som (%) relativ eller absolut(abs%) eller i övrigt gällande enhet t.ex. Mpa, mg/kg.

* SLUT PÅ RAPPORTEN *

Cementa Research
Skeppargatan 1
P.O Box 104
SE-624 22 Slite
Sweden

Phone +46 (0)498-28 11 00
Fax +46 (0)498-28 13 91
www.cementaresearch.se
johan.larsson@cementa.se
VAT no. SE556102778901

Luftporeanalyse (ASTM C 457)

Udført: April 2015 v/AB & PL

Sags nr. 15-044

Prøvemærke : 02 17 02-1

Målelinier : 40 stk.
Pastaindhold : 30 %
(skønnet)

ANALYSE RESULTATER:

Luftindhold	Beton	Kitmasse
Total :	2,6 %	7,9 %
< 0,350 mm :	0,9 %	2,8 %
0,350-1,5 mm :	1,3 %	
1,5 - 2,0 mm :	0,2 %	
>2,0 mm :	0,2 %	

Specifik overflade : 16 mm^{-1}
Afstandsfaktor : 0,43 mm

Bemærkninger
'Kitmasse" er defineret som pastaindhold + luftindhold.
Hvis indhold af indkapslet luft (korder > 2 mm) udelades, kan ovenstående værdier genberegnes til:
Luftporer i beton: 2,4 % (i kitmasse: 7,3 %). Specifik overflade: 17 mm-1. Afstandsfaktor: 0,41 mm.

Luftporeanalyse (ASTM C 457)

Udført: April 2015 v/AB & PL

Sags nr. 15-044

Prøvemærke : 02 27 02-2

Målelinier : 40 stk.
Pastaindhold : 30 %
(skønnet)

ANALYSE RESULTATER:

Luftindhold	Beton	Kitmasse
Total :	2,7 %	8,0 %
< 0,350 mm :	0,9 %	2,8 %
0,350-1,5 mm :	1,2 %	
1,5 - 2,0 mm :	0,2 %	
>2,0 mm :	0,3 %	

Specifik overflade : 17 mm^{-1}
Afstandsfaktor : 0,40 mm

Bemærkninger
'Kitmasse" er defineret som pastaindhold + luftindhold.
Hvis indhold af indkapslet luft (korder > 2 mm) udelades, kan ovenstående værdier genberegnes til:
Luftporer i beton: 2,4 % (i kitmasse: 7,1 %). Specifik overflade: 19 mm-1. Afstandsfaktor: 0,38 mm.

Luftporeanalyse (ASTM C 457)

Udført: April 2015 v/AB & PL

Sags nr. 15-044

Prøvemærke : 02 37 02-3

Målelinier : 40 stk.
Pastaindhold : 30 %
(skønnet)

ANALYSE RESULTATER:

Luftindhold	Beton	Kitmasse
Total :	2,8 %	8,4 %
< 0,350 mm :	1,3 %	3,9 %
0,350-1,5 mm :	1,3 %	
1,5 - 2,0 mm :	0,1 %	
>2,0 mm :	0,1 %	

Specifik overflade : 20 mm^{-1}
Afstandsfaktor : 0,33 mm

Bemærkninger
'Kitmasse" er defineret som pastaindhold + luftindhold.
Hvis indhold af indkapslet luft (korder > 2 mm) udelades, kan ovenstående værdier genberegnes til:
Luftporer i beton: 2,7 % (i kitmasse: 7,9 %). Specifik overflade: 21 mm-1. Afstandsfaktor: 0,32 mm.

Luftporeanalyse (ASTM C 457)

Udført: April 2015 v/AB & PL

Sags nr. 15-044

Prøvemærke : 02 47 02-4

Målelinier : 40 stk.
Pastaindhold : 30 %
(skønnet)

ANALYSE RESULTATER:

Luftindhold	Beton	Kitmasse
Total :	4,1 %	11,9 %
< 0,350 mm :	1,9 %	5,7 %
0,350-1,5 mm :	1,3 %	
1,5 - 2,0 mm :	0,1 %	
>2,0 mm :	0,7 %	

Specifik overflade : 20 mm^{-1}
Afstandsfaktor : 0,27 mm

Bemærkninger
'Kitmasse" er defineret som pastaindhold + luftindhold.
Hvis indhold af indkapslet luft (korder > 2 mm) udelades, kan ovenstående værdier genberegnes til:
Luftporer i beton: 3,4 % (i kitmasse: 9,8 %). Specifik overflade: 24 mm-1. Afstandsfaktor: 0,25 mm.

Luftporeanalyse (ASTM C 457)

Udført: April 2015 v/AB & PL

Sags nr. 14-186

Prøvemærke : 7 F20-1

Målelinier : 40 stk.
Pastaindhold : 30 %
(skønnet)

ANALYSERESULTATER:

Luftindhold	Beton	Kitmasse
Total :	3,5 %	10,3 %
< 0,350 mm :	0,3 %	0,9 %
0,350-1,5 mm :	1,2 %	
1,5 - 2,0 mm :	0,4 %	
>2,0 mm :	1,6 %	

Specifik overflade : 6 mm^{-1}
Afstandsfaktor : 1,00 mm

Bemærkninger
'Kitmasse" er defineret som pastaindhold + luftindhold.
Hvis indhold af indkapslet luft (korder > 2 mm) udelades, kan ovenstående værdier genberegnes til:
Luftporer i beton: 1,9 % (i kitmasse: 5,6 %). Specifik overflade: 10 mm-1. Afstandsfaktor: 0,78 mm.

Luftporeanalyse (ASTM C 457)

Udført: April 2015 v/AB & PL

Sags nr. 14-186

Prøvemærke : 2 F20-2

Målelinier : 40 stk.
Pastaindhold : 30 %
(skønnet)

ANALYSE RESULTATER:

Luftindhold	Beton	Kitmasse
Total :	2,0 %	6,1 %
< 0,350 mm :	0,9 %	2,6 %
0,350-1,5 mm :	0,8 %	
1,5 - 2,0 mm :	0,2 %	
>2,0 mm :	0,1 %	

Specifik overflade : 23 mm^{-1}
Afstandsfaktor : 0,33 mm

Bemærkninger
'Kitmasse" er defineret som pastaindhold + luftindhold.
Hvis indhold af indkapslet luft (korder > 2 mm) udelades, kan ovenstående værdier genberegnes til:
Luftporer i beton: 1,9 % (i kitmasse: 5,6 %). Specifik overflade: 25 mm-1. Afstandsfaktor: 0,32 mm.

Luftporeanalyse (ASTM C 457)

Udført: April 2015 v/AB & PL

Sags nr. 14-186

Prøvemærke : 5 F20-3

Målelinier : 40 stk.
Pastaindhold : 30 %
(skønnet)

ANALYSE RESULTATER:

Luftindhold	Beton	Kitmasse
Total :	3,1 %	9,3 %
< 0,350 mm :	1,1 %	3,3 %
0,350-1,5 mm :	1,2 %	
1,5 - 2,0 mm :	0,2 %	
>2,0 mm :	0,6 %	

Specifik overflade : 15 mm^{-1}
Afstandsfaktor : 0,41 mm

Bemærkninger
'Kitmasse" er defineret som pastaindhold + luftindhold.
Hvis indhold af indkapslet luft (korder > 2 mm) udelades, kan ovenstående værdier genberegnes til:
Luftporer i beton: 2,5 % (i kitmasse: 7,6 %). Specifik overflade: 18 mm-1. Afstandsfaktor: 0,37 mm.

Luftporeanalyse (ASTM C 457)

Udført: April 2015 v/AB & PL

Sags nr. 14-186

Prøvemærke : II F20-4

Målelinier : 40 stk.
Pastaindhold : 30 %
(skønnet)

ANALYSERESULTATER:

Luftindhold	Beton	Kitmasse
Total :	3,5 %	10,3 %
< 0,350 mm :	2,0 %	5,9 %
0,350-1,5 mm :	1,2 %	
1,5 - 2,0 mm :	0,1 %	
>2,0 mm :	0,1 %	

Specifik overflade : 21 mm^{-1}
Afstandsfaktor : 0,28 mm

Bemærkninger
'Kitmasse" er defineret som pastaindhold + luftindhold.
Hvis indhold af indkapslet luft (korder > 2 mm) udelades, kan ovenstående værdier genberegnes til:
Luftporer i beton: 3,4 % (i kitmasse: 9,9 %). Specifik overflade: 22 mm-1. Afstandsfaktor: 0,27 mm.

Luftporeanalyse (ASTM C 457)

Udført: April 2015 v/AB & PL

Sags nr. 15-044

Prøvemærke : F35 13 F35-1

Målelinier : 40 stk.
Pastaindhold : 30 %
(skønnet)

ANALYSERESULTATER:

Luftindhold	Beton	Kitmasse
Total :	1,8 %	5,4 %
< 0,350 mm :	0,3 %	1,0 %
0,350-1,5 mm :	0,8 %	
1,5 - 2,0 mm :	0,0 %	
>2,0 mm :	0,7 %	

Specifik overflade : 15 mm^{-1}
Afstandsfaktor : 0,53 mm

Bemærkninger
'Kitmasse" er defineret som pastaindhold + luftindhold.
Hvis indhold af indkapslet luft (korder > 2 mm) udelades, kan ovenstående værdier genberegnes til:
Luftporer i beton: 1,1 % (i kitmasse: 3,4 %). Specifik overflade: 24 mm-1. Afstandsfaktor: 0,41 mm.

Luftporeanalyse (ASTM C 457)

Udført: April 2015 v/AB & PL

Sags nr. 15-044

Prøvemærke : F35 27 F35-2

Målelinier : 40 stk.
Pastaindhold : 30 %
(skønnet)

ANALYSE RESULTATER:

Luftindhold	Beton	Kitmasse
Total :	3,8 %	11,2 %
< 0,350 mm :	0,8 %	2,2 %
0,350-1,5 mm :	1,3 %	
1,5 - 2,0 mm :	0,3 %	
>2,0 mm :	1,4 %	

Specifik overflade : 13 mm^{-1}
Afstandsfaktor : 0,44 mm

Bemærkninger
'Kitmasse" er defineret som pastaindhold + luftindhold.
Hvis indhold af indkapslet luft (korder > 2 mm) udelades, kan ovenstående værdier genberegnes til:
Luftporer i beton: 2,4 % (i kitmasse: 7 %). Specifik overflade: 20 mm-1. Afstandsfaktor: 0,35 mm.

Luftporeanalyse (ASTM C 457)

Udført: April 2015 v/AB & PL

Sags nr. 15-044

Prøvemærke : F35 37 F35-3

Målelinier : 40 stk.
Pastaindhold : 30 %
(skønnet)

ANALYSE RESULTATER:

Luftindhold	Beton	Kitmasse
Total :	3,2 %	9,5 %
< 0,350 mm :	1,6 %	4,7 %
0,350-1,5 mm :	1,0 %	
1,5 - 2,0 mm :	0,3 %	
>2,0 mm :	0,4 %	

Specifik overflade : 30 mm^{-1}
Afstandsfaktor : 0,20 mm

Bemærkninger
'Kitmasse" er defineret som pastaindhold + luftindhold.
Hvis indhold af indkapslet luft (korder > 2 mm) udelades, kan ovenstående værdier genberegnes til:
Luftporer i beton: 2,9 % (i kitmasse: 8,4 %). Specifik overflade: 34 mm-1. Afstandsfaktor: 0,19 mm.

Luftporeanalyse (ASTM C 457)

Udført: April 2015 v/AB & PL

Sags nr. 15-044

Prøvemærke : F35 47 F35-4

Målelinier : 40 stk.
Pastaindhold : 30 %
(skønnet)

ANALYSE RESULTATER:

Luftindhold	Beton	Kitmasse
Total :	4,8 %	13,8 %
< 0,350 mm :	2,0 %	5,8 %
0,350-1,5 mm :	1,2 %	
1,5 - 2,0 mm :	0,2 %	
>2,0 mm :	1,4 %	

Specifik overflade : 19 mm^{-1}
Afstandsfaktor : 0,27 mm

Bemærkninger
'Kitmasse" er defineret som pastaindhold + luftindhold.
Hvis indhold af indkapslet luft (korder > 2 mm) udelades, kan ovenstående værdier genberegnes til:
Luftporer i beton: 3,4 % (i kitmasse: 9,7 %). Specifik overflade: 27 mm-1. Afstandsfaktor: 0,22 mm.

Luftporeanalyse (ASTM C 457)

Udført: April 2015 v/AB & PL

Sags nr. 14-186

Prøvemærke : 6 S20-1

Målelinier : 40 stk.
Pastaindhold : 30 %
(skønnet)

ANALYSE RESULTATER:

Luftindhold	Beton	Kitmasse
Total :	3,6 %	10,6 %
< 0,350 mm :	0,7 %	2,2 %
0,350-1,5 mm :	1,3 %	
1,5 - 2,0 mm :	0,3 %	
>2,0 mm :	1,3 %	

Specifik overflade : 9 mm^{-1}
Afstandsfaktor : 0,66 mm

Bemærkninger
'Kitmasse" er defineret som pastaindhold + luftindhold.
Hvis indhold af indkapslet luft (korder > 2 mm) udelades, kan ovenstående værdier genberegnes til:
Luftporer i beton: 2,3 % (i kitmasse: 6,8 %). Specifik overflade: 13 mm-1. Afstandsfaktor: 0,55 mm.

Luftporeanalyse (ASTM C 457)

Udført: April 2015 v/AB & PL

Sags nr. 14-186

Prøvemærke : 3 S20-2

Målelinier : 40 stk.
Pastaindhold : 30 %
(skønnet)

ANALYSE RESULTATER:

Luftindhold	Beton	Kitmasse
Total :	5,1 %	14,5 %
< 0,350 mm :	1,1 %	3,0 %
0,350-1,5 mm :	1,3 %	
1,5 - 2,0 mm :	0,5 %	
>2,0 mm :	2,2 %	

Specifik overflade : 10 mm^{-1}
Afstandsfaktor : 0,49 mm

Bemærkninger
'Kitmasse" er defineret som pastaindhold + luftindhold.
Hvis indhold af indkapslet luft (korder > 2 mm) udelades, kan ovenstående værdier genberegnes til:
Luftporer i beton: 2,9 % (i kitmasse: 8,2 %). Specifik overflade: 17 mm-1. Afstandsfaktor: 0,38 mm.

Luftporeanalyse (ASTM C 457)

Udført: April 2015 v/AB & PL

Sags nr. 14-186

Prøvemærke : 8 S20-3

Målelinier : 40 stk.
Pastaindhold : 30 %
(skønnet)

ANALYSE RESULTATER:

Luftindhold	Beton	Kitmasse
Total :	2,3 %	6,9 %
< 0,350 mm :	1,2 %	3,7 %
0,350-1,5 mm :	0,5 %	
1,5 - 2,0 mm :	0,1 %	
>2,0 mm :	0,4 %	

Specifik overflade : 22 mm^{-1}
Afstandsfaktor : 0,32 mm

Bemærkninger
'Kitmasse" er defineret som pastaindhold + luftindhold.
Hvis indhold af indkapslet luft (korder > 2 mm) udelades, kan ovenstående værdier genberegnes til:
Luftporer i beton: 1,9 % (i kitmasse: 5,6 %). Specifik overflade: 27 mm-1. Afstandsfaktor: 0,29 mm.

Luftporeanalyse (ASTM C 457)

Udført: April 2015 v/AB & PL

Sags nr. 14-186

Prøvemærke : 1 S20-4

Målelinier : 40 stk.
Pastaindhold : 30 %
(skønnet)

ANALYSE RESULTATER:

Luftindhold	Beton	Kitmasse
Total :	3,7 %	10,9 %
< 0,350 mm :	2,1 %	6,1 %
0,350-1,5 mm :	1,2 %	
1,5 - 2,0 mm :	0,1 %	
>2,0 mm :	0,3 %	
Specifik overflade :	27 mm^{-1}	
Afstandsfaktor :	0,21 mm	

Bemærkninger
'Kitmasse" er defineret som pastaindhold + luftindhold.
Hvis indhold af indkapslet luft (korder > 2 mm) udelades, kan ovenstående værdier genberegnes til:
Luftporer i beton: 3,4 % (i kitmasse: 9,9 %). Specifik overflade: 30 mm-1. Afstandsfaktor: 0,2 mm.

Luftporeanalyse (ASTM C 457)

Udført: April 2015 v/AB & PL

Sags nr. 15-044

Prøvemærke : S35 14 S35-1

Målelinier : 40 stk.
Pastaindhold : 30 %
(skønnet)

ANALYSE RESULTATER:

Luftindhold	Beton	Kitmasse
Total :	3,1 %	9,1 %
< 0,350 mm :	0,5 %	1,5 %
0,350-1,5 mm :	0,8 %	
1,5 - 2,0 mm :	0,2 %	
>2,0 mm :	1,5 %	

Specifik overflade : 8 mm^{-1}
Afstandsfaktor : 0,75 mm

Bemærkninger
'Kitmasse" er defineret som pastaindhold + luftindhold.
Hvis indhold af indkapslet luft (korder > 2 mm) udelades, kan ovenstående værdier genberegnes til:
Luftporer i beton: 1,5 % (i kitmasse: 4,6 %). Specifik overflade: 16 mm-1. Afstandsfaktor: 0,54 mm.

Luftporeanalyse (ASTM C 457)

Udført: April 2015 v/AB & PL

Sags nr. 15-044

Prøvemærke : S35 26 S35-2

Målelinier : 40 stk.
Pastaindhold : 30 %
(skønnet)

ANALYSE RESULTATER:

Luftindhold	Beton	Kitmasse
Total :	3,6 %	10,4 %
< 0,350 mm :	1,3 %	3,9 %
0,350-1,5 mm :	1,2 %	
1,5 - 2,0 mm :	0,4 %	
>2,0 mm :	0,7 %	

Specifik overflade : 16 mm^{-1}
Afstandsfaktor : 0,37 mm

Bemærkninger
'Kitmasse" er defineret som pastaindhold + luftindhold.
Hvis indhold af indkapslet luft (korder > 2 mm) udelades, kan ovenstående værdier genberegnes til:
Luftporer i beton: 2,9 % (i kitmasse: 8,4 %). Specifik overflade: 19 mm-1. Afstandsfaktor: 0,33 mm.

Luftporeanalyse (ASTM C 457)

Udført: April 2015 v/AB & PL

Sags nr. 15-044

Prøvemærke : S35 37 S35-3

Målelinier : 40 stk.
Pastaindhold : 30 %
(skønnet)

ANALYSE RESULTATER:

Luftindhold	Beton	Kitmasse
Total :	3,1 %	9,1 %
< 0,350 mm :	1,5 %	4,3 %
0,350-1,5 mm :	1,0 %	
1,5 - 2,0 mm :	0,2 %	
>2,0 mm :	0,4 %	

Specifik overflade : 22 mm^{-1}
Afstandsfaktor : 0,29 mm

Bemærkninger
'Kitmasse" er defineret som pastaindhold + luftindhold.
Hvis indhold af indkapslet luft (korder > 2 mm) udelades, kan ovenstående værdier genberegnes til:
Luftporer i beton: 2,7 % (i kitmasse: 8 %). Specifik overflade: 25 mm-1. Afstandsfaktor: 0,27 mm.

Luftporeanalyse (ASTM C 457)

Udført: April 2015 v/AB & PL

Sags nr. 15-044

Prøvemærke : S35 45 S35-4

Målelinier : 40 stk.
Pastaindhold : 30 %
(skønnet)

ANALYSE RESULTATER:

Luftindhold	Beton	Kitmasse
Total :	5,6 %	15,8 %
< 0,350 mm :	2,4 %	6,7 %
0,350-1,5 mm :	2,0 %	
1,5 - 2,0 mm :	0,2 %	
>2,0 mm :	1,1 %	

Specifik overflade : 18 mm^{-1}
Afstandsfaktor : 0,26 mm

Bemærkninger
'Kitmasse" er defineret som pastaindhold + luftindhold.
Hvis indhold af indkapslet luft (korder > 2 mm) udelades, kan ovenstående værdier genberegnes til:
Luftporer i beton: 4,5 % (i kitmasse: 12,8 %). Specifik overflade: 23 mm-1. Afstandsfaktor: 0,23 mm.

Luftporeanalyse (ASTM C 457)

Udført: April 2015 v/AB & PL

Sags nr. 15-044

Prøvemærke : S70 17 S70-1

Målelinier : 40 stk.
Pastaindhold : 30 %
(skønnet)

ANALYSE RESULTATER:

Luftindhold	Beton	Kitmasse
Total :	2,9 %	8,6 %
< 0,350 mm :	0,9 %	2,6 %
0,350-1,5 mm :	1,2 %	
1,5 - 2,0 mm :	0,4 %	
>2,0 mm :	0,4 %	

Specifik overflade : 13 mm^{-1}
Afstandsfaktor : 0,52 mm

Bemærkninger
'Kitmasse" er defineret som pastaindhold + luftindhold.
Hvis indhold af indkapslet luft (korder > 2 mm) udelades, kan ovenstående værdier genberegnes til:
Luftporer i beton: 2,5 % (i kitmasse: 7,4 %). Specifik overflade: 14 mm-1. Afstandsfaktor: 0,48 mm.

Luftporeanalyse (ASTM C 457)

Udført: April 2015 v/AB & PL

Sags nr. 15-044

Prøvemærke : S70 27 S70-2

Målelinier : 40 stk.
Pastaindhold : 30 %
(skønnet)

ANALYSE RESULTATER:

Luftindhold	Beton	Kitmasse
Total :	2,7 %	8,1 %
< 0,350 mm :	1,1 %	3,2 %
0,350-1,5 mm :	1,0 %	
1,5 - 2,0 mm :	0,2 %	
>2,0 mm :	0,5 %	

Specifik overflade : 17 mm^{-1}
Afstandsfaktor : 0,38 mm

Bemærkninger
'Kitmasse" er defineret som pastaindhold + luftindhold.
Hvis indhold af indkapslet luft (korder > 2 mm) udelades, kan ovenstående værdier genberegnes til:
Luftporer i beton: 2,2 % (i kitmasse: 6,7 %). Specifik overflade: 21 mm-1. Afstandsfaktor: 0,35 mm.

Luftporeanalyse (ASTM C 457)

Udført: April 2015 v/AB & PL

Sags nr. 15-044

Prøvemærke : S70 37 S70-3

Målelinier : 40 stk.
Pastaindhold : 30 %
(skønnet)

ANALYSE RESULTATER:

Luftindhold	Beton	Kitmasse
Total :	4,3 %	12,4 %
< 0,350 mm :	1,4 %	4,1 %
0,350-1,5 mm :	1,6 %	
1,5 - 2,0 mm :	0,3 %	
>2,0 mm :	1,0 %	

Specifik overflade : 14 mm^{-1}
Afstandsfaktor : 0,39 mm

Bemærkninger
'Kitmasse" er defineret som pastaindhold + luftindhold.
Hvis indhold af indkapslet luft (korder > 2 mm) udelades, kan ovenstående værdier genberegnes til:
Luftporer i beton: 3,3 % (i kitmasse: 9,5 %). Specifik overflade: 18 mm-1. Afstandsfaktor: 0,35 mm.

Luftporeanalyse (ASTM C 457)

Udført: April 2015 v/AB & PL

Sags nr. 15-044

Prøvemærke : S70 47 S70-4

Målelinier : 40 stk.
Pastaindhold : 30 %
(skønnet)

ANALYSERESULTATER:

Luftindhold	Beton	Kitmasse
Total :	3,3 %	9,6 %
< 0,350 mm :	1,2 %	3,5 %
0,350-1,5 mm :	1,4 %	
1,5 - 2,0 mm :	0,2 %	
>2,0 mm :	0,5 %	

Specifik overflade : 15 mm^{-1}
Afstandsfaktor : 0,42 mm

Bemærkninger
'Kitmasse" er defineret som pastaindhold + luftindhold.
Hvis indhold af indkapslet luft (korder > 2 mm) udelades, kan ovenstående værdier genberegnes til:
Luftporer i beton: 2,7 % (i kitmasse: 8 %). Specifik overflade: 17 mm-1. Afstandsfaktor: 0,38 mm.

Luftporeanalyse (ASTM C 457)

Udført: April 2015 v/AB & PL

Sags nr. 15-044

Prøvemærke : K35 17 K 35-1

Målelinier : 40 stk.
Pastaindhold : 30 %
(skønnet)

ANALYSE RESULTATER:

Luftindhold	Beton	Kitmasse
Total :	3,3 %	9,8 %
< 0,350 mm :	1,0 %	3,0 %
0,350-1,5 mm :	1,5 %	
1,5 - 2,0 mm :	0,2 %	
>2,0 mm :	0,6 %	

Specifik overflade : 14 mm^{-1}
Afstandsfaktor : 0,45 mm

Bemærkninger
'Kitmasse" er defineret som pastaindhold + luftindhold.
Hvis indhold af indkapslet luft (korder > 2 mm) udelades, kan ovenstående værdier genberegnes til:
Luftporer i beton: 2,7 % (i kitmasse: 7,9 %). Specifik overflade: 17 mm-1. Afstandsfaktor: 0,4 mm.

Luftporeanalyse (ASTM C 457)

Udført: April 2015 v/AB & PL

Sags nr. 15-044

Prøvemærke : K35 27 K35-2

Målelinier : 40 stk.
Pastaindhold : 30 %
(skønnet)

ANALYSE RESULTATER:

Luftindhold	Beton	Kitmasse
Total :	3,7 %	10,7 %
< 0,350 mm :	1,2 %	3,5 %
0,350-1,5 mm :	1,4 %	
1,5 - 2,0 mm :	0,3 %	
>2,0 mm :	0,8 %	

Specifik overflade : 15 mm^{-1}
Afstandsfaktor : 0,40 mm

Bemærkninger
'Kitmasse" er defineret som pastaindhold + luftindhold.
Hvis indhold af indkapslet luft (korder > 2 mm) udelades, kan ovenstående værdier genberegnes til:
Luftporer i beton: 2,9 % (i kitmasse: 8,4 %). Specifik overflade: 18 mm-1. Afstandsfaktor: 0,35 mm.

Luftporeanalyse (ASTM C 457)

Udført: April 2015 v/AB & PL

Sags nr. 15-044

Prøvemærke : K35 37 K35-3

Målelinier : 40 stk.
Pastaindhold : 30 %
(skønnet)

ANALYSE RESULTATER:

Luftindhold	Beton	Kitmasse
Total :	3,5 %	10,2 %
< 0,350 mm :	1,5 %	4,5 %
0,350-1,5 mm :	1,2 %	
1,5 - 2,0 mm :	0,3 %	
>2,0 mm :	0,4 %	

Specifik overflade : 20 mm^{-1}
Afstandsfaktor : 0,29 mm

Bemærkninger
'Kitmasse" er defineret som pastaindhold + luftindhold.
Hvis indhold af indkapslet luft (korder > 2 mm) udelades, kan ovenstående værdier genberegnes til:
Luftporer i beton: 3,1 % (i kitmasse: 9,1 %). Specifik overflade: 23 mm-1. Afstandsfaktor: 0,27 mm.

Luftporeanalyse (ASTM C 457)

Udført: April 2015 v/AB & PL

Sags nr. 15-044

Prøvemærke : K35 47 K 35-4

Målelinier : 40 stk.
Pastaindhold : 30 %
(skønnet)

ANALYSE RESULTATER:

Luftindhold	Beton	Kitmasse
Total :	3,2 %	9,5 %
< 0,350 mm :	1,6 %	4,9 %
0,350-1,5 mm :	1,3 %	
1,5 - 2,0 mm :	0,1 %	
>2,0 mm :	0,2 %	

Specifik overflade : 22 mm^{-1}
Afstandsfaktor : 0,28 mm

Bemærkninger
'Kitmasse" er defineret som pastaindhold + luftindhold.
Hvis indhold af indkapslet luft (korder > 2 mm) udelades, kan ovenstående værdier genberegnes til:
Luftporer i beton: 3,1 % (i kitmasse: 9,1 %). Specifik overflade: 23 mm-1. Afstandsfaktor: 0,27 mm.

Paper I

International RILEM Conference on Materials, Systems and Structures in Civil Engineering
Conference segment on Frost Action in Concrete
22-23 August 2016, Lunds University, Lund, Sweden

METHODOLOGY TO ANALYSE THE SALT FROST SCALING MECHANISM(S) IN CONCRETE WITH DIFFERENT BINDERS

Martin Strand [(1)], Katja Fridh [(1)]
(1) Building Materials, Lunds University, Lund, Sweden

Abstract
The purpose of this article is to present a methodology which can be used to evaluate how the salt frost scaling mechanism(s) affects concrete with different air void systems. First, a test is made where the binder is mixed with various combinations of superplasticizer and air entraining agent to find one combination which performs well. The combination is then used when casting concrete to produce four air void systems, from approximately 1.5% to 4.5% in total air content, which are quantified with an air void analysis made on the hardened concrete. The concrete is sealed and hydrated until for over 300 days which results in a high degree of hydration for any binder. Then a salt frost scaling method is used with a temperature cycle which increases the salt frost scaling mechanism(s) load. The results present scaling from concrete with a high degree of hydration, regardless of hydration rate, and the effect the air void system has on the salt frost scaling damage in various binders given an even microstructure since each sample is fully hydrated. This enables a study of how various microstructures are affected by a constant load from the salt frost scaling mechanism(s) and of the salt frost scaling process.

1. Introduction

The purpose of this article is to present a methodology for a salt frost scaling analysis of close to fully hydrated binders with an analysis of the effect various air void systems has on each binder. The degree of hydration has a significant influence when analysing salt frost scaling resistance for different binders [1]. The binders with a slow rate of hydration will produce more scaling when testing after the same amount of time given equal conditions during the hydration. However, by allowing any binder to hydrate in sealed conditions for over 300 days salt frost scaling test results will give information about how the salt frost scaling mechanism affect various binders with fully developed microstructures. The air void system also has a significant effect on the salt frost scaling in concrete containing various binders, therefore it is interesting to study the effect from slight changes in the air void system for various binders.

This paper presents a description of the methodology used, starting with a method to find a combination of superplasticizer (SP) and air entraining agent (AEA) for each binder to enable the creation of various air void systems with small differences. These differences were then quantified by an air void system analysis (linear traverse). Then the article presents the hydration process and briefly mention the salt frost scaling test method which is presented in [2] together with some results from four casts of CEM I concrete. Lastly the methodology is discussed and conclusions are drawn.

2. Test of superplasticizer and air entraining agent combinations

The purpose of this test was to get indications of the difference in performance and learn about the risk of water separation for various combinations of admixtures (one AEA and one SP) given the same recipe (binder and aggregate fractions). The results then enable a choice of a AEA and SP combination (for each binder) which perform well and have a low risk for bleeding, which in turn enables a creation of various air void systems with only small differences. The test measured workability, the air content inside the fresh mortar, and a foam test which gives an idea of the risk for air voids to merge. The mortar recipe contained 2.000 kg binder, 6.000 kg of "0-8" aggregate fraction, and 0.800 kg water.

2.1 Method for the mortar tests

To enable an attempt to produce an acceptable workability for all binders, the AEA was mixed with the water, and then the superplasticizer was added. The following mixing procedure was used:

- The binder and aggregates were blended for 2.5 min ±5 sec
- Water was added and mixed for 2.5 min ±5 sec,
- Mixing continues for 2.5 min ±5 sec and a pipette was used to drip the superplasticizer in to the mix and stop when one of the following occurred
  - the workability looked acceptable.
  - bleeding started (before an acceptable workability was acquired).

The average recommended mass for each AEA was used. When mixing the concrete for the salt frost scaling test a smaller mass of AEA were used to get close to 5% air content. However, at this stage it was assumed that if a larger (average recommended) mass of AEA work well with a specific superplasticizer, then a smaller mass also will perform well.

2.2 Results from the mortar tests

After the mixing procedure was done the workability was measured with a Hägermann cone which is presented in Figure 1a. When the workability was measured the edge of the mortar was studied to look for indications of bleeding (Figure 1b and 1c). The indication of risk for separation was graded "clear", "slight", and "no" from visual observation.

Figure 1. 1a) The Hägermann cone filled with mortar. 1b) When the edge of a mortar is considered to indicate no risk for water separation according to the grading system. 1c) A combination with clear risk for water separation, which happened before the mortar acquired an acceptable workability.

Then the air content was measured on 1 dm³ mortar 5 min after the mixer had stopped. Then circa 0.5 dm³ of mortar were put in to a bucket of water, slowly mixed and dispersed with a large spoon which enabled a comparison between the foam created at the surface when the air inside the mortar ascend. Two different results are shown in Figure 2. In Figure 2b less foam is created since the bubbles come up to the surface and bursts quicker than the bubbles in Figure 2a. The foam created for each mix was graded from zero to two from visual observation in combination with photographs.

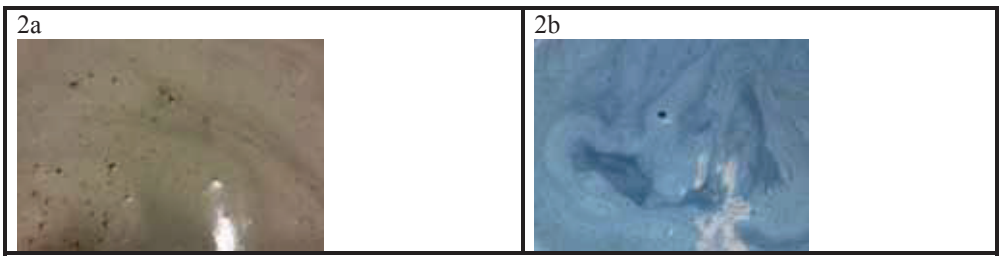

Figure 2. Both figures show an area of approximately 15x15 cm². 2a shows thick foam created at the surface with the foam rating 2. 2b shows less foam created with the foam rating 1.

The results from the admixture combination tests should be compiled according to Table 2. The results presented are from the variation where each of three AEAs has been combined with each of five different superplasticizers for the same binder. Since the recommended average mass of each AEA was used for all mixes, the total air content in the mixes with different SPs should only vary by a few percent if the SPs do not affect the air content.

According to the examples of results in table 2 there is clearly a wide spread of how well different combinations seems to work together with the binder. When evaluating the results a system was made to find the combination which seems to perform best out of the combinations which have been tested. First considerations were taken to the estimated risk for bleeding; the combinations that showed a clear risk were disregarded and focus was put on combinations considered to have no risk for water separation. Then the air content was studied by comparing the air contents for each AEA. As an example, when looking at AEA1 (in table 2) the combination with SP5 resulted in no risk for water separation, therefore approximately 12.5% was considered to be a minimum (or target) air content that the specified mass of AEA1 should result in when mixed with a SP with an acceptable interaction

(i.e. the approximate minimum air content was decided depending on the results from a combination without bleeding). This means that SP4 was also considered since it only had a slight indication of water separation and air content above 12.5%. The third factor which was considered was the workability. Since the SP is added until it looked like the mortar had a workability which was approximately 150 mm (an approved flow-measurement was set to be 130 mm or more). The addition of SP was also stopped when the water started to separate from the paste, hence the mass of SP could become more than the maximum recommended amount. When focusing on the combinations which performed well, the results presented a strong correlation between no indication of separation, high air content and a larger volume of stable foam.

Table 2. Compiled results from the mortar test of one binder.

Combination	Indication of water separation	Air content [%]	Workability [mm]	Superplasticizer[1] [%]	Foam
SP1[2]+AEA1[3]	Slight	9,6	170	112,0	1
SP2[2]+AEA1	Clear	5,2	170	126,8	1
SP3[2]+AEA1	Clear	7,2	175	126,5	1
SP4[2]+AEA1	Slight	15,1	155	257,8	2
SP5[2]+AEA1	No	12,5	170	196,7	2
SP1+AEA2[3]	Clear	4,3	175	417,3	0
SP2+AEA2	Clear	6,0	165	244,8	1
SP3+AEA2	Clear	18,5	120	103,8	1
SP4+AEA2	Slight	5,2	150	318,0	1
SP5+AEA2	No	11,5	180	125,7	2
SP1+AEA3[3]	Slight	13,5	225	65,0	2
SP2+AEA3	Slight	18,5	140	37,0	2
SP3+AEA3	Slight	15,0	185	33,0	2
SP4+AEA3	No	20,0	120	69,5	2
SP5+AEA3	No	21,5	130	68,3	2

[1] Mass of superplasticizer used divided by mass of maximum recommended amount.
[2] SP4 is based on a sulphonate melamine-formaldehyde condensate. The rest of the SPs is based on different modified polycarboxylates.
[3] AEA1 and AEA3 are based on a synthetic detergent. AEA2 is based on Vinsol resin.

When a combination which performed well had been found from evaluating the results another complementing test was made to get an indication if this combination would release air over time from the fresh concrete. This was done by measuring the air content after 5 min (same as before), 30 min and 60 min on the same recipe as before. Results from these tests were also considered before a combination of AEA and SP for each binder was determined for the concrete recipe which was used for the salt frost scaling test. The measurements made on the combination SP5+AEA3 showed the air content between 17.0 and 19.0% for the three measurements and not indicating a decrease over time. This was considered a good result, therefore the combination was chosen without doing the same test with other combinations.

3. Concrete for salt frost scaling test

3.1 Recipe and casting the concrete

To keep the binder content close to 430 kg/m³ the mass of aggregates was adjusted with consideration to the anticipated air content. The anticipated air content was 1.5, 2.5, 3.5 and 4.5 % and the mass of AEA was adjusted with the goal for the measured air content in the fresh concrete to be close to the anticipated air content for each cast. The air content was measured in a 8 dm³ of the fresh concrete, which was approximately 35% of the total mass of concrete mixed. Considering that the air content measurement was made on a large fraction of the cast, the measurement should be a good indication for the entire cast. When casting the concrete the mass of superplasticizer was constant for the four recipes which resulted in a slump of more than 150 mm (when no AEA was added) to facilitate the casting.

3.2 Curing

To enable the tested binder to come as close as possible to fully hydrated conditions, the concrete was cured for 1 day inside a covered steel mould, 7 days submerged in water (approximately 20°C), and 300 days sealed inside a climate room with 20.0±0.1°C. The purpose of the relatively short hydration in water counteracted any early drying shrinkage at the same time as should have added a negligible additional mass of water to the concrete surfaces. Therefore the long hydration in the climate room was constantly 100% RH with a limited mass of water at the set temperature.

3.3 Air void analysis

The air void analysis was done with the linear traverse methodology, according to the ASTM C 457 standard method [3], with one sample per cast. Linear traverse measurements are done by scanning a sample with a small light beam and at the same time measure the reflection. It requires thorough sample preparations to get accurate results from the reflections. First the sample surface is polished, then it is coloured with a black paint and the air voids are filled with zinc paste. When the light beam hits the zinc there is a strong reflection and the machine starts to draw a cord (line), when the light beam has past the air void filled with zinc and is back on the surface painted black there is much less reflecting light and the cord is finished. When approximately 3.5 meters has been measured on a sample (100x150 mm²), calculations are made to estimate the air content, spacing factor and specific surface from all of the cords. In table 4 results from linear traverse measurements are presented for four casts of concrete with 100 mass% CEM I as binder. Cast #4 contained ca 0.015 mass% of the air entraining agent.

Table 4. Results from four casts made with 100% CEM I. The variables presented are calculated from the linear traverse analysis.

Cast	Fresh Concrete [%][1)]	Air void content Total [%][2)]	<2 mm [%][2)3)]	<0.35 mm [%][2)4)]	Air void content in paste <2.00 mm [%][2)5)]	<0.35 mm [%][2)6)]	Specific surface [mm^{-1}][2)7)]	Spacing factor [mm][2)8)]
#1	1,10	3,6	0,8	0,3	2,3	0,9	15	0,76
#2	2,40	5,8	2,5	1,2	7,0	3,4	19	0,37
#3	3,50	5,2	3,9	1,7	11,1	4,9	19	0,30
#4	4,80	2,2	2,2	1,5	6,7	4,6	33	0,22

The results show that the specific surface increase and the spacing factor decrease when an increased mass of AEA is added to the mix. This trend is consistent when comparing the results from all voids and when looking at voids less than 2 mm. When all results was considered a general conclusion was drawn that the air void system was improved when the mass of AEA was increased.

4. Salt frost scaling test

4.1 Method

The salt frost scaling method is developed for the methodology described in this paper where concrete with a high degree of hydration and with various air void systems are tested. During development some factors were chosen to enhance the effect from the salt frost scaling damage e.g. the temperature cycle which is used has been shown to increase the salt frost scaling damage in comparison to the CDF-cycle [1, 4]. This enabled the present methodology to test how the salt frost scaling mechanism(s) is affected by different factors and the effect the mechanism(s) has on concrete with favourable conditions (high degree of hydration and various air void systems) with a high resolution while using climate chambers with air as a thermal conductor. This enables a study as to which properties have the biggest impact on concrete salt frost scaling resistance. These must be considered when varying the binders used for the concrete in structures which is exposed to de-icing salts and freezing temperatures. A detailed description is given in [2].

4.2 Scaling results

The figures below show scaling results from four CEM I concrete casts presented in table 4.

Figure 3 presents non-cumulative results from each separate cast including the mean scaling from all (six) samples together with the standard deviation. In [2] an argument is made that the salt frost scaling method contributes to a relatively constant salt frost scaling load. Considering this with the fact that Figure 3 shows non-cumulative results with measurements of the total scaling per seven cycles, the general gradient of the curve highlights information about an acceleration or deceleration of the scaling damage.

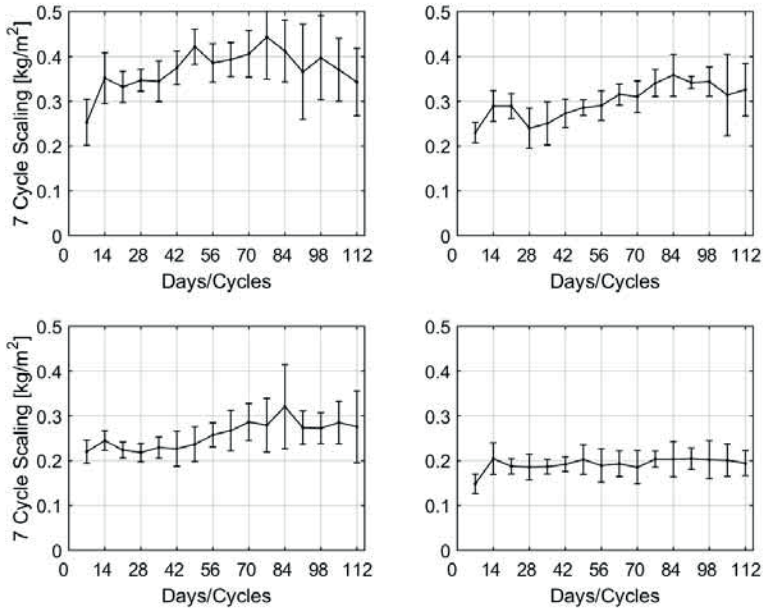

Figure 3. Scaling results measured at each measurement occasion (not cumulative). The line presents the mean scaling from the six samples from each cast after 112 cycles. The error bars present the standard deviation for the six samples at each occasion measurements were done. Upper left show the results from cast #1. Upper right show the results from cast #2. Lower left show the results from cast #3. Lower right show the results from cast #4.

Figure 4 presents a compilation of all mean values of the results, 4a non-cumulative and 4b cumulative. Both highlight the decrease in salt frost scaling damage when improving the air void system, however, they should be presented together to complement each other. 4a shows indications of acceleration and the rate of the salt frost scaling process, while 4b highlights distinctions between each cast at the same time as it presents the total average scaling.

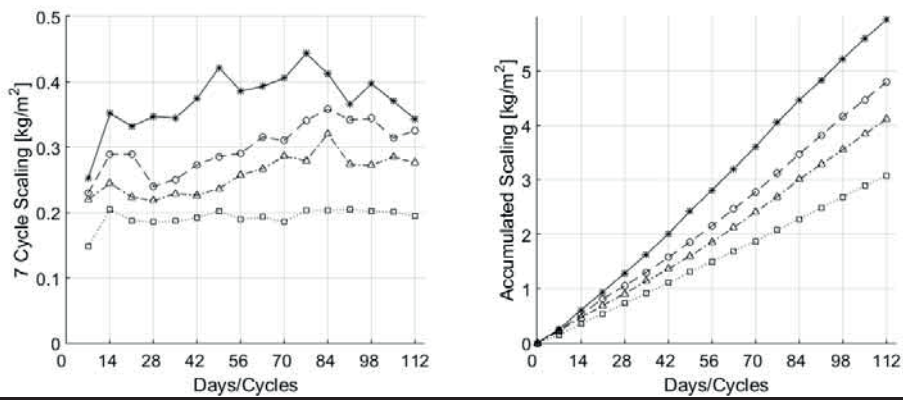

Figure 4. The average mass of scaling for one sample for each cast. 4a shows scaling measured at each measurement occasion. 4b shows the cumulative mass of scaling.

Figure 5 shows a general summary of the results by presenting the total average mass of scaling for all samples, and the error bars show the total mass of scaling from the sample with the most and least mass of scaling after 112 cycles from each cast. This highlights the decrease in salt frost scaling damage, but a slight con is that there is no information provided about the salt frost scaling process for each material.

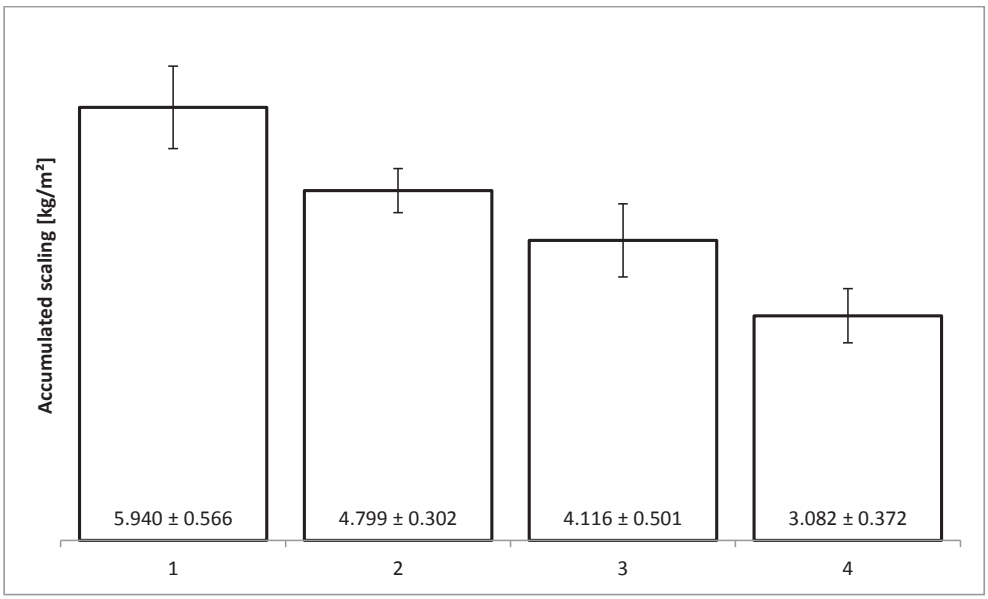

Figure 5. The numbers present the average mass of scaling per sample (6 samples per cast) after 112 cycles. The error bars present the total mass of scaling for the sample with the most and least mass of scaling after 112 cycles.

5. Discussion

When analysing the results from the mortar test, air void analysis and salt frost scaling test it is clear that they seem to agree with three main ideas. First, the mortar test showed that the combination of AEA and SP is vital for minimizing the risk of bleeding and to enable the creation of a relatively stable air void system. Secondly, the results from the air void analysis show that it is also possible to create slightly different air void systems by changing the amount of AEA when using the combination from the mortar test. Finally, by testing concrete which have been sealed for a long time all samples from the same batch will have a high degree of hydration with little variation. This means that the microstructure will not change due to hydration during the testing which contributes to more constant conditions for the material during the test. By using the salt frost scaling method with a high precision and presenting the results according to the diagrams used in chapter 4, the air void systems effect on the salt frost scaling damage on the concrete can be observed for the binder (or binder combination) of interest.

Considering results presented in the current article, the methodology is considered to contribute information of the salt frost scaling mechanism(s) and how it affects various binders given favourable conditions. When a binder is hydrated according to this methodology it will be as close to fully hydrated as can be, given the water binder ratio used. When testing cast #1 (which is the fully hydrated concrete, only containing a SP which provides an excellent workability) with a salt frost scaling method which contributes a relatively constant salt frost scaling load, a non-accumulative and cumulative baseline is acquired for the binder's (or concrete's) salt frost scaling resistance. When this baseline for the binder is known, the impact in salt frost scaling resistance from adding AEA and thereby improving the air void system can then be measured for the specific binder. The salt frost scaling method used also contributes information about the salt frost scaling process over time for the binder.

5.2 Future studies

To obtain more information about the salt frost scaling mechanism(s) and how it varies for concrete with various properties (e.g. concrete containing different SCMs) a grading analysis should be made on the scaled material. The grading will contribute more information about how the average size of the scaled material varies from the beginning of the test until the end of the test, which will give information about the salt frost scaling process. This would also enable an analysis of how the average scaling size varies when the air void system changes. When considering different additives it would be interesting to compare the difference in average scale size between different additives.

Additional salt frost scaling tests should be made with AEA and SP combinations which do not seem to perform well according to the first mortar test results. This would acquire more information about the effectiveness and reliability of the mortar test used. It would also give a better comprehension about the difference in scaling for the salt frost scaling method which increases the mass of scaling damage and enhance knowledge about the salt frost scaling mechanism(s). The results from these complementary tests could also give information about the robustness of a certain binder to various admixtures combinations.

Since the salt frost scaling test method which has been used differs from the standard methods the following should be noted. This method is designed to contribute to a large amount of scaling damage from the salt frost scaling mechanism(s) and provide a higher resolution in the results when testing concrete with a water binder ratio of 0.40 (which could concrete considered when building e.g. a bridge). This means that any claim of a limit for the mass of scaling for a concrete to be considered salt frost scaling resistant cannot be made without much more testing preferably with a lot of field tests to verify the lab results. Another option could be a large round robin test where concrete with various salt frost scaling resistances is tested according to the method presented in [2] together with some of the standard methods [5, 6]. This would provide information about how the salt frost scaling method used in this methodology compares to the other methods, considering relative mass of scaling when testing concrete with the same binder/binder combination. The results would also show if all methods give the same indications about how the salt frost scaling damage increase or decrease when testing various factors, e.g. when varying binder combination, binder content, or air content in the same binder.

6. Conclusions

- The methodology enables a study of the salt frost scaling mechanism(s) in concrete with a high degree of hydration which contributes to an optimal microstructure for any binder regardless of hydration rate. Therefore more constant material conditions during the salt frost scaling test in comparison to tests of young concrete.
- This methodology enables an analysis of how differences in the air void system affects the mass of salt frost scaling damage from a relatively constant salt frost scaling mechanism(s) load for a concrete with a given microstructure.

References

[1] Sjöbeck H (2015) The time dependency of salt-frost damage at low temperature on concrete with SCMs. Lund University, (in Swedish), Master of Science thesis, https://lup.lub.lu.se/student-papers/search/publication/7454864

[2] Strand MJ (2016), Salt frost scaling in uncarbonated concrete containing fly ash and slag with various air void contents, Licenciate thesis, Lunds University, TVBM 3181

[3] ASTM (2012) ASTM C457 / C457M - 12, Standard Test Method for Microscopical Determination of Parameters of the Air-Void System in Hardened Concrete.

[4] Jacobsen S, Saether DH, Sellevold EJ (1997) Frost testing of high strength concrete: Frost/salt scaling at different cooling rates Materials and Structures/Materiaux et Constructions 30:33-42

[5] Setzer MJ, Fagerlund G, Janssen DJ (1996) CDF Test - Test method for the freeze-thaw resistance of concrete - tests with sodium chloride solution (CDF) Materials and Structures 29:523-528 doi:10.1007/bf02485951

[6] SS137244 (2005) Concrete Testing – Hardened Concrete – Scaling at freezing, Swedish Standards Institute, (in Swedish) 10 p.

Paper II

MethodsX 5 (2018) 1299–1310

Contents lists available at ScienceDirect

MethodsX

journal homepage: www.elsevier.com/locate/mex

Method Article

Test method for de-icing salt-frost scaling in high-performance concrete

Martin J. Strand*, Katja Fridh

Division of Building Materials, Lund University, Lund, Sweden

A B S T R A C T

This paper describes a de-icing salt-frost scaling test method for analysis of the salt-frost scaling behaviour in high-performance concrete with various binders. The method was therefore designed to result in considerable scaling damage for the concrete considered to be salt-frost resistant. In addition, the experimental set-up was designed to avoid leakage, and to allow testing of a large number of samples. The method was validated by testing concrete with three different binders with a water–binder ratio of 0.40 with 5% air content. Various preconditioning procedures and freeze–thaw cycles were evaluated. The results show that the freeze–thaw cycle chosen results in a large mass of scaling and the salt-frost scaling behaviour agreed with the findings of previous studies. Thus, the method was considered suitable to study the salt-frost scaling behaviour in high-performance concrete. Three distinguishing features of the method are the following:

- The freeze–thaw cycle result in a large mass of salt-frost scaling to enable study of high-performance concrete.
- The concrete sample is above the salt solution to prevent leakage. The test surface is submerged 2 mm into the salt solution inside a cup.
- Freezers with air as the thermal medium are used to allow a large number of samples.

A R T I C L E I N F O

Method name: De-icing salt-frost scaling in high-performance concrete

Keywords: Test method, High-performance concrete, Durability, De-icing salt-frost scaling, Freeze–thaw cycle

Article history: Received 4 June 2018; Accepted 4 October 2018; Available online 9 October 2018

* Corresponding author.
E-mail address: martin.strand@byggtek.lth.se (M.J. Strand).

https://doi.org/10.1016/j.mex.2018.10.007

Specifications Table

Subject area	• *Materials Science*
More specific subject area	This is a method testing the de-icing salt-frost scaling behaviour in high-performance concrete. De-icing salt-frost scaling is a type of superficial damage that occurs when a low concentration of de-icing salt solution freezes in contact with a concrete surface.
Method name	De-icing salt-frost scaling in high-performance concrete
Name and reference of original method	CEN/TS 12390-9 (2006) Testing hardened concrete - Part 9: Freeze–thaw resistance - Scaling. 24 p. Fagerlund G (1982) The influence of slag cement on the frost resistance of the hardened concrete vol 1. Swedish Cement and Concrete Research Institute, Stockholm Lindmark S (2010) On the Relation between Air void system parameters and Salt frost scaling. Nordic Miniseminar: Freeze–thaw testing of concrete, Vedbaek, Denmark. Nordic Concrete Federation, pp 41-58 Utgenannt P (2004) The influence of ageing on the salt-frost resistance of concrete. Doctoral Thesis, Faculty of Engineering, LTH, Lund University
Resource availability	Concrete mixer and related equipment for casting concrete. Air content tester for fresh concrete. Materials desired in the concrete. Cylinder moulds with 100-mm diameter. Concrete saw. Climate chamber with a stable temperature, relative humidity and carbon dioxide concentration. Logger able to record temperature, relative humidity, and carbon dioxide concentration. Freezer able to cycle between –25 °C and +25 °C. Materials specified in section '1. Method details'.

Method details

De-icing salt-frost scaling is a type of superficial damage that occurs on concrete structures. This happens when water with a low concentration of de-icing salt freezes in contact with a concrete surface. The outermost layer of the concrete structure protects the reinforcement bars. Thus, if the concrete is not salt-frost scaling resistant, the protective concrete layer will scale off as a result of repeated freezing and thawing. This will in turn shorten the period of time until the reinforcement bars start to corrode; thus, the service life of the concrete structure is shortened. There are various methods to assess the salt-frost scaling resistance of concrete [1–7]. All of these methods use a low-concentration salt solution. This solution is in contact with the concrete test surface during the test. The salt solution and concrete are then exposed to a freeze–thaw cycle. The conditions of the freeze–thaw cycle are different (cycle duration, max and min temperature) for each salt-frost scaling test method.

Two important features of the proposed method are the freeze–thaw cycle and the sample setup. The method was designed to enable the testing of high-performance concrete, which generally has a high salt-frost scaling resistance. Hence, the selected freeze–thaw cycle should result in a large mass of scaled material. The method should also be able to detect how different preconditioning processes affect the salt-frost scaling behaviour with various binders. Since a large mass of scaled material can result in leakage of salt solution if the solution is on top of the surface, the test surface was instead submerged into a salt solution inside a cup. The sample size was chosen to allow a large number of samples to be tested at the same time.

Sample preparation

The preparation and preconditioning of the test surface have a large influence on the salt-frost scaling results [6,8–12]. It is therefore essential that the preconditioning process is controlled and documented. Here, 200 mm long concrete cylinders with a diameter of 100 mm were cast. Each cylinder was later sawed into four concrete samples. Therefore each sample had a length of approximately 49 mm and a diameter of 100 mm. Only sawed surfaces were tested to minimise the influence of inhomogeneity at the cast surface which can increase the spread in the results.

The preconditioning of the test surfaces comprised three stages, as shown in Fig. 1, namely, internal curing (IC), drying and carbonation (DaC), and resaturation (RS). IC consisted of sealed hydration before the concrete cylinders were sawn. Here, the cylinders were cured in the moulds for 24 ± 2 h. After de-moulding, the cylinders were submerged in lime-saturated tap water for seven days and were then placed in plastic bags

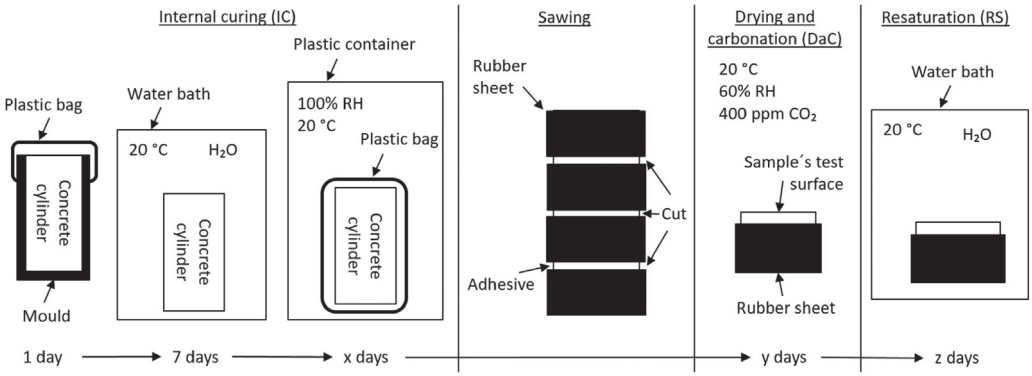

Fig. 1. Overview of the preconditioning process and preparation of the concrete samples including internal curing (IC), sawing, drying and carbonation (DaC), and resaturation (RS).

until they were sawn. DaC occurred after the concrete cylinders had been sawn. In this step, the concrete sample test surfaces were exposed to +20 ± 0.5 °C, 60 ± 2% relative humidity (RH) and about 400 ppmv CO_2. During the RS period, the test surfaces were exposed to tap water before the start of the salt-frost scaling test.

The sides of each concrete sample were sealed with a rubber sheet (length: 330 ± 1 mm, width: 40 ± 1 mm). This was normally done during the DaC period, but if the preconditioning did not include a DaC period, this was done during the IC period. The rubber sheet was fastened with an adhesive. To enable the adhesive to attach to the surface, the concrete cylinders were taken out of the plastic bags for about 1 h to dry before the rubber sheet was fastened to the surface by the adhesive. Since the rubber sheet was only 40 mm wide, sections of the cylinder were left with only a layer of adhesive where the saw was applied (Fig. 1). This was done to avoid sawing into the rubber which would rip the rubber off. The sawn concrete samples were then placed back into the plastic bags. If the preconditioning did not include any DaC, the samples were placed directly into water after they had been sawn, for the RS period.

Preparation of sample setup

The sample setup is presented in Fig. 2. The insulation mould was made by gluing two pieces of insulation together. Before the two pieces were fastened together, a hole (ø 105 mm) was drilled in the bottom piece. Since the elastic rubber sheet had a thickness of 3 mm, the total diameter of the sample,

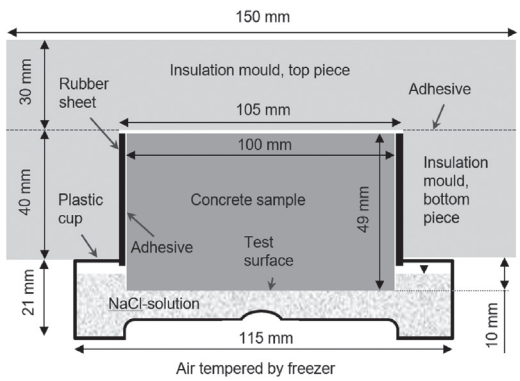

Fig. 2. Section of the sample setup including the extruded polystyrene insulation mould (XES 300 j, Paroc AB, Skövde, Sweden), the EPDM-rubber sheet (3 mm 120 ± 20 kg/cm^3, Lundgrens Sverige AB, Gothenburg, Sweden) fastened with a silyl-modified polymer adhesive (Xtreme fix, Casco, Sika Sverige AB, Spånga, Sweden), and a polypropylene plastic cup (S Unipac Square, Nordic Pack, Nykvarn, Sweden). The 3 mass% NaCl solution was deionised water and 99.9% NaCl (Falksalt, Gothenburg, Sweden).

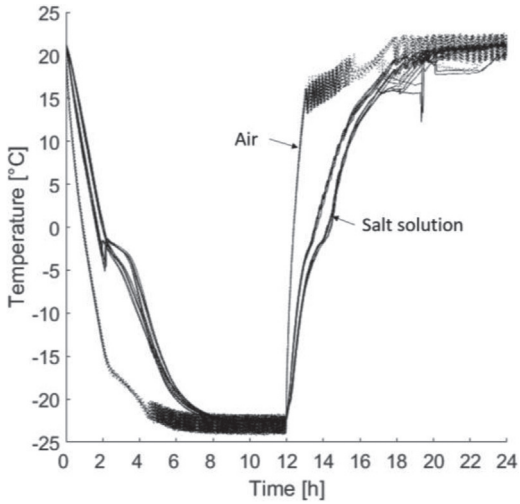

Fig. 3. Temperature cycle measured in the air inside a freezer and in the salt solution in a cup.

adhesive, and elastic rubber sheet was 106 mm. This meant that the sample could be pressed into the insulation mould. This eliminated the need for any spacers inside the cup for the sample to stand on.

The test surface was submerged 2 mm into the salt solution. To achieve this, the sample test surface should be 10 mm from the insulation mould. This was accomplished consistently by using a distance aid with a thickness of 10 mm (length: 150 mm, width: 150 mm) and a hole in the middle with a diameter of 120 mm. The concrete sample was placed inside the hole in the distance aid, with the test surface in contact with the table. The insulation mould was then pressed down on the sample until it was in contact with the distance aid.

Each cup was cut from the bottom of a plastic jar. The cup were then filled with 100 ± 1 ml of 3 mass % NaCl solutions using a 100 ml plastic syringe. The 3 mass% NaCl solution was made by mixing 4850 g deionised water and 150 g salt with NaCl. The insulation mould together with the concrete samples were then placed on top of the cup. This resulted in the sample setup shown in Fig. 2.

Measurement procedure

The samples were placed inside a freezer (CF-A700, Kylcity, Skogås, Sweden). Each freezer had seven shelves and nine samples were placed on each shelf. The samples were then exposed to a pre-defined temperature cycle in which the air inside the freezers was maintained at $-22\,^{\circ}$C for 12 h and $+22\,^{\circ}$C for 12 h. Fig. 3 presents the temperature cycle, both in the salt solution and in air. It was important to always measure the temperatures inside the freezer and inside at least one cup in each freezer with a known position of the thermocouple. For additional information regarding the temperature cycle, see section '2.2 Methodical aspects – *Temperature cycle*'.

Fig. 4 show all the equipment used during the measurements. The following measurement procedure was done every seventh cycle. First, paper filters were prepared, and a batch of salt solution was mixed. The filters were marked with the sample name and the number of freeze–thaw cycles that each sample had been exposed to. When new salt solution and filters had been prepared, one shelf at a time was taken out of the freezer. All the samples from the shelf were placed on a working bench in the same order as on the shelf (⑦ in Fig. 4). Each sample was gently removed from its plastic cup and was placed inside an open tray (②, ⑧ and ③ in Fig. 4). At that point, it was important to check that the test surface has been in contact with the salt solution. This was done by observing whether there was any notable movement in the salt solution during removal of each concrete sample. If this was not the case, some solution was assumed to have leaked from the cup, and this was noted. Then the salt solution and the scaled off material was poured into a paper filter (⑥ in Fig. 4). The test surface of each sample was

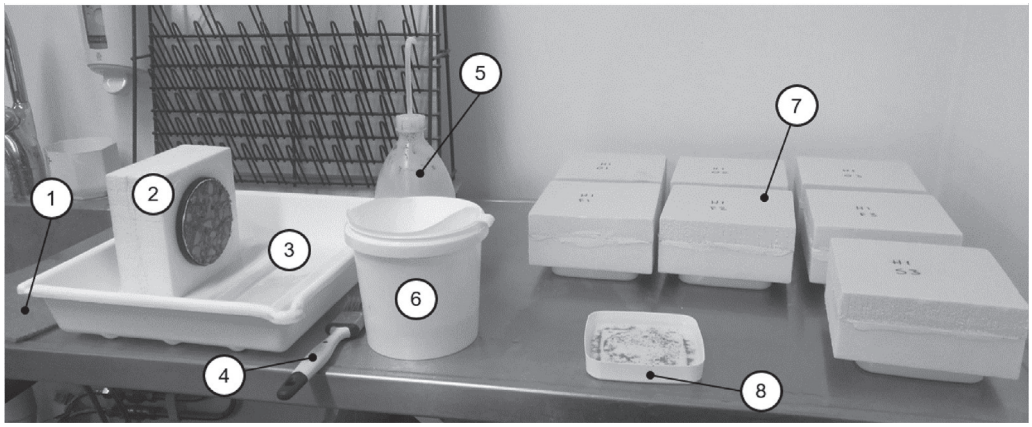

Fig. 4. Equipment used during a measurement. ① Wet cellulose-based cloth (Wettex, Norrköping, Sweden), ② sample ready to be brushed, ③ open plastic tray for brushing test surface, ④ paint brush, ⑤ plastic flask with tap water, ⑥ plastic container with holder for filters and filter (Melitta Original 1 × 4 coffee filters (white), Melitta Unternehmensgruppe Bentz KG, Minden, Germany), ⑦ samples from the same shelf inside the freezer, and ⑧ plastic cup containing scaled material and salt solution.

brushed about 15 to 25 times in four perpendicular directions (fewer times when there was less mass scaling and vice versa) with a paint brush (④ in Fig. 4). Thereafter, the surface was rinsed with tap water which was collected in an open tray (⑤ and ③ in Fig. 4), and the sample was placed on a wet cellulose-based cloth (① in Fig. 4). All water on the test surface and the insulation mould was then wiped off. Then, the mass of each sample, including the insulation mould, rubber sheet, and adhesive was determined using a balance with 0.1 g resolution. The cup was then refilled with new salt solution, and the sample was placed back into the cup. The sample together with the plastic cup were then placed at the same position on the shelf as before. The scaled material that was collected in the tray was then poured into the filter as well. The filters containing the scaled material were then dried at 105 ± 5 °C until the change in mass was less than 0.001 g. The dry mass of the scaled off concrete was determined using a balance with 0.001 g resolution, and the mass of the filter was subtracted. Each step in the measuring procedure was designed with the aim to minimise spread in the results due to the method.

Methodical aspects

Choice of cups

With the proposed sample setup, the choice of material and size of the cup is important. Pre-tests were performed using petri dishes made of tempered glass, but they cracked during the measurements. A second test of cups was made using polypropylene plastic cups with the diameter of 115 mm. During this test, the solution sometimes leaked from the cups. This leaking was believed to be caused by insufficient volume of the cup. Instead, quadratic polypropylene plastic cups with the 115 mm sides were tested and did not leak. Thus, these cups were chosen to be used in the method.

Temperature cycle

When designing the freeze–thaw cycle, the aim was to create a tough cycle that would yield a large mass of scaled material. The reason for this was to enable testing of high-performance concrete with a water binder ratio of 0.40 with 5% air content. The chosen temperature settings gave a cycle where the test surfaces were exposed to −22 °C for slightly more than four hours. Previous studies have shown that lowering the minimum temperature increases the mass of scaling [10,13–15]. Therefore, this cycle

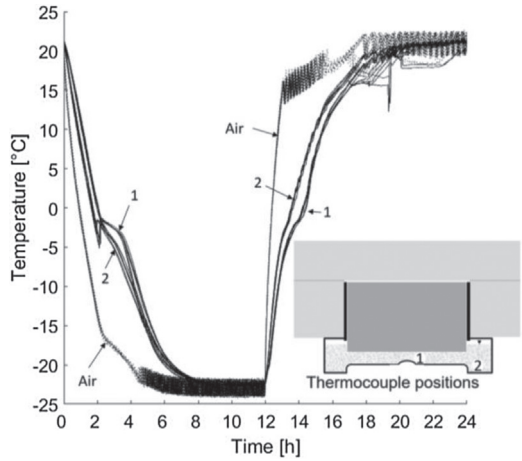

Fig. 5. Temperature measurements from 14 freeze–thaw cycles. Seven measured cycles in position 1 and seven measured cycles in position 2 with the same thermocouple.

can be considered tough with regard to the minimum temperature. Another factor that makes the cycle tough is that an increased period of time when the samples are exposed to the minimum temperature increases the mass of scaled material [11]. An additional advantage of the temperature cycle is that it provides more than eight hours to perform the salt-frost scaling measurements after each freezing period. This is enough to finish measurements on 63 samples during one thawing period.

To investigate the importance of the position of the thermocouple, measurements were made inside in the solution of seven samples during 14 cycles each. During seven of these cycles the thermocouple was in position 1, shown in Fig. 5, and in position 2 for the other seven. The difference in temperature between the two positions was investigated because the bottom of the plastic cup was not flat. However, the position of the thermocouple had no significant impact on the temperature. In Fig. 6, measurements from 14 cycles for seven different samples inside the solution are presented. Seven cycles was measured in each of the two positions. These seven samples were on seven different

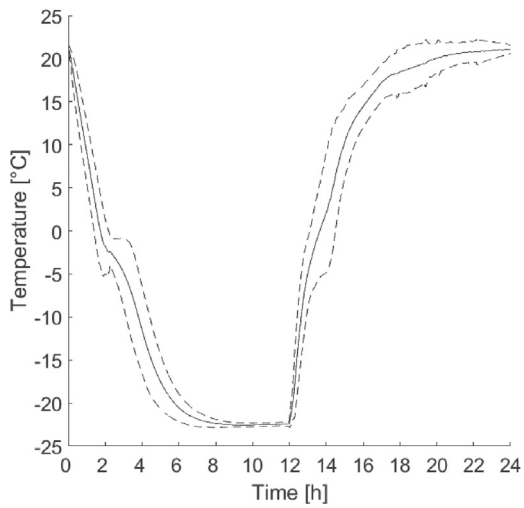

Fig. 6. Mean value and mean value plus or minus two times the standard deviation of 98 cycles.

Table 1
Basic recipes for the materials used in testing of the method.

Binder	CEM I	Fly ash	Slag	Water	Aggregates		Air content
	[kg/m^3]	[kg/m^3]	[kg/m^3]	[kg/m^3]	0–8 [kg/m^3]	8–16 [kg/m^3]	[%]
100% CEM I	430.0	0	0	172	925.5	786.7	ca. 5
65% CEM I + 35% Fly ash	279.5	150.5	0	172	925.5	786.7	ca. 5
65% CEM I + 35% Slag	279.5	0	150.5	172	925.5	786.7	ca. 5

Table 2
Preconditioning of the samples used for each test during the validation of the method.

Factor tested	Internal curing (IC) [days]	Drying and carbonation (DaC) [days]	Resaturation (RS) [days]	Internal curing + resaturation (IC + RS) [days]
Shortened freezing period	36	0	1	37
Prolonged freezing period	64	0	1	65
DaC period	30	0	1	31
	30	87	1	31
RS period	28	31	28	56
	55	31	1	56
	56	32	0	56

shelves during the measurements. These measurements show that the setup gives a low spread in temperature during the cycle despite the different locations of the thermocouple.

Tests were made to optimise the positioning of the samples inside the freezer. This was done to obtain a low spread in the temperature cycle for each sample and to maximise the number of samples that could be placed in the freezer. This was done by varying the number of shelves and the number of samples on each shelf. However, the air circulation inside the freezers gave an even temperature cycle for all samples. Thus, the number of samples that could be tested in the freezer simultaneously was only limited by the available space.

Method validation

The method was assessed to confirm that it can differentiate between concrete with three different binders preconditioned in different ways. Three different factors were studied: the freeze–thaw cycle, the DaC period, and the RS period. The basic recipes are presented in Table 1 and the preconditioning process of each cast is presented in Table 2. Comparisons between the results are made of samples with the same total hydration period without external drying of the test surface, i.e. IC plus RS according to Table 2. The hydration of the test surface during the DaC period is assumed to be negligible. Therefore, comparing samples with the same binder that had the same total period of IC plus RS, it is considered a fair comparison with regards to the degree of hydration. One cast was made with each recipe for each of the three tests. More information about the materials can be found in 'Additional information'.

Freeze–thaw cycles

The first validation test studied the effect of different freeze–thaw cycles, with three variations of the freezing and thawing times, as shown in Fig. 7. The times each sample was exposed to temperatures below −21 °C in each cycle were approximately 2 h, 4 h, and 12 h. All cycles were 24 h in total. The results are presented in Figs. 8 and 9. For a comparison of the 2-h and 4-h cycles, the samples were preconditioned in the same way ('Shortened freezing period' in Table 2). The samples used to

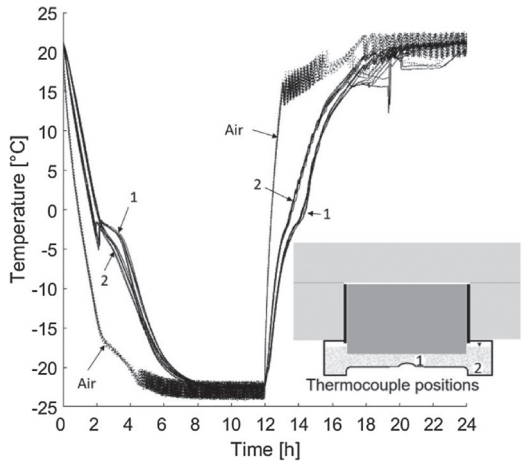

Fig. 7. Freeze–thaw cycles studied; data from [16]. The graph shows two measurements for each cycle. All measurements were made inside the salt solution with the thermocouple at position 1 according to Fig. 4.

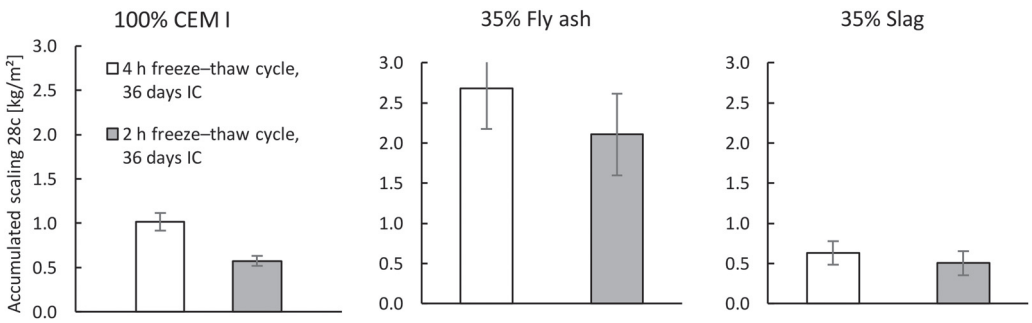

Fig. 8. Influence of a shortened freezing period (cycles '4 h' and '2 h' in Fig. 6) on the salt-frost scaling for each binder. All samples had 36 days of IC and one day of RS (no DaC period). Mean accumulated salt-frost scaling and standard deviation for six samples (from cast #3 of each binder) after 28 cycles; data from [16].

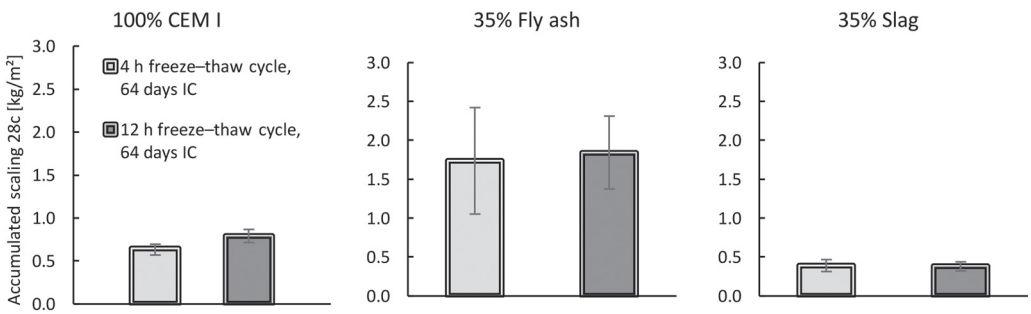

Fig. 9. Influence of a prolonged freezing period (cycles '4 h' and '12 h' in Fig. 6) on the salt-frost scaling for each binder. All samples had 64 days of IC and one day of RS (no DaC period). Mean accumulated salt-frost scaling and standard deviation for six samples (from cast #3 of each binder) after 28 cycles; data from [16].

compare the 4-h and 12-h cycles were also preconditioned in the same way ('Prolonged freezing period' in Table 2). In addition, a comparison was made between the two different preconditioning processes with samples exposed to the 4-h cycle as shown in Fig. 10.

The results presented in Figs. 8 and 9 indicate that the salt-frost scaling increases when the freezing time is prolonged and the thawing time is shortened. These results agree with the findings of previous research [11,15]. As seen in Fig. 10, a comparison of the samples exposed to the 4-h cycle with either 36 days or 64 days of IC, the scaling decreased with increased hydration time. These results also agree with the findings of previous research [6,17–20]. Therefore, the method can evaluate the effect of different freeze–thaw cycles as well as the effect of increased hydration time on concrete with various binders.

Drying and carbonation

The second validation test studied the effect of the DaC period by comparing samples that were exposed to 87 days of DaC (at 20 °C with 60% RH and about 400 ppmv CO_2) with samples exposed to zero days of DaC. Since water evaporates during the DaC period, the samples exposed to DaC contained a lower water content before the salt-frost test began. In addition, the surface of the samples exposed to DaC were carbonated before the salt-frost scaling test began. The samples that were not exposed to any DaC period were assumed to have had an uncarbonated surface and a higher water content after the RS period. The accumulated mass of scaling is presented in Fig. 11.

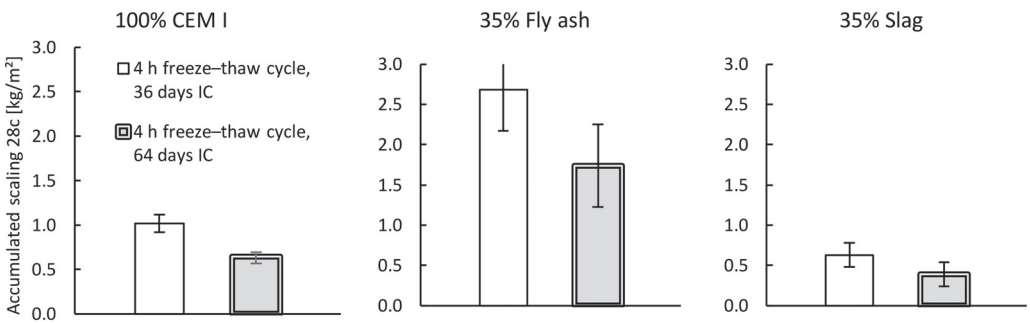

Fig. 10. Influence of an increased period of IC when samples were exposed to a 4-h cycle on the salt-frost scaling for each binder. Mean accumulated salt-frost scaling and standard deviation for six samples (from cast #3 of each binder) after 28 cycles; data from [16].

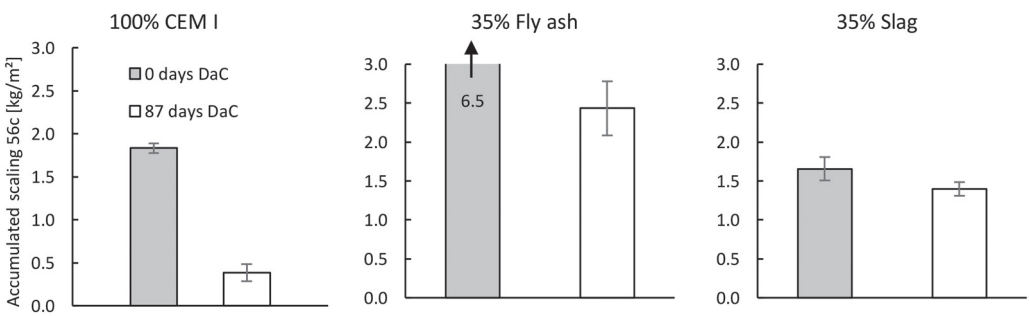

Fig. 11. Influence of two different DaC periods on the salt-frost scaling for each binder. All samples were subjected to IC for 30 days and had one day of RS, in addition to the DaC period. Mean accumulated salt-frost scaling and standard deviation for six samples (from cast #1 of each binder) after 56 cycles.

DaC resulted in a lower mass of salt-frost scaling for concrete containing 100% CEM I, which also was found by [6]. DaC also decreased the salt-frost scaling for concrete containing 35 mass% fly ash, but the samples still showed a large mass of salt-frost scaling. The concrete containing slag showed a very small decrease in the mass of salt-frost scaling from drying and carbonation. These results indicate that the method can distinguish the differences in the salt-frost scaling behaviour for the three different binders preconditioned with and without a DaC period.

Resaturation

The third validation test studied the effect of changing the RS period through a comparison of samples with three different RS periods, namely, 0 days, 1 day, and 28 days. Therefore, the main factor that was varied was the water content of the samples at the start of the salt-frost test. Fig. 12 presents the total mass change from the start of the DaC period until the end of the RS period, before the start of the scaling test. The IC was varied to have the same total period of IC and RS for all the samples to decrease the effect of different degrees of hydration when the salt-frost test began. The samples with 0 days RS were placed directly into the salt solution 2 ± 1 h before the first freezing cycle began. All of these samples were dried and carbonated for approximately 32 days before the RS period. The salt-frost scaling results are presented in Fig. 13.

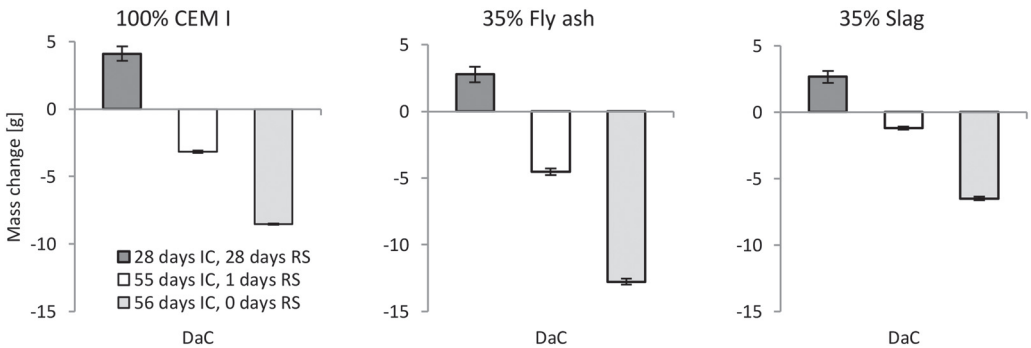

Fig. 12. Mean mass change for three samples (from cast #2 of each binder) during the DaC and various RS periods along with the total mass change from the beginning of the DaC begins until the end of the RS period.

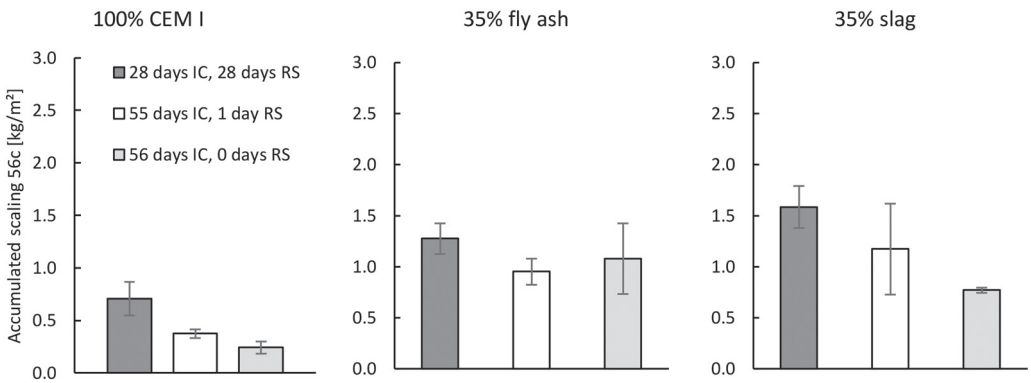

Fig. 13. Influence of the RS period on the salt-frost scaling for each binder. All samples had 32 or 31 days of DaC in addition to IC and RS. Mean accumulated salt-frost scaling and standard deviation for three samples (from cast #2 of each binder) after 56 cycles.

DaC results in a reduction in mass due to evaporation of moisture close to the test surface, and RS results in an increase in mass due to water uptake. As seen in Fig. 12, the mass of samples exposed to 28 days of RS increased from the start of the DaC period until after the RS period. The samples exposed to 1 and 0 days of RS showed a decrease in mass, where samples with 0 days of RS had the lowest water content at the start of the salt-frost test.

The salt-frost scaling results are presented in Fig. 13. An increased RS period increased the mass of salt-frost scaling for concrete with 100% CEM I and concrete containing 35% slag. The results from concrete containing 35% fly ash are not as clear, but [10] also found the moisture history of the test surface is an important factor of the salt-frost scaling damage. Again, the method is able to distinguish the different behaviours of different binders preconditioned in different ways.

Conclusions

- The sample setup and temperature cycles gave a tough temperature cycle with a small spread. This resulted in a large mass of scaling and enabled testing of high-performance concrete (water binder ratio of 0.40 with 5% air content).
- The method detects differences in de-icing salt-frost scaling behaviour for various factors, such as different binders, preconditioning processes, and freeze–thaw cycles.
- The method allows for a large number of samples to be tested simultaneously.

Acknowledgements

We would like to express our sincere gratitude to Dr Maria Fredriksson for invaluable support when writing this paper. We also acknowledge the support from Henrik Sjöbeck who tested the method in his Master's thesis. Additional thanks to Dr Sture Lindmark and Dr Peter Utgenannt who contributed important input during the development of the method and sample setup. This research was funded by The Development Fund of the Swedish Construction Industry (SBUF) and Cementa AB (a part of Heidelberg Cement Group).

Appendix A. Supplementary data

Supplementary material related to this article can be found, in the online version, at doi:https://doi.org/10.1016/j.mex.2018.10.007.

References

[1] CEN/TS, CEN/TS 12390-9 in Testing Hardened Concrete - Part 9: Freeze-Thaw Resistance - Scaling, (2006) , pp. 24.
[2] ASTM, ASTM C672/C672M-12, in Standard Test Method for Scaling Resistance of Concrete Surfaces Exposed to Deicing Chemicals, (2012) .
[3] MTO, M.o.T.O., MTO LS-142, in Scaling Resistance of Concrete Surfaces Exposed to Deicing Chemicals, (2012) Ontario, Canada.
[4] BNQ, S.o.t.P.o.Q., NQ 2621-900, (2002) Montréal, Quebec, Canada.
[5] G. Fagerlund, The Influence of Slag Cement on the Frost Resistance of the Hardened Concrete, Swedish Cement and Concrete Research Institute, Stockholm, 1982.
[6] P. Utgenannt, The Influence of Ageing on the Salt-Frost Resistance of Concrete. Doctoral Thesis, Department och Building and Environmental Technology. Faculty of Engineering, LTH, Lund University, 2004 TVBM 1021.
[7] S. Lindmark, On the Relation between Air Void System Parameters and Salt Frost Scaling. in Nordic Miniseminar: Freeze-Thaw Testing of Concrete Vedbaek, Denmark, (2010) .
[8] S. Jacobsen, E.J. Sellevold, Frost/Salt scaling testing of concrete - importance of absorption during test, Nordic Concr. Re. 14 (1994) 26–44.
[9] E. Helsing, P. Utgenann, The salt-frost resistance of concrete with supplementary cementitoius materials (SCM), Materials, Systems and Structures in Civil Engineering 2016, Technical University of Denmark, Lyngby, Denmark, 2016.
[10] E.J. Sellevold, T. Farstad, Frost/Salt-Testing of Concrete: Effect of Test Parameters and Concrete Moisture History, (1991) .
[11] S. Jacobsen, D.H. Saether, E.J. Sellevold, Frost testing of high strength concrete: Frost/salt scaling at different cooling rates, Mater. Struct./Materiaux et Constructions 30 (195) (1997) 33–42.
[12] S. Jacobsen, et al., Frost deicer salt scaling testing of concrete: effect of drying and natural weathering, Cem. Concr. Aggreg. 19 (1) (1997) 8–16.
[13] W. Studer, Internal comparative tests on frost-deicing-salt resistance, International Workshop in the Resistance of Concrete to Scaling Due to Freezing in the Presence of De-Icing Salts, (1997) Sainte-Foy, Québec, Canada.

[14] P.-E. Petersson, Influence of Minimum Temperatures on the Scaling Resistance of Concrete. Part 1: Portland Cement Concrete, SP Swedish National Testing and Research Institute, 1994, pp. 30.
[15] S. Lindmark, Mechanisms of Salt Frost Scaling of Portland Cement-Bound Materials: Studies and Hypothesis. Doctoral Thesis, Department of Building and Environmental Technology. Faculty of Engineering, LTH, Lund University, 1998 TVBM 1017.
[16] H. Sjöbeck, The Time Dependency of Salt-Frost Damage at Low Temperature on Concrete With SCMs. Master Thesis, Building and Environmental Technology, Lund University, 2015 TVBM-5101.
[17] A. Krishnan, et al., Technical Issues Related to the Use of Fly Ash and Slag During Late-Fall (Low Temperature) Construction Season, Indiana Department of Transportation, Purdue University, 2006, pp. 358.
[18] N. Bouzoubaâ, et al., Deicing salt scaling resistance of concrete incorporating supplementary cementing materials: laboratory and field test data, Can. J. Civ. Eng. 35 (2008) 1261–1275.
[19] J. Marchand, M. Jolin, Y. Machabée, Deicer salt scaling resistance of supplementary cementing material concrete: laboratory results against field performance, Cement Combinations for Durable Concrete, University of Dundee, Scotland, UK, 2005.
[20] H. Arnfelt, Damage on Concrete Pavements by Wintertime Salt Treatment, Statens Väginstitut, 1943, pp. 28.

Paper III

The air void contents effect on the salt frost scaling of uncarbonated concrete containing siliceous fly ash or slag

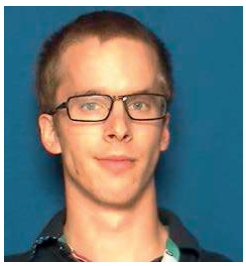

Martin Strand
M.Sc. PhD Student
Building Materials
Department of Building and Environmental Technology
Faculty of Engineering, LTH, Lund University
P O Box 188, SE-221 00 Lund, Sweden
Phone +46 46 222 4260
E-mail: martin.strand@byggtek.lth.se

Katja Fridh
M.Sc., PhD., Supervisor
Building Materials
Department of Building and Environmental Technology
Faculty of Engineering, LTH, Lund University
P O Box 188, SE-221 00 Lund, Sweden
Phone +46 46 222 3323
E-mail: katja.fridh@byggtek.lth.se

ABSTRACT
The first half of this PhD project has analysed the effect various air void contents has on the mass of de-icing salt frost scaling (DISFS) of uncarbonated concrete containing siliceous fly ash or slag. This has been done by finding a combination of air entraining agent and superplasticizer for each binder combination that has been used to enable the creation of various air void contents. Then the concrete has been cured moisture sealed for 307 days hydrated before the DISFS test began. The results show that the DISFS resistance vary between the different binders and the air void content clearly has various impacts on the DISFS depending on the binder combination.

Key words: Frost action, Supplementary Cementitious Materials (SCM), Testing, Admixtures, De-Icing Salt Frost Scaling

1. INTRODUCTION

To lower the energy consumption and carbon dioxide (CO_2) emissions from cement production fractions of the binder can be replaced with supplementary cementitious materials (SCMs) such as fly ash, slag and lime filler which has been used in this project. However, when adding these SCMs the hydration products and therefore final microstructure of the concrete changes in comparison to when only ordinary Portland cement is used [1]. This can affect the mass of de-icing salt frost scaling (DISFS) resistance of various concrete surfaces.

Two other factors which affect the DISFS of concrete is the air void system [2, 3] and preconditioning; carbonation [4], temperature and moisture history of the concrete test surface [5]. According to the theories and observations regarding the mechanisms of the DISFS in concrete containing 100% CEM I is that when creating an air void system (e.g. by including an air entraining agent (AEA)) in the concrete the mass of DISFS will decrease [2, 3]. However, it is uncertain if the air void system has the same effect when the concrete contain siliceous fly ash

(SFA) or ground granulated blast furnace slag (GGBFS) since the microstructure will differ. Therefore this project have tested concrete containing various fractions of SFA or GGBFS and made each recipe with 4 different air void contents. In addition to this, the DISFS test is split in to two different series. The first series is finished, where the concrete had hydrated for 307 days and never dried before the DISFS test began. Since it had never dried it can be assumed that the surface is uncarbonated. In the second large series samples from the same casts will be tested. These samples have hydrated for the same time, however then they have dried and carbonated in 20 °C and 60% RH for approximately 700 days before the test start. This study will therefore result in more information regarding how the mass of DISFS varies for concrete containing different binder combinations and how various air void systems affect these. The present article will present some of the results from the first series which have tested the never dried and therefore uncarbonated test surfaces.

2. MATERIALS

One type of ordinary Portland cement (CEM I) is used in all recipes, one type of siliceous fly ash is used and one type of ground granulated blast furnace slag is used. The name of the cement, according to the European standards [6], is CEM I 42,5 N - SR 3 MH/LA. Table 1 present each binder combination that has been tested.

Table 1 – Binder combinations used in the studies.

Binder	Abbreviation
100% CEM I 42,5 N - SR 3 MH/LA	CEM I
80+20 mass% CEM I + SFA	F20
65+35 mass% CEM I + SFA	F35
80+20 mass% CEM I + GGBFS	S20
65+35 mass% CEM I + GGBFS	S35
30+70 mass% CEM I + GGBFS	S70
65+25+10 mass % CEM I + GGBFS + LF	K35

The project also tested three air entraining agents and five superplasticizers to find one combination of AEA and SP which work well together with each binder combination. When one combination of AEA and SP had been found for each binder combination, four air void systems were created by varying the mass of AEA.

3. RESULTS

To get an indication of the air void system inside the casts air void analysis was made on one sample (100x150 mm²) per cast with linear traverse according to the standard [7]. When varying the mass of AEA the air void analysis showed that the amount of small air voids increased according to Table 2.

Table 2 – Air voids <0.35 mm in the paste for each binder combination and each cast

	Air voids <0.35 mm in the paste [%]						
Cast	CEM I	F20	F35	S20	S35	S70	K35
1	2,8	0,9	1,0	2,2	1,5	2,6	3,0
2	2,8	2,6	2,2	3,0	3,9	3,2	3,5
3	3,9	3,3	4,7	3,7	4,3	4,1	4,5
4	5,7	5,9	5,8	6,1	6,7	3,5	4,9

The increase in small air voids was expected when increasing the mass of added AEA. Other results from the air void analysis did not show the same consistency, e.g. spacing factor and specific surface presented in Table 3. These results would most likely show a clearer trend (e.g. smaller spacing factor with increasing AEA) if more samples, i.e. larger total surface area, had been analysed with linear traverse from the same casts.

Table 3 – Air content in the concrete for each binder combination and each cast

	Specific surface [mm^{-1}]						
Cast	CEM I	F20	F35	S20	S35	S70	K35
1	16	6	15	9	8	13	14
2	17	23	13	10	16	17	15
3	20	15	30	22	22	14	20
4	20	21	19	27	18	15	22
	Spacing factor [mm]						
Cast	CEM I	F20	F35	S20	S35	S70	K35
1	0,43	1,00	0,53	0,66	0,75	0,52	0,45
2	0,40	0,33	0,44	0,49	0,37	0,38	0,40
3	0,33	0,41	0,20	0,32	0,29	0,39	0,29
4	0,27	0,28	0,27	0,21	0,26	0,42	0,28

Figure 1 and 2 present the accumulated scaling after 56 cycles for the different binder combinations. Each binder combination has four bars that present the different casts with different masses of AEA that created four different air void systems with an increased amount of small air voids.

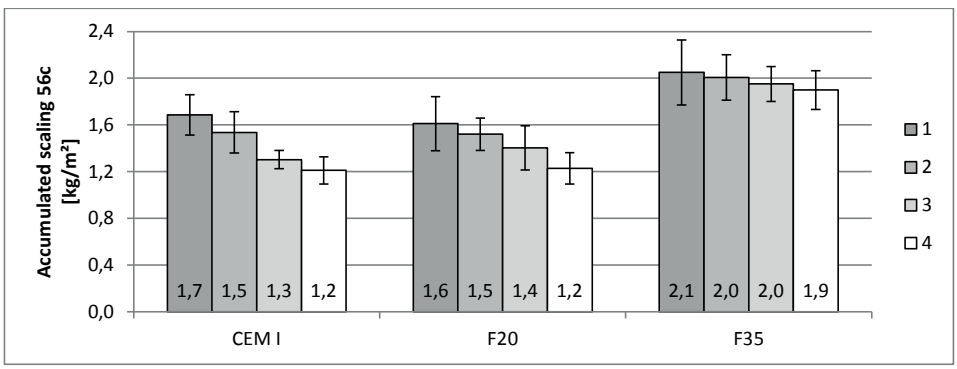

Figure 1. Each bar present the mean accumulated scaling together with the standard deviation for 6 samples after 56 cycles. Cast #1 contained 0 g AEA and cast #4 contained the largest mass of AEA.

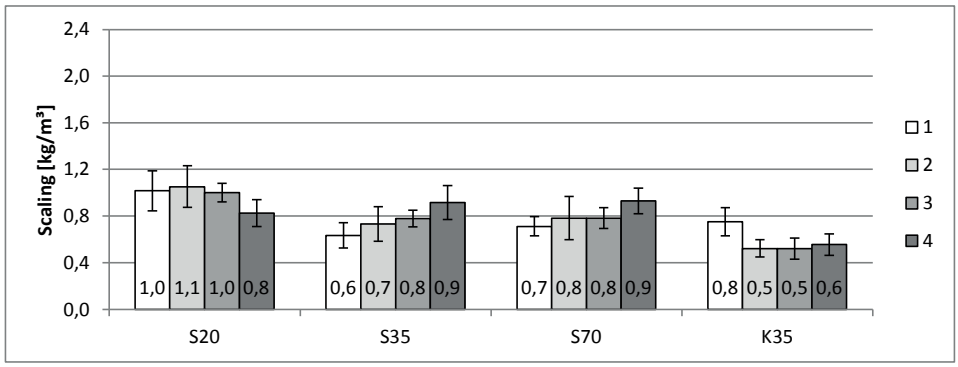

Figure 2. Each bar present the mean accumulated scaling together with the standard deviation for 6 samples after 56 cycles. Cast #1 contained 0 g AEA and cast #4 contained the largest mass of AEA.

4. CONCLUSIONS

Here are some of the conclusions drawn so far from the DISFS test results.

- The various binder combinations that have been tested produce various masses of DISFS which mean that the differences in the structure and properties between them could contribute to resisting the DISFS mechanism to various extents.
- An increased amount of small air voids in the hardened cement paste has various effects on the mass of DISFS for the various binder combinations.
    - There seems to be a consistent decrease in mass of DISFS with an increased amount of small air voids for CEM I and CEM I + siliceous fly ash concrete.
    - The concrete containing CEM I with GGBFS seems to generally have a lower mass of scaling, however the recipes does not seem to gain the same consistent effect as the concrete with SFA from the increased amount of small air voids.

REFERENCES

[1] K., B.E.S., *Evolution of pore structure in blended systems.* Cement and Concrete Research, 2015. **73**: p. 25-35.

[2] Valenza II, J.J. and G.W. Scherer, *A review of salt scaling: II. Mechanisms.* Cement and Concrete Research, 2007. **37**(7): p. 1022-1034.

[3] Powers, T.C., *The mechanism of frost action in concrete (Part II).* Cement, Lime and Gravel, 1966. **41**(6): p. 5.

[4] Utgenannt, P., *The influence of ageing on the salt-frost resistance of concrete*, in *Department och Building and Environmental Technology*. 2004, Faculty of Engineering, LTH, Lund University: Lund. p. 346.

[5] Sellevold, E.J. and T. Farstad, *Frost/Salt-testing of Concrete: Effect of Test Parameters and Concrete Moisture History.* 1991.

[6] 197-1, S.-E., *Cement - Part 1: Composition, specifications and conformity criteria for common cements*. 2011. p. 48.

[7] ASTM, *ASTM C457 / C457M - 12, Standard Test Method for Microscopical Determination of Parameters of the Air-Void System in Hardened Concrete*. 2012.

Paper IV

Experimental study of the influence of carbonation, SCMs, and air content on the de-icing salt-frost scaling of well-hydrated concrete. Part 1: Concrete containing low-calcium fly ash

Martin J. Strand, Katja Fridh

Division of Building Materials, Lund University, Lund, Sweden

Corresponding author's info.

E-mail: martin.strand@byggtek.lth.se

Abstract

This is the first part in a two-part series on de-icing salt frost scaling (DISFS) in well-hydrated concrete containing low-calcium fly ash or slag with various low air contents that were carbonated or noncarbonated. This first part presents the methods used and aims to answer how drying and carbonation and various air contents affect DISFS in concrete hydrated for over 300 days containing 20 or 35 mass% fly ash. The second part presents results from concrete containing slag. The approach has been to perform capillary suction, low-temperature calorimetry; pH measurements; thin sections, linear traverse, and DISFS tests. The carbonation of concrete containing 100% CEM I decreased the DISFS. The noncarbonated and carbonated concrete with 20% fly ash resulted in the same DISFS. For concrete with 35% fly ash, carbonation increased the DISFS. The effect of the air content on the DISFS varied depending on the binder and preconditioning.

Keywords: Concrete, de-icing salt frost scaling, low-calcium fly ash, carbonated, noncarbonated, air void system, capillary suction, low-temperature calorimetry

Introduction

Concrete is the most common building material in the world and represents 5-8% of man-made carbon dioxide emissions [1]. These emissions can be reduced by replacing some of the CEM I with supplementary cementitious materials (SCMs) such as low-calcium fly ash (LCFA). An understanding of the climate to which concrete with LCFA can be exposed requires a study of the durability of this material. This study focuses on the de-icing salt frost scaling (DISFS) of concrete

with LCFA. The DISFS is a superficial damage that occurs when a low concentration salt solution freezes in contact with concrete. This can occur on constructions such as bridges, pavements and balconies made of concrete if a de-icing salt is used during freezing periods.

The DISFS of concrete has been studied since at least the first half of the 20th century to understand the mechanism and to see how different environmental and material factors affect DISFS [2]. Different theories regarding the underlying mechanisms and what factors most influence the mechanisms have been presented [3-11]. The early theories were that hydraulic pressures, osmotic pressures and pressures exerted on the wall from the growing ice body (or ice lens) were the main reasons behind the DISFS [3-11]. The hydraulic pressures are created from solution being squeezed through small pores when ice nucleation starts in voids that do not contribute to a freezing depression [4]. The osmotic pressure is enabled due to gradients of salt concentrations that also force moisture transport to thermodynamic equilibrium [12]. The ice body (or ice lens) growth is created by to the moisture transport caused by both the gradients of salt concentrations and accessibility to an outer reservoir of liquid [7]. For all of these mechanisms moisture uptake and ice formation are believed to be two of the most important factors. The moisture uptake relates to the ability of the sample to saturate, and if the degree of saturation increases, the pressures from the stated mechanisms increase. The same applies to ice formation; if more ice is formed, the pressures from the stated mechanisms increase. Therefore, it is natural that some research regarding the DISFS mechanism focuses on the moisture uptake before and during the DISFS test and ice formation [7, 8, 13]. Valenza and Scherer showed that the osmotic pressures caused by differences in the ion concentration will not reach destructive levels due to hydrodynamic relaxation [9]. The reason for this is that the moisture flow is much faster than the ion diffusion in concrete [9]. Instead, they suggest glue spalling as the main mechanism behind the salt frost scaling [9]. The glue-spalling mechanism is caused by the combined ice and brine layer on top of the concrete shrinking more than the concrete due to thermal contraction. This creates shear stresses large enough to cause the removal of scallops [9]. However, they also mention the bursting of air voids, which is described in the same way as the critical degree of saturation [14]. This is caused by the 9 vol% expansion of ice in pores with a degree of saturation larger than 91%. (highest critical degree of saturation [14]). This causes unfrozen liquid to be pressed through the microstructure, thus the pressure on the pore walls increases [9, 14]. The pressure on the pore wall due to the nucleation can be determined by the Clausius-Clapeyron condition, which reveals that a freezing point depression as small as 0.25 °C will be large enough to damage the concrete [9].

Concrete is a complex material in which the microstructure will change over time due to e.g. hydration, leaching, and carbonation. When there is a change in the

material properties, this most likely means that the durability also changes. Therefore, it is important to know how the carbonation will change the properties of the hardened paste made with a certain binder. Previous research has shown that carbonation of different binders results in various changes in the microstructure [8, 15]. Carbonation is a spontaneous chemical reaction between the hardened binder paste and the carbon dioxide (CO_2) in the atmosphere [15]. When the concrete contains only ordinary Portland cement, carbonation primarily consists of CO_2 from the atmosphere reacting with portlandite ($Ca(OH)_2$) [15]. The products of this reaction are calcium carbonate ($CaCO_3$) and water (H_2O) [15]. In addition, the calcium silicate hydrates and ettringite also carbonates, since the CO_2 reacts with hydrates containing Ca resulting in a decalcification [15]. When adding low-calcium fly ash the Ca/Si ratio decreases, which results in an increased vulnerability to carbonation since the calcium content is lower [15]. Carbonation results in a change in the structure and porosity [16-25]. When the porosity and microstructure changes, the DISFS also changes [8].

There have been many previous studies on the DISFS of concrete containing LCFA [26-37]. However, there is a lack of research on carbonation combined with drying and how various air contents affect DISFS in concrete. In addition, most studies use standard test methods that test concrete that is approx. 30 days old, whereas this study used concrete that had hydrated for over 300 days, i.e., making the conditions more favourable for blended cements with low hydration rates. This study presents results from pH measurements, capillary suction, low-temperature calorimetry (LTC), thin section analysis, linear traverse analysis, and the DISFS test. All these tests, except for the thin section and linear traverse analysis, have been made on both carbonated and noncarbonated samples from the same batches. The pH measurements were made to estimate the extent of carbonation of the samples used for the LTC measurements and the capillary suction measurements. These samples were exposed to accelerated carbonation. The LTC measurements show how much ice has formed at different temperatures. The capillary suction measurements give information about the moisture uptake into the materials. LTC and capillary suction both also give information about the microstructure. The LTC gives information about the pore volume <50 nm [38] since these pores infer a freezing suppression. The capillary suction gives information about the total permeability for the entire pore volume since a coarse permeability results in a high initial absorption rate and a fine permeability results in a low initial absorption rate. The thin section analysis was made on a carbonated sample to show the carbonation depth before the DISFS test. The linear traverse analysis gives information about the air void content for voids larger than approx. 10 µm [39]. The DISFS test was made on concrete exposed to more than 300 days of internal curing (the time before the sample was sawn. Only sawn surfaces were tested). The noncarbonated samples were sawn and then resaturated for one day

before the DISFS began. For each noncarbonated sample, another adjacent sample was taken from the same cylinder that was dried and carbonated for 735 days before resaturation and the beginning of the DISFS test. Therefore, all of the samples used during the DISFS test were well hydrated. These measurements have been made to discuss the following questions: How does an increased fraction of LCFA affect the microstructure? How does drying and carbonation of each binder change the microstructure? How does an increased fraction of LCFA affect DISFS? How does drying and carbonation of each binder affect the DISFS? How does an increased air content affect DISFS in concrete with various fractions of LCFA? Does the effect of the air content on DISFS change depending on whether the surface is carbonated?

Method and materials

Concrete recipes

The cement used in all concrete recipes was a low-alkali CEM I 42,5 N SR 3 classified according to EN197-1 [40]. The low-calcium fly ash (Class F according to [41]) is a waste product that comes from coal power plants. To enable a comparison with other studies the binders were characterized by X-ray fluorescence (XRF), inductively coupled plasma (ICP), Blaine measurement, laser diffraction analysis and compressive strength on the hardened paste. These measurements on the binders are presented in the supplementary materials attached to this article.

The recipes were designed to test the effect the air content has on the DISFS for each binder. Four batches with different air contents were made for each binder according to Table 1. The target air contents for batches 1, 2, 3, and 4 were 1.5, 2.5, 3.5, and 4.5% respectively. Batch 1 only included a superplasticizer, whereas batch 2, 3, and 4 also contained an air entraining agent to get the air content as close as possible to the target air content. The method for selecting the combination of admixtures and additional information about the methodology are given in [42]. The measured air contents in the fresh pastes are presented in Table 1. The grain-size fraction curve of the aggregates used had a combined fineness modulus of 4.79 [43].

Table 1
Concrete recipes for each batch.

Batch	CEM I[1] kg/m³	LCFA[2] kg/m³	Aggregate[3], kg/m³ 0-8	8-12	12-16	Air[4] %	Slump mm	Density[5] kg/m³
CEM I-1	430	0	966	285	536	3.2[6]	165	2399
CEM I-2	430	0	953	281	529	3.0[6]	160	2405
CEM I-3	430	0	939	277	521	4.5[6]	200	2375
CEM I-4	430	0	926	273	514	5.1[6]	220	2331
F20-1	344	86	966	285	536	1.6[7]	190	2413
F20-2	344	86	953	281	529	2.6[7]	220	2367
F20-3	344	86	939	277	521	3.5[7]	200	2371
F20-4	344	86	926	273	514	4.5[7]	210	2339
F35-1	280	151	966	285	536	2.1[7]	220	2382
F35-2	280	151	953	281	529	2.7[7]	230	2327
F35-3	280	151	939	277	521	4.1[7]	230	2309
F35-4	280	151	926	273	514	5.1[7]	240	2277

[1] CEM I 42,5 N - SR 3 LA (Degerhamn anläggningscement, Cementa AB).
[2] Low-calcium fly ash from Emineral A/S.
[3] Calculated with consideration of the target air contents of 1.5, 2.5, 3.5 and 4.5% for batches 1, 2, 3, and 4 respectively.
[4] Air content was measured in 8 dm³ of the fresh concrete.
[5] Density was determined on the same concrete as the air content.
[6] Superplasticizer was based on a polycarboxylate and the air entraining agent was based on a synthetic detergent.
[7] Superplasticizer was based on sulphonated melamine-formaldehyde condensate and the air entraining agent was based on a synthetic detergent.

pH measurement of samples exposed to accelerated carbonation

In the capillary suction measurements and in the LTC measurements, samples that had been exposed to an accelerated carbonation were used. To quantify the extent of the carbonation, pH measurements were made on noncarbonated and carbonated samples. The pH in the concrete is a measure of the alkalinity in the pore solution, which is approx. 12.7 to 13.1 for the low-alkali cement used in the current study [44]. The carbonation of concrete, when calcium hydroxide turns into calcium carbonate, reduces the pH below 10 [45]. Therefore, pH measurements give an indication of the extent of the carbonation.

The preconditioning process is presented in Table 2. “Internal curing” is the time from casting until the sample was sawn from the cylinder and the sawn test surface was exposed to drying and carbonation. “Accelerated carbonation” is the time that the samples were exposed to 0.5-1.1 vol% CO_2 in boxes with 56% relative humidity (RH). According to [8, 46], an accelerated carbonation with increased CO_2 concentration can change the carbonation process in comparison to a natural carbonation. However, when limiting the concentration to 1 vol% CO_2, it is likely to resemble natural carbonation in 0.04 vol% to a large extent [46]. The high CO_2

concentration was created by manually adding CO_2. The climates inside the boxes were logged during the carbonation. “Drying without carbonation” is the time the samples were exposed to 0% CO_2 inside a glovebox with 35% RH. The 0% CO_2 concentration was created by using a CO_2 absorbent. The samples used for the pH measurements were preconditioned in the same way as the samples used for the capillary absorption and LTC measurements.

Table 2
Preconditioning of samples used for the pH measurements, capillary absorption measurements, and LTC measurements.

Process	Internal curing, days	0.5-1.1% CO_2, 56% RH, and 20 °C, days	0% CO_2, 35% RH and 20 °C, days
Drying without carbonation	1053 – 1204	0	49 – 77
Accelerated carbonation	1221 – 1387	83	0

The measurements were made on samples from the batches with the highest air content. The samples were 2-5 mm particles, similar to those used for the LTC. They were ground by hand into powder and placed in deionized water (10 g powder in 200 g deionized H_2O). The measurements were made in a fume cupboard that contributed to a variation of the temperature during the measurements. All measurements were made in 19±1 °C

The pH metre (Thermo Scientific Orion, model 720A 220 VAC) was first calibrated with two buffer solutions (pH 7 and 12). After the calibration the measurements were made by first rinsing the metre with deionized H_2O, measuring in the sample solution for 5 min, and rinsing the metre with deionized H_2O. The pH metre was then used to measure on a 7.00 pH buffer solution for 1 min and rinsed in deionized H_2O, before the next sample was measured. The measurement inside the 7.00 pH buffer was made to get a baseline to see if the measurements change over time. This baseline did not change much. Therefore, the temperature variation during the measurements did not significantly contribute to a variation in the pH measurements. Since the whole sample was crushed, the pH of the carbonated samples was expected to be below the pH of the noncarbonated samples. If the sample is completely carbonated the pH is expected to be below 10.

During the preconditioning inside the box, the CO_2 concentration decreased from approx. 1.00 vol% - 0.80 vol% (10 000 ppmv - 8 000 ppmv) after approx. 16 h. However, when the container was tested without concrete samples inside it, the concentration did not decrease as much. This means that the decrease in CO_2 concentration could be used to get an indication of when the samples are completely carbonated.

Low-temperature calorimetry

The LTC measurements were made to get information about the microstructures and how carbonation affects the microstructure of each material. This enables an analysis of what properties of the microstructure are favourable and non-favourable for the DISFS. A measurement shows how much ice is formed at each temperature. According to the Gibbs-Thomson equation, the melting point is dependent on the pore size [47]. Therefore, the thawing curves of these measurements give some information about the pore size distribution [47]. The pore size needed for a significant freezing depression to occur is a radius of 50 nm or lower [38, 48]. Therefore, an LTC measurement gives information on the microstructure and pores with a radius smaller than 50 nm. The pores with a radius between 2 nm and 50 nm are called mesopores [38, 47, 48]. The method used in the current study is the same as that used in [38], which was shown to be reliable for studying the mesopores.

The hysteresis between the freezing and thawing curves gives some information about the microstructure based on the theory presented by [49]. The hysteresis is created from large pores being surrounded by smaller pores [49]. Another factor contributing to the hysteresis is that the ice formation is a stochastic process. The water inside the large pores cannot freeze before the water has frozen in the smaller surrounding pores [49]. When the water thaws, the water inside the small pores thaws before the surrounding ice in the larger pores has thawed [49]. The results also enable an analysis of how carbonation affects the amount of ice that is formed at different temperatures and how the hysteresis is affected by carbonation, i.e., how the microstructure changes due to the carbonation of each binder.

All tests were performed with samples from batch 4 of each binder (Table 1). The samples are placed inside a 3 ml plastic container and consist of 2-5 mm concrete particles (taken from crushed cylinders) that each weighed approximately 0.3 g. The total mass of each sample was 2.0-2.5 g. For each measurement two samples were used, one vacuum-saturated sample and one reference sample, both with approx. the same masses. The reference samples were taken from the same batch to minimize the difference in heat capacity between the reference and the vacuum-saturated sample. The noncarbonated and carbonated samples were preconditioned according to Table 2 before the drying or vacuum saturation. The vacuum saturation was performed in three steps. First, the samples were placed in a desiccator at approx. 40 mbar pressure for 60-70 minutes. Then, the desiccator was filled with deionized water and the low pressure was maintained for another 60-70 minutes. Finally, the pump was switched off and the samples were kept in the water for 46 to 142 h at normal indoor air pressure. Before the vacuum-saturated samples were placed in the calorimeter, the particles were wiped with a wet cellulose-based cloth and weighed. The reference samples were dried at 105 °C for 24 h before the measurements. After the measurements, the samples were dried at

105 °C to obtain the dry mass and to calculate the evaporable water content that each sample contained during the test.

The LTC measurements were made with a Setaram BT 2.15 temperature scanning calorimeter. The results show the heat flow produced from the exothermic phase change of water to ice, and the reverse during thawing. The temperature cycle started at +20 °C with a ramp of -6 °C/h to the minimum temperature of -80 °C, then a ramp of +6 °C/h back to +20 °C. Since the samples are small, the temperature is more or less the same through the entire sample at a given time. To evaluate the results, the baseline and the amount of ice formed were calculated according to the J-method presented in [50].

Capillary absorption

The capillary absorption measurements were made to give information about the water absorption of the total pore volume, and how the water absorption changes with carbonation. This also gives information about the microstructure and permeability since a pore system with large pores and a high connectivity will absorb water faster than an air void system with small pores and low connectivity. When comparing the LTC and the capillary absorption measurements, the LTC primarily gives information about the mesopores with a radius between 2 nm and 50 nm, whereas the capillary absorption measurements give information about the entire pore structure (primarily pores larger than the mesopores). To quantify the properties related to the moisture absorption three factors are calculated: the resistance to water penetration (Eq. 1), the coefficient of capillarity (Eq. 2) and the porosity (Eq. 3). This enables an analysis of how these factors are changed by the carbonation of each binder. This also enables an analysis to see if these factors seem to affect the DISFS and if so, how the changes in these factors affect the DISFS for the different binders. To get more information about the microstructure, the samples were first dried at 35% RH and room temperature, and then at 105 °C. An RH of 35% dries all pores larger then approx. 2 nm [51], whereas 105 °C will overestimate the total porosity since some of the chemically bound water evaporates [52]. Since the samples were dried at 35% RH and vacuum saturated before they were dried at 105 °C, the damage caused by the drying at 105 °C did not affect the previous measurements. The drying at 105 °C was made to enable comparisons with e.g., [8], since drying in 105 °C has been widely used in previous studies.

$$m = \frac{t}{h^2} \quad \text{Eq. 1}$$

$$c = \frac{W_n - W_i}{\sqrt{t}} \quad \text{Eq. 2}$$

$$P_{tot} = \frac{V_{open}}{V_{tot}} = \left(\frac{Q_{sat,air} - Q_{dry}}{\rho_w}\right) / \left(\frac{Q_{sat,air} - Q_{sat,water}}{\rho_w}\right) \quad \text{Eq. 3}$$

t = time when knickpoint is reached, s

h = thickness of specimen, mm

W_n = mass water of absorbed water per unit area at knickpoint, kg

W_i = initial mass of water in sample at start of test, kg

V_{open} = open pore volume, %

V_{tot} = total sample volume, %

$Q_{sat,a}$ = mass of vacuum-saturated sample in air, kg

$Q_{sat,w}$ = mass of vacuum-saturated sample in water, kg

$Q_{dry,35\%}$ = mass of sample dried in 35% RH, kg

$Q_{dry,105\ °C}$ = mass of sample dried in 105 °C, kg

ρ_w = density of water, kg/m³

The measurements were made with samples that were 100 mm in diameter and 5 mm thick in Petri dishes with cellulose-based cloth and deionized water. The samples were laid on the cellulose-based cloth. Deionized water was added to each dish until there was visible free water on top of the cloth. The samples were taken from the petri dish and placed on a slightly wet cellulose-based cloth before it was placed on the balance, and then returned to the Petri dish. Each measurement took approx. 20 s. At least 12 measurements were made during the first 8 h, then 4 additional measurements were made during two weeks after the first measurements. Measurements were made on three samples for each binder. The samples were taken from batches with the highest air content (batches #4 in Table 1). The noncarbonated and carbonated samples were preconditioned according to Table 2.

Air void analysis by linear traverse measurements

The air void analysis with linear traverse was made to quantify the air void system. This enables an analysis of how the DISFS is affected by an increased amount of air entraining agent, which result in an increased air content. The air void system

was quantified by calculating the specific surface, spacing factor and a rough air void size distribution.

The linear traverse measurement was performed by Pelcon Materials & Testing ApS (Copenhagen, Denmark) according to ASTM C457 [39]. One sample of 150x100 mm test surface from each batch was analysed after at least 36 days of hydration.

Thin section analysis

Microscopic analysis was made on thin section samples that had been preconditioned in the same way as the DISFS samples. Therefore, the thin section analysis shows the same carbonation depth as the DISFS samples. The depth of carbonated layer can be correlated to an accumulated mass of scaling since 1 mm deep scaling corresponds to approx. 1 kg/m² scaling. Therefore, by quantifying the carbonation depth the effect from the carbonated layer can be seen in the DISFS results. Second, a check was performed for micro cracks in the surface from sawing the samples or drying shrinkage that could increase the DISFS. Third, the homogeneity in the paste was analysed to see if the hydration of the paste was even and make sure that no water separation has occurred adjacent to aggregates. Finally, an examination for agglomeration of air voids was made. The third and fourth points were made to ensure that the combination of superplasticizer and air entraining agent was working well together with the binder. Previous tests have shown that the combination of superplasticizer and air entraining agent increases the risk of bleeding for some binders [53].

The preconditioning process for the thin section samples and carbonated samples used for the DISFS test are presented in Table 3. “Internal curing” represents the time from casting until the sample was sawed and the test surface was exposed to a different climate. “Drying and carbonation” represents the time the test surfaces were exposed to 60±5% RH, 0.04% CO_2. After the drying and carbonation the samples were sent to RISE (Research Institutes of Sweden) for the sample preparation.

Table 3
Preconditioning of samples used for thin section analysis and carbonated samples used for the DISFS test.

Test	Internal curing (IC), days	Drying and carbonation (DC), days
Thin section	307 – 308	707 – 873
Dried and carbonated DISFS samples	307 – 308	733 – 735

The thin section samples were cut from samples similar to the DISFS samples (100 mm diameter and 50 mm high) to the dimensions 90x40 mm² with a thickness of approx. 25 µm. One thin section sample was made from batch 4 (with

the highest air content) of each binder (Table 1). The microscopic analysis was made with fluorescence and polarized light. The fluorescent light enabled quantification of micro cracks, analysis of the homogeneity and denseness of the paste, water separation and agglomeration of air voids. When polarized light was used, the carbonated layer was seen as a beige colour that enabled a quantification of the carbonation depth. The homogeneity and denseness analysis was done according to NT Build 361 [54] where 10 images are taken on noncarbonated concrete and these are compared relative to each other. The barrier filter was in the range 510 to 530 nm and the lens used had a magnification of 5x.

De-icing salt frost scaling method

To test the effect of various air contents, the effect of carbonation and the effect of the fraction of LCFA content on the DISFS, all batches (according to Table 1) were tested after two different preconditioning processes. The two preconditioning processes were either never-dried and never-carbonated, or dried and carbonated. Two samples were cut from a cylinder that was 100 mm long and 100 mm in diameter. One of the samples was never-dried and never-carbonated, whereas the other was dried and carbonated. The test surfaces were only separated by the saw blade (ca 3 mm). The samples that were dried and carbonated were preconditioned according to Table 3 with the addition of 1 day of resaturation after the drying and carbonation (before the DISFS test began). In contrast, the never-dried or carbonated samples were exposed to internal curing according to Table 3, then to 1 day of resaturation before the DISFS test began. This enabled a comparison between the never-dried and never-carbonated samples, and the dried and carbonated samples in order to study the effect of carbonation on the DISFS on each binder.

The DISFS method that was used to test all batches is presented in [55]. The method tests samples with 100 mm diameter and 50 mm thickness with insulation surrounding all sides except for the test surface. The test surface protrudes from the insulation and was submerged into a 3% NaCl solution. Only sawn surfaces were tested to enable a homogeneous internal curing and then a controlled period of drying and carbonation for each binder. The freeze-thaw cycle was 24 h long and goes from +20 to -22 and then back to +20 °C. The samples are exposed to -22 °C for approx. 4 h. This results in a large mass of scaling that enables an analysis of concrete recipes with a water binder ratio of 0.40 [55]. Measurements were made every seventh cycle on each sample and all samples were exposed to 112 cycles.

Results and discussion

The results from each measurement are presented together to enable an analysis of the impact an increased fraction of LCFA has on each measurement. Additionally, the noncarbonated results and carbonated results are presented together to enable an analysis of the effect of carbonation on the results for each binder. The results are presented together with a short analysis of how an increased fraction of LCFA and carbonation affect the result for the specific measurement. A summarizing discussion is given in the end of this chapter.

First, the pH measurements are presented to give an indication of the difference in the carbonation between the noncarbonated samples and the samples exposed to 1% CO_2 used for the capillary absorption and LTC measurements. Then, the capillary absorption and LTC measurements are presented. Thereafter, the results from the air void analysis are presented, followed by the thin slice section that quantifies the carbonation depth of the carbonated samples that have been tested with the salt-frost scaling method. Lastly, the salt-frost scaling results are presented.

pH measurements

Table 4 shows the pH values for the noncarbonated and the carbonated sample. The pH decreases with an increased fraction of LCFA for noncarbonated samples, and when comparing each binder, all carbonated samples have a lower pH in comparison with the noncarbonated samples. With an increased fraction of LCFA the difference in pH between the noncarbonated and carbonated samples increases. This suggests that F35 is carbonated to a greater extent in comparison to the F20. The CEM I samples were carbonated to the smallest extent. This means that the effect carbonation has on the results of the other measurement techniques will be most pronounced for the F35 samples.

Table 4
Measured pH on noncarbonated and carbonated samples conditioned in 1% CO2.

Binder	Noncarbonated	Carbonated	Difference
CEM I	12.24	11.96	0.28
F20	12.18	11.38	0.80
F35	12.03	9.57	2.46

Low temperature calorimetry

Results from the LTC measurements are presented in Figure 1. The dashed lines represent the noncarbonated samples and the solid lines represent the carbonated samples. The y-axis shows the fraction of frozen water inside the vacuum-

saturated sample at a given temperature in relation to the total amount of evaporable water inside the sample. This enables a relevant comparison between the fractions of frozen water between samples with different porosities. For each sample, the lower curve shows the amount of ice formed during freezing and the upper curve shows the amount of ice remaining during thawing.

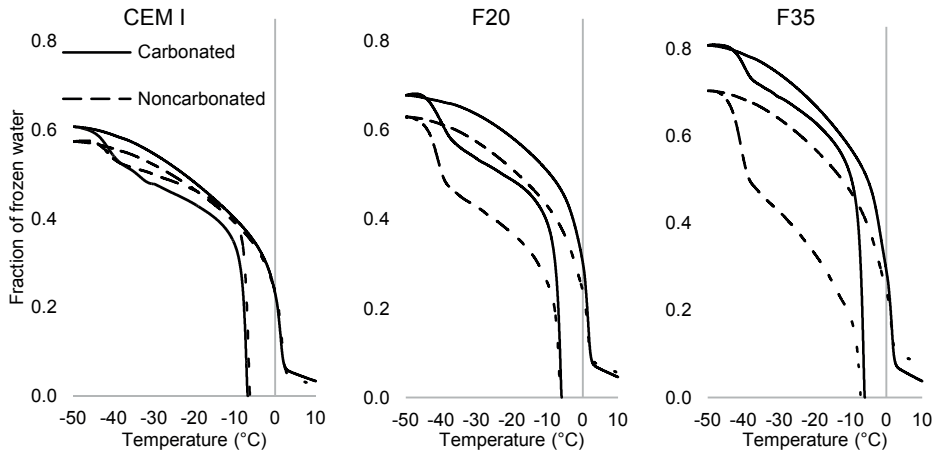

Figure 1
LTC measurements on samples from CEM I-4, F20-4 and F35-4 according to Table 1. Dashed lines represent the noncarbonated samples and solid lines represent the carbonated samples. The lower lines represent the fraction of water frozen during freezing and the upper curves show the fraction of frozen water during thawing.

Since the Gibbs-Thomson equation gives the melting point temperature as a function of the pore radius, the thawing curves give information about the pore size distributions of the mesopores. According to the thawing curves in Figure 1, 24 to 29% of the water is frozen close to ±0 °C, and 57 to 81% of the water content is frozen at -50 °C. This enables a rough estimate of how large a fraction of the pores have a radius larger than 50 nm, the fraction of mesopores and the fraction of pores with a radius shorter than 2 nm. The total porosities measured for each binder on the samples used for the capillary measurements and are presented in Table 5.

Figure 2 presents the differences between the thawing curves presented in Figure 1 to show what effect an increased fraction of LCFA and carbonation has for each binder. Figure 2-A shows the difference between the thawing curve of noncarbonated F20 and noncarbonated CEM I, and the difference between the thawing curve of noncarbonated F35 and noncarbonated CEM I. Figure 2-B shows the same differences as Figure 2-A for the carbonated samples. Figure 2-C shows the increased fraction of ice that can form in carbonated samples compared to the noncarbonated samples for each binder.

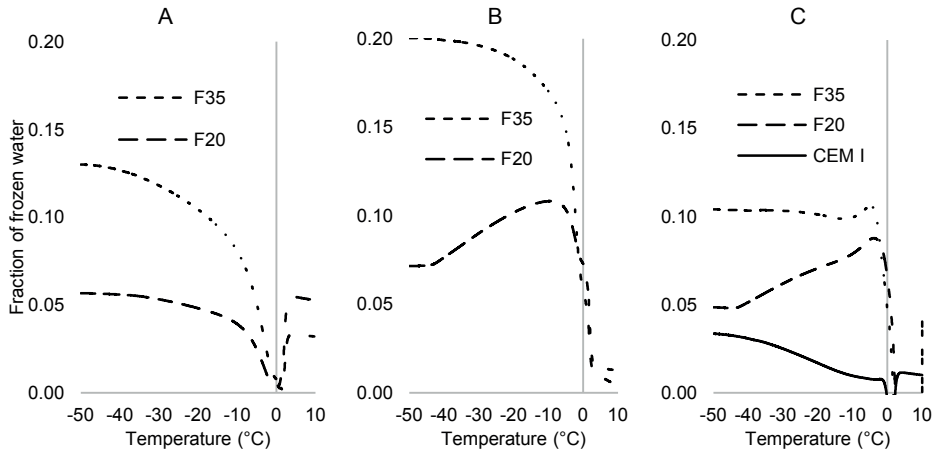

Figure 2
Differences between thawing curves presented in Figure 1 from the LTC measurements on CEM I-4, F20-4 and F35-4.

According to Figure 2-A, an increased fraction of LCFA increases the fraction of pores <50 nm in noncarbonated concrete. By comparing Figure 2-A and Figure 2-B, it can be seen that carbonation increases this effect. According to 2C, carbonation increases the fraction of pores <50 nm slightly for CEM I and this effect increases when the replacement of LCFA increases. The same trend from LTC results was presented in [35].

Another factor seen in Figure 1 for the noncarbonated concrete is that the hysteresis between freezing and thawing curves increases with an increased fraction of LCFA. The carbonation contributes to a large decrease in the hysteresis for the F35 concrete, and a slight decrease in the hysteresis for the F20 concrete. The carbonation of the 100% CEM I concrete increased the hysteresis. The hysteresis of the carbonated CEM I and the carbonated F35 is about the same. A large hysteresis suggests that there are many bottlenecks, whereas a small hysteresis indicates few bottlenecks in the voids <50 nm according to [49].

Capillary absorption

The results from the capillary absorption measurements are presented in Figure 3 and Table 5. Figure 3 presents the average degree of saturation from three samples, i.e., capillary absorption in relation to the saturated mass. There were three carbonated samples (solid lines), and three noncarbonated samples (dashed lines). Table 5 presents the resistance to water penetration (Eq. 1), the coefficient of capillarity (Eq. 2) and porosities (Eq. 3) for each binder. The coefficient of capillarity, which is the initial slope of each curve, was determined by calculating the average slope for $0 < t^{1/2} < 100$.

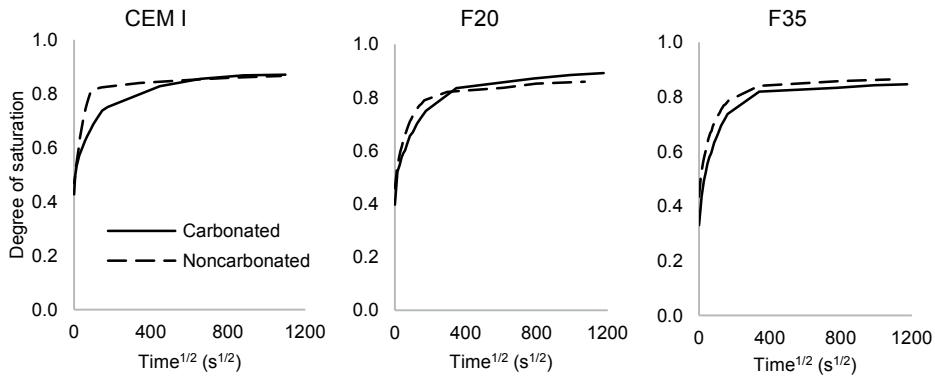

Figure 3
Mean value for capillary absorption from three samples of the batches CEM I-4, F20-4, and F35-4.

Table 5
Resistance to water penetration, coefficient of capillarity and porosity calculated from the mean values presented in Figure 3.

Binder	Coefficient of capillarity kg/(m²s^1/2)		Resistance to water penetration, ·10⁶ s/m²		Porosity[1] %		Porosity[2], pores >2 nm, %	
	Noncarb.	Carb.	Noncarb.	Carb.	Noncarb.	Carb.	Noncarb.	Carb.
CEM I	0.0040	0.0017	325	1135	14.9	13.5	9.2	7.9
F20	0.0027	0.0016	559	879	16.2	13.1	10.5	8.2
F35	0.0031	0.0025	607	788	16.8	15.2	10.9	10.6

[1] Porosities are calculated with dry mass when samples were dried at 105 °C.
[2] Porosities are calculated with dry mass when samples were dried at 35% RH. Therefore, pores larger than approx. 2 nm have been dried according to [51].

For the noncarbonated concrete, the results suggest that added LCFA decreases the coefficient of capillarity and increases the resistance to water penetration. Carbonation decreases the coefficient of capillarity, increases the resistance to water penetration and decreases the porosity. This effect from carbonation decreases with an increased fraction of LCFA. When CEM I carbonates, it goes from having the coarsest and most well-connected microstructure to having the densest microstructure.

These results from the capillary absorption measurements agree with results presented in [16-18]. They also found that both concrete with CEM I and concrete containing LCFA exhibit a lower porosity after they have carbonated [16-18]. The decrease in porosity for concrete with 100% CEM I can be attributed to the increased molar volume when CH forms $CaCO_3$ [56-60]. The pore volume >2 nm for F35 seems to be unaffected by the carbonation according to the porosity measurements.

Air Void Analysis

Table 6 presents results from the air void measurements made on the fresh and hardened concrete for each batch. An increased mass of air entraining agent increases the air content and the amount of air voids smaller than 2 mm. When the air content increases, the specific surface of the voids should increase, and the spacing factor should decrease.

Table 6
Air content measured in fresh concrete and results from linear traverse measurements according to ASTM C 457 [39].

Cast	Fresh Concrete[1] %	Air void content			Air void content in paste		Specific surface[2][7] mm^{-1}	Spacing factor[2][8] mm
		Total %[2]	<2 mm %[2][3]	<0.35 mm %[2][4]	<2.00 mm %[2][5]	<0.35 mm %[2][6]		
CEM I-1	3.20	2.6	2.4	0.9	7.1	2.8	17	0.41
CEM I-2	3.00	2.7	2.4	0.9	6.8	2.8	19	0.38
CEM I-3	4.50	2.8	2.7	1.3	8.0	3.9	21	0.32
CEM I-4	5.10	4.1	3.4	1.9	9.4	5.7	24	0.25
F20-1	1.60	3.5	1.9	0.3	5.5	0.9	10	0.78
F20-2	2.60	2.0	1.9	0.9	5.8	2.6	25	0.32
F20-3	3.45	3.1	2.5	1.1	7.3	3.3	18	0.37
F20-4	4.45	3.5	3.4	2.0	9.6	5.9	22	0.27
F35-1	2.05	1.8	1.1	0.3	3.4	1.0	24	0.41
F35-2	2.70	3.8	2.4	0.8	6.9	2.2	20	0.35
F35-3	4.05	3.2	2.9	1.6	8.5	4.7	34	0.19
F35-4	5.05	4.8	3.4	2.0	9.5	5.8	27	0.22

[1] Total air content measured in 8 dm^3 fresh concrete. Read and rounded to closest 0.05%.
[2] Calculated from results from linear traverse measurements according to ASTM C 457 [39].
[3] Total air content from air voids <2.0 mm.
[4] Total air content from air voids <0.350 mm.
[5] Voids <2.0 mm / (vol% CEM I paste + vol% of total voids). CEM I paste is calculated to 31 vol%.
[6] Voids <0.350 mm / (vol% CEM I paste + vol% of total voids). CEM I paste is calculated to 31 vol%.
[7] Specific surface ($mm^2/mm^3=mm^{-1}$) calculated from results of voids <2.0 mm.
[8] Spacing factor calculated from results of voids <2.0 mm.

According to Table 6, the increased mass of air entraining agent increases the amount of air voids in the ranges of 0 to 2 mm and 0 to 350 µm for all binders. There are some inconsistencies in the results for the specific surface and spacing factor, where air contents of air voids <2 mm increase, whereas the specific surface does not increase, and the spacing factors do not decrease. The reason for this is believed to be the stochastic variation in the air content. If measurements had been made on more samples from each batch the results would likely show more consistent results.

Thin section analysis

Examples of results from the thin section analysis for each batch are shown in Figures 4, 5 and 6. The left images are taken in polarized light where the light beige area shows carbonated cement paste. These images show that the air voids and the cement paste closest to some of the aggregates enable a faster carbonation. The images with fluorescent light show that there do not seem to be any cracks or decreases in the denseness in the hardened pastes that would contribute to the fast carbonation rate. The effect on carbonation from air voids is seen in all of the polarized images, while the effect from aggregates is most clear in the polarized image in Figure 4 and 6. It is important to be aware of these phenomena since they have a large influence on the carbonation depth, and could also affect the DISFS depending on the properties of the carbonated layer for each binder. However, they make it difficult to estimate an average carbonation depth. Therefore, images where these phenomena were not visible were used when estimating an average carbonation depth for each binder. The average carbonation depths of CEM I, F20, and F35 were approx. 0.2, 1, and 2 mm respectively. Therefore, an increased fraction of LCFA increases the carbonation rate. These results agree with previous studies [19-21].

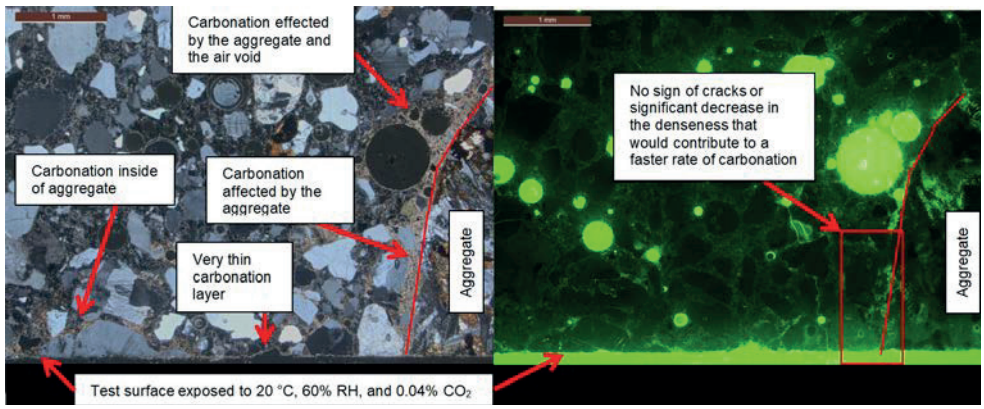

Figure 4
Carbonated CEM I thin section sample with the test surface in the bottom of the figure. The left figure shows a polarized image and right shows a fluorescence image of the same surface. Some large aggregates are marked with red lines to facilitate the interpretation of the images.

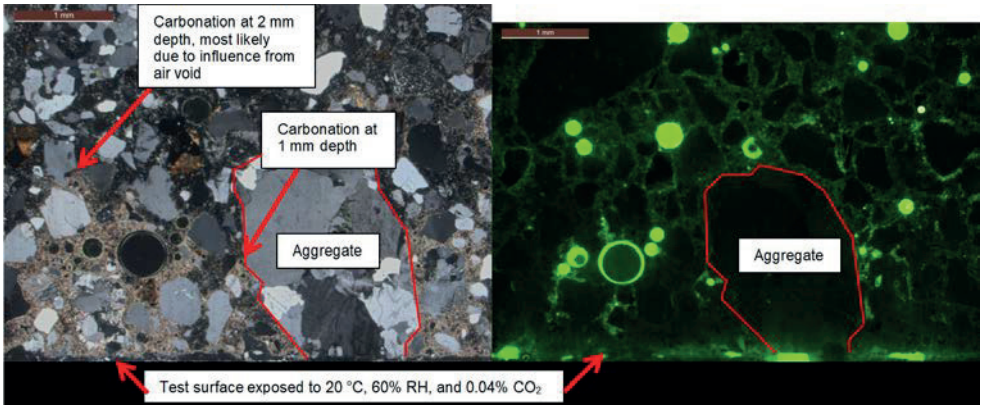

Figure 5
Carbonated F20 thin section sample (see caption Fig. 4).

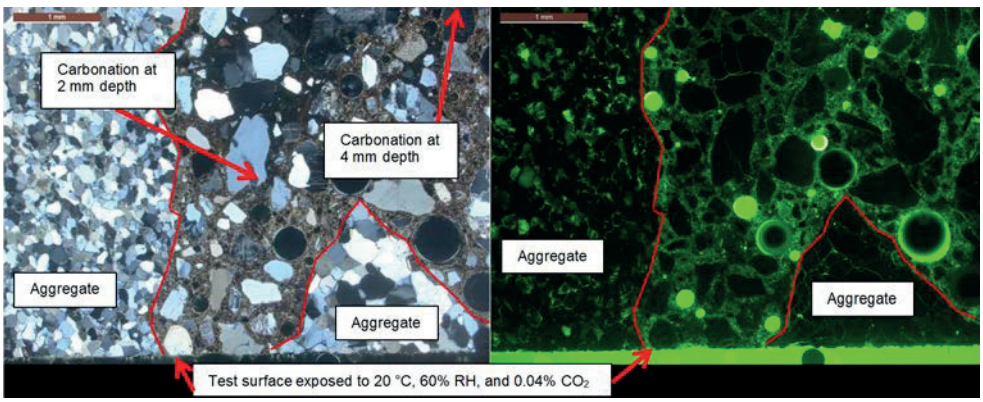

Figure 6
Carbonated F35 thin section sample (see caption Fig. 4).

There was no indication of water separation in any of the three samples. This means that the combination of superplasticizer and air entraining agent was working well with the specific binder. There was no pattern of micro-cracks perpendicular to the test surfaces in the hardened paste. When comparing the noncarbonated paste with the carbonated zone along the surface there were not more cracks observed in the carbonated zone. This means that the drying and carbonation most likely does not contribute to micro-cracks for any of the binders. Some of the micro cracks perpendicular to the test surface were found to have occurred in the aggregates. This suggests that the hardened paste has a higher strength than the aggregate due to the long and favourable hydration.

Agglomerated air voids were defined as two or more small air voids that merge together. Some air voids were close to each other, similar to the air voids in the top right corner in Figure 4. However, these are not merged together and therefore are not agglomerated. There were almost no agglomerated air voids found in any of the samples. This also confirmed that the superplasticizer and air entraining agent worked well together for each batch. The analysis according to [54] showed that the hardened paste for each binder was homogeneous and had an even denseness.

De-Icing Salt Frost Scaling

The DISFS results are presented in Figure 7-9 for each binder. The left figures show the mean accumulated scaling. The right figures show the accumulated scaling after every seventh cycle in relation to the total accumulated scaling. The seven-cycle scaling is the derivative of the accumulated scaling according to the left figures, which is the scaling rate of the accumulated scaling. The scaling rates are presented to highlight when the carbonated layer is scaled off. Since the scaling depth of 1 mm can be translated to (roughly) 1 kg/m² accumulated scaling, the average carbonation depth of according to the thin slice analysis can be marked for each binder. These were 0.2 mm, 1 mm, and 2 mm for the CEM I concrete, F20 concrete, and the F35 concrete. These carbonation depths are translated to 0.2 kg/m², 1 kg/m², and 2 kg/m². They are marked in the right scaling rate diagrams with a vertical dotted black line. It is important to remember that the number of cycles that have passed when each line passes the dotted black lines (that mark the carbonated zone) differs. To assist in the analysis of the scaling rate diagrams, Table 7 presents the number of cycles that have passed for each batch when it passes the dotted lines in the diagrams on the right in Figures 7-9. Diagrams showing the coefficient of variation for the accumulated scaling measurements are presented in supplementary information attached to this paper.

The solid lines present the results from six noncarbonated and never-dried samples, whereas the dashed lines present the mean values from five carbonated and dried samples. The name of each batch in the legend is the same name as the name given in Table 1 with the addition of “C” for the samples exposed to drying and carbonation during the preconditioning process. Batches 1, 2, 3, and 4 have black, blue, green, and red colours, respectively.

To enable an easier comparison between the measurements, the results from each measurement are divided into three groups according to Table 8. Note that during the discussion of the LTC and capillary absorption measurements, only F35 seemed to be completely carbonated according to the pH measurements.

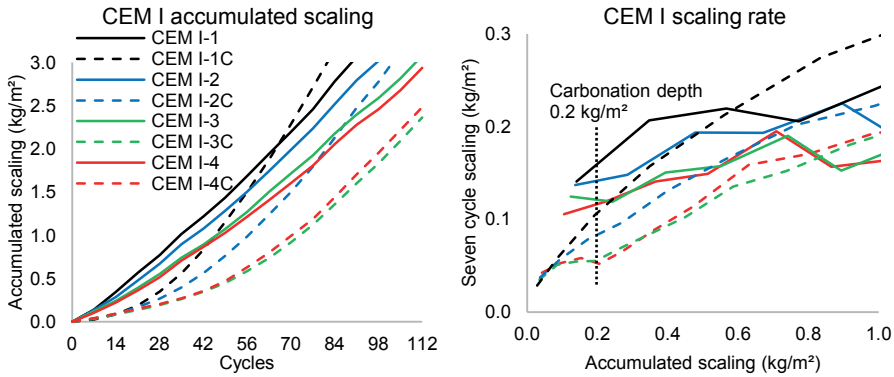

Figure 7
The left figure shows the mean accumulated scaling and the right figure shows the mean seven-cycle scaling for the accumulated scaling curves. Each line for noncarbonated samples represents the mean value of six samples. Each line for the carbonated samples represents the mean value of five samples. The value of 0.2 kg/m² is marked with vertical dotted line in the right figure since the estimated carbonation depth from the thin slice analysis was on average 0.2 mm.

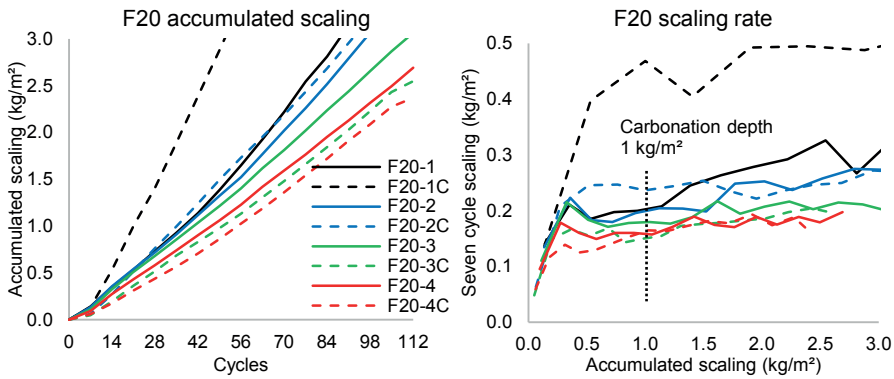

Figure 8
Results for F20 concretes (see caption of Fig. 7).

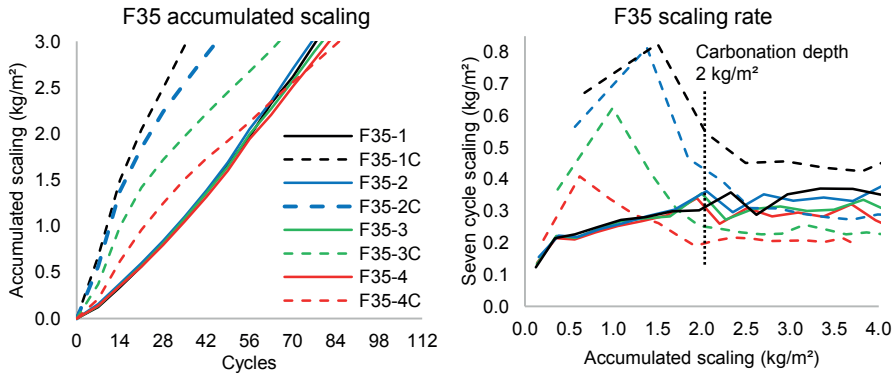

Figure 9
Results for F35 concretes (see caption of Fig. 7).

Table 7
Cycles when the accumulated scaling is 0.2, 1.0, and 2.0 kg/m² for CEM I, F20 and F35 respectively.

Binder	Noncarbonated	Carbonated	Difference
CEM I-1	9	21	12
CEM I-2	10	23	13
CEM I-3	11	28	17
CEM I-4	12	27	15
F20-1	37	21	-16
F20-2	38	35	-3
F20-3	41	50	9
F20-4	46	55	9
F35-1	57	20	-37
F35-2	55	24	-31
F35-3	56	36	-20
F35-4	58	52	-6

Table 8
Summary of how the microstructure affects the DISFS and how large an effect increased air content has on the DISFS. Fraction of frozen water at -50 °C according to the LTC results: dense < 65% < medium < 75% < coarse. Resistance to water penetration according to capillary absorption measurements: coarse < $650 \cdot 10^6$ < medium < $1300 \cdot 10^6$ < dense. 7 cycle scaling: low < 0.15 kg/m² < medium < 0.3 kg/m² < high. Effect from increased air content (7 cycle scaling for batch 1 – batch 4): low < 0.1 kg/m² < medium < 0.2 kg/m² < high.

Binder	Preconditioning	LTC, porosity of mesopores (structure / fraction of ice)	Cap.absorption porosity of pores r>50 nm (structure / permeability)	Seven-cycles scaling	Effect from air voids on the DISFS
CEM I	Noncarbonated	Dense / Low	Coarse / High	Medium	Medium
	Carbonated	Dense / Low	Medium / Medium	Low	Low
F20	Noncarbonated	Dense / Low	Coarse / High	Medium	Medium
	Carbonated	Medium / Medium	Medium / Medium	Medium	High
F35	Noncarbonated	Medium / Medium	Coarse / High	Medium	Low
	Carbonated	Coarse / High	Medium / Medium	High	High

Effect of Carbonation

The DISFS results indicate that an increased fraction of LCFA contributes to an increased mass of scaling, which agrees with previous research [28, 30-32, 34-37]. The effect from drying and carbonation varies depending on the fraction of LCFA added to the concrete. When comparing the carbonated and the noncarbonated samples, the DISFS show large differences for the CEM I and F35 concrete, whereas the F20 concrete does not change as much (Figure 8). According to Figure 7, the carbonated 100% CEM I samples have a lower mass of scaling in the beginning compared to the 100% CEM I noncarbonated samples. According to Figure 9, the carbonated F35 samples have a larger mass of scaling in the beginning compared to the F35 noncarbonated samples. Therefore, the effect from carbonation decreases the DISFS for CEM I and increases the DISFS for F35. With the assumption that 1 kg/m² corresponds to approximately 1 mm scaling depth, the right figures show a correlation between the carbonation depth (according to the thin section analysis) and the DISFS depth of these two binders. The results from the concrete containing 100% CEM I agree with the results presented by [8]. Figure 8 shows that the carbonation does not seem to have any notable effect on the DISFS for the F20 batches that contained air entraining agent.

Noncarbonated CEM I has the coarsest porosity according to the capillary suction measurements whereas the LTC measurements suggest that is has the finest porosity of pores <50 nm. When looking at the effect carbonation has on the LTC measurements, there is almost no difference. The amount of water that can freeze and the number of bottlenecks (hysteresis) slightly increase. The capillary absorption suggests that the carbonated CEM I become denser. Considering the LTC results, this means that the products from carbonation fill pores larger than 50 nm. Since the carbonated CEM I has the lowest DISFS these results suggest that a fine pore structure <50 nm and a low permeability >50 nm are two important properties for a concrete with a low DISFS.

Noncarbonated F35 has a medium coarse porosity according to both the capillary suction measurements, and the LTC measurements. When looking at the effect carbonation has on the LTC measurements, there is an increased fraction of pores <50 nm and a large decrease in bottlenecks (hysteresis). The capillary absorption results show almost no difference; only a small decrease in the permeability. The noncarbonated and carbonated F35 have the second highest and highest DISFS. Therefore, a coarse pore volume <50 nm results in a high DISFS and an increased amount of coarse pores <50 nm increases the DISFS further.

Effect from air void system

According to the linear traverse analysis, the CEM I, F20 and F35 batches got an increased amount of small air voids (<0.35 mm) when more air entraining agent

was added. Noncarbonated and carbonated 100% CEM I and F20 concretes showed a decreased DISFS from the increased air content. This was also the case for carbonated F35, but not for the noncarbonated F35 concrete. One possible reason for the air void system not having any effect for noncarbonated F35 could be the large fraction of bottlenecks in this material. The bottlenecks could prevent moisture transport in the microstructure and therefore reduce the moisture transport that provides a beneficial effect of the air voids on the DISFS resistance.

When looking at the carbonated batches without air entraining agent (CEM I-1 C, F20-1 C and F35-1 C), the DISFS is higher than for the noncarbonated samples (CEM I-1, F20-1 and F35-1) after the carbonated layer has scaled off. Since the carbonated material has scaled off, this effect is believed to have been caused by the drying. This could mean that when the concrete does not have a sufficient amount of air voids, the drying shrinkage will result in more micro cracks that reduces the DISFS resistance. However, this cannot be confirmed here since the thin section analysis was only made on the samples with the highest mass of air entraining agent.

When the carbonated layer has scaled off from F35-3C and F35-4C, the scaling rate is lower than the noncarbonated and never-dried samples. This could have been caused by an increased degree of hydration in the noncarbonated layer.

According to the scaling rate figure for concrete with CEM I, the rates of CEM I-3C and CEM I-4C increase at 0.2 kg/m² accumulated scaling, whereas the rates of CEM I-1C and CEM I-2C increase at an earlier accumulated scaling. This suggests that an increased amount of air voids increases the average carbonation depth (as seen in the thin section analysis), which in turn decreases the initial DISFS that can be observed from the carbonated layer of CEM I-4C in Figure 7.

Research questions

How does an increased fraction of LCFA affect the microstructure?

- For noncarbonated concrete an increased fraction of LCFA lowers the permeability for pores >50 nm, but increases the fraction of pores <50 nm, which increases the amount of ice that can form at a given freezing temperature.

How does the carbonation of each binder change the microstructure?

- Carbonation of concrete with 100% CEM I or LCFA decreases the permeability of pores >50 nm; this effect decreases as the fraction of LCFA increases.
- Carbonation results in a coarser pore volume <50 nm, which increases the fraction of water that can freeze at a given freezing temperature; this effect increases as the fraction of LCFA increases.

- Carbonation of concrete for all studied material decreases the porosity. For 35 mass% LCFA the pore volume >2 nm does decrease to a smaller extent.

How does an increased fraction of LCFA affect DISFS?

- For noncarbonated concrete, F20 replacement seems to have approximately the same DISFS as noncarbonated concrete with 100% CEM I; noncarbonated concrete with F35 has a higher DISFS.

How does the drying and carbonation of each binder affect DISFS?

- The carbonation of concrete containing LCFA decreases the DISFS resistance in comparison to concrete containing 100% CEM I. This effect increases with an increased fraction of LCFA.
- Drying increases the DISFS for samples from all batches without air entraining agent in comparison to samples from the same batches that have never been dried or carbonated.

How does increased air content affect the DISFS in noncarbonated concrete with various fractions of fly ash?

- An increased air void content decreases the DISFS on noncarbonated concrete containing CEM I and F20, whereas the DISFS for noncarbonated F35 is not affected by the increased air content. The proposed explanation is that a large number of bottlenecks inside the mesoporous system of F35 cause the introduced air content to be insufficient. The effect of an increased air void content is therefore dependent on the fine porosity.

How does increased air content affect the DISFS in carbonated concrete with various fractions of fly ash?

- An increased air void content decreases the DISFS in all tested carbonated concrete, including F35.

Conclusions

- A fine structure for pores <50 nm that reduces the fraction of ice that can form at a given temperature, combined with a low permeability for the structure of pores >50 nm results in the lowest DISFS.
- A coarse structure for pores <50 nm that increases the fraction of ice that can form at a given temperature combined with a medium permeability for the structure of pores >50 nm results in the highest DISFS.

Acknowledgement

This research was funded by SBUF (The Development Fund of the Swedish Construction Industry) and supported by Skanska AB and Cementa AB (a part of the Heidelberg Group). Cementa AB performed the measurements on the binders. Thin section samples were polished and prepared by RISE (Research institute of Sweden AB), and Jan Erik Lindqvist at RISE assisted the author in the microscopic analysis.

References

1. Scrivener, K.L., *Options for the future of cement.* The Indian Concrete Journal, 2014. **88**(7): p. 11.
2. Arnfelt, H., *Damage on Concrete Pavements by Wintertime Salt Treatment*. 1943, Statens Väginstitut. p. 28.
3. Liu, Z. and W. Hansen, *A hypothesis for salt frost scaling in cementitious materials.* Journal of Advanced Concrete Technology, 2015. **13**: p. 403-414.
4. Powers, T.C. and R.A. Helmuth, *Theory of volume changes in hardened portland-cement paste during freezing.* Proceedings, Highway Research Board 32, PCA Bull 46, 1953.
5. Verbeck, G.J. and P. Klieger, *Studies of "Salt" Scaling of Concrete*, H.R.B. 150, Editor. 1957: Washington D.C. p. 13.
6. Powers, T.C., *The mechanism of frost action in concrete (Part II).* Cement, Lime and Gravel, 1966. **41**(6): p. 5.
7. Lindmark, S., *Mechanisms of Salt Frost Scaling of Portland Cement-bound Materials: Studies and Hypothesis*, in *Department of Building and Environmental Technology*. 1998, Faculty of Engineering, LTH, Lund University: Lund. p. 266.
8. Utgenannt, P., *The influence of ageing on the salt-frost resistance of concrete*, in *Department och Building and Environmental Technology*. 2004, Faculty of Engineering, LTH, Lund University: Lund. p. 346.
9. Valenza II, J.J. and G.W. Scherer, *A review of salt scaling: II. Mechanisms.* Cement and Concrete Research, 2007. **37**(7): p. 1022-1034.
10. Yuan, J., et al., *Mechanisms on the Salt–Frost Scaling of Concrete.* Journal of Materials in Civil Engineering Structures, 2017. **29**(3).
11. Liu, Z., W. Hansen, and F. Wang, *Pumping effect to accelerate liquid uptake in concrete and its implications on salt frost durability.* Construction and Building Materials, 2018. **158**: p. 181-188.
12. Powers, T.C., *Freezing effects in concrete.* ACI, 1975. **SP-47**(Durability of Concrete): p. 1-11.

13. Liu, Z., *Frost Deterioration in Concrete due to Deicing Salt Exposure: Mechanism, Mitigation and Conceptual Surface Scaling Model*. 2014, University of Michigan. p. 211.

14. Fagerlund, G., *Critical degrees of saturation at freezing of porous and brittle materials*. 1972, The Lund Institute of Technology: Lund, Sweden.

15. Herterich, J.A., *Microstructure and phase assemblage of low-clinker cements during early stages of carbonation*. 2017, School of Civil Engineering, The University of Leeds. p. 265.

16. Wu, B. and G. Ye, *Development of porosity of cement paste blended with supplementary cementitious materials after carbonation.* Construction and Building Materials, 2017. **145**: p. 52-61.

17. Morandeau, A., M. Thiéry, and P. Dangla, *Impact of accelerated carbonation on OPC cement paste blended with fly ash.* Cement and Concrete Research, 2015. **67**: p. 226-236.

18. Hussain, S., D. Bhunia, and S.B. Singh, *Comparative study of accelerated carbonation of plain cement and fly-ash concrete.* Journal of Building Engineering, 2017. **10**: p. 26-31.

19. Shi, H.-s., B.-w. Xu, and X.-c. Zhou, *Influence of mineral admixtures on compressive strength, gas permeability and carbonation of high performance concrete.* Construction and Building Materials, 2009. **23**(5): p. 1980-1985.

20. Khan, M.I. and C.J. Lynsdale, *Strength, permeability, and carbonation of high-performance concrete.* Cement and Concrete Research, 2002. **32**(1): p. 123-131.

21. Papadakis, V.G., *Effect of supplementary cementing materials on concrete resistance against carbonation and chloride ingress.* Cement and Concrete Research, 2000. **30**(2): p. 291-299.

22. Papadakis, V.G., *Effect of fly ash on Portland cement systems: Part I. Low-calcium fly ash.* Cement and Concrete Research, 1999. **29**(11): p. 1727-1736.

23. Frías, M. and M.I.S. de Rojas, *Microstructural alterations in fly ash mortars: Study on phenomena affecting particle and pore size.* Cement and Concrete Research, 1997. **27**(4): p. 619-628.

24. Chindaprasirt, P., C. Jaturapitakkul, and T. Sinsiri, *Effect of fly ash fineness on compressive strength and pore size of blended cement paste.* Cement and Concrete Composites, 2005. **27**(4): p. 425-428.

25. Yu, Z., et al., *Effect of fly ash on the pore structure of cement paste under a curing period of 3years.* Construction and Building Materials, 2017. **144**: p. 493-501.

26. Pigeon, M., et al., *Surface microstructure and scaling resistance of concrete.* Cement and Concrete Research, 1996. **26**(10): p. 1555-1566.

27. Marchand, J., M. Jolin, and Y. Machabée, *Deicer salt scaling resistance of supplementary cementing material concrete: laboratory results against field*

performance, in *Cement Combinations for Durable Concrete*, R.K. Dhir, T.A. Harrison, and M.D. Newlands, Editors. 2005, MPG Books: University of Dundee, Scotland, UK. p. 579-590.

28. Bouzoubaâ, N., et al., *Deicing salt scaling resistance of concrete incorporating supplementary cementing materials: laboratory and field test data.* Canadian Journal of Civil Engineering, 2008. **35**: p. 1261-1275.

29. Bouzoubaâ, N., et al., *Deicing salt scaling resistance of concrete incorporating fly ash and (or) silica fume - laboratory and field sidewalk test data.* Canadian Journal of Civil Engineering, 2011. **38**: p. 373-382.

30. Nowak-Michta, A., *Water-binder Ratio Influence on De-icing Salt Scaling of Fly Ash Concretes.* Procedia Engineering, 2013. **57**: p. 823-829.

31. Bilodeau, A. and V.M. Malhotra. *Deicing salt scaling resistance of concrete incorporating supplementary cementing materials CANMET research*. in *Freeze-Thaw Durability of Concrete - rilem proceedings 30*. 1997. E & FN SPON.

32. Zhang, M.H., et al., *De-Icing Salt Scaling of Concrete Incorporating Different Types and Percentages of Fly Ashes*, in *Sixth CANMET/ACI International Conference on Fly Ash, Silica Fume, Slag, and Natural Pozzolans in Concrete*, V.M. Malhotra, Editor. 1998, ACI: Bangkok, Thailand. p. 493-525.

33. Nili, M. and M. Zaheri, *Deicer salt-scaling resistance of non-air-entrained roller-compacted concrete pavements.* Construction and Building Materials, 2011. **25**(4): p. 1671-1676.

34. Sun, C.T., W.H. Li, and B.R. Hou, *Study on Frost-Salt Resistance of Fly Ash Concrete.* Architecture and Urban Development, 2012. **598**: p. 432-437.

35. Marchand, J., et al., *Effects of fly ash on microstructure and deicer salt scaling resistance of concrete*, in *Frost Resistance of Concrete*, M.J. Setzer and R. Auberg, Editors. 1997, E&FN Spon: University of Essen. p. 11-20.

36. Baert, G., A.-M. Poppe, and N. De Belie, *Evaluation and comparison of mechanical characteristics and durability of concrete with different cement replacement levels by fly ash*, in *Cement Combinations for Durable Concrete*, R.K. Dhir, T.A. Harrison, and M.D. Newlands, Editors. 2005, MPG Books: University of Dundee, Scotland, UK. p. 787-797.

37. Bilodeau, A., et al., *Effect of Curing Methods and Conditions on the Performance of Fly Ash Concrete in De-Icing Salt Scaling*, in *Sixth CANMET/ACI International Conference on Fly Ash, Silica Fume, Slag, and Natural Pozzolans in Concrete*, V.M. Malhotra, Editor. 1998, ACI: Bangkok, Thailand. p. 361-384.

38. Wu, M. and B. Johannesson, *Impact of sample saturation on the detected porosity of hardened concrete using low temperature calorimetry.* Thermochimica Acta, 2014. **580**: p. 66-78.

39. ASTM, *ASTM C457 / C457M - 12, Standard Test Method for Microscopical Determination of Parameters of the Air-Void System in Hardened Concrete*. 2012.

40. 197-1, S.-E., *Cement - Part 1: Composition, specifications and conformity criteria for common cements*. 2011. p. 48.

41. ASTM, *ASTM C618-12a Coal fly ash and raw or calcined natural pozzolan for use in concrete*, in *ASTM C618 Standard Spec. Coal Fly Ash and Raw or Calcined Natural Pozzolan*. 2013.

42. Strand, M.J. and K. Fridh, *Methodology to analyse the salt frost scaling mechanism(s) in concrete with different binders*, in *Materials, Systems and Structures in Civil Engineering 2016*. 2016: Technical University of Denmark, Copenhagen, Denmark.

43. SS-EN12620, *SS-EN 12620+A1:2008*, in *Aggregates for concrete*. 2008.

44. Jennifer A. Grubb, H.S.L. and M.K. Ashok, *Testing pH of Concrete.* Concrete International. **29**(4).

45. McPolin, D.O., P.A. Basheer, and A.E. Long, *Carbonation and pH in Mortars Manufactured with Supplementary Cementitious Materials.* Journal of Materials in Civil Engineering, 2009. **21**(5): p. 217-225.

46. Morandeau, A., M. Thiéry, and P. Dangla, *Investigation of the carbonation mechanism of CH and C-S-H in terms of kinetics, microstructure changes and moisture properties.* Cement and Concrete Research, 2014. **56**: p. 153-170.

47. Scherer, G.W., *Crystallization in pores.* Cement and Concrete Research, 1999. **29**(8): p. 1347-1358.

48. Valenza II, J.J. and G.W. Scherer, *Mechanism for salt scaling.* Journal of the American Ceramic Society, 2006. **89**(4): p. 1161-1179.

49. Fagerlund, G., *Non-freezable water contents of porous building materials*. 1974, Lund Institute of Technology: Lund, Sweden. p. 186.

50. Wu, M., B. Johannesson, and M. Geiker, *Determination of ice content in hardened concrete by low-temperature calorimetry Influence of baseline calculation and heat of fusion of confined water.* Journal of Thermal Analysis and Calorimetry, 2014. **115**(2): p. 1335-1351.

51. Jennings, H.M., A. Kumar, and G. Sant, *Quantitative discrimination of the nano-pore-structure of cement paste during drying: New insights from water sorption isotherms.* Cement and Concrete Research, 2015. **76**: p. 27-36.

52. Gallé, C., *Effect of drying on cement-based materials pore structure as identified by mercury intrusion porosimetry: A comparative study between oven-, vacuum-, and freeze-drying.* Cement and Concrete Research, 2001. **31**(10): p. 1467-1477.

53. Strand, M.J., *De-icing salt frost scaling in concretes with fly ash or slag with low air void contents*, in *Building Materials*. 2016, Lunds University. p. 222.

54. Nordtest, *NT Build 361*, in *Concrete hardened - Water-cement ratio*. 1999.

55. Strand, M.J. and K. Fridh, *Test Method for De-Icing Salt Frost Scaling in High Performance Concrete.* MethodsX, 2018.

56. Pihlajavaara, S.E., *Some results of the effect of carbonation on the porosity and pore size distribution of cement paste.* Matériaux et Construction, 1968. **1**(6): p. 521-527.

57. Pihlajavaara, S.E. and E. Pihlman, *Effect of carbonation on microstructural properties of cement stone.* Cement and Concrete Research, 1974. **4**(2): p. 149-154.

58. Patel, R.G., et al., *Influence of curing at different relative humidities upon compound reactions and porosity in Portland cement paste.* Materials and Structures, 1988. **21**(3): p. 192-197.

59. Ngala, V.T. and C.L. Page, *EFFECTS OF CARBONATION ON PORE STRUCTURE AND DIFFUSIONAL PROPERTIES OF HYDRATED CEMENT PASTES.* Cement and Concrete Research, 1997. **27**(7): p. 995-1007.

60. Delmi, M.M.Y., A. Aı¨t-Mokhtar, and O. Amiri, *Modelling the coupled evolution of hydration and porosity of cement-based materials.* Construction and Building Materials, 2006. **20**(7): p. 504-514.

61. EN196-6, *Methods of testing cement- Part 6: Determination of fineness*. 2010.

62. EN196-1, *Methods of testing cement - Part 1: Determination of strength*. 2005.

Supplementary information

Binder characterization tests

Table 8 presents the XRF analysis of the LCFA and each binder combination that has been tested. The CEM I contained 2.36% lime filler.

Table 8

X-ray fluorescence (XRF) analysis of the binders according to the ER 9214 method. SO_3 measurements according to the ER 9212-method. Loss on ignition measurements according to the ER 9213:2005-method.

Binder	CaO[1] %	SiO_2[1] %	Al_2O_3[1] %	Fe_2O_3[1] %	MgO[1] %	K_2O[1] %	Na_2O %	Na_2Oe[2] %	SO_3[1] %	LOI[1] %
CEM I	63.60	21.30	3.80	4.56	0.86	0.65	0.07	0.50	2.45	1.84
LCFA	3.53	57.00	21.60	7.33	1.95	2.16	0.00	1.42	0.65	2.71
F20	52.40	28.60	7.38	5.17	1.09	1.00	0.25	0.91	2.05	2.00
F35	44.00	33.50	9.88	5.52	1.26	1.24	0.38	1.20	1.78	2.09

[1] The precision of the measurements are CaO±0.233%, SiO_2±0.100%, Al_2O_3±0.052%, Fe_2O_3±0.019%, MgO±0.025%, K_2O±0.032%, SO_3±3%, (loss on ignition=) LOI ±0.18%.

[2] Na_2O-equivalent from K_2O and Na_2O.

Table 9 presents the results from the Blaine fineness-, laser diffraction and compressive strength measurements. The ICP analysis shows how soluble the fraction of the alkalis contained in each binder are in water. According to the results, the mass of soluble alkalis decreases when increasing the mass of LCFA. The Blaine and laser diffraction measurements show that the LCFA has a smaller specific surface in comparison and therefore has on average larger particle sizes than the CEM I. The compressive strength tests show that an increased amount of LCFA decreases the strength.

Table 9

H_2O soluble alkalis, Blaine value, laser diffraction and compressive strength measurement. Cementa performed the measurements.

Binder	ICP analysis[1] %			Blaine[2]	LD[3]	Strength after presented days of hydration[4] MPa			
	K_2O	Na_2O	Na_2Oe	m^2/kg	µm	2 days	28 days	56 days	91 days
CEM I	0.44	0.03	0.32	343	17.305	21.8±0.3	55.1±0.3	62.3±1.2	66.1±2.0
F20	0.35	0.03	0.26	340	18.097	17.0±0.3	45.5±1.0	56.4±0.6	62.7±1.5
F35	0.29	0.04	0.23	328	18.556	13.3±0.2	37.4±0.4	49.6±1.1	56.9±0.6

[1] ICP analysis of soluble K_2O, Na_2O and Na_2O-equivalent in H_2O according to the "CR 0401"-method.

[2] Blaine value of specific surface area per mass binder measured according to [61].

[3] Laser diffraction measurement on the size of the 50th percentile particle size.

[4] Compressive strength measured according to the [62] with the standard deviation.

Table 10 presents a summary of the preconditioning processes for the measurements.

Table 10
Preconditioning of the batches used for each test.

Test	Process name	Internal curing (IC), days	Drying and carbonation (DC), days	Drying days
pH measurements	Dried and never-carbonated (DNC)	1053 – 1204	0	49 – 77 (35% RH, 0% CO_2)
	Dried and carbonated (DC)[1)]	1221 – 1387	83 (55% RH, 0.5-1% CO_2)	0
Capillary suction	Dried and never carbonated (DNC)	1053 – 1204	0	49 – 77 (35% RH, 0% CO_2)
	Dried and carbonated (DC)[1)]	1221 – 1387	83 (55% RH, 0.5-1% CO_2)	0
Low temperature calorimetry	Dried and never carbonated (DNC)	1053 – 1204	0	49 – 77 (35% RH, 0% CO_2)
	Dried and carbonated (DC)[1)]	1221 – 1387	83 (55% RH, 0.5-1% CO_2)	0
Air void analysis		36 – 120[2)]		
Thin section	Dried and carbonated (DC)	307 – 308	707 – 873 (60±5% RH, 0.04% CO_2)	0
DISFS	Never-dried, never-carbonated (NDNC)	307 – 308	0	0
	Dried and carbonated (DC)	307 – 308	733 – 735 (60±5% RH, 0.04% CO_2)	0

[1)] Drying and carbonation with increased CO2 concentration.
[2)] Days hydrated before the samples were delivered to Pelcon Materials & Testing ApS (Copenhagen, Denmark).

Salt-frost scaling results supplementary information

Figures 10, 11, and 12 show the coefficient of variation in relation to the accumulated scaling from the CEM I, F20, and F35 concretes. The coefficient of variation is the standard deviation of the accumulated scaling divided by the accumulated scaling.

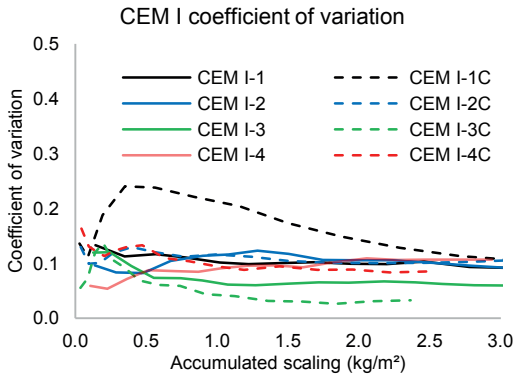

Figure 10
Coefficient of variation for the accumulated scaling presented in Figure 7.

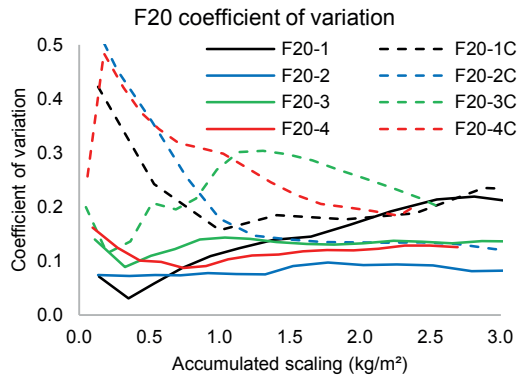

Figure 11
Coefficient of variation for the accumulated scaling presented in Figure 8.

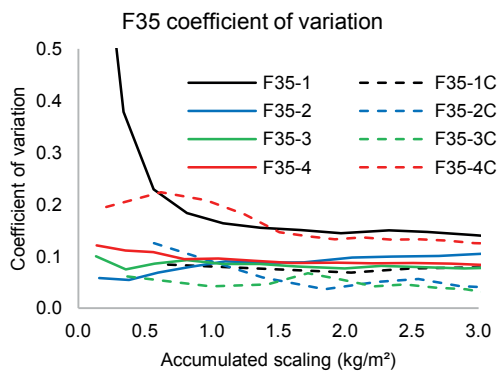

Figure 13
Coefficient of variation for the accumulated scaling presented in Figure 9.

Paper V

Experimental study of the influence of carbonation, SCMs, and air content on the de-icing salt-frost scaling of well-hydrated concrete. Part 2: Concrete containing slag

Martin J. Strand, Katja Fridh

Division of Building Materials, Lund University, Lund, Sweden

Corresponding author's info:

E-mail: martin.strand@byggtek.lth.se

Telephone: (+46)7 02 95 68 75

Abstract

This is the second part in a series of two articles on the de-icing of salt frost scaling (DISFS) in well-hydrated concrete containing low-calcium fly ash, or slag. This second part aims to investigate how drying and carbonation affect the DISFS in concrete containing 20, 35, or 70 mass% slag, or concrete containing 25+10 mass% slag + lime filler. The same tests were performed as in Part 1. The results show that slag decreases the DISFS in noncarbonated concrete. Carbonation of concrete containing up to 35% slag also decreases the DISFS. However, when concrete containing 70% slag becomes carbonated, the DISFS increases. An increased fraction of slag seems to decrease the positive effect from an increased air void content. The DISFS was low for the concrete with lime filler regardless of carbonation. The increased air void content slightly reduces the DISFS in the concrete containing lime filler.

Keywords: Concrete, De-Icing Salt Frost Scaling, Ground Granulated Blast Furnace Slag, Carbonated, Noncarbonated, Air Void System

Introduction

Concrete causes 5-8% of anthropogenic carbon dioxide emissions [1]. One way of decreasing these emissions is to replace some of the cement with supplementary cementitious materials, such as ground granulated blast furnace slag. However, slag changes the hydration process and results in changed material properties that may influence the durability of the concrete. In order to know in what climate

these blended binder combinations can be used, it is important to study how durability is affected by the use of slag. This study focuses on the de-icing of salt frost scaling (DISFS), which is briefly described in the introduction to the first part of this series [2].

It is known that when slag is included in the binder, some properties of concrete change, e.g. the permeability decreases [3], and the rate of chloride ion diffusion also decreases [4]. In addition to the changes that result directly from adding slag, the carbonation of concrete containing slag changes its microstructure in a different way than for a CEM I binder [5-8]. When comparing carbonated CEM I concrete with carbonated concrete containing slag, the concrete containing slag becomes coarser [5]. Previous research has also shown that these changes affect the DISFS [5-8].

There have been many previous studies on the DISFS of concrete containing slag [5-15]. The present paper complements the current knowledge with results from concretes that were hydrated for a long time (more than 300 days). DISFS studies on concretes that have hydrated this long are rare, because most studies are conducted according to standard DISFS methods that test the concrete after approximately 30 days, at which point concrete with slag has a relatively low degree of hydration compared with CEM I concrete. In addition to the long hydration time, this article also analyses what effect the air void content has on concrete that has been dried and carbonated, and on that which has never-dried and has not carbonated.

This paper is the second in a series of two, where the effects of drying and carbonation are studied together with the effect of different air void content levels. In the first part, concretes containing 20 and 35 mass% low-calcium fly ash were studied. In this second part, concretes containing 20, 35, and 70 mass% slag were studied along with concrete containing 25 + 10 mass% slag + lime filler (LF). In both papers, capillary suction and low temperature calorimetry measurements were performed to give information about the microstructure; thin section analysis was used to measure the carbonation depth of the carbonated samples for the DISFS test, and to look for micro cracks and water separation; and linear traverse analysis was performed to quantify the air void system in order to see what effect an increased air void content would have on the DISFS. This paper aims to answer the following questions: How does an increased fraction of slag affect the microstructure? How does the carbonation of each binder change the microstructure? How does an increased fraction of slag affect the DISFS? How does the drying and carbonation of each binder affect the DISFS? How does increased air content affect the DISFS in concrete with various fractions of slag? Does the effect that the air content has on the DISFS change depending on whether the surface is c arbonated or not? The paper concludes with a discussion

of how results presented in this paper and in reference [2] relate to the theories for DISFS.

Method and materials

Concrete recipes

Concrete was mixed with four slag-containing binders (Table 1); for each binder, four concrete batches with different air void content levels were prepared.

Table 1
Concrete recipes for each batch.

Batch	Binder[1] kg/m³	Slag[2] kg/m³	Limestone filler[3], kg/m³	Aggregate[4], kg/m³			Air[5] [6] %	Slump mm	Density[7] kg/m³
				0-8	8-12	12-32			
CEM I-1	430	0	0	966	285	536	3.2	165	2399
CEM I -2	430	0	0	953	281	529	3.0	160	2405
CEM I -3	430	0	0	939	277	521	4.5	200	2375
CEM I -4	430	0	0	926	273	514	5.1	220	2331
S20-1	344	86	0	962	284	534	2.0	210	2417
S20-2	344	86	0	949	280	527	2.9	210	2391
S20-3	344	86	0	937	276	520	3.7	220	2375
S20-4	344	86	0	924	272	513	4.7	220	2345
S35-1	280	151	0	959	283	532	2.3	210	2398
S35-2	280	151	0	941	277	522	3.8	220	2354
S35-3	280	151	0	930	274	516	4.5	220	2336
S35-4	280	151	0	919	271	510	5.2	240	2314
S70-1	129	301	0	951	280	528	3.2	220	2364
S70-2	129	301	0	938	277	521	4.1	230	2332
S70-3	129	301	0	930	274	516	4.5	240	2328
S70-4	129	301	0	924	272	513	4.7	240	2324
K35-1	280	108	43	948	280	526	3.5	210	2389
K35-2	280	108	43	942	278	523	3.7	210	2379
K35-3	280	108	43	926	273	514	5.0	220	2327
K35-4	280	108	43	920	271	511	5.1	220	2338

[1] CEM I 42,5 N - SR 3 LA (Degerhamn anläggningscement, Cementa AB)
[2] Merit 5000, Merox.
[3] Limus 25, Nordkalk.
[4] Calculated with consideration for the target air content levels of 1.5, 2.5, 3.5, and 4.5% for batches 1, 2, 3, and 4 respectively.
[5] Superplasticizer was based on a polycarboxylate, and air-entraining agent was based on a synthetic detergent.
[6] Air content of the fresh concrete was measured within 8 dm³. Target air content was 1.5, 2.5, 3.5, and 4.5% for batches 1 to 4.
[7] Density was determined on the same concrete as the air content.

Summary of methods

Because the first article in this series, [2], includes detailed descriptions of the methods used, this article only presents a summary of the methods and why each measurement was performed.

The microstructure was characterised by low temperature calorimetry (LTC) and capillary absorption measurements. The carbonated samples used for these measurements were exposed to an accelerated carbonation with 1% CO_2. To quantify the extent of the carbonation in these samples, pH measurements were made. The LTC measurements gives information about the temperature at which water freezes in mesopores that have a radius between 2 nm and 50 nm, as there is a freezing suppression depending on the size of the pores according to the Gibbs-Thomson equation [16]. The capillary suction measurements give information about the moisture uptake of the entire pore structure. Drying the samples in 35% RH gives information about the porosity for pores with a radius as small as approximately 2 nm [17]; further drying at 105 °C removes all bound water (and may also dehydrate some of the chemically-bound water and therefore overestimate the total porosity [18]). The capillary suction measurements also give some indication of the permeability of the concrete by comparing its resistance to water penetration and its coefficient of capillarity (defined in the first part in this series [2]). To quantify the carbonation depth of the DISFS samples that had carbonated, thin section analysis was done. In addition to this, DISFS measurement was made according to a newly developed freeze-thaw method described in reference [19]. Two samples were cut from a cylinder that was 100 mm long and 100 mm in diameter. One of the samples was never-dried or carbonated, whereas the other sample was dried and carbonated. The test surfaces were separated by distance no larger than the width of a saw blade (ca 3 mm). To enable comparisons with other studies, measurements of the binders (the same as in [2]) are presented in the supplementary information attached to this paper.

Results and discussion

The results from each measurement are presented in the same way as in reference [2]. The results from the concrete containing 100% CEM I are included in this paper as well so as enable an analysis of the impact the increased fraction of slag had on each measurement. Note that the results of the concrete containing 100% CEM I are the same as those presented in [2].

pH measurements

Table 2
Measured pH on noncarbonated and carbonated samples conditioned in 1% CO_2.

Binder	Noncarbonated	Carbonated	Difference
CEM I	12.24	11.96	0.29
S20	12.16	11.79	0.37
S35	12.07	11.58	0.49
S70	11.82	9.45	2.37
K35	12.02	11.39	0.63

Table 2 shows the pH values for noncarbonated samples, and samples carbonated in 1% CO_2. The pH decreases with an increased fraction of slag in the noncarbonated samples. When each binder is compared individually, all carbonated samples have a lower pH than the noncarbonated samples. With an increase in the fraction of slag, the difference in pH between the noncarbonated and carbonated samples increases. The results suggest that S70 is carbonated to the greatest extent of all the binders. The effect carbonation has on capillary absorption and LTC is clearest for the S70 samples, whereas the K35, S35, and S20 samples only give some indications of the effect from carbonation.

Low temperature calorimetry

Figure 1 presents results from the LTC measurements. The solid lines are for the noncarbonated samples, and the dashed lines are for the carbonated samples. The y-axis represents the quantity of ice formed at a given temperature in relation to the total evaporable water content inside the sample.

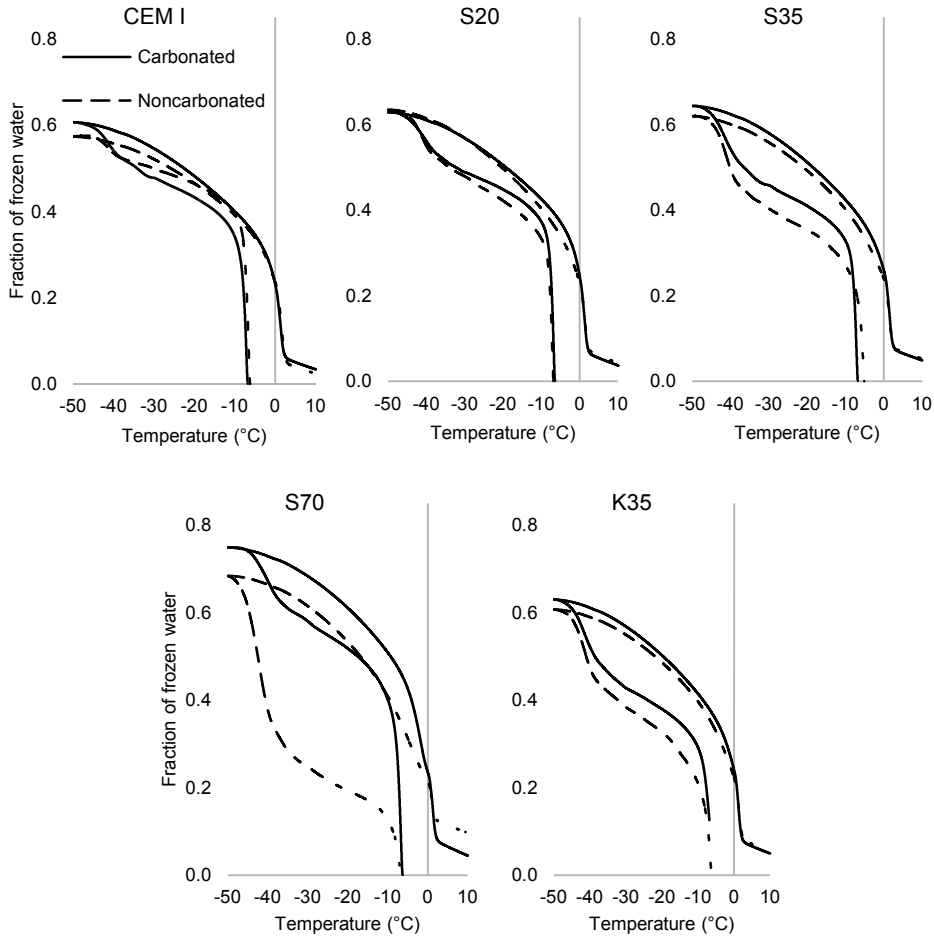

Figure 1
LTC measurements on samples from CEM I-4, S20-4, S35-4, S70-4, and K35-4 according to Table 1. The dashed lines are for the noncarbonated samples and the solid lines are for the carbonated samples. The lower lines present the fraction of ice during freezing, and the upper curves show the fraction of ice during thawing.

Thawing curves are used to study the pore size distribution according to the Gibbs-Thomson equation [20]. The reason for this is that during freezing, the water can supercool, and freezing is a stochastic process. By analysing the thawing curves, these two factors are avoided, and the thawing process comes closer to meeting thermodynamic equilibrium, which means that the measurements are closer to the Gibbs-Thomson equation [20, 21]. According to the thawing curves in Figure 1, 22% to 26% of the water content is frozen close to ±0 °C, and 57% to 75% of the water content is frozen at -50 °C. This enables a rough estimate of the volume fraction of pores having a radius larger than 50 nm, the fraction of the volume of mesopores, and the fraction of the volume of pores with a radius shorter than 2

nm. The total porosities were measured for each binder in the samples used for the capillary measurements and are presented in Table 3.

Figure 2 presents the differences between the thawing curves of each binder presented in Figure 1. These differences show the effect an increased fraction of slag had, and the effect carbonation had on the microstructure for each binder. Figure 2-A shows the increased fraction of ice that forms in noncarbonated samples of S20, S35, S70, and K35 compared with noncarbonated CEM I. Figure 2-B shows the increased fraction of ice that can form in carbonated samples of S20, S35, S70, and K35 compared with carbonated CEM I. Figure 2-C shows the increased fraction of ice that can form in carbonated samples compared with the noncarbonated samples for each binder.

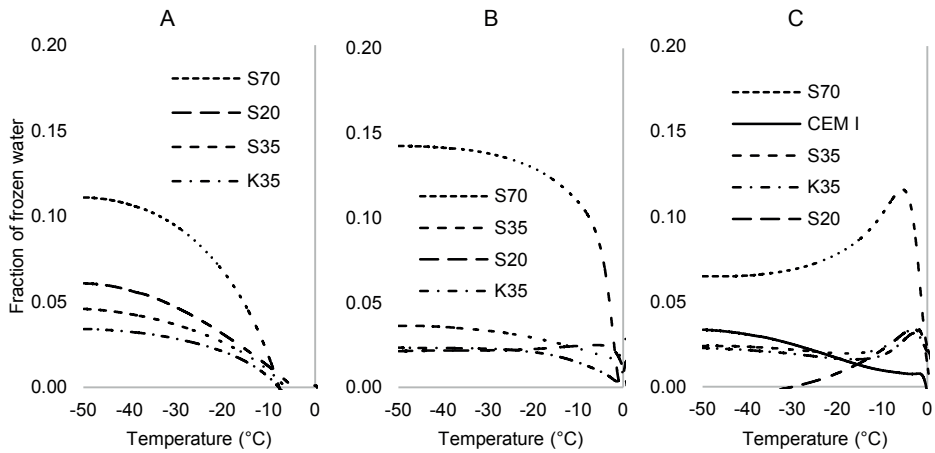

Figure 2
Differences between thawing curves presented in Figure 1 from the LTC measurements for CEM I-4, S20-4, S35-4, S70-4, and K35-4.

According to Figure 2-A, noncarbonated concrete with replacement of slag up to 35 mass%, or 25 + 10 mass% of slag + LF contributes a small increase in the fraction of mesopores compared to CEM I. For noncarbonated S70 concrete, there is a large increase in the fraction of mesopores compared with CEM I. These results agree with comparable LTC results in reference [5]. By comparing Figure 2-A and Figure 2-B, it can be seen that the carbonation reduces, or does not affect, the fraction of mesopores for S20, S35, and K35 compared with CEM I. However, carbonation increases the fraction of mesopores for the S70 concrete, according to the Figure 2-C carbonation results for a slight increase or no increase in the fraction of mesopores when the replacement of cement with slag is restricted to 35 mass% or less. Also, carbonation contributes only a slight increase to the fraction

of mesopores for concrete K35. However, carbonation of the S70 concrete results in a large increase in the volume fraction of mesopores.

According to Figure 2-A, the hysteresis between freezing and thawing increases with an increased fraction of slag in the noncarbonated concrete. The carbonation increases the hysteresis slightly for the CEM I concrete, whereas the carbonation reduces the hysteresis for all concrete samples containing slag. The reduction in the hysteresis by carbonation becomes greater as the fraction of slag increases. The hysteresis of the carbonated S70 is similar to the concrete containing 35 mass% low-calcium fly ash in [2]. These trends for the hysteresis also agree with the comparable measurements by [5].

Capillary absorption

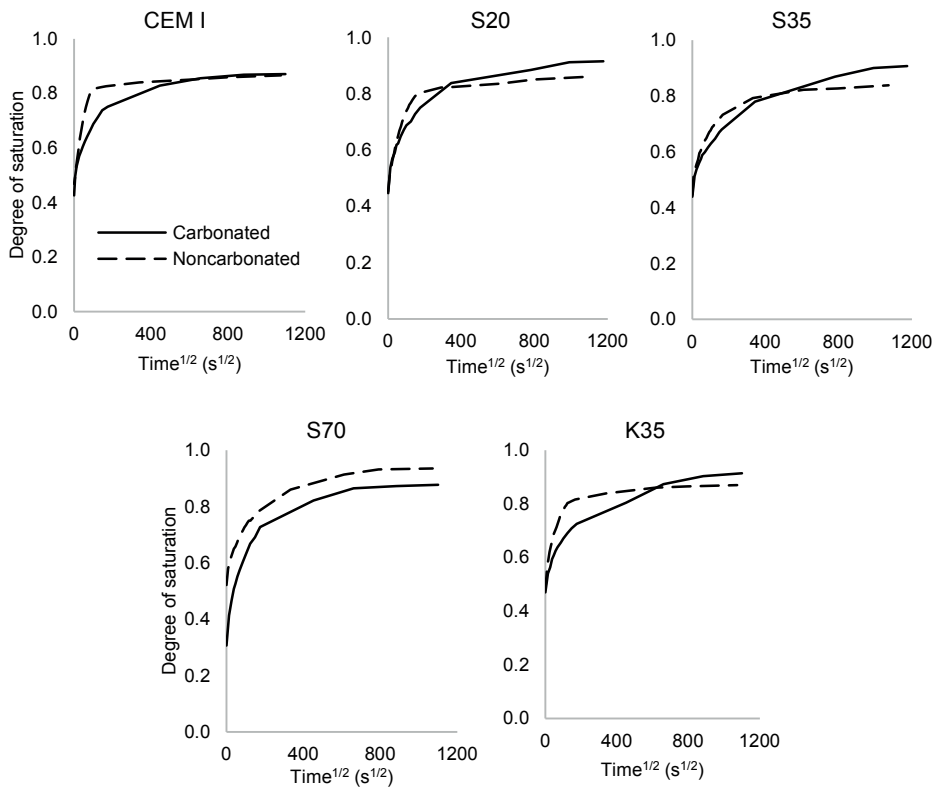

Figure 3
Mean value for capillary absorption from three samples of the batches CEM I-4, S20-4, S35-4, S70-4, and K35-4.

Table 3
Resistance to water penetration, coefficient of capillarity, and porosity calculated from the mean values presented in Figure 3.

Binder	Coefficient of capillarity kg/(m²s$^{1/2}$)		Resistance to water penetration, ·10^6 s/m²		Porosity[1] %		Porosity[2], pores >2 nm %	
	Noncarb.	Carb.	Noncarb.	Carb.	Noncarb.	Carb.	Noncarb.	Carb.
CEM I	0.0040	0.0017	325	1135	14.9	13.5	9.2	7.9
S20	0.0025	0.0013	579	1020	14.3	12.2	9.1	7.2
S35	0.0023	0.0013	783	1958	15.2	13.3	9.5	8.0
S70	0.0019	0.0023	1200	1046	13.8	12.9	9.2	9.3
K35	0.0028	0.0013	461	1795	13.9	12.5	8.9	7.2

[1] Porosities are calculated with dry mass when samples have dried at 105 °C.
[2] Porosities are calculated with dry mass when samples have dried in 35% RH and at 20 °C. Therefore, pores larger than approximately 2 nm have dried according to [17].

Capillary absorption measurements are presented in Figure 3 and Table 3. A high coefficient of capillarity with a low resistance to water penetration is regarded as a coarse porosity, and the opposite is regarded as a fine porosity. For the noncarbonated concrete, additional slag decreases the coefficient of capillarity and increases the resistance to water penetration. The noncarbonated K35 concrete has a higher coefficient of capillarity and lower resistance to water penetration than the S20 concrete. Carbonation decreases the coefficient of capillarity, increases the resistance to water penetration, and decreases the porosity for the CEM I, S20, S35, and K35 concretes. For the S70 concrete, the coefficient of capillarity increases, and the resistance to water penetration decreases. The noncarbonated 100% CEM I, noncarbonated S20, and noncarbonated K35 concrete have the highest permeability. The carbonated S35 and the carbonated K35 concrete have the lowest permeability. Carbonation resulted in a decrease in porosity for all of the samples. S70 shows the smallest decrease in porosity (0.9%), and the decrease seems to be only for pore volume <2 nm, whereas all other binders showed a decrease of between 1.2% and 2.1% both for voids >2 nm and for total porosity. The decrease in porosity for carbonated samples can be explained by the positive difference in molar volume between CH and the formed $CaCO_3$ [22-26]. These results show the same trends as those presented by [5].

Air Void Analysis

Table 4 presents results from the linear traverse analysis made on each concrete batch. An increased mass of air-entraining agent increases the number of air voids in the range of 0.0 mm to 2.0 mm and in the range of 0 µm to 350 µm for all binders. The CEM I, S20, and S35 batches have a slightly higher increase in the number of air voids than the S70 and K35 batches.

Table 4
Air content measured in fresh concrete and results from linear traverse measurements according to ASTM C 457.

Cast	Fresh concrete %[1]	Air void content			Air void content in paste		Specific surface[2][7] mm^{-1}	Spacing factor[2][8] mm
		Total %[2]	<2 mm %[2][3]	<0.35 mm %[2][4]	<2.00 mm %[2][6]	<0.35 mm %[2][6]		
CEM I-1	3.2	2.6	2.4	0.9	7.1	2.8	17	0.41
CEM I-2	3.0	2.7	2.4	0.9	6.8	2.8	19	0.38
CEM I-3	4.5	2.8	2.7	1.3	8.0	3.9	21	0.32
CEM I-4	5.1	4.1	3.4	1.9	9.4	5.7	24	0.25
S20-1	2.0	3.6	2.3	0.7	6.6	2.2	13	0.55
S20-2	2.9	5.1	2.9	1.1	8.0	3.0	17	0.38
S20-3	3.7	2.3	1.9	1.2	5.4	3.7	27	0.29
S20-4	4.7	3.7	3.4	2.1	9.8	6.1	30	0.20
S35-1	2.3	3.1	1.5	0.5	4.4	1.5	16	0.54
S35-2	3.8	3.6	2.9	1.3	8.4	3.9	19	0.33
S35-3	4.5	3.1	2.7	1.5	7.9	4.3	25	0.27
S35-4	5.2	5.6	4.5	2.4	12.6	6.7	23	0.23
S70-1	3.2	2.9	2.5	0.9	7.4	2.6	14	0.48
S70-2	4.1	2.7	2.2	1.1	6.8	3.2	21	0.35
S70-3	4.5	4.3	3.3	1.4	9.3	4.1	18	0.35
S70-4	4.7	3.3	2.7	1.2	8.2	3.5	17	0.38
K35-1	3.5	3.3	2.7	1.0	7.9	3.0	17	0.40
K35-2	3.7	3.7	2.9	1.2	8.4	3.5	18	0.35
K35-3	5.0	3.5	3.1	1.5	8.7	4.5	23	0.27
K35-4	5.1	3.2	3.1	1.6	8.8	4.9	23	0.27

[1] Total air content measured in 8 dm^3 fresh concrete. Read and rounded to closest 0.05%.
[2] Calculated from results from linear traverse measurements according to ASTM C 457.
[3] Total air content from air voids <2.0 mm.
[4] Total air content from air voids <0.350 mm.
[5] Voids <2.0 mm / (vol% cement paste + vol% of total voids). Vol% cement paste is calculated to 31%.
[6] Voids <0.350 mm / (vol% cement paste + vol% of total voids). Vol% cement paste is calculated to 31%.
[7] Specific surface ($mm^2/mm^3=mm^{-1}$) calculated from results of voids <2.0 mm.
[8] Spacing factor calculated from results of voids <2.0 mm.

Thin section analysis

Images from the thin section analysis for each batch are shown in Figures 4-8. An increased fraction of up to 35 mass% slag does not significantly affect the carbonation rate, but a large fraction (70 mass%) of slag increases the carbonation rate in a way similar to 35 mass% fly ash [2]. The average carbonation depth of CEM I, S20, S35, and K35 were approximately 0.2 mm, whereas the carbonation depth of S70 was approximately 2 mm. The images presented are used to show that the carbonation depth is not a constant depth for each binder, because the

aggregates and air voids affect the carbonation rates. Figure 4 and Figure 6 show examples of the carbonation of the paste along a large aggregate (light beige colour), whereas the carbonated layer along the test surface (bottom of the picture) has a smaller depth. Figure 7 shows an example where an air void seems to have increased the carbonation rate in the adjacent paste, resulting in a larger carbonation depth.

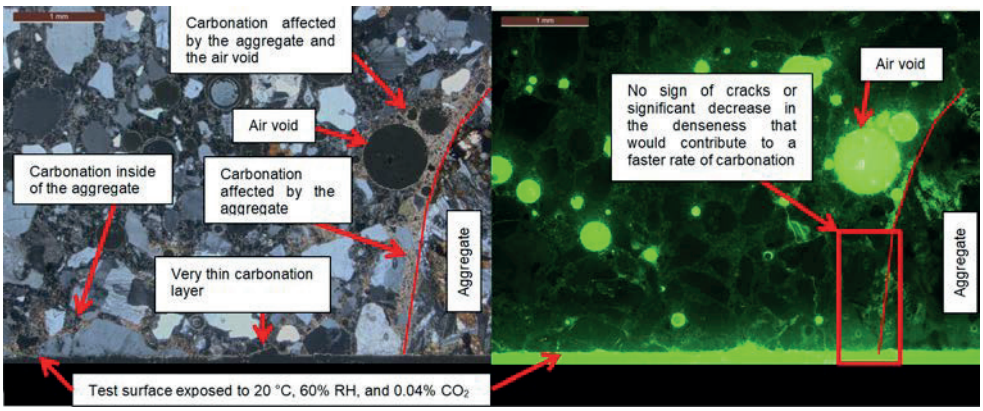

Figure 4
Carbonated CEM I thin section sample with the test surface at the bottom of the figure. The left figure shows a polarised image, and the right shows a fluorescence image of the same surface. Large aggregates are marked with red lines to facilitate interpretation of the images.

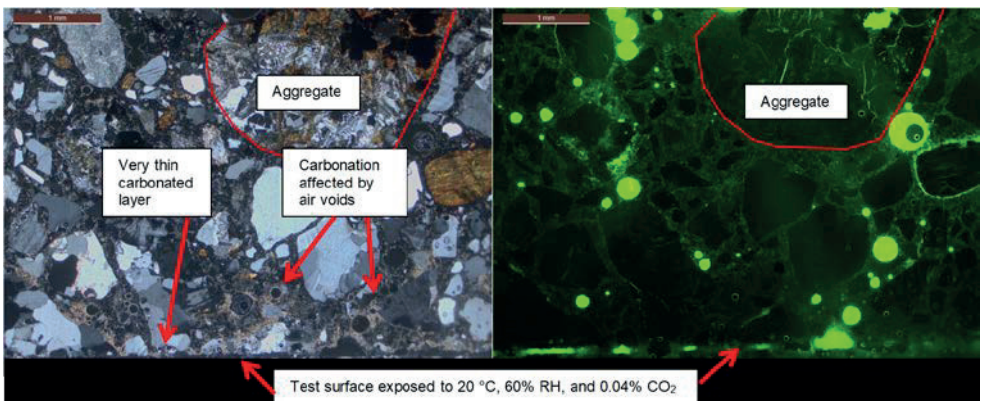

Figure 5
Carbonated S20 thin section (see caption, Fig. 4).

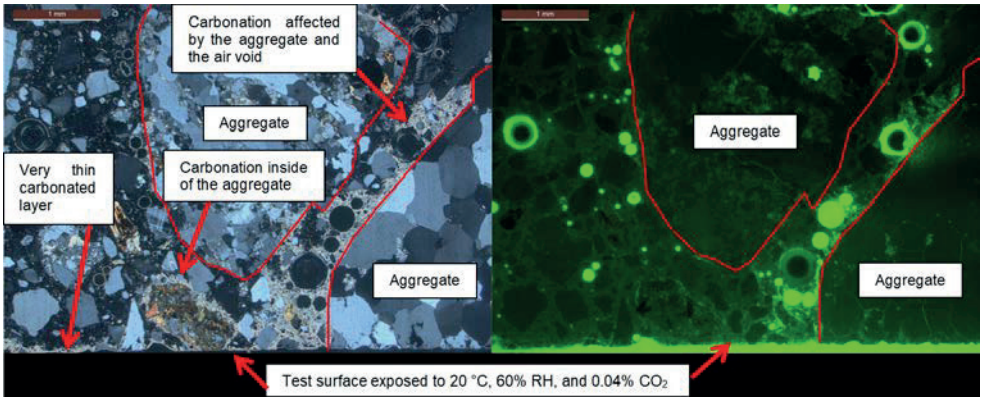

Figure 6
Carbonated S35 thin section (see caption, Fig. 4).

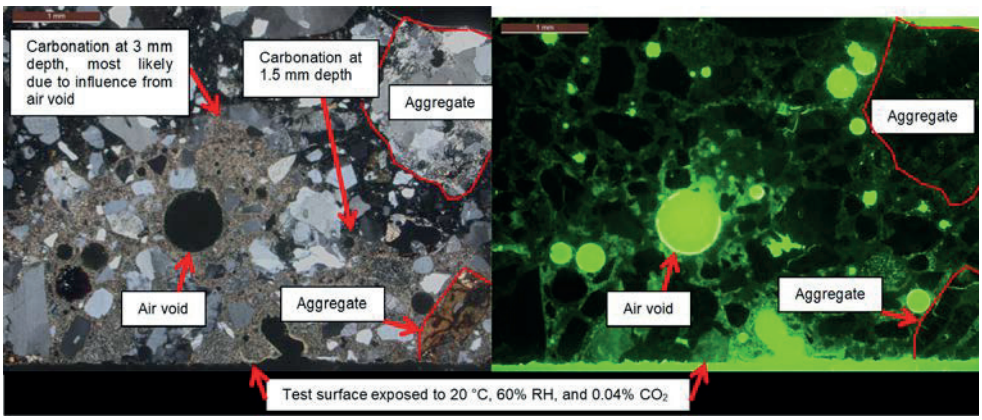

Figure 7
Carbonated S70 thin section (see caption, Fig. 4).

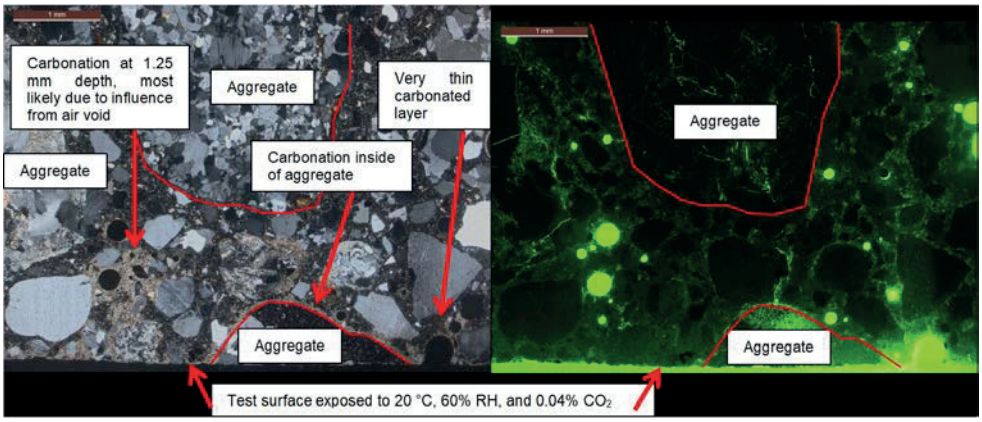

Figure 8
Carbonated K35 thin section sample (see caption, Fig. 4).

There were no indications of water separation, patterns of micro cracks, or agglomerated air voids. Also, the analysis according to NT Build 361 [27] showed that the hardened noncarbonated pastes for each binder had a homogeneous denseness.

De-Icing Salt Frost Scaling

The DISFS results are presented in Figures 9-13. The left figures show the mean accumulated scaling, and the right figures show the scaling rate in relation to the accumulated scaling. The average carbonation depths for each binder according to the thin section analysis are marked in the figures to the right. This is done with the rough estimate that a 1 mm scaling depth corresponds to 1 kg/m². The CEM I-4, S20-4, S35-4, and K35-4 concrete batches had an average carbonation depth of approximately 0.2 mm, therefore, this was converted to 0.2 kg/m². The S70 concrete had a carbonation depth of approximately 2.0 mm, this was converted to 2 kg/m². In order to help the analysis of the scaling rate diagrams, Table 5 presents the average number of cycles that had passed for each batch at the point marked by the dotted lines in diagrams to the right in Figures 9-13. Diagrams showing the coefficient of variation for the accumulated scaling measurements are presented in the supplementary information. All results are generalised, with consideration for the results presented in [2], and are summarised in Table 6.

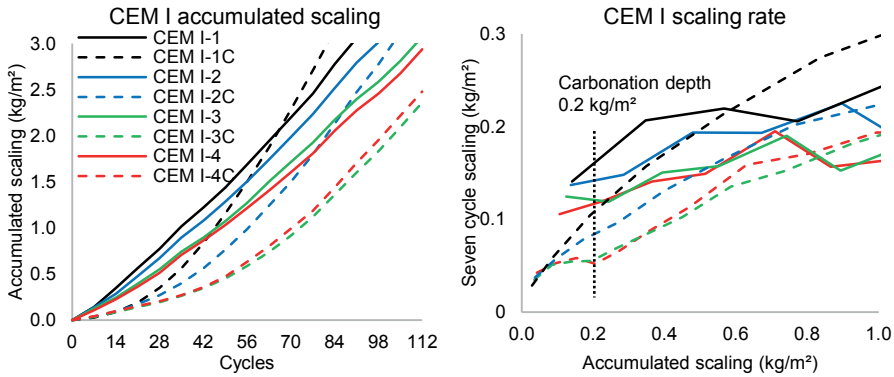

Figure 9
Left: mean accumulated scaling. Right: mean seven-cycle scaling for the accumulated scaling curves. Each line presenting results for noncarbonated samples represents the mean value of six samples. Each line presenting results for carbonated samples represents the mean value of five samples. 0.2 kg/m² is marked with an orange dashed line in the figure on the right because the estimated carbonation depth from the thin section analysis was, on average, 0.2 mm.

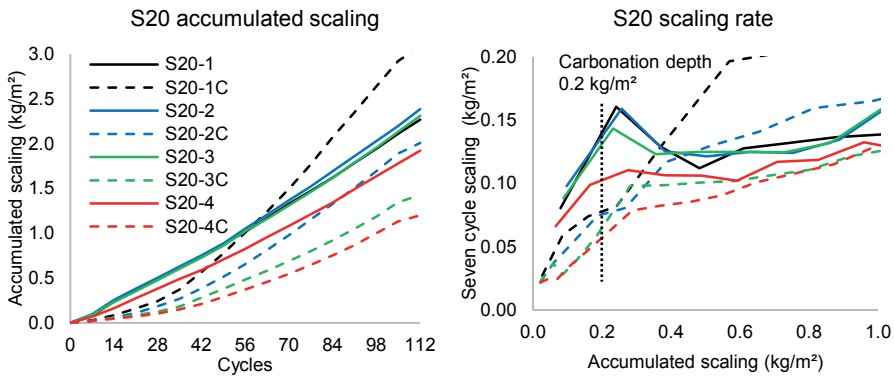

Figure 10
Results for S20 concretes (see caption of Fig. 9).

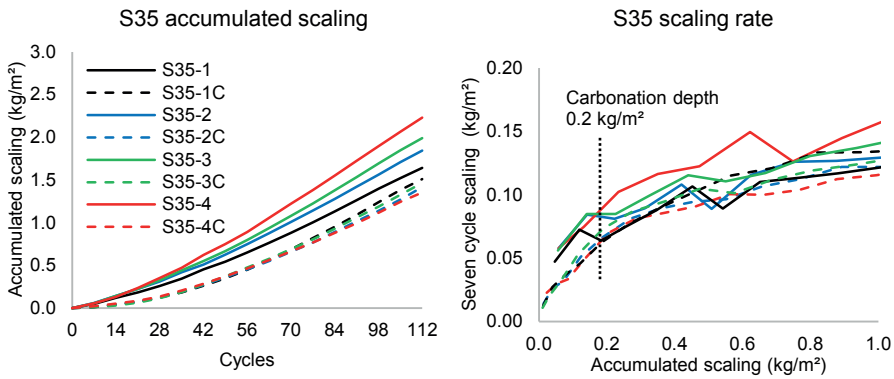

Figure 11
Results for S35 concretes (see caption of Fig. 9).

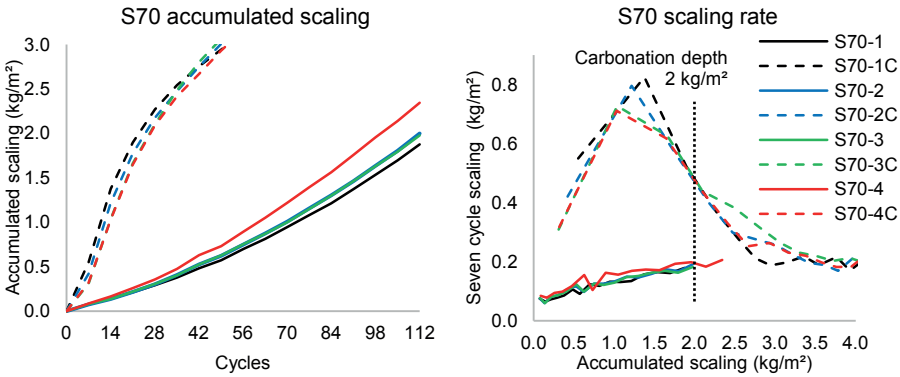

Figure 12
Results for S70 concretes (see caption of Fig. 9).

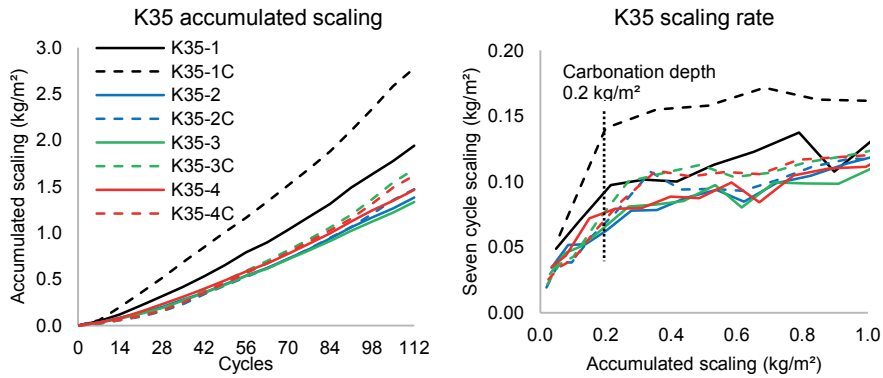

Figure 13
Results for K35 concrete (see caption of Fig. 9).

Table 5
Number of cycles when the accumulated scaling was 0.2 kg/m² for CEM I, S20, S35, and K35, and the number of cycles when the accumulated scaling was 2.0 kg/m² for S70.

Binder	Noncarbonated	Carbonated	Difference
CEM I-1	9	21	12
CEM I-2	10	23	13
CEM I-3	11	28	17
CEM I-4	12	27	15
S20-1	12	24	12
S20-2	11	29	18
S20-3	12	36	24
S20-4	16	41	25
S35-1	22	34	12
S35-2	19	36	17
S35-3	19	36	17
S35-4	19	36	17
S70-1	>112	23	<-89
S70-2	>112	25	<-87
S70-3	>112	26	<-86
S70-4	100	27	-73
K35-1	20	14	-6
K35-2	28	32	4
K35-3	29	30	1
K35-4	25	31	6

Table 6

Summary of the effect of microstructure on the DISFS, and the magnitude of the effect of increased air content on the DISFS. Water frozen at -50 °C according to the LTC results: 'dense' < 65% < 'medium' < 75% < 'coarse'. Resistance to water penetration according to capillary absorption measurements: 'coarse' < $650 \cdot 10^6$ < 'medium' < $1300 \cdot 10^6$ < 'dense'. Seven-cycle scaling: 'low' < 0.15 kg/m² < 'medium' < 0.3 kg/m² < 'high'. Effect from increased air content (Seven-cycle scaling for batch 1 to batch 4): 'low' < 0.1 kg/m² < 'medium' < 0.2 kg/m² < 'high'.

Binder	Preconditioning	LTC porosity of mesopores (structure / fraction of ice)	Cap absorption porosity of pores r>50 nm (structure / permeability)	Seven-cycles scaling	Effect of air voids on the DISFS
CEM I	Noncarbonated	Dense / Low	Coarse / High	Medium	Medium
	Carbonated	Dense / Low	Medium / Medium	Low	Low
S20	Noncarbonated	Dense / Low	Coarse / High	Low	Low
	Carbonated	Dense / Low	Medium / Medium	Low	Medium
S35	Noncarbonated	Dense / Low	Medium / Medium	Low	Low
	Carbonated	Dense / Low	Dense / Low	Low	Low
S70	Noncarbonated	Medium / Medium	Medium / Medium	Medium	Low
	Carbonated	Coarse / High	Medium / Medium	High	Low
K35	Noncarbonated	Dense / Low	Coarse / High	Low	Low
	Carbonated	Dense / Low	Dense / Low	Low	Medium

Effect of carbonation

During the discussion regarding the LTC and capillary absorption measurements, it is important to remember that only S70-4C seemed to be completely carbonated, whereas the samples from CEM I-4C, S20-4C, S35-4C, and K35-4C were not completely carbonated according to the pH measurements.

The DISFS results show that noncarbonated concrete containing up to 70 mass% slag, or 25 + 10 mass% slag + LF has a lower DISFS than 100% CEM I concrete. These results agree with [5, 9, 10], which show that replacing CEM I with slag can decrease the DISFS.

The effects of drying and carbonation are strongly dependent on the fraction of slag added to the concrete. The drying and carbonation of concrete that contains up to 35 mass% slag decreases the DISFS. According to the scaling rate diagrams in Figures 9-12, a correlation was found between the carbonation depth and the DISFS results. The correlation for the carbonated S70 concrete was similar to the correlation for the carbonated F35 concrete found in the first paper in this series (paper I) [2]. When a thin carbonated layer had scaled off, the scaling rate was approximately the same as for the noncarbonated CEM I, S20, S35, and S70 batches. For the K35 concrete with the air-entraining agent, the DISFS either increased or decreased after the carbonation, similar to the F20 batches in paper I [2].

The low DISFS for carbonated CEM I, as mentioned in paper I [2], is believed to be due to the fine porosity of mesopores and the low permeability of pores >50 nm according to the capillary suction measurements. When comparing the noncarbonated concrete containing slag with the noncarbonated CEM I, the results agree with these conclusions. The noncarbonated concrete batches with up to 35 mass% slag have fine-porosity mesopores (similar to CEM I), but a lower permeability than CEM I. After carbonation, the volume fraction of mesopores is almost unchanged, and the permeability of the pores >50 nm decreases for the CEM I, S20, S35, and K35 batches of concrete. This decreases the DISFS for CEM I, S20, and S35.

The DISFS results for the noncarbonated concrete containing K35 stand out. K35 had fine porosity mesopores and coarse porosity for pores >50 nm, similar to the noncarbonated CEM I. However, the DISFS was much lower in noncarbonated K35 than in the noncarbonated CEM I. The microstructure of carbonated K35 is similar to carbonated CEM I. There is almost no change to the porosity of mesopores, and the permeability of pores >50 nm decreases. Still, there is no change to the DISFS. This indicates that the permeability of pores >50 nm is not detrimental to the DISFS for K35. This means that these results contradict the results from CEM I, S20, and S35, and another explanation for the low DISFS is needed. According to the measurements of compressive strength for each binder (found in the supplementary material), the K35 binder has significantly lower compressive strength than the CEM I. This suggests that the tensile strength of the K35 is also lower, yet the noncarbonated K35 still has a much lower DISFS than the CEM I concrete. In order to understand why the noncarbonated K35 has such a low DISFS, measurements are needed for material properties other than the ones that have been taken in this study. Two suggestions for measurements of material properties that could differentiate K35 from the others are the Young's modulus and the pore size distribution between 50 nm and 10 μm.

Effect of air void system

The linear traverse analysis shows that an increased mass of air-entraining agent increases the amount of air voids for all batches, but to a lesser extent for the S70 and K35 batches. However, the effect of an increased amount of air voids on the DISFS varies, depending on the binder. The increased amount of small air voids in noncarbonated S20 results in a slight decrease to the DISFS. The carbonated S20 concrete has a decreased DISFS, similar to carbonated CEM I. Noncarbonated S35 seems to show a negative effect from the increased air void content, whereas the carbonated S35 seems to be unaffected by the increased number of air voids. The DISFS of noncarbonated and carbonated S70 does not seem to show any effect from an increased number of small air voids. Therefore, the results indicate that an

increased fraction of slag reduces the protective effect of an increased number of small air voids.

The noncarbonated and carbonated S20 seem to have a similar mesopore structure, whereas the carbonated S20 has a lower permeability. The reason for the small negative effect from the air voids of noncarbonated S35 is not known; its mesopore porosity seems to be similar to that of CEM I and S20. The reason that the noncarbonated S70 concrete does not show any effect from the addition of air-entraining agent could be due to the large hysteresis, which is believed to be caused by a considerable number of bottlenecks. This would support the theory that bottlenecks <50 nm counteract the positive effect from an air void system, as mentioned in paper I [2] for the F35 noncarbonated concrete. However, the carbonated S70 batches did not have a large number of bottlenecks, and still did not show any decrease in DISFS from an increased number of air voids. The reason is therefore more likely to be that the increase in the number of air voids is too low for the S70 concrete, and the low permeability reduces the effect of the increased number of air voids. The DISFS of the K35 concrete did not seem to be affected by the addition of the air-entraining agent. The reason that carbonated S35 and carbonated K35 were unaffected by the addition of air-entraining agent could be due to their low permeability. These two concrete mixtures had the lowest permeability of all mixtures tested.

Batches S20-1C and K35-1C (without air-entraining agent) had higher DISFS than the corresponding noncarbonated samples after the carbonated layer had scaled off. This is the same observation as the one made in paper I [2] regarding CEM I-1C, F20-1C, and F35-1C. The suggested cause for this is that the drying shrinkage results in more micro cracks, which increases the DISFS when the concrete does not contain air-entraining an agent. However, this cannot be confirmed by the current study because the thin section analysis was only made on the samples with the highest mass of air-entraining agent (as mentioned in paper I [2]).

Discussion considering de-icing salt frost scaling theories

This section will discuss the results presented in the current article and in paper I [2]. However, the measurements were made to study the DISFS in different materials, and were not specifically designed to test mechanism theories. Hence, the discussion here is limited to how the presented results relate to the different theories.

According to Powers [28], the hydraulic pressure created from ice nucleation in non-saturated pastes is higher for an increased fraction of ice formed, a decreased permeability, and an increased freezing rate. This theory was later revised by Powers, so that the damage mechanism of DISFS was thought to be the hydraulic

pressure together with the osmotic pressure and the pressure from the ice lens that grows [29]. This revision was due to new experimental data that the hydraulic pressure mechanism could not explain by itself [30]. The reason for the damage, according to Lindmark [31], is that the salt and an external reservoir enable the ice lenses to continue to grow due to differences in free energy. The samples used in the present DISFS method [19] are cylindrical and insulated on all sides, except the one that is in contact with the salt solution. The temperature of the air inside the freezer is approximately -22 °C during freezing. According to results presented in [21], the freezing rate of the dendritic growth in water was measured to be 0.19 cm/s in a small cylindrical insulated sample with an external temperature of -12 °C. The dendritic growth rate is faster when supercooling occurs [21]. Because the samples in this study were exposed to the same temperature cycle during DISFS, the freezing rate should be approximately the same unless the supercooling varies to a large extent between the samples. According to the temperature measurements, the supercooling does not vary to a large extent in the NaCl solutions that are in contact with the samples. Previous studies have shown that the DISFS damage increases as the minimum temperature decreases [31-34]. This phenomenon cannot be explained by the hydraulic pressure because the observed suction from the ice generates a negative pressure and causes the air-entrained concrete to shrink [30, 35-37]. Therefore, previous observations suggest that the hydraulic pressures damages only concrete with low air content and a high degree of saturation. Considering that a lower minimum temperature increases the DISFS damage [31-34], the LTC measurements from the current study suggest that the damage increases with a larger fraction of ice formed. These results agree with previous research [38]. When the structure is coarse, and mesopores enables more ice to form, the damage increases. When considering the permeability, the results from the current study do not agree with the theory of hydraulic pressure. According to the theory, a low permeability increases the hydraulic pressure, which should result in a higher DISFS. According to the results presented in the current study, a fine structure for mesopores with a low permeability (according to the capillary suction measurements, i.e. S20 carb, S35 carb, and K35 carb) results in a much lower DISFS than a coarse structure for mesopores with a medium permeability (i.e. S70 carb, and F35 carb). Therefore, a higher permeability, which should decrease the pressures according to the theory, does not decrease the damage, because more ice is allowed to form.

According to the micro ice lens growth mechanism presented by Lindmark in [31], DISFS damage is caused by external moisture uptake during freezing due to differences in free energy. His theory is based on earlier theories of the mechanism of soil heaving [31]. The salt enables an outer reservoir of unfrozen brine solution at atmospheric pressure to provide water that can be transported into the concrete [31]. When the temperature decreases, the pressure of the ice body must increase

to return to thermodynamic equilibrium [31]. This means that the ice body must grow until it starts exerting pressure on the pore walls [31]. Because the pressures from the growth of ice lenses is much higher than the strength of concrete, the strength of the concrete is of little importance [31]. However, the depth from the concrete surface where the micro ice lenses form and grow is the deciding factor for how much scaling there will be [31]. As the depth of the micro ice lens increases, the mass of scaling increases. The depth is determined by a coupled heat and mass transfer process [31]. The heat from ice being formed must be transported away from the site, and moisture must be transported to the site [31]. The sites for ice nucleation occur at several depths, which results from the balance between the moisture accessibility, heat flow, and ice lens growth [31]. This mechanism should therefore be strongly connected to the permeability of the concrete, the fraction of ice that can form according to the Gibbs-Thomson equation, and the moisture content in the vicinity of the ice body. When comparing the results to the theory, the LTC results agree with the theory in the sense that an increased fraction of ice formed increases the DISFS. However, the capillary suction results are not as consistent, because a lower permeability should decrease the water content at the surface and reduce the depth to which water can be transported and freeze. However, K35 has a low DISFS, even if it has a high permeability.

According to the glue spall theory proposed by Valenza and Scherer, the DISFS is caused by the thermal contraction of ice that is in contact with the concrete surface [20]. The difference in the coefficient of thermal expansion for cement paste and ice results in an ice contraction five times greater than the concrete contraction [20]. This results in shear stress that exceeds the strength of the concrete surface [20]. This mechanism is strongly related to the strength of the concrete, the coefficients of thermal expansion [20], and the amount of ice that has formed [35]. The theory also points out that the air void system has a protective function [35], because when ice forms in larger pores, the ice bodies creates a suction in surrounding mesopores. This contracts the concrete and therefore reduces the shear stress caused by the ice contracting during freezing [35]. The carbonation of CEM I decreases its permeability and does not change the structure of mesopores. This likely increases the strength of the concrete, and therefore decreases the DISFS. Because the noncarbonated F35 had a larger number of mesopores compared to the noncarbonated F20, F35 had a lower tensile strength compared to F20. Also, when F35 carbonates, the mesopores become even coarser. This is also likely to decrease the tensile strength, resulting in a higher DISFS than the noncarbonated F35 (presented in paper I [2]). The batches containing slag have a fine porosity of mesopores and a low permeability according to the capillary suction measurements. It is reasonable that the dense structure of these batches increases the strength of the concrete and therefore decreases the DISFS according

to the glue spall theory. However, the noncarbonated K35 seems to have approximately the same structure and porosity as the noncarbonated CEM I, but its DISFS is much lower than that of the noncarbonated CEM I. According to the glue spall theory, the DISFS results suggest that the structure of K35 contributes to lowering the difference between the coefficient of thermal expansion in the ice-brine bimaterial and the concrete surface. It would be interesting to do warping tests similar to the ones presented in [39] to see if the deflection for each material correlates with the DISFS results presented in the current study. It would also be interesting to measure the thermal coefficients of expansion for each concrete mixture that have been studied to see if the difference in thermal coefficient of expansion between the paste and ice is lower for the mixtures with a lower mass of scaling.

According to an analysis of the data from Mielenz [40] by Valenza and Scherer [20], the air voids reduce the damage to a greater extent if the air voids are surrounded by a dense structure. The reason for this is that a dense structure prevents ice from growing into the pores due to the freezing depression caused by the small connecting pores [20]. If ice nucleation starts inside an unsaturated air void, the growing ice inside the air void will drain unfrozen fluid from surrounding pores where ice has not yet formed, due to cryo-suction [20, 21, 30, 35]. The results from the current study seem to fully support this theory. Looking at CEM I, S20, and S35, the air-entrained concretes have a fine structure of mesopores that connects larger air voids. After carbonation of the CEM I, pores >50 nm are filled with product, the permeability and porosity decrease, and the structure surrounding the air voids become denser. This results in a decreased DISFS according to the analysis of [40] by [20]. Looking at noncarbonated F35, the air-entrained concrete has a coarse structure of mesopores with an average permeability of pores >50 nm that connects larger entrained air voids. The coarser structure of mesopores contributes to faster growth of ice into these pores and therefore contributes to a higher DISFS. The same can be said of the carbonated F35 and the carbonated S70. Looking at noncarbonated F20, the air-entrained concretes have a dense structure of mesopores with an average permeability of pores >50 nm that connects larger air-entrained voids. This seems to contribute to approximately the same DISFS as the noncarbonated CEM I concrete. After F20 carbonation, the structure of mesopores becomes slightly coarser, and the permeability of the pores >50 nm decreases. These two facts conflict according to the theory (of how the structure surrounding the air voids affects the DISFS), and according to the results the DISFS is approximately the same, therefore these two factors may have cancelled each other out. The noncarbonated S20, S35, and S70 with a dense structure for mesopores and a low-to-medium permeability for pores >50 nm result in a low DISFS. The carbonated S20, S35, and K35 have a dense structure of mesopores and a low permeability for pores >50 nm that results in a

low DISFS. These results therefore also agree with the theory and suggest that a concrete with these properties is likely to have a low DISFS. The noncarbonated K35 with dense structure for mesopores and a high permeability for pores >50 nm is does not fit as well to the theory. Nevertheless, these measurements have been shown in this paper to be useful for comparing the porosities and microstructures, and how these affect the DISFS in concrete.

When considering the DISFS results in relation to compressive strength, the results agree with a previous study by Hooton and Vassilev [14], which also showed that there is no direct correlation between the mass of DISFS and the compressive strength for each binder. This is clearly shown just by looking at the compressive strength for S35 and S70, where S35 had a compressive strength approximately 15.6 MPa higher than S70, yet they still produced approximately the same mass of DISFS in never-dried and noncarbonated samples. A study by Boyd and Hooton [41] tested pull-out strength (which could be considered to be related to the tensile strength of the material) in relation to the scaling test. However, there was no correlation between the results. One reason for this could be that the rupture surface was not in the carbonated zone, i.e. the pull-out strength did not represent the strength of the carbonated layer that was exposed to the DISFS.

Research questions

How does an increased fraction of slag affect the microstructure?

- For noncarbonated concrete, the addition of slag lowers the permeability for pores with a radius greater than 50 nm. Up to 35% replacement with slag, or 25 + 10% slag + LF slightly increases the fraction of the mesopores. When replacing 70 mass% of CEM I with slag, the fraction of mesopores increases more than when the replacement of slag is 35 mass% or lower.

How does the carbonation of each binder change the microstructure?

- Carbonation of concrete with 100% CEM I, up to 35% slag, or 25 + 10% slag + LF causes almost no change to the fraction of mesopores. Carbonation of concrete with 70 mass% slag increases the fraction of mesopores.
- Carbonation of concrete with 100% CEM I, up to 35% slag, or 25 + 10% slag + LF decreases the permeability of pores with a radius larger than 50 nm. Carbonation of concrete with 70% slag slightly increases the permeability of pores with a radius larger than 50 nm.

How does an increased fraction of slag affect the DISFS?

- For noncarbonated concrete, all batches containing slag have lower DISFS than noncarbonated concrete with 100% CEM I.

How does the drying and carbonation of each binder affect the DISFS?

- The carbonation of concrete containing up to 35 mass% slag, or 25 + 10 mass% slag + LF decreases the DISFS, reaching a similar level as concrete containing 100% CEM I. Carbonation of concrete containing 70 mass% slag increases the DISFS similar to that of concrete containing 35 mass% low-calcium fly ash.
- Drying increases the DISFS for CEM I, S20, and K35 without air-entraining agent in comparison to samples from the same batches that have never-dried. This suggests that increased air void content decreases the DISFS more for dried and carbonated concrete compared with noncarbonated and never-dried concrete for CEM I, S20, and K35.

How does increased air content affect the DISFS in concrete with various fractions of slag?

- An increased air void content has a positive effect on concrete containing CEM I and S20. The reason for the small effect from the increased air content in the S35 and K35 concrete could be that the low permeability of pores with a radius longer than 50 nm counteracts this effect. The reason for the small effect from the increased air content in S70 (or K35) could be due to the small increase in the air void content.

Does the effect that the air content has on the DISFS change depending on whether the surface is carbonated or not?

- The results indicate that the protective effect of an increased air void content is dependent on the surrounding paste. Therefore, the change in porosity caused by carbonation changes the effect by the air voids for the same material.

Conclusions

Considering this article and [2].

- A fine structure of mesopores that reduces the fraction of ice that can form at a given temperature combined with low permeability for the structure of pores with a radius longer than 50 nm results in a low DISFS. (Noncarbonated K35 is an exception that has a fine structure of mesopores and a coarse structure of pores with a radius larger than 50 nm with a very low DISFS.)
- A coarse structure of mesopores with a medium or high permeability for the structure of pores with a radius longer than 50 nm results in the highest DISFS.

Acknowledgements

This research was funded by SBUF (The Development Fund of the Swedish Construction Industry) supported by Skanska AB and Cementa AB (a part of Heidelberg Group). Cementa performed the measurements on the binders. Thin section samples were polished and prepared by RISE. The author performed the microscopic analysis with some assistance from Jan Erik Lindqvist at RISE.

References

1. Scrivener, K.L., *Options for the future of cement.* The Indian Concrete Journal, 2014. **88**(7): p. 11.
2. Strand, M.J. and K. Fridh, *De-Icing Salt Frost Scaling part 1: Concrete containing Low Calcium Fly Ash*. Manuscript, Lund University.
3. Özbay, E., M. Erdemir, and H.İ. Durmuş, *Utilization and efficiency of ground granulated blast furnace slag on concrete properties – A review.* Construction and Building Materials, 2016. **105**: p. 423-434.
4. Lang, E., *Durability aspects of CEM II/B-M with blastfurnace slag and limestone*, in *Cement Combinations for Durable Concrete*, R.K. Dhir, T.A. Harrison, and M.D. Newlands, Editors. 2005, MPG Books: University of Dundee, Scotland, UK. p. 55-64.

5. Utgenannt, P., *The influence of ageing on the salt-frost resistance of concrete*, in *Department och Building and Environmental Technology*. 2004, Faculty of Engineering, LTH, Lund University: Lund. p. 346.

6. Stark, J. and H.M. Ludwig. *Freeze-deicing salt resistance of concretes containing cement rich in slag*. in *Frist resistance of concrete*. 1997. London: E & FN Spon.

7. Stark, J. and H.M. Ludwig, *Freeze-thaw and freeze-deicing salt resistance of concretes containing cement rich in granulated blast furnace slag.* Aci Materials Journal, 1997. **94**(1): p. 47-55.

8. Stark, J. and U. Knaack. *Freeze-deicing salt resistance of concretes containing blast-furnace slag-cement*. in *Freeze-thaw durability of concrete*. 1997. United Kingdom, London: E & FN Spon.

9. Helsing, E. and P. Utgenannt, *The salt-frost resistance of concrete with supplementary cementitoius materials (SCM)*, in *Materials, Systems and Structures in Civil Engineering 2016*, M.T. Hasholt, K. Fridh, and R.D. Hooton, Editors. 2016, RILEM publications S.A.R.L: Technical University of Denmark, Lyngby, Denmark. p. 51-60.

10. Boubitsas, D., et al., *Frost resistance of concrete - Experience from long term exposure*, in *Materials, Systems and Structures in Civil Engineering 2016*, M.T. Hasholt, K. Fridh, and R.D. Hooton, Editors. 2016, RILEM publications S.A.R.L: Technical University of Denmark, Lyngby, Denmark. p. 21-30.

11. Bilodeau, A. and V.M. Malhotra. *Deicing salt scaling resistance of concrete incorporating supplementary cementing materials CANMET research*. in *Freeze-Thaw Durability of Concrete - rilem proceedings 30*. 1997. E & FN SPON.

12. Panesar, D.K. and S.E. Chidiac, *Multi-variable statistical analysis for scaling resistance of concrete containing GGBFS.* Cement and Concrete Composites, 2007. **29**(1): p. 39-48.

13. Giergiczny, Z., et al., *Air void system and frost-salt scaling of concrete containing slag-blended cement.* Construction and Building Materials, 2009. **23**(6): p. 2451-2456.

14. Hooton, R.D. and D. Vassilev, *Deicer Scaling Resistance of Concrete Pavements, Bridge Decks, and Other Structures Containing Slag Cement: Phase 2: Evaluation of Different Laboratory Scaling Test Methods*. 2012.

15. Löfgren, I., O. Esping, and A. Lindvall, *The influence of carbonation and age on salt frost scaling of concrete with mineral additions*, in *Materials, Systems and Structures in Civil Engineering 2016*, M.T. Hasholt, K. Fridh, and R.D. Hooton, Editors. 2016, RILEM publications S.A.R.L: Technical University of Denmark, Lyngby, Denmark. p. 91-100.

16. Scherer, G.W., *Crystallization in pores.* Cement and Concrete Research, 1999. **29**(8): p. 1347-1358.

17. Jennings, H.M., A. Kumar, and G. Sant, *Quantitative discrimination of the nano-pore-structure of cement paste during drying: New insights from water sorption isotherms.* Cement and Concrete Research, 2015. **76**: p. 27-36.

18. Gallé, C., *Effect of drying on cement-based materials pore structure as identified by mercury intrusion porosimetry: A comparative study between oven-, vacuum-, and freeze-drying.* Cement and Concrete Research, 2001. **31**(10): p. 1467-1477.

19. Strand, M.J. and K. Fridh, *Test Method for De-Icing Salt Frost Scaling in High Performance Concrete.* MethodsX, 2018.

20. Valenza II, J.J. and G.W. Scherer, *A review of salt scaling: II. Mechanisms.* Cement and Concrete Research, 2007. **37**(7): p. 1022-1034.

21. Sun, Z. and G.W. Scherer, *Measurement and simulation of dendritic growth of ice in cement paste.* Cement and Concrete Research, 2010. **40**(9): p. 1393-1402.

22. Pihlajavaara, S.E., *Some results of the effect of carbonation on the porosity and pore size distribution of cement paste.* Matériaux et Construction, 1968. **1**(6): p. 521-527.

23. Pihlajavaara, S.E. and E. Pihlman, *Effect of carbonation on microstructural properties of cement stone.* Cement and Concrete Research, 1974. **4**(2): p. 149-154.

24. Patel, R.G., et al., *Influence of curing at different relative humidities upon compound reactions and porosity in Portland cement paste.* Materials and Structures, 1988. **21**(3): p. 192-197.

25. Ngala, V.T. and C.L. Page, *EFFECTS OF CARBONATION ON PORE STRUCTURE AND DIFFUSIONAL PROPERTIES OF HYDRATED CEMENT PASTES.* Cement and Concrete Research, 1997. **27**(7): p. 995-1007.

26. Delmi, M.M.Y., A. Aı¨t-Mokhtar, and O. Amiri, *Modelling the coupled evolution of hydration and porosity of cement-based materials.* Construction and Building Materials, 2006. **20**(7): p. 504-514.

27. Nordtest, *NT Build 361*, in *Concrete hardened - Water-cement ratio*. 1999.

28. Powers, T.C. *The Air Requirement of Frost-Resistant Concrete*. 1949. Highway Research Board 29, PCA Bull 33.

29. Powers, T.C., *Freezing effects in concrete.* ACI, 1975. **SP-47**(Durability of Concrete): p. 1-11.

30. Powers, T.C. and R.A. Helmuth, *Theory of volume changes in hardened portland-cement paste during freezing.* Proceedings, Highway Research Board 32, PCA Bull 46, 1953.

31. Lindmark, S., *Mechanisms of Salt Frost Scaling of Portland Cement-bound Materials: Studies and Hypothesis*, in *Department of Building and Environmental Technology*. 1998, Faculty of Engineering, LTH, Lund University: Lund. p. 266.

32. Studer, W., *Internal comparative tests on frost-deicing-salt resistance*, in *International Workshop in the Resistance of Concrete to Scaling Due to Freezing in the Presence of De-icing Salts*, J. Marchand, M. Pigeon, and M.J. Setzer, Editors. 1997, E & FN Spon: Sainte-Foy, Québec, Canada. p. 259-270.

33. Sellevold, E.J. and T. Farstad, *Frost/Salt-testing of Concrete: Effect of Test Parameters and Concrete Moisture History.* 1991.

34. Petersson, P.-E., *Influence of Minimum Temperatures on the Scaling Resistance of Concrete. Part 1: Portland Cement Concrete.* 1994, SP Swedish National Testing and Research Institute. p. 30.

35. Sun, Z. and G.W. Scherer, *Effect of air voids on salt scaling and internal freezing.* Cement and Concrete Research, 2009. **40**: p. 260-270.

36. Coussy, O. and P.J.M. Monteiro, *Poroelastic model for concrete exposed to freezing temperatures.* Cement and Concrete Research, 2008. **38**(1): p. 40-48.

37. Valenza II, J.J. and G.W. Scherer, *Mechanism for salt scaling.* Journal of the American Ceramic Society, 2006. **89**(4): p. 1161-1179.

38. Marchand, J., et al., *Influence of Chloride Solution Concentration on Deicer Salt Scaling Deterioration of Concrete.* ACI Materials Journal, 1999. **96**(4): p. 429-435.

39. Valenza II, J.J., *Mechanism for Salt Scaling*, in *Civil and Environmental Engineering*. 2005, Princeton University. p. 362.

40. Mielenz, R.C., et al., *Origin, evolution, and effects of the air void system in concrete. Part 1 - Entrained air in unhardened concrete.* ACI, 1958. **30**(1): p. 95-121.

41. Boyd, A.J. and R.D. Hooton, *Long-Term Scaling Performance of Concretes Containing Supplementary Cementing Materials.* Journal of Materials in Civil Engineering, 2007. **19**(10): p. 820-825.

Supplementary information

Binders

Table 1 presents the recipes used for each batch that was tested in this article with consideration for the measured air content in the fresh concrete. The binder content was set to be close to 430 kg/m³ for each recipe, given an increased amount of air content. The grain fraction curve of the aggregates used had a fineness modulus of 4.79, and they were designed to have a small number of fractions between 4 and 8 mm.

Table 6 presents X-ray fluorescence (XRF) analysis of the siliceous fly ash, and each binder combination that was tested. CEM I contained 2.36% LF. Table 3 presents the results from the Blaine fineness-, laser diffraction and compressive strength measurements. The Blaine value and laser diffraction measurement results indicate that the slag particles have a larger specific surface and a smaller average size than the CEM I particles, and the LF particles have smaller specific surface and a larger average particle size than the slag. When replacing 20 and 35 mass% of the CEM I content, there is no significant difference in strength other than the early 2-day strength. However, when replacing 70 mass%, there is a significant difference in strength up to 91 days. The LF seems to have a negative impact on the strength in comparison with the slag according to these measurements.

Table 6
XRF – Cement – wroxi.

Binder	CaO[1] %	SiO_2[1] %	Al_2O_3[1] %	Fe_2O_3[1] %	MgO[1] %	K_2O[1] %	Na_2O %	Na_2Oe[2] %	SO_3[1] %	LOI[1] %
CEM I	63.60	21.30	3.80	4.56	0.856	0.650	0.07	0.50	2.45	1.84
S20[3]	57.80	23.90	5.61	3.78	3.68	0.699	0.17	0.63	2.60	1.17
S35[3]	52.70	25.90	7.10	3.11	5.92	0.748	0.26	0.75	2.76	0.56
S70[3]	41.60	29.90	10.20	1.67	10.7	0.842	0.44	1.00	3.02	-0.59
K35[3]	54.10	22.90	5.94	3.11	4.77	0.685	0.21	0.66	2.40	5.04

[1] The precision in the measurements are CaO±0.233%, SiO_2±0.100%, Al_2O_3±0.052%, Fe_2O_3±0.019%, MgO±0.025%, K_2O±0.032%, SO_3±3%, (loss on ignition=) LOI ±0.18% Na

[2] Na_2O-equivalent.

[3] Measured oxide composition from the blended slag and CEM I.

Table 7
Blaine value, laser diffraction, and compressive strength measurements for each binder combination.

Binder	Blaine[1)]	LD[2)]	Strength after given days of hydration[3)], MPa			
	m²/kg	µm	2 days	28 days	56 days	91 days
CEM I	343	17.305	21.8±0.3	55.1±0.3	62.3±1.2	66.1±2.0
S20	371	16.142	16.5±0.2	52.1±0.8	63.3±1.3	65.3±1.3
S35	395	15.339	12.9±0.1	53.9±0.6	63.5±0.7	67.4±0.5
S70	448	13.957	4.4±0.1	42.4±0.4	49.3±0.9	51.8±1.1
K35	397	16.439	12.8±0.3	47.9±1.2	55.2±0.6	58.3±0.6

[1)] Blaine value of specific surface area per mass binder measured according to EN 196-6:2010.
[2)] Laser diffraction measurement of the 50th percentile particle size.
[3)] Compressive strength measured according to EN 196-1:2005 with the standard deviation.

Salt-frost scaling results supplementary information

Figure 14 below show the coefficient of variation in relation to the accumulated scaling from the CEM I, S20, S35, S70, and K35 concrete. The coefficient of variation is the standard deviation of the accumulated scaling divided by the accumulated scaling.

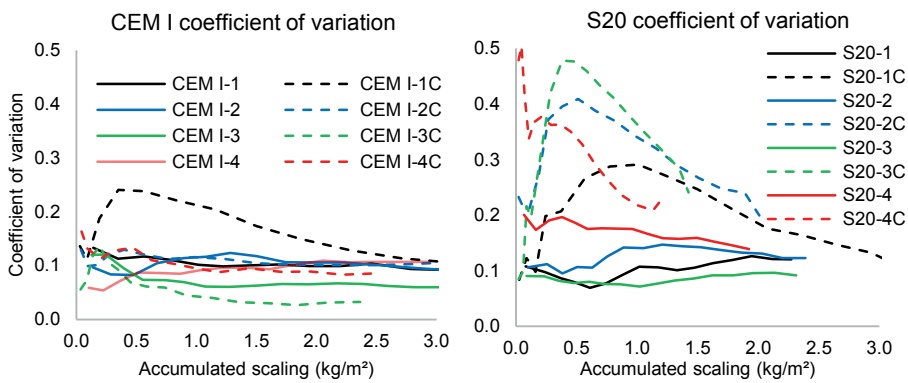

Figure 14
Coefficient of variation for the accumulated scaling presented in Figure 9 and 10 for CEM I and S20 respectively.

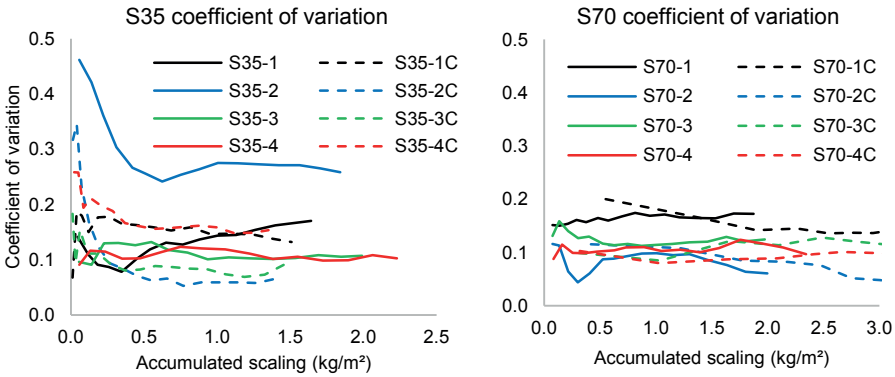

Figure 15
Coefficient of variation for the accumulated scaling presented in Figure 11 and 12 for S35 and S70 respectively.

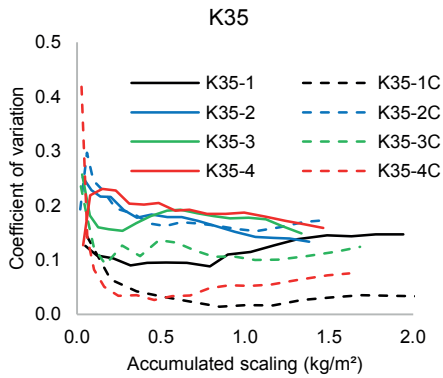

Figure 16
Coefficient of variation for the accumulated scaling presented in Figure 13 for K35.

Paper VI

De-icing salt-frost scaling in concrete containing low-calcium fly ash or slag—Influence of drying and carbonation, air content, and salt solution concentration

Martin J. Strand

Division of Building Materials, Lund University, Lund, Sweden

Corresponding author's info.

E-mail: martin.strand@byggtek.lth.se

Telephone: (+46)7 02 95 68 75

Abstract

The de-icing salt-frost scaling (DISFS) mechanism, how it is affected by preconditioning, and how it affects various materials are not completely understood. This paper presents a comprehensive study of the influence of the preconditioning process, air content, and salt solution concentration on the DISFS. Three different materials have been tested: concrete containing 100% CEM I, 35 mass% low-calcium fly ash, and 35 mass% slag. Six mixes of each binder have been prepared, one of which has no entraining agent. Fourteen different preconditioning processes and three salt concentrations have been tested. In total, 87 different groups have been tested where each group consisted of three samples (replicas). The results show that the DISFS is affected by different factors to various extents depending on the binder. Some unexpected results provide clear impetus to further the studies on the DISFS.

Keywords: Concrete, De-icing salt-frost scaling, Preconditioning, Fly ash, Slag, Supplementary cementitious materials (SCMs)

Introduction

Concrete is one of the most common building materials in the world, and de-icing salt-frost scaling (DISFS) is a known problem in northern countries with low temperatures. Cement production is energy-intensive and releases carbon dioxide from limestone; moreover, concrete is widely used. Consequently, the anthropogenic carbon dioxide emissions from cement and concrete is 5–8% of the world's total [1]. Nevertheless, such emissions can be reduced by replacing some

of the binder contents with supplementary cementitious materials, such as fly ash from coal power plants and slag from the iron industry. However, these additions change the properties of the material, such as porosity and permeability; consequently, its resistance to DISFS is also modified [2, 3]. The DISFS in concrete occurs when a low-concentration salt solution freezes in contact with a concrete surface. This usually occurs when de-icing salt is used on concrete during winter.

Previous research has shown that the DISFS is affected by various factors related either to the material being tested or the DSFS testing method [2-27]. Two previous studies [2, 3] analysed the effect of drying and carbonation, and the effect of various air contents on concrete exposed to more than 300 d of favourable hydration (the period before sawing the samples) with a water–binder ratio of 0.40. These studies show that drying and carbonation, and various air contents affect the DISFS in well-hydrated concrete in various ways depending on the fraction of supplementary cementitious material (SCM). The present article complements these two studies on 35 mass% low-calcium fly ash (LCFA) or slag by showing how concrete containing these SCMs with a shorter period of hydration (degree of hydration) influences the DISFS.

As the period of hydration increases, the amount of products from cement and pozzolanic reactions increases; consequently, this affects the properties of concrete [28]. Two of the changes in concrete properties include the increase in strength and the decrease in permeability. The mechanism causing the DISFS is presumed to be the shear stress on the surface [29] or pressures generated inside the pore system [30], or both. In any case, an increased tensile strength should decrease the DISFS. Conversely, a shorter period of favourable hydration results in a lower tensile strength and increases the DISFS. Moreover, when the period of hydration is shorter, it is inferred that the amounts of products from the cement and pozzolanic reactions are small. When the amount of hydration products is low, it is inferred that a coarser porosity increases permeability and drying rate. With the increased drying rate, the initial water content would be lower. When the initial water content is lower than the critical water content [31], the risk is low for any high pressure to occur inside the pore structures because the water is squeezed out of them (when the concrete has entrained air).

Furthermore, concrete that has been exposed to long drying and carbonation periods and internal curing would more probably differ in some important ways from concrete that has been dried and carbonated for a short period after a short internal curing period. The important differences between them are that the younger concrete has a lower degree of hydration and therefore has a more porous structure. When the structure is more porous, both drying and carbonation processes will be faster. However, because the periods of drying and carbonation

are considerably shorter, drying is more probably less extensive, and the depth of carbonation into the concrete is more probably not extreme.

This article have focuses on three factors: test surface preconditioning, air content, and salt solution concentration. These are known to affect the DISFS. However, there is a dearth of comprehensive studies that compare how the three factors (preconditioning, air content, and concentration of NaCl solution) affect the DISFS. Furthermore there is a dearth of studies that show how these three factors affect the DISFS in concrete containing LCFA or slag. Because different concrete recipes have various material properties (such as porosity, permeability, and strength), the aforementioned factors (preconditioning, air content, and salt solution concentration) affect the DISFS of each material in different ways.

The preconditioning of concrete test surfaces can be classified into three: curing, drying and carbonation, and resaturation [2-5]. The increased curing period of concrete results in a higher degree of hydration, a lower permeability, and an increased strength. Drying results in a lower moisture content before the DISFS test begins. Furthermore, it lowers the risk of the moisture content approaching the critical degree of saturation [31]; previous results show that an increased moisture content seemingly increases the DISFS [32]. If drying occurs in high temperatures or extremely low relative humidity (RH), the microstructure of concrete can be damaged [33-36]; consequently, any damage to the microstructure will increase the DISFS. In the present article, drying and carbonation have been set to a condition where the temperature is 20 °C and humidity is 35% RH or higher. Accordingly, the concrete surfaces should not be damaged by drying. Carbonation is a chemical reaction of the hardened paste with carbon dioxide (CO_2) in the atmosphere. It changes the microstructure of the material as well as its material properties. These properties in turn change the resistance to the DISFS. According to [2, 3], the porosity decreases as the structures of small pores (radius less than 50 nm) and larger capillary pores (>50 nm) change to various extents. However, the DISFS results show that these properties of porosity are not sufficient predictors of the DISFS. Nevertheless, the results from [2, 3] clearly show that the preconditioning of the test surface has a significant impact on the DISFS.

An increased air content, together with an increased amount of air voids, decreases the DISFS [5, 8, 29, 37-46]. With the use of air-entraining agents, small and stable air voids are created, the air content increases, and the spacing between air voids shortens. However, according to results that are presented in [2, 3], the effect of an increased amount of air voids depends on the surrounding microstructure. Furthermore, the concentration of the de-icing solution influences salt-frost scaling [8, 10-18].

There seems to exist a pessimum salt concentration for sodium chloride of approximately 3 mass% that produces the largest DISFS mass [8, 10-18]. The salt

solution concentration affects two important factors: the amount of ice that can form and the absorption of solution [10, 15, 29, 47].

This study complements previous studies [2, 3] by presenting the effect drying and carbonation, and entrained air content have on young concrete exposed to a much shorter period of hydration (8 to 63 d compared to 308 d). Furthermore, results that show the effect of NaCl concentration on the DISFS in three concrete recipes are presented in this paper. The NaCl concentration affects the absorption and fraction of ice formed at a specific freezing temperature. Well hydrated concrete based on different recipes have different structure and porosity [2, 3]. Therefore, it is likely that this is the case also in younger concrete, and that the effect of NaCl concentration on young concretes will be different for different recipes. This study fills the gap in the lack of knowledge on the effect NaCl concentration has on the DISFS in concrete containing LCFA or slag.

This article presents a comprehensive DISFS study where the results aim to answer the following questions for concrete containing 35 mass% LCFA or 35 mass% slag: How do short periods of hydration, and drying and carbonation affect the DISFS? How does drying, with and without carbon dioxide, affect the DISFS? How does the air content affect the DISFS in concrete exposed to short periods of hydration (with or without exposure to drying and carbonation)? How does the NaCl concentration affect the DISFS in concrete with LCFA or slag?

Method and Materials

The salt-frost scaling method used in this study is presented in a previous paper [6]. The materials utilised—CEM I, LCFA, slag and aggregates—are the same as those used in [2, 3]. The current study presents results from concrete with aggregate sizes up to 16 mm and micro-concrete with aggregates up to 8 mm; accordingly, these could provide some indications on the effect of aggregates. Because concrete and micro-concrete differ in binder contents, their paste volumes vary; consequently, the analysis of aggregates becomes more difficult. To compare air contents among the recipes considering various paste volumes, the measured air content is recalculated as air content in paste (ACP) using Eq. 6b, which is derived from Eqs. 1–5. The measured air contents are 1.6, 3.2, 4.8, and 6.4 vol%, which are equivalent to 5, 10, 15, and 20 ACP, respectively, in concrete with a 430-kg/m³ cement content, water–binder ratio of 0.40, and aggregate–cement ratio of 3.98; material densities are summarised in Table 1.

$$\frac{m_{\text{binder}}}{\rho_{\text{binder}}} + \frac{m_{\text{SCM}}}{\rho_{\text{SCM}}} = V_{\text{paste}} \qquad \textit{Eq. 1}$$

m_{binder} = mass of CEM I, kg

ρ_{binder} = density of CEM I as listed in Table 1, kg/m³

m_{SCM} = mass of SCM (LCFA or slag), kg

ρ_{SCM} = density of SCM (LCFA or slag) as listed in Table 1, kg/m³

V_{paste} = volume of paste, m³

$$\frac{m_{\text{aggregate}}}{\rho_{\text{aggregate}}} = V_{\text{aggregate}} \qquad \text{Eq. 2}$$

$m_{\text{aggregate}}$ = mass of aggregates, kg

$\rho_{\text{aggregate}}$ = density of aggregates as listed in Table 1, kg/m³

$V_{\text{aggregate}}$ = volume of paste, m³

$$V_{\text{total batch}} = (V_{\text{aggregate}} + V_{\text{paste}}) \cdot (1 + V_{\text{measured air content}}) \qquad \text{Eq. 3}$$

$V_{\text{total batch}}$ = volume of total batch, m³

$$V_{\text{measured air content}} = \frac{V_{\text{air content batch}}}{V_{\text{total batch}}} \qquad \text{Eq. 4}$$

$V_{\text{measured air content}}$=measured air contents in 8 and 1 dm³ of concrete and micro-concrete batches, respectively, %

$$FP = \frac{V_{\text{paste}} \cdot (1 + V_{\text{measured air content}})}{V_{\text{total batch}}} \qquad \text{Eq. 5}$$

$$ACP = \frac{V_{\text{measured air content}}}{FP} \qquad \text{Eq. 6a}$$

$$ACP = \left(\frac{V_{\text{air content batch}}}{V_{\text{total batch}}}\right) / \left(\frac{V_{\text{paste}} \cdot (1 + V_{\text{measured air content}})}{V_{\text{total batch}}}\right) \qquad \text{Eq. 6b}$$

ACP = Air content in paste, %

Table 1
Specifications of materials used—Densities.

Material	Density [kg/m³]
Cement (CEM I 42,5 N - SR 3 LA)	3200
Ground-granulated blast-furnace slag	2920
Low-calcium fly ash	2300
Tap water	1000
Aggregates	2650

Recipes

The recipes, along with the measured slump, air content, and density in fresh concrete, are summarised in Tables 2, 3, and 4. All recipes have a water binder ratio of 0.40 and a binder content of 430 kg/m³; the replacement level of LCFA or slag is 35%. In the general discussion in this paper, the binder combinations containing 35% LCFA and 35% slag are denoted F35 and S35, respectively. Table 2 lists batches with 100% CEM I, Table 3 summarises batches containing LCFA, and Table 4 tabulates batches containing slag. A polycarboxylate superplasticiser is used in batches containing 100% CEM I and 35% slag. A superplasticiser based on sulphonate melamine–formaldehyde condensate is used in batches containing 35% LCFA. The air-entraining agent in all three binders is based on a synthetic surfactant. Batches 1–4 and 6 contain air-entraining agents; batch 5 only contains a superplasticiser. The added mass of air-entraining agent in relation to the binder mass is 1.7‰ in the batches containing 100% CEM I and S35. Batches 1–4 and 6 with F35 contain 3.1‰ air-entraining agent relative to the binder content. The density measurements summarised in Tables 2–4 are made on the same concrete used in the air-content measurements. Air contents ($V_{\text{measured air content}}$) are measured in 8 and 1 dm³ of the fresh concrete and micro-concrete, respectively.

Table 2
Specifications of the batches containing 100% CEM I.

Batch	CEM I kg/m³	SCM kg/m³	Water kg/m³	Aggregate, kg/m³ 0-8	8-16	Slump[1] mm	AC[2] vol%	ACP vol%	Density kg/m³
CEM I-1	430	0	172	932	792	210	4.8	14.9	2351
CEM I-2	430	0	172	932	792	60	4.9	15.3	2347
CEM I-3	430	0	172	932	792	200	7.1	22.1	2278
CEM I-4	682	0	273	1363	0	160	6.4	13.2	2143
CEM I-5	682	0	273	1363	0	115	3.0	6.2	2272
CEM I-6	682	0	273	1363	0	115	9.6	19.8	2061

[1] The slumps in batches 1, 2, and 3 were measured with a regular cone for concrete, and those in batches 4, 5, and 6 were measured with a Hägermann cone used for mortar.

Table 3
Specifications of batches containing 65% CEM I and 35% LCFA.

Batch	CEM I kg/m³	LCFA kg/m³	Water kg/m³	Aggregate, kg/m³ 0–8	8–16	Slump[1] mm	AC[2] vol%	ACP vol%	Density kg/m³
F35-1	280	150	172	932	792	240	5.5	16.5	2266
F35-2	280	150	172	932	792	30	5.7	17.1	2283
F35-3	280	150	172	932	792	155	4.7	14.1	2324
F35-4	443	239	273	1363	0	125	7.8	16.5	1946
F35-5	443	239	273	1363	0	150	0.5	1.0	2270
F35-6	443	239	273	1363	0	130	8.1	16.2	2034

[1] The slumps in batches 1, 2, and 3 were measured with a regular cone for concrete, and those in batches 4, 5, and 6 were measured with a Hägermann cone used for mortar.

Table 4
Specifications of batches containing 65% CEM I and 35% slag.

Batch	CEM I kg/m³	Slag kg/m³	Water kg/m³	Aggregate, kg/m³ 0-8	8-16	Slump[1] mm	AC[2] vol%	ACP vol%	Density kg/m³
S35-1	280	150	172	932	792	230	5.6	17.3	2280
S35-2	280	150	172	932	792	60	4.9	15.1	2307
S35-3	280	150	172	932	792	195	7.2	22.2	2249
S35-4	443	239	273	1363	0	140	5.7	11.8	2171
S35-5	443	239	273	1363	0	150	4.5	9.2	2207
S35-6	443	239	273	1363	0	135	8.0	16.4	2096

1) The slumps in batches 1, 2, and 3 were measured with a regular cone for concrete, and those in batches 4, 5, and 6 were measured with a Hägermann cone used for mortar.
2) AC is the measured air content in 8 dm³ of the concrete batch and 1 dm³ of the micro-concrete batch.

Preconditioning processes

Table 5 summarises the preconditioning processes for the batches listed in Tables 2, 3, and 4. In this work, only sawn surfaces have been tested. This has contributed to the high consistency in the preconditioning of the different tested samples. When sawn surfaces are tested, the preconditioning process can be classified into three periods: internal curing (IC), drying and carbonation (DC), and resaturation (RS). In this article, the IC is defined as the hydration of the test surface before the sample is sawn; the DC period is the time when the test surface is exposed to 20.0±0.2 °C, 60±5% RH and 400±50 ppmv (0.040±0.005 vol%) CO_2. A special case of the DC period is used when the sample is only dried and not carbonated (called dried and never-carbonated (DNC) samples). The DNC is accomplished by using magnesium chloride tetrahydrate ($Cl_2Mg{\cdot}4H_2O$) and CO_2 absorber inside a sealed box. Salt is used to maintain 35% RH (this is a low and an unfavourable humidity for the carbonation process [48]). The CO_2 absorber maintains the CO2 concentration close to 0 ppmv CO_2 (measured with a Testo 160 IAQ). The RS is defined as the period when the sample is immersed in water, enabling the test surface to absorb water during a specified period. The RS period is one day for all preconditioning processes except for preconditioning process p5 and p7, which have been used with batch 2 to examine the effect of an increased RS period on the DISFS.

Table 5.
Preconditioning processes. Preconditioning of each batch and number of days the samples are exposed to different stages.

Process	Batches[1)]	Internal curing (IC)	Drying & carbonation (DC)	Dried & never carbonated (DNC)	Resaturation (RS)
p1	1	30	0	0	1
p2	1	30	87	0	1
p3	1	23	7	0	1
p4	1	8	22	0	1
p5	2	28	31	0	28
p6	2	55	31	0	1
p7	2	55	32	0	0
p8	3, 4	29	0	0	1
p9	3, 4	8	21	0	1
p10	3	29	59	0	1
p11	5, 6	28	0	0	1
p12	5, 6	8	20	0	1
p13	5, 6	63	28	0	1
p14	5, 6	63	0	28	1

[1)] Batch 1 corresponds to CEM I-1, F35-1, and S35-1 as listed in Tables 2, 3, and 4.

To study the effect of the preconditioning process, results from each batch are separately compared; this comparison is performed because the air content affects the DISFS. If it is assumed that the air content only varies to a small degree in each batch, then the comparison among the samples from the same batch minimises the influence of varied air content on the DISFS. For the comparison, six groups are formed; one batch is one group.

When analysing the effect of air content, samples from different batches (with different air contents) are exposed to the same preconditioning process; thereafter, results are compared. These can be classified into four groups. One group consists of samples that have a medium period (29±1 d) of IC and NDNC; these are p1, p8, and p11 for samples from batches 1, 3, 4, 5, and 6 as listed in Table 5. Another group is composed of samples with a short IC period (8 d) and a medium DC period. These are p4, p9, and p12 for samples from batches 1, 3, 4, 5, and 6 as listed in Table 5. The third group contains samples with a medium IC period and a long DC period (55 d or more). These are p2 and p10 for samples from batches 1 and 3 as listed in Table 5. The fourth group has samples with a long IC period and a medium DC period. These are p6 and p13 for samples from batches 2, 5, and 6 as listed in Table 5.

The influence of salt concentration is studied by comparing samples with different salt concentrations from the same batch exposed to the same preconditioning process. The three salt concentrations used in the tests are 1, 3, and 9 mass% NaCl with deionised water. This analysis includes four groups. One group of concrete samples is exposed to a medium IC period and NDNC with a high ACP (batch 3). Another group of concrete samples is exposed to a medium IC period and long DC period with a high ACP (batch 3). A group of micro-concrete samples is exposed to a long IC period and medium DC period with a low ACP (batch 5). Another group of micro-concrete samples is exposed to a long IC period and medium DC period with a high ACP (batch 6).

Salt-frost scaling test method

The salt-frost scaling test method is presented in [6]. The freeze–thaw cycle that is used is designed to result in a large mass of salt-frost scaling and thereby enable the testing of concrete with a water–binder ratio of 0.40, such as the concrete tested in the present study. The test method uses freezers with air as the thermal medium, and the samples are submerged a few millimetres in the NaCl solution. The method has been proven capable of enabling relative comparisons among the DISFS from various binders. Moreover, it shows how factors related to the method (such as the time and temperatures of the freeze–thaw cycle) affect the DISFS [2, 3, 6].

Results and discussion

The results are presented together with the groups described in the section 'Preconditioning processes' in this article in order to emphasise the effect of drying and carbonation, air content, and salt solution concentration; some results are presented in multiple figures. All figures show the average accumulated scaling of samples of either three or six. To understand the variation in results, the coefficient of variation in relation to the accumulated scaling is presented for each figure in the supplementary materials. In the various tests, two preconditioning processes have been applied to all batches (except batch 2) in order to enable comparisons among them. These are IC8 DC21±1 RS1 and IC29±1 NDNC RS1.

Drying and carbonation

Figures 1–5 show the testing results of the effect of drying and carbonation on the salt-frost scaling in concrete with 100% CEM I, 35% LCFA, and 35% slag. The internal curing varies between 8, 21, 30 and 63 d. To analyse the effect of drying and carbonation, and to minimise the influence of air content, the results from each batch are separately compared. The figure title indicates the ACP and binder, whereas the legend indicates the preconditioning processes. Consider the following two examples: IC8 DC22 RS1 means 8 d of internal curing, 22 d of drying and carbonation in 60% RH and 400 ppmv CO_2, and 1 d of RS; IC63 D28NC RS1 means 63 d of internal curing, 28 d of drying in 35% RH and 0 ppmv CO_2, and 1 d of RS.

Concrete with air-entraining agent

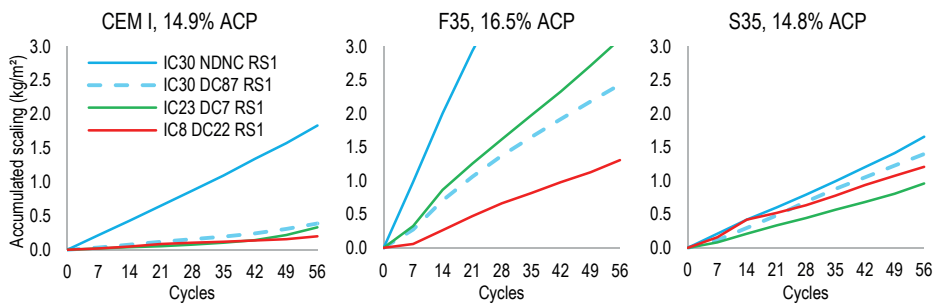

Figure 1
Mean accumulated scaling in three concrete samples from batches CEM I-1, F35-1, and S35-1 with air-entraining agents and exposed to different preconditioning processes.

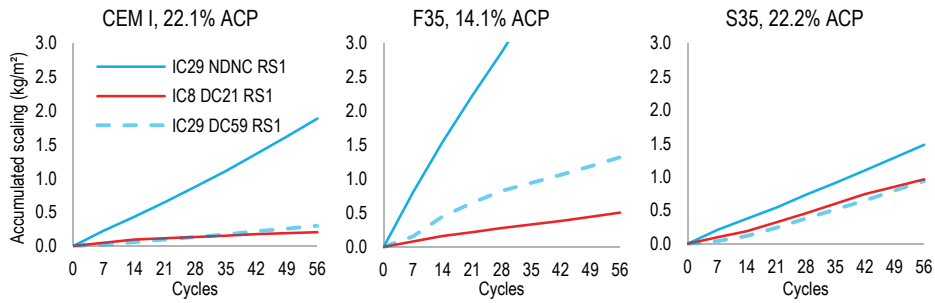

Figure 2
Mean accumulated scaling in three concrete samples from batches CEM I–3, F35-3, and S35-3 with air-entraining agents and exposed to different preconditioning processes.

Figures 1 and 2 present results that show the effect of drying and carbonation on concrete samples containing air-entraining agent and with a short or medium IC period. By comparing the blue solid and dashed lines, the effect of drying and carbonation on concrete with 29 or 30 d of internal curing can be observed. The results show that drying and carbonation reduces the DISFS in concrete with 100% CEM I and F35; the DISFS in S35 concrete either remains unchanged or slightly decreases. By comparing the dashed and red lines, the effect of drying and carbonation when the concrete has a long IC period compared to concrete with a short IC period is observed. The results show that an increased IC period increases the DISFS in F35. The DISFS remains unchanged in concrete with CEM I and S35 when the IC is increased. The comparison between the green line and the other lines in Fig. 1 shows some indication of the DISFS when the samples are exposed to a preconditioning process similar to that in the standard process in [49] of the current DISFS method. This provides some indication of how the standard preconditioning method compare with other preconditioning processes. However, note that the salt-frost test method used in article [6] has a different sample setup and a different freeze–thaw cycle compared with the standard test method [49]; this affects the DISFS mass. Therefore, the specific DISFS (in kg/m²) presented here cannot be compared directly with the results of samples tested using the standard method. The results show that a preconditioning process similar to that used in the standard method [49] yields a low DISFS in CEM I, similar to the other preconditioning processes that expose the samples to the DC. In F35, the preconditioning similar to that in the standard process results in a higher DISFS compared with other preconditioning processes that similarly expose the samples to the DC. For S35, the preconditioning process similar to the process in [49] results in a DISFS similar to that of other preconditioning processes that expose the samples to the DC. These results indicate that drying and carbonation have the most significant impact on concrete with CEM I and F35. When CEM I is exposed to the DC, the DISFS is extremely low in all cases. When F35 is exposed to the

DC, the DISFS is high; however, it is lower than the DISFS in the NDNC samples. The S35 concrete has a high accumulated 56-cycle scaling of approximately 1 kg/m²; it has a slightly lower DISFS when the samples are exposed to the DC. Regardless of the preconditioning process, the DISFS values of all samples are similar overall.

Micro-concrete with air-entraining agent

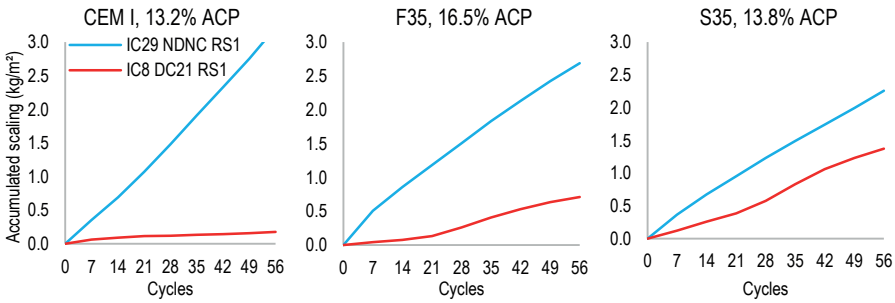

Figure 3
Mean accumulated scaling in three micro-concrete samples from batches CEM I-4, F35-4, and S35-4 with air-entraining agents and exposed to different preconditioning processes.

Figure 3 presents results that show the effect of drying and carbonation on micro-concrete samples containing air-entraining agents and with a short or medium IC period. Generally, the results are the same as those of concrete samples presented in Figs. 1 and 2; the ACPs slightly differ between the figures. Apart from that, they differ in terms of large aggregates that cover a considerable part of the sawed test surface. Results from the NDNC samples with 100% CEM I and S35 show that the DISFS has slightly increased compared to that in the concrete shown in Figs. 1 and 2. On the other hand, F35 NDNC micro-concrete samples have decreased DISFS compared with the NDNC concrete samples in Figs 1 and 2. In comparing the red lines of each binder in Fig. 3 with the red lines of each binder in Figs. 1 and 2, it is found that the results are similar. This suggests that micro-concrete and concrete samples have approximately the same DISFS when preconditioned with a short IC period followed by a medium DC period.

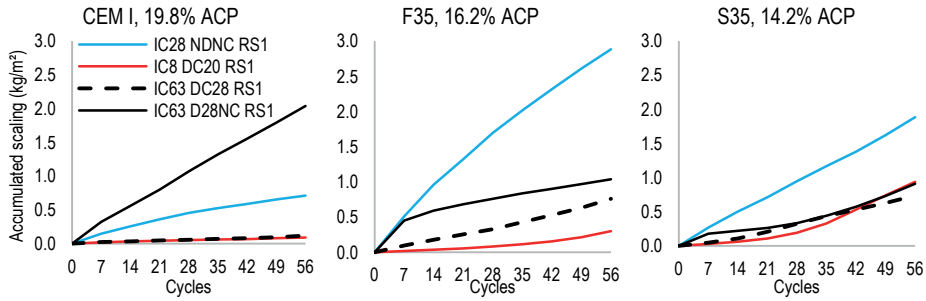

Figure 4
Mean accumulated scaling in three micro-concrete samples from batches CEM I-6, F35-6, and S35-6 with air-entraining agents and exposed to different preconditioning processes.

Figure 4 presents results that show the effect of DC and DNC on micro-concrete samples with a short, medium, and long IC periods containing air-entraining agents. In comparing the red and dashed lines, the effect of an increased IC period is observed in samples exposed to drying and carbonation. The results show that both these processes result in a low DISFS in micro-concrete with 100% CEM I. However, the increased IC period in F35 micro-concrete seems to increase the DISFS when the samples are exposed to the DC. The reason could be that F35 with a shorter IC period dries faster because of a lower degree of hydration (IC8 compared with IC63) and higher porosity. When porosity is higher, the drying is probably faster. This means that at the start of the DISFS test, the samples represented by the red lines will probably have a faster drying rate and lower initial moisture content when compared with samples represented by the dashed lines. Moreover, a longer period of hydration could increase the constraint in the pore system and thereby increase the scaling when the IC period with a favourable hydration is increased.

In comparing the dashed and black lines, the results show the effect of drying and carbonation when the micro-concrete samples have a long IC period. The carbonation significantly decreases the DISFS in micro-concrete with 100% CEM I. However, in comparing the blue and black lines, the results show that drying (without carbonation) increases the DISFS in micro-concrete with 100% CEM I, whereas S35 micro-concrete appears unaffected by the carbonation. The carbonation in F35 micro-concrete slightly decreases the DISFS. In comparing the blue and black lines of F35 and S35, the drying (without carbonation) seems to decrease the DISFS. This suggests that the carbonation of CEM I generally reduces the DISFS, whereas drying increases the DISFS in micro-concrete with 100% CEM I. However, drying results in a lower DISFS in F35 and S35 micro-concretes. The reason why drying decreases the DISFS in micro-concrete with F35 or S35 and increases it in micro-concrete with 100% CEM I is unknown. Because

drying without carbonation only contributes to lowering the initial moisture content of the samples at the start of the DISFS test, the relationship between the blue and black lines is expected to follow the same pattern in all binders.

Micro-concrete without air-entraining agent

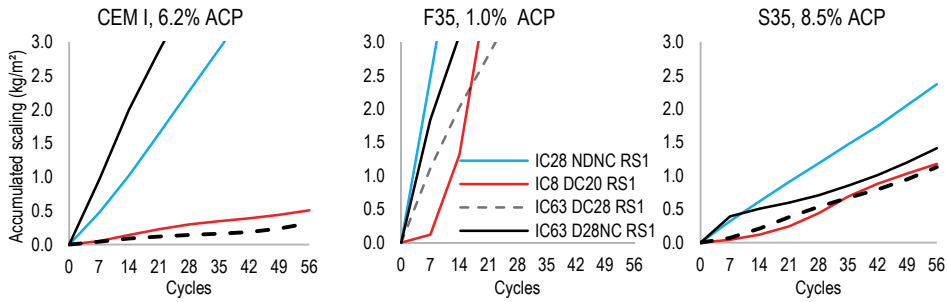

Figure 5
Mean accumulated scaling in three micro-concrete samples from batches CEM I-5, F35-5, and S35-5 without air-entraining agents and exposed to different preconditioning processes.

Figure 5 presents results that show the effect of DC and DNC on micro-concrete samples with a short, medium, or long IC period and without air-entraining agents (low ACP). The results of F35 micro-concrete exhibit considerably high DISFS in all preconditioning processes. The high DISFS in all samples with LCFA is probably because the low air content outweighs other effects. Therefore, no further comments regarding the results of F35 are required. In comparing the red and dashed lines, the effect of an increased IC period is observed in samples exposed to drying and carbonation. The results show that an increased IC period results in a slightly lower or similar DISFS in micro-concrete samples with a low ACP and 100% CEM I when these are exposed to the DC. When the red and dashed lines are compared, it is observed that the samples of S35 have approximately the same DISFS. This suggests that an increased IC does not decrease the DISFS when the samples are exposed to the DC. In comparing the dashed and blue lines, the results show the effect of drying when the micro-concrete samples have a long IC period and low ACP. Furthermore, it is observed that drying increases the DISFS in micro-concrete with 100% CEM I and low ACP (the same result trend as that presented in Fig. 4); conversely, it decreases the DISFS in S35 micro-concrete (the same result trend as that presented in Fig. 4).

In comparing the blue and red lines in Figs. 1–5, it is evident that IC8 and DC21±1 generally result in practically no DISFS in CEM I. Furthermore, this preconditioning process seems to be favourable for F35 samples when the results are compared with those of other processes; IC8 DC21±1 process also appears to

contribute to the DISFS decrease in S35. However, the effect of drying and carbonation in S35 is minimal.

Air content

Figures 6–9 show the testing results of the effect of air content on the salt-frost scaling in concrete with 100% CEM I, F35, or S35 exposed to various preconditioning processes. To analyse this effect, results from different batches exposed to similar preconditioning processes are compared. The title in each figure indicates the binder and preconditioning process that the samples are exposed to. The batches in Figs. 6–9 are classified into three groups based on the ACP: <10% (red lines), 10–15% (blue), >15% (green); the dashed and solid lines represent the micro-concrete (MC) and concrete (C) materials, respectively. The ACP is found in the legend under each diagram.

Medium internal curing, never-dried or carbonated

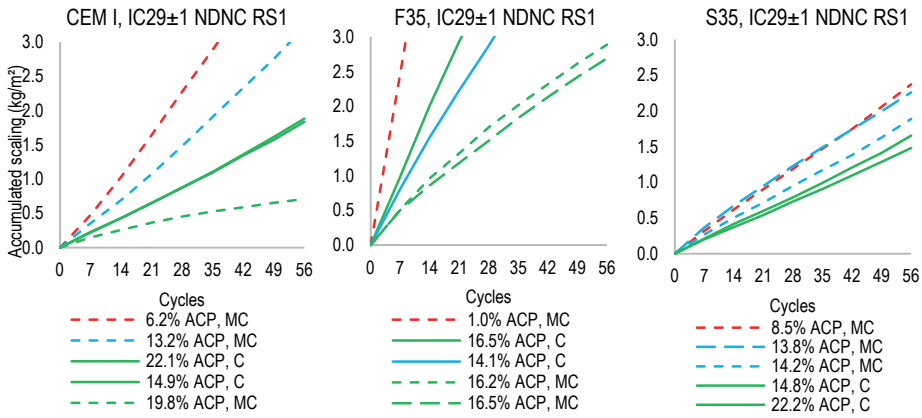

Figure 6
Mean accumulated scaling in three samples from batches 1 and 3–6 for each binder and exposed to a medium IC period (without drying and carbonation periods).

Figure 6 shows the effect of various ACPs in NDNC samples with a medium IC period. The results suggest that an increased ACP decreases the DISFS in concrete or micro-concrete with 100% CEM I. The results of F35 exhibit a similar pattern as the aforementioned (with the exception of 16.5% ACP, C); however, the DISFS is generally high in F35 recipes. When compared with the other two binders, an increased ACP has a minimal effect on S35.

Short internal curing followed by drying and carbonation

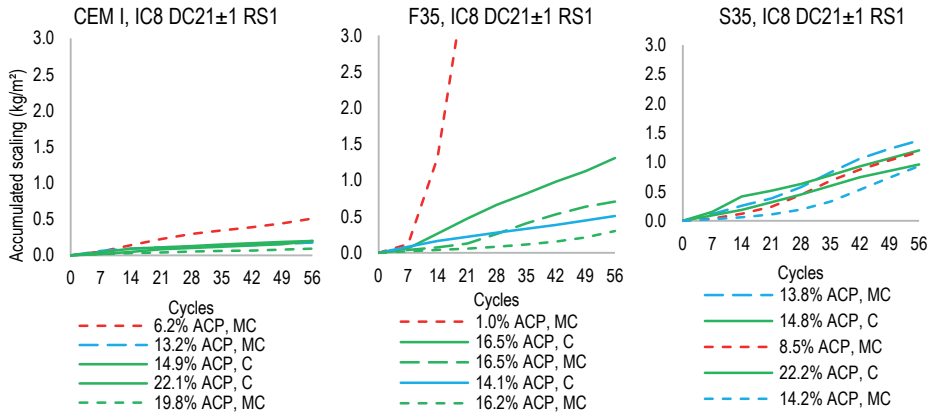

Figure 7
Mean accumulated scaling in three samples from batches 1 and 3–6 for each binder and exposed to a short IC period followed by DC.

Figure 7 shows the effect of various ACPs in samples exposed to a short IC period followed by a medium DC period. The results suggest that concrete and micro-concrete with 100% CEM I and exposed to this preconditioning process has a considerably low DISFS. The micro-concrete with a low ACP slightly increases the DISFS in micro-concrete with 100% CEM I. The results show the same trend as that presented in Fig. 6 (although not as clear because the DISFS is extremely low). The results of F35 samples show an evident difference in the DISFS between samples with extremely low and high ACPs. The results of S35 samples exposed to this preconditioning process do not indicate any distinct effect of an increased ACP. In analysing Figs. 6 and 7, it is observed that all binders seem to be affected by the preconditioning process to a considerable extent by the ACP. The samples of S35 generally appear to be insignificantly affected by an increased ACP.

Medium internal curing followed by drying and carbonation

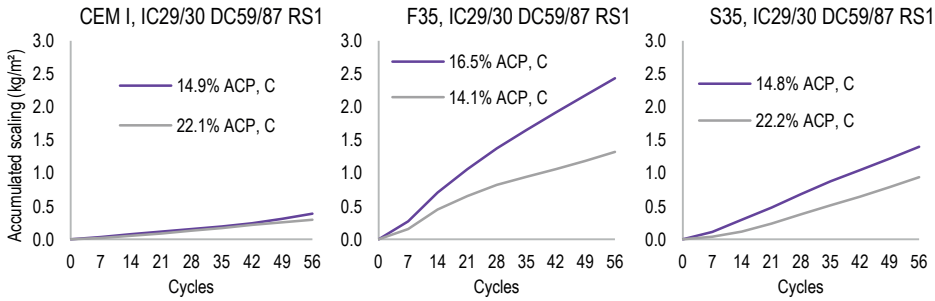

Figure 8
Mean accumulated scaling in three samples from batches 1 and 3 for each binder and exposed to a medium IC period followed by DC. Purple lines represent samples exposed to IC30 DC87 RS1, and orange lines are samples exposed to IC29 DC59 RS1.

Figure 8 shows the effect of air content when the samples are exposed to a medium IC period followed by a long DC period. The purple lines represent samples exposed to 87 d of DC, and the orange lines represent samples exposed to 59 d of DC. The DISFS is low in all samples that contain 100% CEM I; the effect of an increased ACP appears to be insignificant. The DISFS in F35 samples exposed to a longer DC increased although the ACP is slightly higher. It is possible that the longer DC exposure is unfavourable when the sample is exposed to a medium IC period. The DISFS in S35 samples, with a longer DC exposure, increased; however, this increase could either be because of the longer DC or the lower ACP.

Long internal curing followed by drying and carbonation

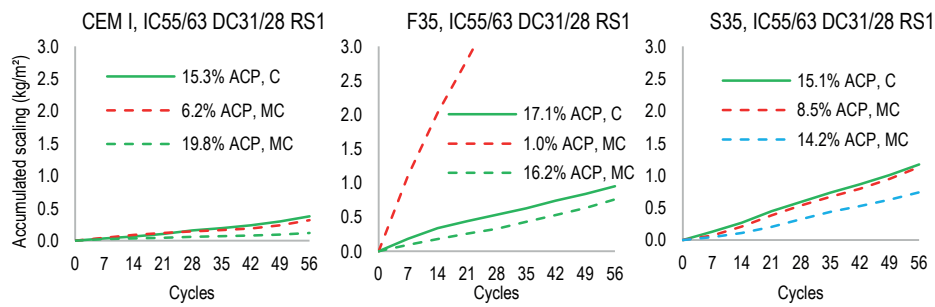

Figure 9
Mean accumulated scaling in three samples from batches 2, 5, and 6 for each binder and exposed to a long IC period followed by DC.

Figure 9 shows the effect of air content when the samples are exposed to a long IC period followed by a medium DC period. The results show that the DISFS is extremely low in concrete with 100% CEM I regardless of the ACP. In the samples of F35, it is observed that an increased ACP decreases the DISFS. The accumulated scaling after 56 cycles is approximately 1 kg/m² when the ACP is high (over 15%). In the samples of S35, it appears that an increased ACP does not affect the DISFS (the same trends as those shown in Figs. 6 and 7).

Figures 6–9 show that the effect of air content varies according to the preconditioning process and binder. An increased air content reduces the salt-frost scaling in all recipes when the samples have never been dried or carbonated (Fig. 6). The effect in recipes that contain 100% CEM I and F35 is larger when compared with that containing S35. For samples exposed to a period of DC, the air content has a minimal effect on concrete that contains 100% CEM I. It is assumed that the reduction in the DISFS is because the carbonation in 100% CEM I outweighs the effect of air content. The recipes with S35 are seemingly unaffected by the increased air content when the samples are dried and carbonated. The air content appears to have the largest influence on recipes with F35 regardless of drying and carbonation. The combination of preconditioning IC8 DC21 with a high air content results in the lowest DISFS in F35 samples. The reason for this is unknown because the results seem to contradict those reported in [2]. This should be examined further by measuring the pore size distribution. The largest difference between well-hydrated F35 concrete exposed to IC308 DC735 in [2], and less hydrated F35 concrete exposed to IC8 DC21, is most probably the structure of pores smaller than a few microns, i.e. capillary pores and mesopores . The explanation for this is that, when the concrete is hydrated for a longer time, the smaller pores are filled with hydrates to a higher degree.

Salt solution concentration

Figures 10 and 11 show the testing results of the effect of different salt solution concentrations on the DISFS in concrete that has been hydrated for a medium period. Figure 10 shows the NDNC samples, whereas those shown in Fig. 11 have been exposed to the DC for 59 d. Figures 12 and 13 show the testing results of the effect of different salt solution concentrations on the DISFS in micro-concrete that has been hydrated for a long period and thereafter exposed to a medium DC period. The samples in Fig. 12 have low ACPs, whereas those in Fig. 13 have high ACPs. Each figure title indicates the binder, preconditioning, and ACP. The red, black, and blue lines show the results of 1, 3, and 9 mass% NaCl solutions, respectively.

Never-dried or never-carbonated concrete

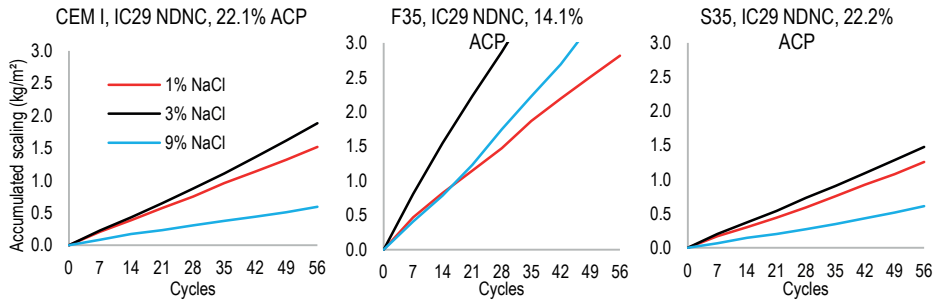

Figure 10
Mean accumulated scaling in three samples—Concrete samples (batches CEM I-3, F35-3, and S35-3) with a high air content and exposed to a medium IC period (NDNC).

According to Fig. 1–5, samples that have not been exposed to the DC are expected to have a high DISFS. Results show that the DISFS in CEM I and S35 samples exposed to low salt concentrations (1 or 3%) are higher compared with the DISFS in the same type of samples exposed to a high salt concentration (9%). These results agree with the previous research, which found a low pessimum concentration of approximately 3% [8, 10-18]. However, the scaling in samples exposed to a 9% salt concentration is expected to be either negligible or non-existent [17, 18, 50] because it is presumed that only approximately 61% of the solution is frozen at −21 °C [51], and the samples are not saturated. On the contrary, these results show that when the materials have not been dried or carbonated, a 9% NaCl solution results in the DISFS in all binders. The DISFS in F35 samples is high when the samples have not been exposed to the DC; however, it is remarkable that the 9% solution results in a high DISFS in this case. The presence of the DISFS when the salt solution concentration is high is presumed to be because the high NaCl concentration enables the samples to absorb more of the salt solution. Consequently, the degree of saturation is higher when the water freezes.

Dried and carbonated concrete with high air content

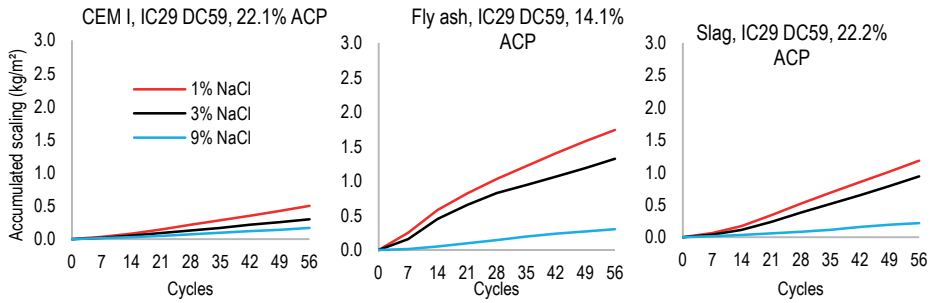

Figure 11
Mean accumulated scaling in three samples—Concrete samples (batches CEM I-3, F35-3, and S35-3) with a high air content and exposed to a medium IC period followed by DC.

By comparing Fig. 11 with Fig. 10, it is observed that when the samples have been exposed to a DC period, the DISFS significantly decreases in CEM I and F35, whereas the DISFS decrease in S35 is slight. These results agree with those presented above regarding the effect of drying and carbonation. Moreover, the results exhibit a clear trend for S35 and F35: low NaCl concentrations result in a higher DISFS in samples exposed to the DC. Because the carbonation results in a low DISFS in samples with 100% CEM I, the influence of different NaCl concentrations is not as clear; however, the low concentrations appear to result in a higher DISFS compared to the effect of the 9% concentration.

Dried and carbonated micro-concrete with low air content

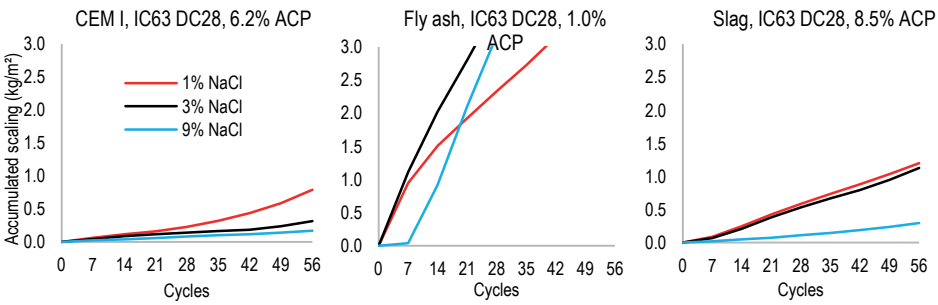

Figure 12
Mean accumulated scaling in three samples—Micro-concrete samples (batches CEM I-5, F35-5, and S35-5) with a low air content and exposed to a long IC period followed by DC.

The results presented in Fig. 12 show the same trends for samples with 100% CEM I and S35 as those shown in Fig. 11; the low salt concentrations result in a greater amount of the DISFS. The DISFS is extremely high in all F35 samples. It

is supposed that this is because low air content outweighs any effect of the salt concentration.

Dried and carbonated micro-concrete with high air content

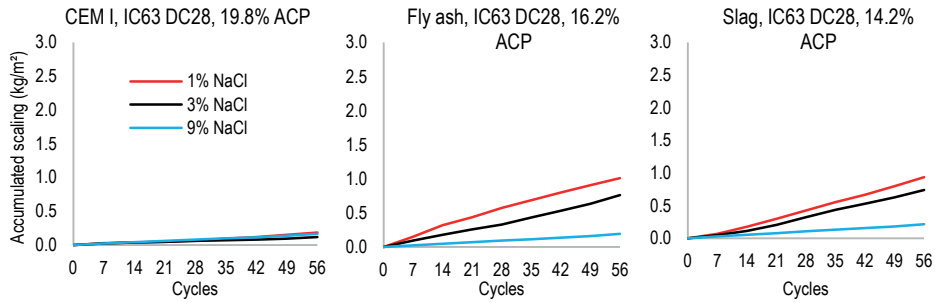

Figure 13
Mean accumulated scaling in three samples—Micro-concrete samples (batches CEM I-6, F35-6, and S35-6) with a high air content and exposed to a long IC period followed by DC.

Figure 13 shows that when samples with high ACPs have been exposed to the DC period, the low NaCl concentrations result in greater amounts of the DISFS in both F35 and S35. By comparing Figs. 12 and 13, the influence of an increased air content on the binder in F35 can be seen. The increased air content in dried and carbonated F35 samples decreases the DISFS. These results agree with those presented above (Figs. 7 and 9). However, the influence of the NaCl concentration cannot be observed in samples with 100% CEM I and high ACP that have been exposed to the DC because the DISFS is extremely low.

According to Figs. 10–13, the DISFS in samples with binders are affected to various extents by different NaCl solution concentrations. According to previous studies [8, 10-18], there exists a pessimum concentration. This suggests that the low salt concentration (1 or 3%) is expected to result in the highest DISFS; the results generally agree with those of previous findings. However, there are three exceptions. First, the pessimum is not clear in NDNC F35 concrete (Fig. 10); this is because the DISFS is high when the samples have not been dried or carbonated. Second, in F35 micro-concrete (Fig. 12), the low air content results in a high DISFS that outweighs any effect of the NaCl concentration. Third, in the samples of CEM I shown in Fig. 13, the carbonation and high ACP result in a low DISFS in all samples exposed to NaCl concentrations.

Additional observations

In addition to the influence of DC, ACP, and NaCl concentrations, two other factors have been tested. Figure 14 shows the results of changing the number of

cycles between each scaling measurement (including changing the salt solution concentration) from 7 to 14. This is tested to determine whether changing the solution more frequently could increase the leaching of the test surface and therefore result in a higher DISFS. Figure 15 shows the effect of an increased RS period before the DISFS test begins.

Measurement frequency comparison

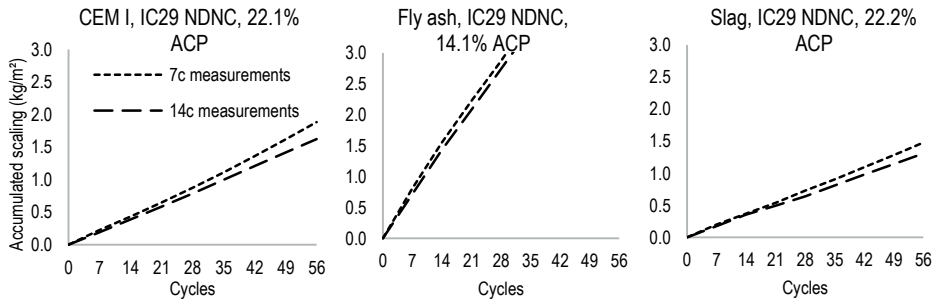

Figure 14
Mean accumulated scaling in three samples—Concrete samples (batches of CEM I-3, F35-3, and S35-3) with a high air content and exposed to NDNC.

Effect from an increased period of resaturation

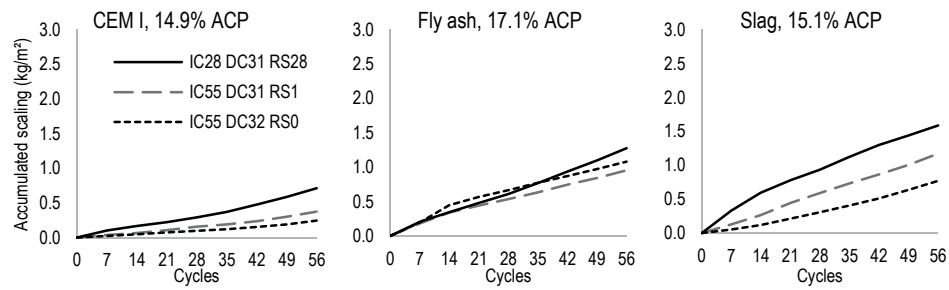

Figure 15
Mean accumulated scaling in three samples—Concrete batches (batches of CEM I-2, F35-2, and S35-2) samples with high air contents exposed to various periods of RS. Results are the same as those found in [32]; however, only accumulated scaling after 56 cycles is presented.

Figure 14 shows that conducting measurements every seventh cycle, instead of every fourteenth, does not influence the DISFS; this suggests that changing the solution more frequently does not affect the DISFS. This test is performed to study the difference between the frequency variation in the above and that in the slab method according to [49].

The results presented in Fig. 15 indicate that the initial water content in samples subjected to a longer RS period contributes to a slight increase in the DISFS; the

effect is more evident in CEM I and S35 samples. This could be because F35 samples with long RS have been dried and carbonated at a young age; previous results (Figs. 2 and 4) show that the DISFS increases when the IC increases. Therefore, for F35 samples shown in Fig. 15, the DC with RS28 is probably more favourable compared to those exposed to the DC with RS0 and RS1.

Answers to research questions

The answers to the research questions in this study are based on results presented in this article, i.e., answers pertaining to concrete or micro-concrete containing 100% CEM I, or 65+35% CEM I+low-calcium fly ash, or 65+35% CEM I+slag.

How do short period of hydration, and drying and carbonation affect the DISFS?

Curing of approximately one week followed by approximately three weeks of drying and carbonation have been found favourable for all binders when compared to a longer period of curing before testing. Whereas, a longer period of curing before the DISFS test begin seems unfavourable for the concrete containing 35% LCFA. The results show that concrete with 35% slag is not affected by increasing the period of curing before the drying and carbonation.

The reason for these results is believed to be due to changes to the microstructure from the binder reactions. According to [52], the degree of reaction for the cement in concrete containing 100% CEM I is approx. 75% after 7 d and increases to approx. 83% after 28 days. The degree of reaction for the cement in concrete containing LCFA is approx. 80% after 7 d and increases to approx. 87% after 28 days. Whereas, the degree of reaction for the LCFA in the concrete containing 35% fly ash is approx. 6% after 7 days and 21% after 28 days. Therefore, the increased DISFS when comparing F35 samples that have cured for 8 d (with exposure to DC) with F35 samples that have cured for approx. 28 days (with exposure to DC, see Fig. 1, 2, and 4) should therefore be studied further. Because a longer period of curing result in an increased degree of reaction of the LCFA, products from the LCFA reaction is likely to fill some of the fine porosity and change the microstructure. To find the properties of the microstructure that reduce the DISFS it is suggested that measurements should performed on the changes to the microstructure (pore size distribution of capillary pores and mesopores with capillary suction measurements and low-temperature calorimetry), and connecting the changes to the entrained air void system (pores radius of ca 25 and 250 μm with air void analysis, these voids are effective in decreasing the DISFS). The results is believed to give crucial information to what type of microstructure and entrained air void system that result in a low DISFS for a concrete.

The reason why concrete containing 35% slag is affected to the lowest degree when considering all factors tested in the current study should also be studied further. According to [53], the degree of reaction for slag (Fig. 12c, C-S8 in [53]

was considered closest to materials used in this study) is approx. 40% after 7 d and 55% after 28 days. Therefore, the products will have contributed to a change to the microstructure. However, the DISFS results indicate that this change to the microstructure, from the continued reaction of the slag, does not affect the DISFS. It is suggested that the same measurements as those suggested earlier for the concrete with 35% LCFA (changes to the capillary pores, and mesopores, and measuring the entrained air void system) are performed for the slag concrete also. The results will give information to the question why 35% slag concrete is not affected to the same extent as 35% LCFA from drying and carbonation, increased curing, and increased air content.

How does drying, with and without carbon dioxide, affect the DISFS?

In concrete with 100% CEM I, drying without CO_2 increases the DISFS compared with drying with CO_2. Drying with and without carbon dioxide seem to result in approximately the same DISFS in concrete containing 35% slag or LCFA.

The reason why drying without CO_2 increase the DISFS for concrete containing 100% CEM I should be studied further by analysing if drying concrete containing 100% CEM I in 35% RH more probably cause micro cracks compared to 35% slag or LCFA. Measurements should also be made on the properties of the surface, e.g. indention measurement, in order to study the difference between noncarbonated and carbonated concrete surface that have been cured for 8 d.

The reason why the DISFS is much lower for slag and LCFA compared to CEM I should be studied further by analysing how the microstructures of these young materials differ. Measurements on the microstructure according to previous suggestions (capillary suction, and low-temperature calorimetry) will give information regarding what structures are more probable to result in a low DISFS.

How does the air content affect the DISFS in concrete exposed to short periods of hydration (with or without exposure to drying and carbonation)?

An increased air content decreases the DISFS more in all tested concrete that has never been dried or carbonated than in all tested concrete that has been dried and carbonated.

The reason for this is also unknown and should be studied further by analysing what properties increase the effectiveness from the entrained air void system. Results in [2, 3] indicate that a microstructure with a large fraction of bottle-necks in the capillary and mesopores decrease the effectiveness from the entrained air void system. Another factor that affects the effect the entrained air void system could be the water content in the sample. When the samples are dried at a certain relative humidity, the water content inside all pores with a radius larger than a certain value will dry out. Therefore, a study should be made where samples are dried to equilibrium with a certain relative humidity. This gives detailed

information about what pores are filled in the beginning of the DISFS test. When combining the information about what pores are filled with measurements of the microstructure, this will contribute with information regarding drying of pores down to a certain radius contribute to reduce the DISFS.

How does the NaCl concentration affect the DISFS in concrete with low-calcium fly ash or slag?

Low concentrations of NaCl increase the DISFS; however, this effect is seemingly outweighed by air content and preconditioning process.

The low air content is believed to outweigh the other factors for the 35% LCFA samples because samples with low air contents makes it more probable for less air to be trapped inside the entrained air void system. When less air is trapped the critical degree of saturation is exceeded and the pressure from growing ice damage the concrete. Because 9% NaCl is absorbed more readily into concrete the critical degree of saturation is exceeded and that is believed to be the reason why the 9% NaCl solution was able to damage the 35% fly ash concrete with low air content. This is also believed to be the reason to the high DISFS to the 35% concrete containing LCFA that have never-dried or carbonated. Because this concrete have never-dried and that 9% NaCl more readily fills the porosity, the critical degree of saturation is believed to be exceeded, which caused the damage. The other concrete samples are believed to have enough air trapped inside the entrained air voids, i.e. the critical degree of saturation is not exceeded. When there is air trapped inside the entrained air voids, the damaging DISFS mechanism is believed to be according to the theory presented by Valenza and Scherer [29].

Conclusions

This paper has provided a broad overview of the effect of various preconditioning processes on the materials tested in this study. The results show that the DISFS in each material is highly dependent on drying and carbonation, air content, and salt solution concentrations. The results also show some that these factors influence each other. The carbonation of the surface has the largest influencing factor in concrete containing CEM I. When samples with 100% CEM I is subjected to an NDNC preconditioning process, the air content has a large influence on the DISFS. The foremost influencing factor on concrete containing 35% low-calcium fly ash is drying at a young age together with high air content. The high NaCl solution concentration (9%) has resulted in a lower DISFS mass only when the samples with high ACP have been dried and carbonated. The foremost influencing factors on concrete containing 35% slag are drying and carbonation. Moreover, the high salt solution concentration (9%) has consistently resulted in a lower DISFS mass in concrete with 35% slag regardless of the preconditioning or air content.

This paper also shows that there is impetus for future studies where material characterisations are made on the microstructure of young concrete (e.g. samples that have cured for 8 and 28 days) with capillary suction and low-temperature calorimetry. This could answer the question why concrete with 35% low calcium fly ash that have cured for 8 d, and dried and carbonated, have lower DISFS compared to samples (from the same batches) that have cured for 28 days (or more), and dried and carbonated. This could also answer the question why concrete with 35% slag is affected by each tested factor to a lower extent when compared to the other materials tested. Another future question is the importance of trapped air inside the entrained air void system and how various drying conditions affect the DISFS. This paper also shows that some preconditioning processes are favourable to certain recipes. Because some studies have criticised the lack of agreement between field studies and standard DISFS test studies [19, 21, 22, 54-58], the results presented in this paper should be considered if future adjustments are made to the standard preconditioning processes to improve the agreement.

Acknowledgement

This research received financial support from the SBUF (The Development Fund of the Swedish Construction Industry) and assisted by Skanska AB and Cementa AB (a part of Heidelberg Cement Group).

References

1. Scrivener, K.L., *Options for the future of cement.* The Indian Concrete Journal, 2014. **88**(7): p. 11.
2. Strand, M.J. and K. Fridh, *De-Icing Salt Frost Scaling part 1: Concrete containing Low Calcium Fly Ash*. Manuscript, Lund University.
3. Strand, M.J. and K. Fridh, *De-Icing Salt Frost Scaling part 2: Concrete containing Ground Granulated Blast-Furnace Slag*. Manuscript, Lund University.
4. Jacobsen, S., et al., *Frost deicer salt scaling testing of concrete: Effect of drying and natural weathering.* Cement Concrete and Aggregates, 1997. **19**(1): p. 8-16.
5. Utgenannt, P., *The influence of ageing on the salt-frost resistance of concrete*, in *Department och Building and Environmental Technology*. 2004, Faculty of Engineering, LTH, Lund University: Lund. p. 346.
6. Strand, M.J. and K. Fridh, *Test Method for De-Icing Salt Frost Scaling in High Performance Concrete.* MethodsX, 2018.

7. Nili, M. and M. Zaheri, *Deicer salt-scaling resistance of non-air-entrained roller-compacted concrete pavements.* Construction and Building Materials, 2011. **25**(4): p. 1671-1676.

8. Lindmark, S., *Mechanisms of Salt Frost Scaling of Portland Cement-bound Materials: Studies and Hypothesis*, in *Department of Building and Environmental Technology*. 1998, Faculty of Engineering, LTH, Lund University: Lund. p. 266.

9. Studer, W., *Internal comparative tests on frost-deicing-salt resistance*, in *International Workshop in the Resistance of Concrete to Scaling Due to Freezing in the Presence of De-icing Salts*, J. Marchand, M. Pigeon, and M.J. Setzer, Editors. 1997, E & FN Spon: Sainte-Foy, Québec, Canada. p. 259-270.

10. Sellevold, E.J. and T. Farstad, *Frost/Salt-testing of Concrete: Effect of Test Parameters and Concrete Moisture History.* 1991.

11. Ghazy, A. and M.T. Bassuoni, *Resistance of concrete to different exposures with chloride-based salts.* Cement and Concrete Research, 2017. **101**: p. 144-158.

12. Liu, Z. and W. Hansen, *Freezing characteristics of air-entrained concrete in the presence of deicing salt.* Cement and Concrete Research, 2015. **74**: p. 10-18.

13. Setzer, M.J., *Frost-attack on concrete - modeling by the micro-ice-lens model - evaluating by RILEM CIF test.* Creep, Shrinkage and Durability Mechanics of Concrete and Concrete Structures, 2009: p. 971-977.

14. Setzer, M.J., S. Palecki, and F. Tauscher, *Einfluss der NaCl konzentration auf das abwitterungsverhalten von beton unter frost-tausalzbelastung.* Forschungsbericht BAST, 2007.

15. Marchand, J., et al., *Influence of Chloride Solution Concentration on Deicer Salt Scaling Deterioration of Concrete.* ACI Materials Journal, 1999. **96**(4): p. 429-435.

16. G., F., *Studies of the Scaling, the Water Uptake and the Dilation of Mortar Specimens Exposed to Freezing and Thawing in NaCl Solutions*, in *Freeze-Thaw and De-Icing Resistance of Concrete*, G. Fagerlund and M.J. Setzer, Editors. 1992, Lund Institute of Technology: Lund, Sweden. p. 36-66.

17. Verbeck, G.J. and P. Klieger, *Studies of "Salt" Scaling of Concrete*, H.R.B. 150, Editor. 1957: Washington D.C. p. 13.

18. Arnfelt, H., *Damage on Concrete Pavements by Wintertime Salt Treatment*. 1943, Statens Väginstitut. p. 28.

19. Löfgren, I., O. Esping, and A. Lindvall, *The influence of carbonation and age on salt frost scaling of concrete with mineral additions*, in *Materials, Systems and Structures in Civil Engineering 2016*, M.T. Hasholt, K. Fridh, and R.D. Hooton, Editors. 2016, RILEM publications S.A.R.L: Technical University of Denmark, Lyngby, Denmark. p. 91-100.

20. Ahani, R.M. and M.R. Nokken, *Salt scaling resistance – The effect of curing and pre-saturation.* Construction and Building Materials, 2012. **26**(1): p. 558-564.

21. Bouzoubaâ, N., et al., *Deicing salt scaling resistance of concrete incorporating supplementary cementing materials: laboratory and field test data.* Canadian Journal of Civil Engineering, 2008. **35**: p. 1261-1275.

22. Marchand, J., M. Jolin, and Y. Machabée, *Deicer salt scaling resistance of supplementary cementing material concrete: laboratory results against field performance*, in *Cement Combinations for Durable Concrete*, R.K. Dhir, T.A. Harrison, and M.D. Newlands, Editors. 2005, MPG Books: University of Dundee, Scotland, UK. p. 579-590.

23. Zhang, M.H., et al., *De-Icing Salt Scaling of Concrete Incorporating Different Types and Percentages of Fly Ashes*, in *Sixth CANMET/ACI International Conference on Fly Ash, Silica Fume, Slag, and Natural Pozzolans in Concrete*, V.M. Malhotra, Editor. 1998, ACI: Bangkok, Thailand. p. 493-525.

24. Bilodeau, A., et al., *Effect of Curing Methods and Conditions on the Performance of Fly Ash Concrete in De-Icing Salt Scaling*, in *Sixth CANMET/ACI International Conference on Fly Ash, Silica Fume, Slag, and Natural Pozzolans in Concrete*, V.M. Malhotra, Editor. 1998, ACI: Bangkok, Thailand. p. 361-384.

25. Thomas, M.D.A., *Laboratory and field studies of salt scaling in fly ash concrete*, in *Frost Resistance of Concrete*, M.J. Setzer and R. Auberg, Editors. 1997, E&FN Spon: University of Essen. p. 21-30.

26. Bilodeau, A. and V.M. Malhotra. *Deicing salt scaling resistance of concrete incorporating supplementary cementing materials CANMET research*. in *Freeze-Thaw Durability of Concrete - rilem proceedings 30*. 1997. E & FN SPON.

27. Pigeon, M., et al., *Surface microstructure and scaling resistance of concrete.* Cement and Concrete Research, 1996. **26**(10): p. 1555-1566.

28. Paris, J.M., et al., *A review of waste products utilized as supplements to Portland cement in concrete.* Journal of Cleaner Production, 2016. **121**: p. 1-18.

29. Valenza II, J.J. and G.W. Scherer, *A review of salt scaling: II. Mechanisms.* Cement and Concrete Research, 2007. **37**(7): p. 1022-1034.

30. Powers, T.C., *Freezing effects in concrete.* ACI, 1975. **SP-47**(Durability of Concrete): p. 1-11.

31. Fagerlund, G., *Critical degrees of saturation at freezing of porous and brittle materials*. 1972, The Lund Institute of Technology: Lund, Sweden.

32. Strand, M.J. and K. Fridh, *Test Method for De-Icing Salt-Frost Scaling in High-Performance Concrete.* MethodsX, 2018.

33. Gallé, C., *Effect of drying on cement-based materials pore structure as identified by mercury intrusion porosimetry: A comparative study between oven-, vacuum-, and freeze-drying.* Cement and Concrete Research, 2001. **31**(10): p. 1467-1477.

34. Muller, A.C.A., et al., *Use of bench-top NMR to measure the density, composition and desorption isotherm of C–S–H in cement paste.* Microporous and Mesoporous Materials, 2013. **178**: p. 99-103.

35. Feldman, R.F. and V.S. Ramachandran, *Differentiation of interlayer and adsorbed water in hydrated portland cement by thermal analysis.* Cement and Concrete Research, 1971. **1**(6): p. 607-620.

36. Feldman, R.F. and V.S. Ramachandran, *A study of the state of water and stoichiometry of bottle-hydrated Ca3SiO5.* Cement and Concrete Research, 1974. **4**(2): p. 155-166.

37. Powers, T.C. *The Air Requirement of Frost-Resistant Concrete*. 1949. Highway Research Board 29, PCA Bull 33.

38. Lindmark, S. *On the Relation between Air void system parameters and Salt frost scaling*. in *Nordic Miniseminar: Freeze-thaw testing of concrete*. 2010. Vedbaek, Denmark: Nordic Concrete Federation.

39. Yuan, J., Y. Wu, and J. Zhang, *Characterization of air voids and frost resistance of concrete based on industrial computerized tomographical technology.* Construction and Building Materials, 2018. **168**: p. 975-983.

40. Shon, C.-S., et al., *Determination of air-void system and modified frost resistance number for freeze-thaw resistance evaluation of ternary blended concrete made of ordinary Portland cement/silica fume/class F fly ash.* Cold Regions Science and Technology, 2018. **155**: p. 127-136.

41. Van den Heede, P., J. Furniere, and N. De Belie, *Influence of air entraining agents on deicing salt scaling resistance and transport properties of high-volume fly ash concrete.* Cement and Concrete Composites, 2013. **37**: p. 293-303.

42. Sun, C.T., W.H. Li, and B.R. Hou, *Study on Frost-Salt Resistance of Fly Ash Concrete.* Architecture and Urban Development, 2012. **598**: p. 432-437.

43. Giergiczny, Z., et al., *Air void system and frost-salt scaling of concrete containing slag-blended cement.* Construction and Building Materials, 2009. **23**(6): p. 2451-2456.

44. Valenza II, J.J. and G.W. Scherer, *A review of salt scaling: I. Phenomenology.* Cement and Concrete Research, 2007. **37**(7): p. 1007-1021.

45. Du, L. and K.J. Folliard, *Mechanisms of air entrainment in concrete.* Cement and Concrete Research, 2005. **35**(8): p. 1463-1471.

46. Powers, T.C., *Void spacing as a basis for producing air-entrained concrete.* Journal of the American Concrete Institute, 1954. **50**(9): p. 741-760.

47. Yuan, J., et al., *Mechanisms on the Salt–Frost Scaling of Concrete.* Journal of Materials in Civil Engineering Structures, 2017. **29**(3).

48. Herterich, J.A., *Microstructure and phase assemblage of low-clinker cements during early stages of carbonation*. 2017, School of Civil Engineering, The University of Leeds. p. 265.

49. CEN/TS, *CEN/TS 12390-9* in *Testing hardened concrete - Part 9: Freeze-thaw resistance - Scaling*. 2006. p. 24.

50. Valenza II, J.J., *Mechanism for Salt Scaling*, in *Civil and Environmental Engineering*. 2005, Princeton University. p. 362.

51. Haynes, W.M., *CRC Handbook of Chemistry and Physics 93rd edition*, ed. W.M. Haynes. 2012.

52. De Weerdt, K., et al., *The effect of temperature on the hydration of composite cements containing limestone powder and fly ash.* Materials and Structures, 2012. **45**(7): p. 1101-1114.

53. Kocaba, V., E. Gallucci, and K.L. Scrivener, *Methods for determination of degree of reaction of slag in blended cement pastes.* Cement and Concrete Research, 2012. **42**(3): p. 511-525.

54. Hooton, R.D. and A. Boyd, *Effect of finishing, forming and curing on de-icer salt scaling resistance of concretes*, in *Frost Resistance of Concrete*, M.J. Setzer and R. Auberg, Editors. 1997, E&FN Spon: University of Essen. p. 174-183.

55. Krishnan, A., et al., *Technical issues related to the use of fly ash and slag during late-fall (low temperature) construction season*. 2006, Indiana department of transportation, Purdue University. p. 358.

56. Boyd, A.J. and R.D. Hooton, *Long-Term Scaling Performance of Concretes Containing Supplementary Cementing Materials.* Journal of Materials in Civil Engineering, 2007. **19**(10): p. 820-825.

57. Boubitsas, D., et al., *Frost resistance of concrete - Experience from long term exposure*, in *Materials, Systems and Structures in Civil Engineering 2016*, M.T. Hasholt, K. Fridh, and R.D. Hooton, Editors. 2016, RILEM publications S.A.R.L: Technical University of Denmark, Lyngby, Denmark. p. 21-30.

58. Bouzoubaâ, N., et al., *Deicing salt scaling resistance of concrete incorporating fly ash and (or) silica fume - laboratory and field sidewalk test data.* Canadian Journal of Civil Engineering, 2011. **38**: p. 373-382.

59. EN196-6, *Methods of testing cement- Part 6: Determination of fineness*. 2010.

60. EN196-1, *Methods of testing cement - Part 1: Determination of strength*. 2005.

Supplementary information

Binder characterisation tests

Table 8 summarises the XRF analysis of the LCFA and each binder combination that has been tested; CEM I contains 2.36% lime filler.

Table 8
X-ray fluorescence analysis (XRF) of binders according to ER 9214 method; SO3 measurements according to ER 9212 method; loss on ignition measurements according to ER 9213:2005 method.

Binder	CaO[1] [%]	SiO_2[1] [%]	Al_2O_3[1] [%]	Fe_2O_3[1] [%]	MgO[1] [%]	K_2O[1] [%]	Na_2O [%]	Na_2Oe[2] [%]	SO_3[1] [%]	LOI[1] [%]
CEM I	63.60	21.30	3.80	4.56	0.86	0.65	0.07	0.50	2.45	1.84
LCFA	3.53	57.00	21.60	7.33	1.95	2.16	0.00	1.42	0.65	2.71
F20	52.40	28.60	7.38	5.17	1.09	1.00	0.25	0.91	2.05	2.00
F35	44.00	33.50	9.88	5.52	1.26	1.24	0.38	1.20	1.78	2.09
S20[3]	57.80	23.90	5.61	3.78	3.68	0.699	0.17	0.63	2.60	1.17
S35[3]	52.70	25.90	7.10	3.11	5.92	0.748	0.26	0.75	2.76	0.56
S70[3]	41.60	29.90	10.20	1.67	10.7	0.842	0.44	1.00	3.02	−0.59
K35[3]	54.10	22.90	5.94	3.11	4.77	0.685	0.21	0.66	2.40	5.04

[1] Measurement precisions: CaO±0.233%, SiO2±0.100%, Al2O3±0.052%, Fe2O3±0.019%, MgO±0.025%, K2O±0.032%, SO3±3%, (loss on ignition=) LOI±0.18%.
[2] Na2O-equivalent from K2O and Na2O.
[3] Measured oxide composition from blended slag and CEM I.

The measurement results of the ICP, Blaine, laser diffraction, and compressive strength are summarised in Table 9. The ICP analysis shows the fractional amounts of alkalis contained in each binder combination that are soluble in water. According to the results, the mass of soluble alkalis decreases when the LCFA mass increases. The Blaine and laser diffraction measurements show that the particles of LCFA have a smaller specific surface in comparison with that of CEM I; therefore, on average, the particle size of the former is larger than that of the latter. The compressive strength tests show that an increased amount of the LCFA decreases the strength.

Table 9
H2O-soluble alkalis, Blaine value, laser diffraction, and compressive strength measurements; Cementa performed the measurements.

Binder	ICP analysis[1] [%]			Blaine[2]	LD[3]	Strength after presented days of hydration[4] [MPa]			
	K_2O	Na_2O	Na_2Oe	[m²/kg]	[µm]	2 d	28 d	56 d	91 d
CEM I	0.44	0.03	0.32	343	17.305	21.8±0.3	55.1±0.3	62.3±1.2	66.1±2.0
F20	0.35	0.03	0.26	340	18.097	17.0±0.3	45.5±1.0	56.4±0.6	62.7±1.5
F35	0.29	0.04	0.23	328	18.556	13.3±0.2	37.4±0.4	49.6±1.1	56.9±0.6
S20				371	16.142	16.5±0.2	52.1±0.8	63.3±1.3	65.3±1.3
S35				395	15.339	12.9±0.1	53.9±0.6	63.5±0.7	67.4±0.5
S70				448	13.957	4.4±0.1	42.4±0.4	49.3±0.9	51.8±1.1
K35				397	16.439	12.8±0.3	47.9±1.2	55.2±0.6	58.3±0.6

[1] ICP analysis of soluble K2O, Na2O, and Na2O-equivalent in H2O according to 'CR 0401' method.
[2] Blaine value of specific surface area per mass binder measured according to [59].
[3] Laser diffraction measurement of the size of the 50th percentile particle size.
[4] Compressive strength measurement according to [60] with standard deviation.

Supplementary information on salt-frost scaling results

The figures below show the coefficient of variation in relation to the accumulated scaling. The coefficient of variation is the standard deviation of the accumulated scaling divided by the accumulated scaling.

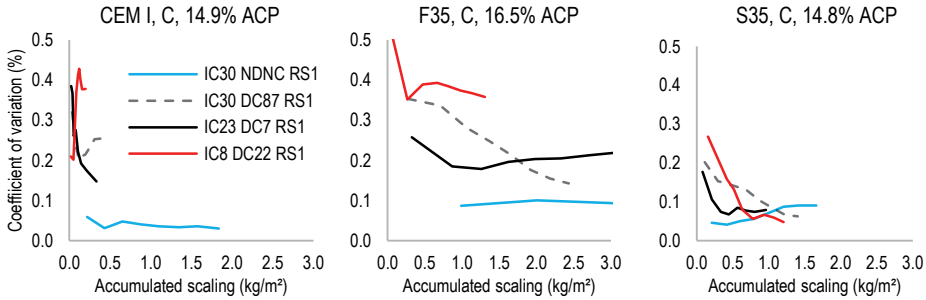

Figure 16
The coefficient of variation in relation to the accumulated scaling for Fig. 1 in the paper.

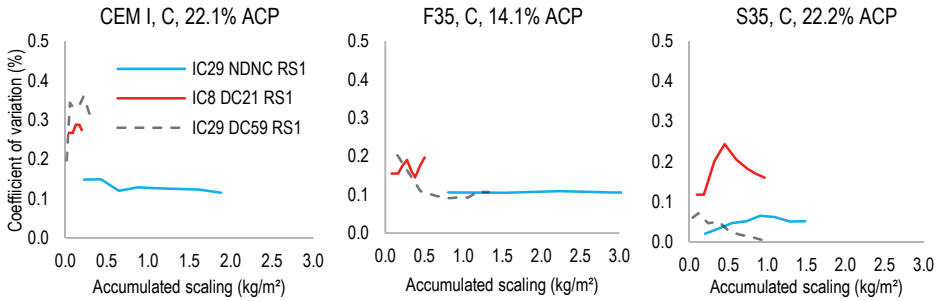

Figure 17
The coefficient of variation in relation to the accumulated scaling for Fig. 2 in the paper.

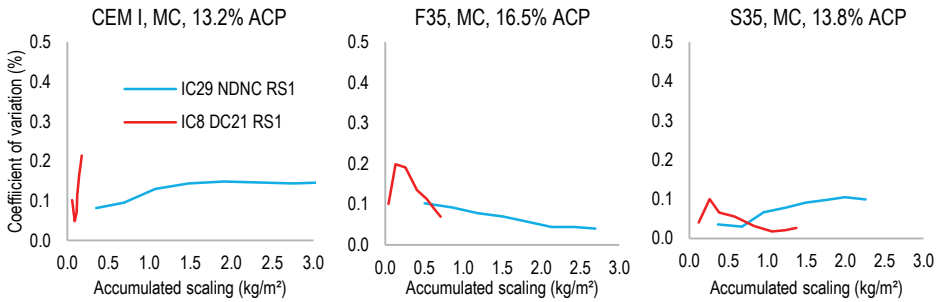

Figure 18
The coefficient of variation in relation to the accumulated scaling for Fig. 3 in the paper.

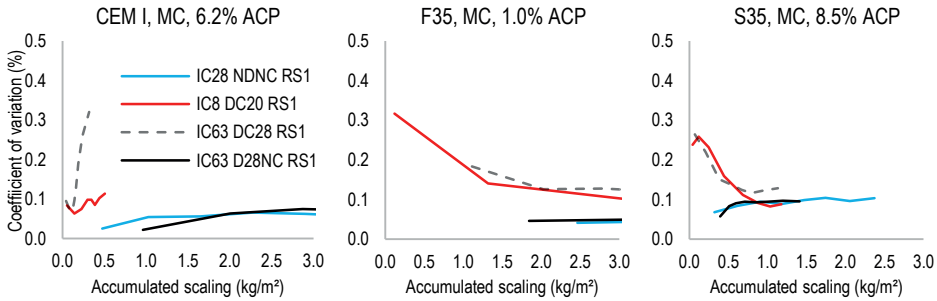

Figure 19
The coefficient of variation in relation to the accumulated scaling for Fig. 4 in the paper.

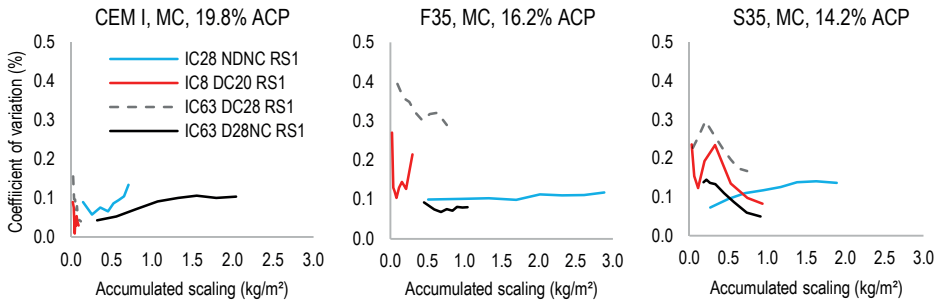

Figure 20
The coefficient of variation in relation to the accumulated scaling for Fig. 5 in the paper.

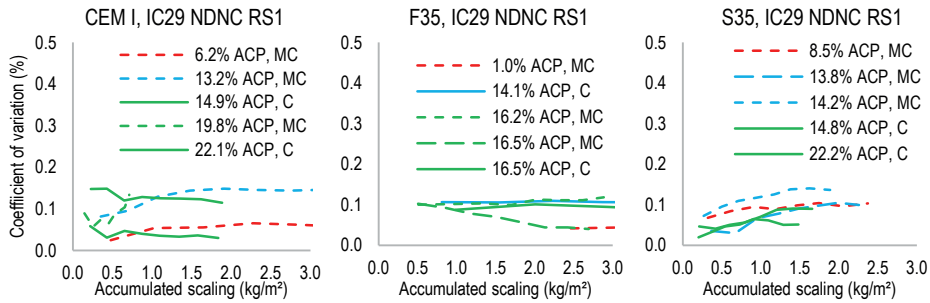

Figure 21
The coefficient of variation in relation to the accumulated scaling for Fig. 6 in the paper.

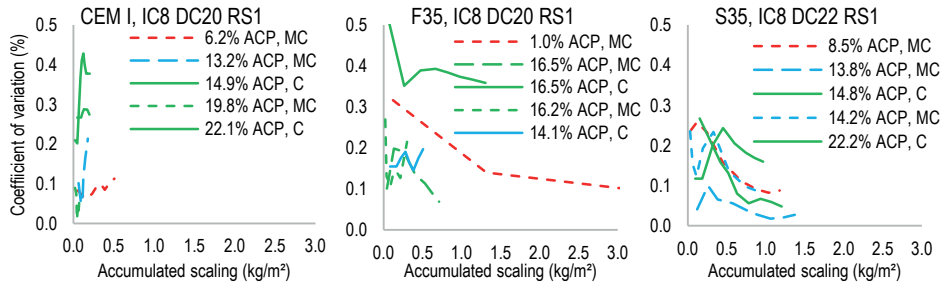

Figure 22
The coefficient of variation in relation to the accumulated scaling for Fig. 7 in the paper.

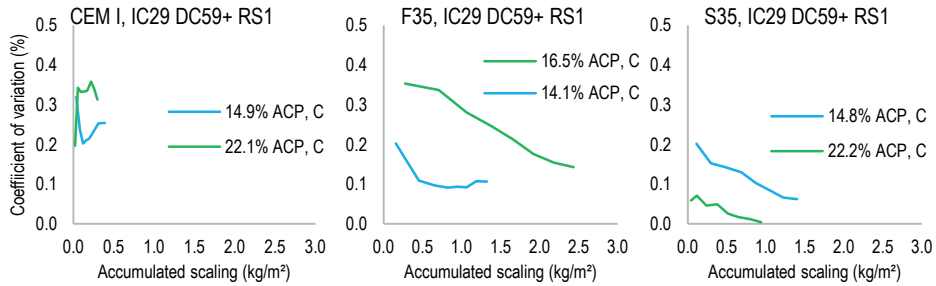

Figure 23
The coefficient of variation in relation to the accumulated scaling for Fig. 8 in the paper.

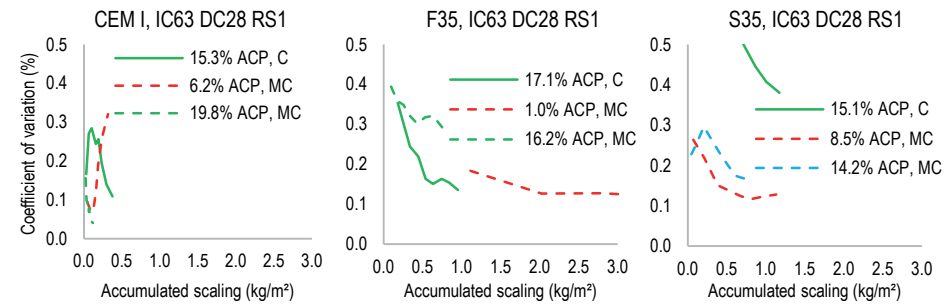

Figure 24
The coefficient of variation in relation to the accumulated scaling for Fig. 9 in the paper.

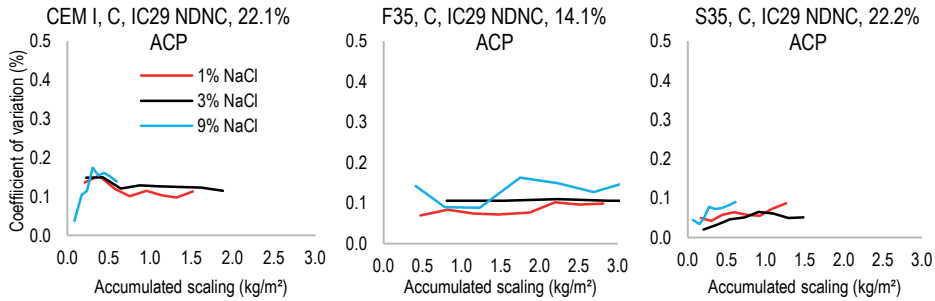

Figure 25
The coefficient of variation in relation to the accumulated scaling for Fig. 10 in the paper.

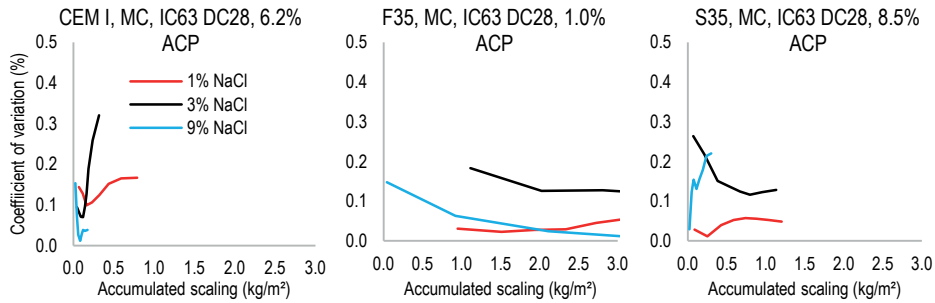

Figure 26
The coefficient of variation in relation to the accumulated scaling for Fig. 11 in the paper.

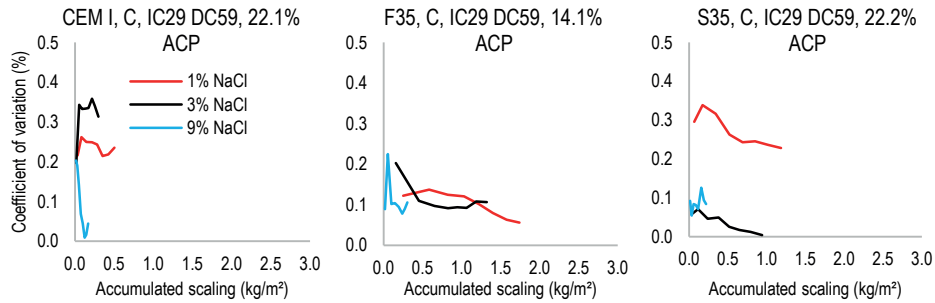

Figure 27
The coefficient of variation in relation to the accumulated scaling for Fig. 12 in the paper.

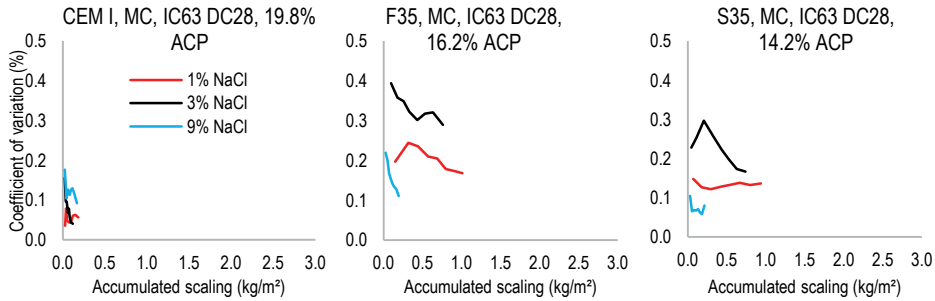

Figure 28
The coefficient of variation in relation to the accumulated scaling for Fig. 13 in the paper.

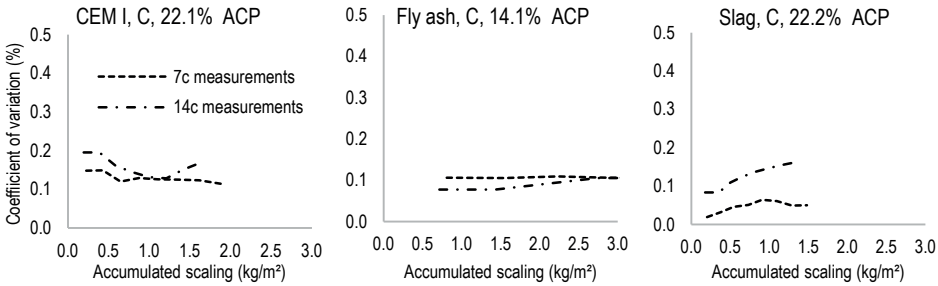

Figure 29
The coefficient of variation in relation to the accumulated scaling for Fig. 14 in the paper.

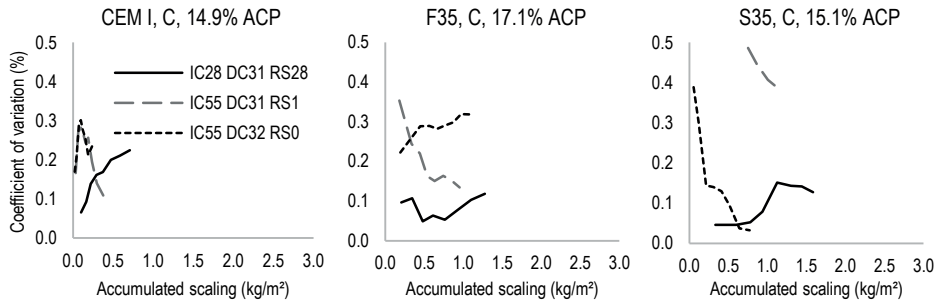

Figure 30
The coefficient of variation in relation to the accumulated scaling for Fig. 15 in the paper.

Printed by Media-Tryck, Lund 2018 NORDIC SWAN ECOLABEL 3041 0903

Faculty of Engineering
Division of Building Materials
ISRN LUTVDG/TVBM--18/1038--SE(1-73)
ISBN 978-91-7753-940-7 (Print)
ISBN 978-91-7753-941-4 (Pdf)
ISSN 0348-7911